Copper(I)-catalyzed azide–alkyne cycloaddition as synthetic tool for triazole-based ligands

Dissertation

zur Erlangung des akademischen Grades

doctor rerum naturalium (Dr. rer. nat.)

seit 1558

vorgelegt dem Rat der Chemisch-Geowissenschaftlichen

Fakultät der Friedrich-Schiller-Universität Jena

von Diplom-Chemiker Bobby Happ

geboren am 2. Mai 1984 in Suhl

Gutachter:

    1. ....

    2. ....

Tag der öffentlichen Verteidigung:

"*Zwei Dinge sind zu unserer Arbeit nötig: Unermüdliche Ausdauer und die Bereitschaft, etwas, in das man viel Zeit und Arbeit gesteckt hat, wieder wegzuwerfen.*" (Albert Einstein)

Table of contents

Documentation of Authorship

This section contains a list of the individual authors' contributions regarding the publications reprinted in this thesis.

A1) <u>B. Happ</u>, D. Escudero, M. D. Hager, C. Friebe, A. Winter, H. Görls, E. Altuntas, L. González, U. S. Schubert — *J. Org. Chem.* **2010**, *75*, 4025–4038.

B. Happ:	syntheses, preparation of the manuscript
D. Escudero:	DFT calculations
C. Friebe:	photophysical measurements
H. Görls:	X-ray crystallography
E. Altuntas:	mass spectrometry measurements
L. González, U. S. Schubert:	revision of the manuscript, supervision

A2) D. Escudero, <u>B. Happ</u>, A. Winter, M. D. Hager, U. S. Schubert, L. González — *Chem. Asian J.* **2012**, *7*, 667–671.

B. Happ:	syntheses, preparation of the manuscript
D. Escudero:	DFT calculations, preparation of the manuscript
M. D. Hager, U. S. Schubert:	revision of the manuscript, supervision
L. González:	revision of the manuscript, supervision

A3) <u>B. Happ</u>, A. Winter, M. D. Hager, U. S. Schubert — *Chem. Soc. Rev.* **2012**, *41*, 2222–2255.

B. Happ:	preparation of the manuscript
A. Winter, M. D. Hager:	revision of the manuscript, supervision
U. S. Schubert:	revision of the manuscript, supervision

A4) <u>B. Happ</u>, J. Schäfer, R. Menzel, M. D. Hager, A. Winter, J. Popp, R. Beckert, B. Dietzek, U. S. Schubert — *Macromolecules* **2011**, *44*, 6277–6287.

B. Happ, R. Menzel:	syntheses, preparation of the manuscript
J. Schäfer:	photophysics, preparation of the manuscript
M. D. Hager, A. Winter:	revision of the manuscript, supervision
J. Popp, R. Beckert:	revision of the manuscript, supervision

B. Dietzek, U. S. Schubert: revision of the manuscript, supervision

A5)   B. Happ, C. Friebe, A. Winter, M. D. Hager, U. S. Schubert — *Eur. Polym. J.* **2009**, *45*, 3433–3441.

B. Happ:	syntheses, preparation of the manuscript
C. Friebe:	photophysical measurements
A. Winter, M. D. Hager:	revision of the manuscript, supervision
U. S. Schubert:	revision of the manuscript, supervision

A6)   B. Happ, G. M. Pavlov, E. Altuntas, C. Friebe, M. D. Hager, A. Winter, H. Görls, W. Günther, U. S. Schubert — *Chem. Asian J.* **2011**, *6*, 873–880.

B. Happ:	syntheses, preparation of the manuscript
G. M. Pavlov:	analytical ultracentrifuge measurements
E. Altuntas:	mass spectrometry measurements
C. Friebe:	photophysical measurements
H. Görls:	X-ray crystallography
W. Günther:	2D-NOESY measurements
M. D. Hager, A. Winter:	revision of the manuscript, supervision
U. S. Schubert:	revision of the manuscript, supervision

A7)   B. Happ, G. M. Pavlov, I. Perevyazko, M. D. Hager, A. Winter, U. S. Schubert — *Macromol. Chem. Phys.* **2012**, 213, 1339–1348.

B. Happ:	syntheses, preparation of the manuscript
G. M. Pavlov:	analytical ultracentrifuge measurements
I. Perevyazko:	viscosity measurements
A. Winter, M. D. Hager:	revision of the manuscript, supervision
U. S. Schubert:	revision of the manuscript, supervision

Signature of the supervisor:

_____

Prof. Dr. Ulrich S. Schubert

1 Introduction

In the last decades, transition metal complexes have played a crucial role in many domains of chemistry, such as supramolecular self-assembly, catalysis, photo-generated processes, chemosensors, and material science.[1-16] In particular, the d^6-configured metal ions (i.e. Fe^{II}, Ru^{II}, Os^{II}, Ir^{III}, Co^{III} and Re^{I}) were intensively applied in coordination chemistry and represent nowadays a well-studied and well-understood field.[11, 17-29] The lingering attractiveness can be explained by their exceptional photophysical properties (photostability and broad absorption in the visible region) as well as their chemical attributes (kinetic and thermodynamic stability in solution). The latter consideration can be ascribed to the electronic low-spin configuration for most octahedral d^6 complexes which bear organic ligands causing a considerable high ligand-field splitting, and make these complexes inert with respect to unmeant substitution or oxidation-reduction processes. The coordinative bond, which is set up between a metal center and the donor atom(s) of the organic ligand, has to be assessed as an ambivalent interaction. It is (i) weak enough to keep the intrinsic properties – *e.g.*, the redox properties of the metal ion, ligand-centered and metal-centered absorption bands – of the metal ion as well as ligand and (ii) sufficiently strong to enable new features (phosphorescent complexes as sensors, metal-to-ligand or ligand-to-metal charge-transfer bands) of the compound at the same time. An essential requirement to deliver transition metal ion complexes with desired chemical and physical properties is the creation of chelating ligand systems, whereby a certain alignment of fundamental features, such as chemical stability, redox properties, and excited-state quality, can be developed. Hence, an important challenge is to identify strategies which enable avenues to synthesize potential metal chelators, while at the same time the synthetic complexity of the ligand preparation should be minimized. Ideally, those methods provide functionalized ligand scaffolds by the use of modular building blocks.

The phrase "click chemistry", which was first introduced by Sharpless and co-workers in 2001, describes such a modular approach to organic synthesis.[30] Click chemistry is defined by a set of criteria: a chemical reaction has to be stereospecific (but not necessarily enantioselective), give high yields, generates only minor byproducts and is wide in scope. Furthermore, the reaction must be easy to perform, be inert to oxygen or water, and the product isolation should be undemanding (no chromatographic

purification). Chemical transformations, which obey these criteria, can be primarily ascertained in the field of carbon–heteroatom bond formations comprising common reactions as: (a) additions to unsaturated carbon–carbon bonds (epoxidation, Michael additions and thiol–ene reaction), (b) nucleophilic substitutions (ring-opening of strained electrophiles, azidations) and (c) cycloaddition of unsaturated species (Diels–Alder reactions, 1,3-dipolar cycloaddition).

In this respect, the regioselective Cu[I]-catalyzed Huisgen 1,3-dipolar cycloaddition of organic azides with terminal alkynes (CuAAC) nearly fulfills these criteria and yields only 1,4-substituted 1*H*-1,2,3-triazoles (Scheme 1–1).[31-32] Indeed, 1,2,3-triazoles are not a discovery of the 21st century, since the first synthesis of a 1,2,3-triazole was already described in 1893 by A. Michael from phenyl azide and diethyl acetylenedicarboxylate and was thoroughly studied by Huisgen and coworkers in the 1960s in the course of a detailed investigation toward 1,3-dipolar cycloaddition reactions.[33] Although the reaction of organic azides with alkynes is highly exothermic ($\sim$220 kJ·mol^{-1}), its high activation barrier in the range of 100 kJ·mol^{-1} results in low reaction rates for electronically inactivated reactants even at elevated temperature.[34] Overcoming the lack of selectivity (the non-catalyzed reaction generates the 1,4- and 1,5-regioisomers) and the low reaction rates of the non-catalyzed 1,3-dipolar cycloaddition by the discovery of the CuAAC in 2001, the 1,2,3-triazole emerged as an important scaffold and found numerous application in the field of polymer chemistry and material science.[35-40] Medicinal chemistry uses the 1*H*-1,2,3-triazole moiety as a stable linkage between chemical or biological systems, which is based on its low liability to hydrolytic cleavage and reduction/oxidation processes.[35, 41-44]

In general, the CuAAC reveals a high thermodynamic driving force of about $\Delta G \approx 250$ kJ·mol^{-1}, and the outcome of the reaction is considerably dependant on the used copper(I)-catalyst system.[35] The rate increase relative to the non-catalyzed process is about seven orders of magnitude, which results in a fast reaction even below room temperature. In general, the reaction performance does not suffer from sterical and electronic properties of the groups attached to the azide and alkyne entities. Solvents, which maintain ligand exchange during the process (alcohols and water) mostly, lead to high conversions, though the reaction runs in a broad range of protic and aprotic solvents. In most cases, there is no need for protecting group chemistry, since the most common organic and inorganic functional groups do not impair the CuAAC.

I) 1,3-dipolar cycloaddition of azides and alkynes
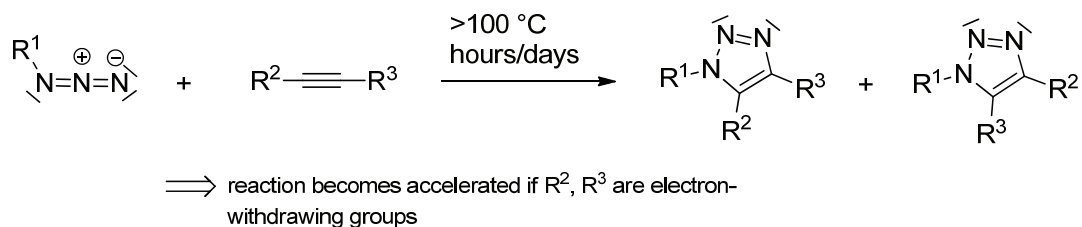
II) Copper(I)-catalyzed azide-alkyne cycloaddition
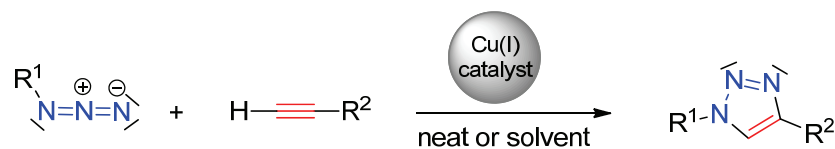
Scheme 1–1. Schematic representation of the difference of the non-catalyzed and the copper(I)-catalyzed 1,3-dipolar cycloaddition.

Up to date the mechanism of the CuAAC is not well-understood because of a complicated and discontinuous behavior, but the latest hypotheses are: (i) copper acetylide species are easily formed during the reaction and are crucial components for the catalysis cycle, (ii) a weak interaction of organic azides with the copper metal center inhibits the formation of disturbing polymeric acetylides or complexes and guides the acetylides into the productive catalytic cycle, and (iii) the catalytic active species may be a dinuclear copper complex and the nuclearity is continuously kept up during the catalysis.[45]

Within in the last five years, chemists have identified a wide range of additional applications for the 1H-1,2,3-triazole heterocycle, *e.g.*, synthesizing bidentate 2-pyridyl-substituted 1H-1,2,3-triazole (trzpy) ligands. The system itself is known since 1970 and has been obtained by recyclization of *v*-triazolo[l,5-a]pyridines.[46] In 1977, Seebach *et al.* combined non-enolizable nitriles and lithiated nitrosamines providing N^1-substituted trzpys.[47] The regioselective CuAAC of 2-ethynylpyridines with organic azides exclusively yields 1,4-substituted trzpys, a very versatile scaffold offering plenty of beneficial properties (Figure 1–1). Different groups have shown that the bidentate pocket of the trzpy can coordinate to a variety of transition metal ions, such as Ru^{II},[48-51] Ir^{III},[52-54] Re^I,[38, 55-56] Pt^{II},[57-58] Pd^{II},[57-59] Cu^I,[60-61] Cu^{II},[62] Ag^I,[62-64] Ni^{II},[65] and Zn^{II},[65] whereby different kind of metal complexes were obtained. The structural and

photophysical properties, in particular coordination compounds of the electronically d^6- and d^8-configurated transition metal ions, resemble their relevant bipyridine counterparts. Recently, trzpy-based ruthenium(II) and iridium(III) complexes were used as photosensitizers for the catalytic production of hydrogen as well as in dye-sensitized solar cells, whereas the device performances were comparable to appropriate reference systems.[66-67]
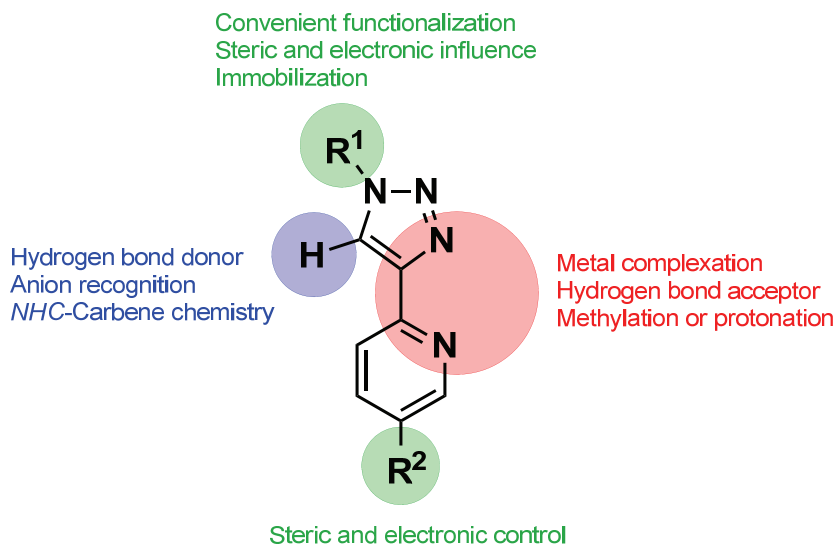
Figure 1–1. Versatility of 2-(1*H*-1,2,3-triazol-4-yl)pyridine-based ligands.

The nitrogen donor atoms may also be a target for protonation[68] and methylation.[69] The unique position of the proton on the C-5 atom of the 1,2,3-triazole subunit permits additional features of the trzpy ligand. The C–H bond of the triazole has a strong dipolar disposition and is able to act as a hydrogen bond donor in contrast to 2,2´-bipyridines.[70] Furthermore, those ligands are used in anion recognition[71-73] and open the door for carbene chemistry.[69, 74] The moiety R^1 allows a straightforward functionalization by simply varying the organic azides in order to introduce polymerizable groups or enables immobilization on a surface.

This thesis specifically covers events of the trzpy ligand that occur in the red- and green-marked region of Figure 1–1. The synthesis, characterization and investigation of photophysical properties of trzpy-based d^6 metal complexes and the self-assembly of d^{10} metal complexes as well as the preparation of polymeric architectures comprises the main part of this work.

2 Tuning the electronic properties of trzpy-based ruthenium(II) complexes

Parts of this chapter have been published including: A1) B. Happ, D. Escudero, M. D. Hager, C. Friebe, A. Winter, H. Görls, E. Altuntas, L. González, U. S. Schubert, *J. Org. Chem.* **2010**, *75*, 4025–4038. A2) D. Escudero, B. Happ, A. Winter, M. D. Hager, U. S. Schubert, L. González, *Chem. Asian J.* **2012**, *7*, 667–671. A3) B. Happ, A. Winter, M. D. Hager, U. S. Schubert, *Chem. Soc. Rev.* **2012**, *41*, 2222–2255.

Polypyridines, such as 2,2′-bipyridine (bpy) and 2,2′:6′,2′′-terpyridine (tpy) and their derivatives, are a well-established and well-studied class of organic ligands due to a predictable coordination behavior and interesting photochemical properties that result from their corresponding metal complexes.[6, 18, 75-77] In particular, the d^6-configured metal ions Ru^{II}, Ir^{III}, Os^{II} and Re^{I} have been chosen as transition metal ions, because of their useful spectroscopic properties comprising photostability and a broad absorption in the visible region.[18-21] As a result, d^6 metal polypyridine compounds are extensively involved as photosensitizers in photochemical processes. For an ideal photosensitizer some requirements can be proposed: a reversible redox behavior, suitable ground and excited state potentials, durability towards thermal and photochemical decomposition, as high as possible extinction coefficients in a suitable spectral region (commonly >300 nm), and a high quantum yield as well as a proper lifetime of the reactive excited state. The excited state properties, *i.e.* excited state lifetime, exited state energy and emission quantum yield as central parameters, determine crucial characteristics of the photosensitizer, such as (photo)chemical stability and redox properties. Chemists have been trying for decades to understand the tuning of the excited state properties. The relatively long-lived excited states of the late d^6 metal complexes (10^{-6} to 10^{-9} s), which are usually of MLCT character, were investigated in detailed photophysical and photochemical studies since the early 1970s leading to a well-understood field of chemistry nowadays.[26, 78-79]

Apart from several photophysical and photochemical similarities, there exist fundamental dissimilarities with respect to the redox behavior of d^6 metal complexes, for instance, when comparing Ru^{II} and Ir^{III} as frequently used transition metal ions. Cyclic voltammetric studies of Ru^{II} polypyridine complexes have shown that they undergo a reversible oxidation associated with the metal-centered Ru^{II}/Ru^{III} couple as well as a

reversible ligand-centered py/py$^-$ (py = polypyridine ligand) reduction to generate Ru^I. In general, the existence of both an oxidizable Ru^{II} center and a reducible ligand establishes a relatively long-lived (up to microseconds) low energy MLCT-associated excited state.[79] In contrast, when it comes to charged Ir^{III} polypyridine complexes, cyclic voltammetric studies indicated that oxidation of Ir^{III} to Ir^{IV} is often irreversible, which was attributed to the preference of oxidation rather at the ligand entity than at the metal ion center. As expected from charge pre-conditions, reduction of Ir^{III} occurs at a much less negative potential than it does in the corresponding Ru^{II} complexes (this process is a reversible one related to reduction at the ligand). In contrast to Ru^{II}, the oxidation and reduction potentials of Ir^{III} complexes suggest a relatively high energy MLCT excited state and, consequently, Ir^{III} is by far a stronger oxidizing agent than Ru^{II}, but a weaker reducing agent.[80] The latter considerations resulted in the utilization of ruthenium(II) polypyridine complexes as prototype for photosensitizers in the first instance.

The following achievements were established in order to tune the electronic properties of bidentate trzpy ligands by introducing electron-donating and electron-withdrawing phenylacetylene units on the 5-position of the pyridine ring. The syntheses of the trzpy ligands were accomplished by the CuAAC, yet having a straightforward access to the central structural trzpy scaffold, whereby the donor and acceptor units were introduced by the Pd^0-catalyzed Sonogashira cross–coupling reaction of various phenylacetylene moieties. Subsequently, the trzpy ligands were attached to the *cis*-dichloro-*bis*(4,4′-dimethyl-2,2′-bipyridine)ruthenium [Ru(dmbpy)$_2$Cl$_2$] precursor (Scheme 2–1). The heteroleptic ruthenium(II) complexes **2-8** to **2-14** of the general structure [(dmbpy)$_2$Ru**L**](PF$_6$)$_2$ were synthesized by heating Ru(dmbpy)$_2$Cl$_2$ and the appropriate ligands (L = **2-1** to **2-7**) under microwave irradiation. After 2 h, the reactions were completed and a 10-fold excess of NH$_4$PF$_6$ was added to precipitate the products. In most cases, precipitation occurred after 15 min and the pure complex was isolated after washing with different solvents in moderate to very good yields. The verification of the structures of **2-8** to **2-14** was carried out by ^{1}H and ^{13}C NMR spectroscopy as well as HR-ESI mass spectrometry.

I) Synthesis of the donor and acceptor ligand systems
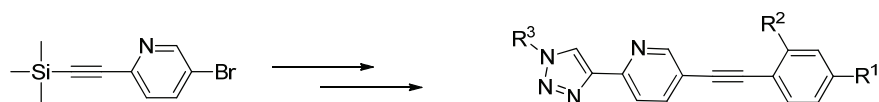
2-1: $R^1 = O-C_6H_{13}$, $R^2 = H$, $R^3 = C_{10}H_{21}$
2-2: $R^1 = NO_2$, $R^2 = H$, $R^3 = C_{10}H_{21}$
2-3: $R^1 = H$, $R^2 = NO_2$, $R^3 = C_{10}H_{21}$
2-4: $R^1 = CF_3$, $R^2 = H$, $R^3 = C_{10}H_{21}$
2-5: $R^1 = H$, $R^2 = H$, $R^3 = C_{10}H_{21}$
2-6: $R^1 = NO_2$, $R^2 = H$, $R^3 = Ph$

2-7
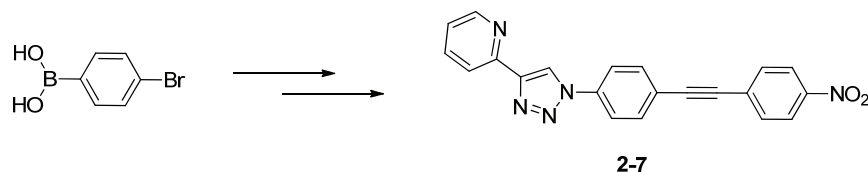
II) Synthesis of the ruthenium(II) complexes
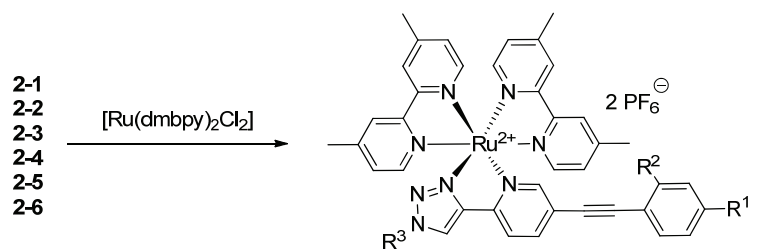
2-8: $R^1 = O-C_6H_{13}$, $R^2 = H$, $R^3 = C_{10}H_{21}$
2-9: $R^1 = NO_2$, $R^2 = H$, $R^3 = C_{10}H_{21}$
2-10: $R^1 = CF_3$, $R^2 = H$, $R^3 = C_{10}H_{21}$
2-11: $R^1 = H$, $R^2 = NO_2$, $R^3 = C_{10}H_{21}$
2-12: $R^1 = H$, $R^2 = H$, $R^3 = C_{10}H_{21}$
2-13: $R^1 = NO_2$, $R^2 = H$, $R^3 = Ph$
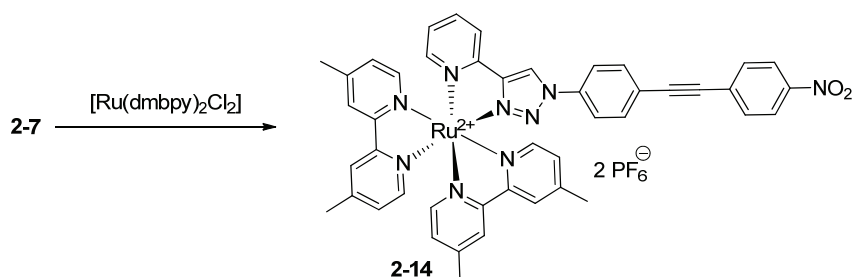
2-14

Scheme 2–1. Schematic representation of the synthesis of the *N*-heterocyclic ligands and their corresponding heteroleptic Ru^{II} complexes.

The complexes **2-8** to **2-12** were characterized by cyclic voltammetry (CV) and the electrochemical properties are presented in Table 2–1. In all cases, a first reversible oxidation wave occurred at around +0.85 V (*vs.* Fc/Fc$^+$) that can be assigned to a

Ru^{II}/Ru^{III} oxidation process. Compound **2-8** showed a second oxidation process at +1.28 V, probably originating from an oxidation process of the triazole ligand. Due to the absence of electron-donating substituents at the triazole ligand, the respective ligand-centered π-orbitals are more stabilized for complexes **2-9** to **2-12** and, therefore, no such oxidation processes were visible in the CV spectrum. In contrast to the other systems, the nitro-containing complexes **2-9** and **2-11** featured a single reversible reduction wave at around −1.35 V (*vs.* Fc/Fc$^+$) that could be assigned to a trzpy-based reduction process. Both complexes provided a strongly electron-withdrawing substituent causing a stabilization of the trzpy-located antibonding π*-orbitals (compare results of the DFT calculations). Starting at −1.8 V all five complexes showed additional reduction waves deriving from ligand-based (dmbpy and triazole ligand) π*-orbitals.

Table 2–1. Electrochemical data of selected Ru^{II} complexes.

Complex	$E_{1/2,ox}$ [V]^a	$E_{1/2,red}$ [V]^a	E^{HOMO} [eV]^b	E^{LUMO} [eV]^b	E_g^{opt} [eV]^c
2-8	+0.82, +1.28	−1.85, −2.06, −2.23	−5.62	−3.18	+2.48
2-9	+0.88	−1.34, −1.97, −2.18	−5.67	−3.70	+2.43
2-10	+0.84	−1.89, −2.13	−5.69	−3.21	+2.44
2-11	+0.88	−1.36, −1.98, −2.11	−5.64	−3.62	+2.43
2-12	+0.84	−1.85, −2.03, −2.18	−5.64	−3.17	+2.49

a) Measurements were performed in CH$_3$CN containing 0.1 M TBAPF$_6$. The potentials are given *vs.* the ferrocene/ferricinium (Fc/Fc$^+$) couple. b) Determined by using $E^{HOMO} = − [(E_{onset,ox} − E_{onset,Fc/Fc+}) − 4.8]$eV and $E^{LUMO} = − [(E_{onset,red} − E_{onset,Fc/Fc+}) − 4.8]$eV, respectively.[81] c) Estimated from the UV/vis spectra at 10% of the maximum of the longest-wavelength absorption band on the low-energy side.[81]

The resulting photophysical properties of the heteroleptic ruthenium(II) complexes are summarized in Table 2–2. In the case of the acceptor-type complexes, referring to representative DFT calculations for complex **2-9**, the broad absorption band between 400 to 500 nm was assigned to various MLCT transitions between the ruthenium metal center and either the dmbpy or the triazole ligand (see Publication A1, Table 5 for details). For the donor-based complex **2-8**, DFT calculations suggested a considerable contribution of LLCT transitions, in addition to MLCT transitions, from the π-orbital localized on the trzpy unit to the π*-orbital of one dmbpy ligand (Figure 2–1, see Publication A1, Table 5

for details). Between 300 and 400 nm, the complexes investigated herein exhibited different absorption behavior concerning their wavelength maxima and band shape. This region was dominated by IL transitions, namely located at the triazole and dmbpy ligand, respectively. More bands were present below 280 nm arising from further MLCT, LLCT and MC d-d transitions, respectively. The observed emission energies (Table 2–2) showed a clear dependency on the used substituent. Starting at 602 nm in the case of the alkoxy-containing system, the emission was strongly red-shifted to 621 nm for the unsubstituted triazole ligand and to 640 and even 674 nm in the case of the complexes possessing an *ortho-* and *para-*nitrophenyl moiety, respectively. This trend was most likely caused by the stabilization of the π*-orbitals located at the triazole ligand *via* introduction of electron-withdrawing groups. These orbitals are involved in the emissive [3]MLCT state (compare DFT ground state calculations in Figure 2–1) in the case of the acceptor-based complex **2-9**, so that a lower energy level led to a decreased emission energy.

Table 2–2. Photophysical data recorded for the Ru[II] complexes.

Complex	λ_{abs} [nm] (ε [10^3 L·mol^{-1}·cm^{-1}])[a,b]	λ_{em} [nm][a]	Φ_{PL}[a,c]
2-8	206 (145.6), 286 (133.1), 333 (59.8), 435 (23.6)	602	0.001 < 0.005[d]
2-9	209 (58.4), 286 (63.4), 328 (38.6), 441 (11.6)	674	0.001 0.022[d]
2-10	209 (88.1), 286 (103.9), 312s (51.6), 440 (18.3)	620	0.002
2-11	208 (66.6), 286 (74.7), 341s (22.6), 442 (12.4)	640	0.001
2-12	205 (131.1), 286 (125.6), 315s (60.9), 438 (20.6)	621	0.001
2-13	206 (83.7), 286 (76.9), 326 (52.5), 440 (12.8)	642	< 0.001
2-14	195 (102.9), 286 (83.1), 316s (40.5), 442s (12.5)	610	0.003

a) For all measurements: 10^{-6} M solution in aerated CH$_3$CN at room temperature. For emission measurements: excitation at longest absorption wavelength. b) "s" signifies absorption shoulder. c) Photoluminescence quantum yields determined using [Ru(bpy)$_3$](PF$_6$)$_2$ (Φ_{PL} = 0.062) as standard. d) Measured in aerated CH$_2$Cl$_2$ solution at room temperature (10^{-6} M).
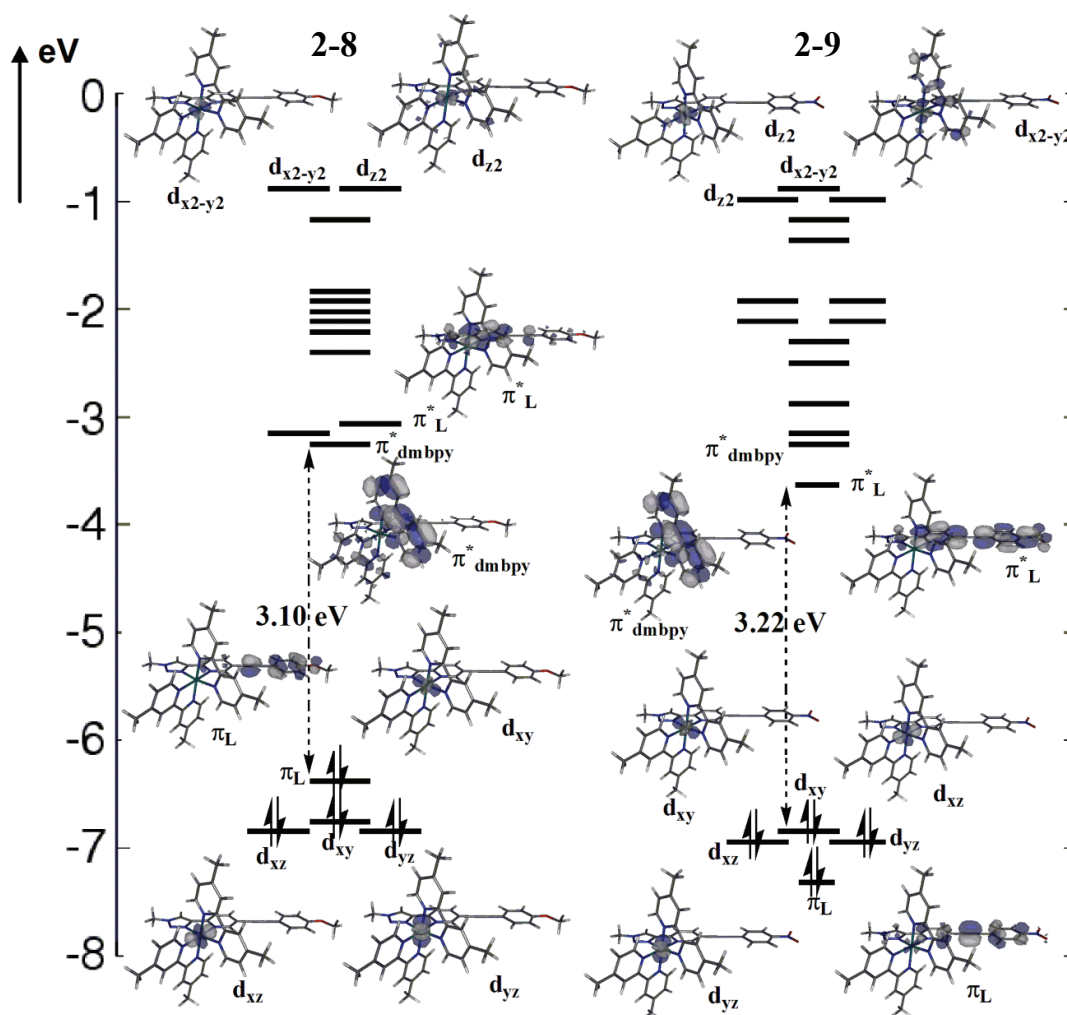
Figure 2–1. Energy levels for the most relevant Kohn-Sham orbitals of complexes **2-8** and **2-9** including the HOMO-LUMO gaps calculated with B3LYP/6-31G*.

The measured emissive behavior revealed a clear dependency on the electronic character of the peripheral substitution as well as on the polarity of the solvent. Similar observations on solvent-dependent luminescence have been reported in literature recently.[82-83] Therefore, TD-DFT calculations were performed to gain a deeper insight into the photophysical processes. The Jablonski diagrams was computed for simplified complexes (**2-8** and **2-9**, respectively) in CH_2Cl_2 (Figure 2–2). The most important singlet–singlet and singlet–triplet electronic excitations computed in CH_2Cl_2 at the S_0 geometry as well as some important triplet excited states at the T_1 geometry are depicted in Figure 2–2a and b, respectively. The biggest SOC elements are obtained between ^{1}MLCT and ^{3}MLCT states, particularly those possessing the same π^* orbital but with

participation of different 4d orbitals (in the case of S_2 interacting with T_6 in complex **2-8** or with T_5 in complex **2-9**, see Figure 2–2).

Figure 2–2. Jablonski diagrams of a donor-type (a: resembles compound **2-8**) and acceptor-type (b: resembles compound **2-9**) Ru^{II} complex with TD-B3LYP singlet-singlet and singlet-triplet vertical excitations (in nm) computed in CH_2Cl_2. The main absolute SOCs (cm^{-1}) and the main k_r values (s^{-1}) are highlighted. The magnitude of the oscillator strengths (f) at the S_0 geometry are pictorially indicated by the width of the vertical transition.

Only the largest radiative rate constant (k_r) obtained for each complex is shown in Figure 2–2. The k_r value for complex **2-9** [$k_r(T_7 \rightarrow S_0) = 5.4 \times 10^7$ s^{-1}] is approximately one

order of magnitude larger than for complex **2-8** [$k_r(T_6{\rightarrow}S_0) = 3.0{\times}10^6$ s^{-1}]. A detailed analysis exhibited that in complex **2-8** the largest radiative rate is due to the interaction of T_6 and S_2 and both states are of MLCT character at S_0 geometry. From T_6, IC processes lead to the lowest T_1, which is the emissive state as stated by Kasha's rule.[84] In the case of complex **2-9**, the ISC is due to the interaction of T_7 with S_4 at the Franck-Condon geometry and further IC to T_1 follows. In both complexes, the T_1 state is a ^{3}MLCT state with $4d_2{\rightarrow}\pi^*_{dmbpy}$ character, as reflected by both the spin-density analysis and the TD-DFT calculations at the T_1 geometry. The reason behind the different orders of magnitude in the radiative rates can be correlated with the electronic nature of the substituent.

Electron-rich substituents on the trzpy ligand stabilize the related π_L orbitals and destabilize the π^*_L orbitals and, consequently, less ^{1}MLCT states are excited below the experimental excitation wavelength. In complex **2-9**, charge transfer transitions to the trzpy with high oscillator strengths are additionally present. The presence of these states is crucial to provide smaller ^{1}MLCT–^{3}MLCT gaps that contribute to a more efficient horizontal ISC and, thus, a larger radiative rate constant. Since larger k_r values entail higher Φ_P [$\Phi_P = k_r/(k_r+k_{nr})$] the expected increase of the k_{nr} value for complex **2-9**, as compared to complex **2-8**, is overcompensated. Therefore, the combination of both effects finally leads to a higher Φ_P value for complex **2-9**.

In summary, bidentate trzpy ligands were synthesized, whereas different phenylacetylene moieties of donor and acceptor nature, respectively, were attached on the 5-position of the pyridine unit. The moieties featured a crucial influence on the electronic properties of these ligands. The *N*-heterocyclic ligands were coordinated to the Ru^{II} ion by using the Ru(dmbpy)$_2$Cl$_2$ precursor. The Ru^{II} complex with electron-donor nature revealed no luminescence at room temperature in contrast to the one with acceptor capability revealing remarkable luminescence at room temperature in CH$_2$Cl$_2$. Radiative rate constants (k_r) have been calculated using a mixed TD-DFT/CASSCF approach for the complexes **2-8** and **2-9**. The calculated k_r values could be used to explain the considerable decrease in quantum yield of the donor-type compound **2-8**.

3 Light-harvesting metallopolymers

A general target of current research is the establishment of new synthetic approaches allowing the facile and straightforward covalent or non-covalent linkage of functionalized ligands or transition metal complexes to polymers. Covalent linkages are the basis for potential functional materials, which are able to avoid aggregation of the incorporated metal complexes, while maintaining the photophysical properties of the appropriate complex at the same time. Considerable effort in the synthesis of metal-containing polymers has been invested for combining the beneficial properties of a metal ion complex, which provides the optoelectronic capacity in many examples, and a polymer backbone enhancing the processability of the materials, *e.g.*, using spin-coating and inkjet-printing, respectively. Applications in the field of supramolecular chemistry, conducting and photoresponsive materials, and catalysis were established.[7-9, 12, 85-87]

In general, a metal complex can be incorporated into a polymer as part of the main chain or as a pendant group. It is also possible to prepare materials in which the metal complex is present in both the side and main chains (dendrimers). Mainly three different types of metal-containing polymers have been emerged: (i) the metal ions/complexes are attached to the polymer backbone at the side chain or as an end group by electrostatic interactions, metal–ligand coordination or covalent bonds, (ii) the metal complexes are part of the polymer main chain (coordination or covalent connection), and (iii) the metal ions are embedded in the polymer matrix by physical interaction. From the synthesis point of view, two primary procedures were applied to prepare the metal-containing polymers: (i) the transition metal complex was attached to a polymer backbone after the polymerization process (grafting), and (ii) the metal complex served itself as the monomer and was incorporated into the polymer by (co)polymerzation.

The latter approach was used for the synthesis of a light-harvesting terpolymer by controlled RAFT radical polymerization containing a luminescent Ru^{II} complex coordinated by an acceptor-type trzpy chelate, a 2-(pyridine-2-yl)thiazole donor-type system and methyl methacrylate (Scheme 3–1). This terpolymer was designed in order to

mimic natural strategies for light harvesting systems for the conversion of energy from sunlight into chemical energy. The thiazole dye is supposed to absorb photons with an energy higher than 2.95 eV ($\lambda < 420$ nm) and transfers a decisive fraction of the excitation energy by the emission of photons ($\lambda_{em,max} = 450$ nm) to the Ru^{II} unit, where a MLCT state ($\lambda_{abs,max} = 450$ nm) is directly excited for charge separation. Hence, the transition metal complex might act as a primary electron donor in any photocatalytic process when, in perspective, combined with a suited electron acceptor. For the system under investigation, the focus was on the energy transfer, which may take place in the random donor−acceptor terpolymer.
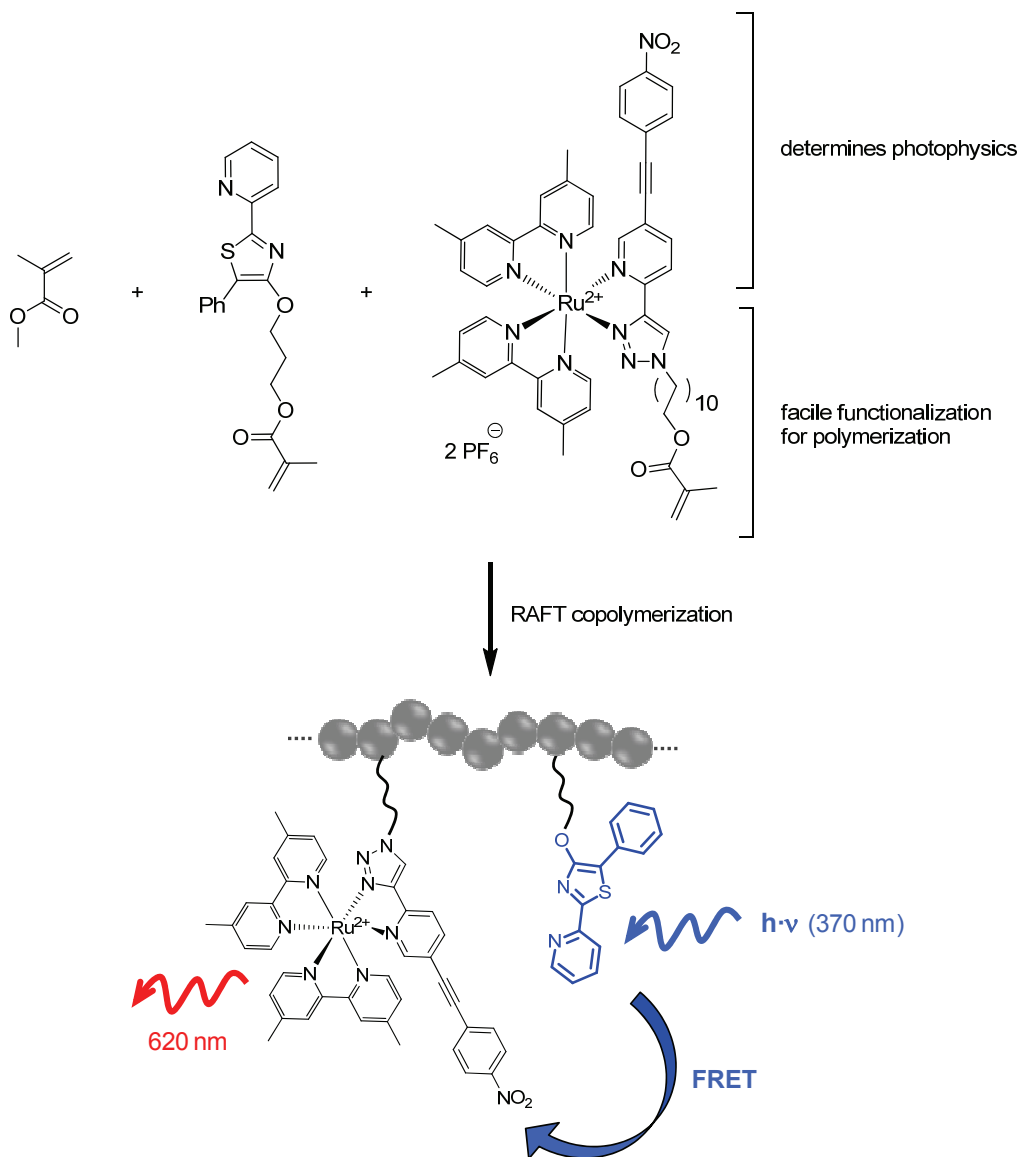
Scheme 3–1. Schematic representation of the synthesis of the donor−acceptor terpolymer capable of transferring energy upon light excitation of the donor-type thiazole entity.

The general synthesis route of the monomers is depicted in Schemes 3–2 and 3–3. In the first three steps, CuAAC and Pd^0-catalyzed Sonogashira coupling were used to set up the trzpy scaffold bearing an electron-withdrawing 4-nitrophenylacetylene moiety on the 5-position of the pyridine ring. The CuAAC of 2-ethynyl-5-bromopyridine and 11-azidoundecan-1-ol yielded **3-1** under typical reaction conditions, using 10 mol% of $CuSO_4$ and 0.5 equiv. of sodium ascorbate as Cu^I source. Consecutive Sonogashira cross-coupling with TMSA and $Pd^0(PPh_3)_4$, as catalytic active Pd^0 source, as well as subsequent deprotection of the TMS by potassium fluoride afforded **3-2** in moderate yield (47%). The following Sonogashira coupling with 4-nitro-1-iodobenzene provided component **3-3**. The hydroxyl moiety was changed to methyl methacrylate in order to introduce a polymerizable group. The esterification of **3-3** with methacryloyl chloride gave **3-4** in good yield (89%). The heteroleptic ruthenium(II) complex **3-5** was synthesized by heating $Ru(dmbpy)_2Cl_2$ and ligand **3-4** under microwave irradiation for 2 h at 120 °C. The methacryl-moiety was found to be stable under these conditions as confirmed by preliminary experiments. After the reaction was completed, a 10-fold excess of NH_4PF_6 was added to precipitate the ruthenium(II) complex. Precipitation occurred usually within 30 min, and the complex was finally purified by recrystallization from ethanol and subsequent washing with cold ethanol (yield >90%). The verification of the structure was carried out by ^1H and ^{13}C NMR spectroscopy as well as by high-resolution mass spectrometry.

The 4-hydroxythiazole **3-6** was prepared by a cyclization process of pyridine-2-carbothioamide with ethyl 2-bromophenylacetate. Williamson-type etherification of **3-6** with 3-bromopropan-1-ol as electrophile yielded **3-7** in good yield (68%) under mild conditions. Subsequently, the hydroxyl group was reacted with methacryloyl chloride under basic conditions to yield the polymerizable ester **3-8** (Scheme 3–3). All compounds had to be purified by column chromatography to ensure a proper reagent grade for the following radical polymerization. The confirmation of the structures was performed by NMR spectroscopy, mass spectrometry and elemental analysis.

Two copolymers and one terpolymer were synthesized based on a PMMA backbone, where **3-8** served as the donor and **3-5** as the acceptor unit, respectively (Scheme 3–4). The conversion of the reactions was roughly 80% using a standard reaction time of 16 h.

I) Synthesis of the ligand scaffold
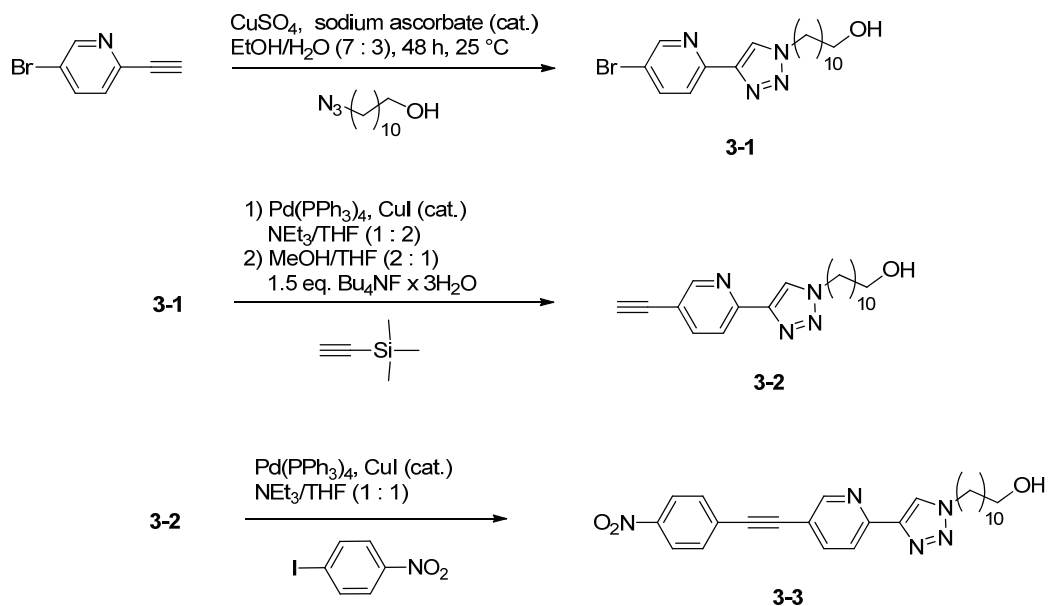
3-1

3-2

3-3

II) Functionalization with a polymerizable group

3-4

III) Synthesis of the Ru^{II} complex

3-5
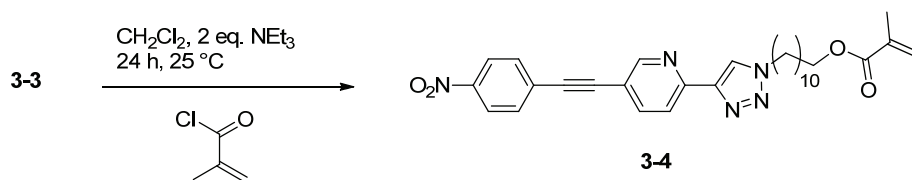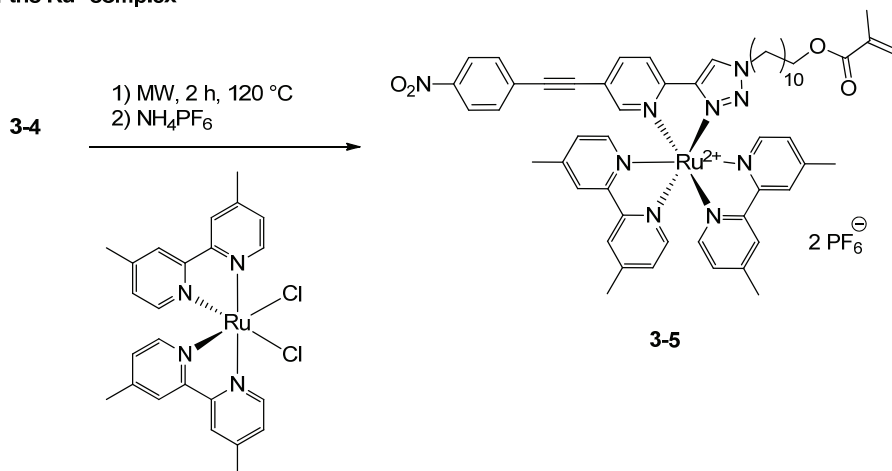
Scheme 3–2. Schematic representation of the synthesis of the polymerizable acceptor-type ruthenium(II) complex **3-5**.
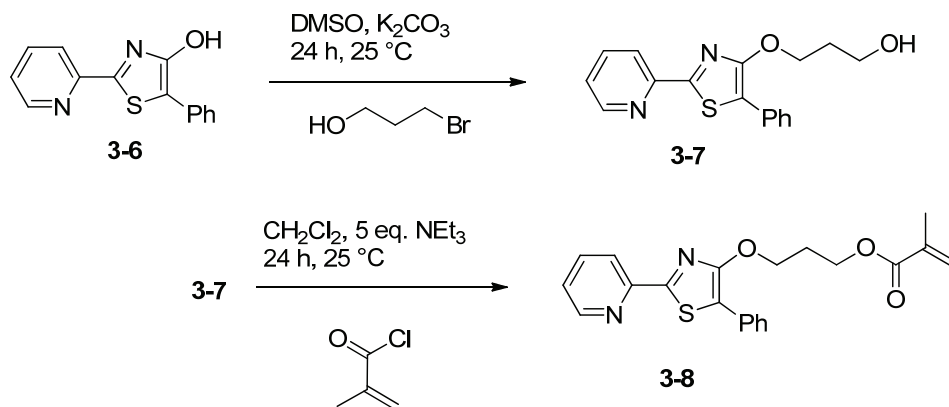
Scheme 3–3. Schematic representation of the synthesis of the polymerizable donor-type thiazole ligand **3-8**.

3-9a: n = 3, m = 87, p = 0
3-9b: n = 0, m = 84, p = 6
3-9c: n = 7, m = 108, p = 12
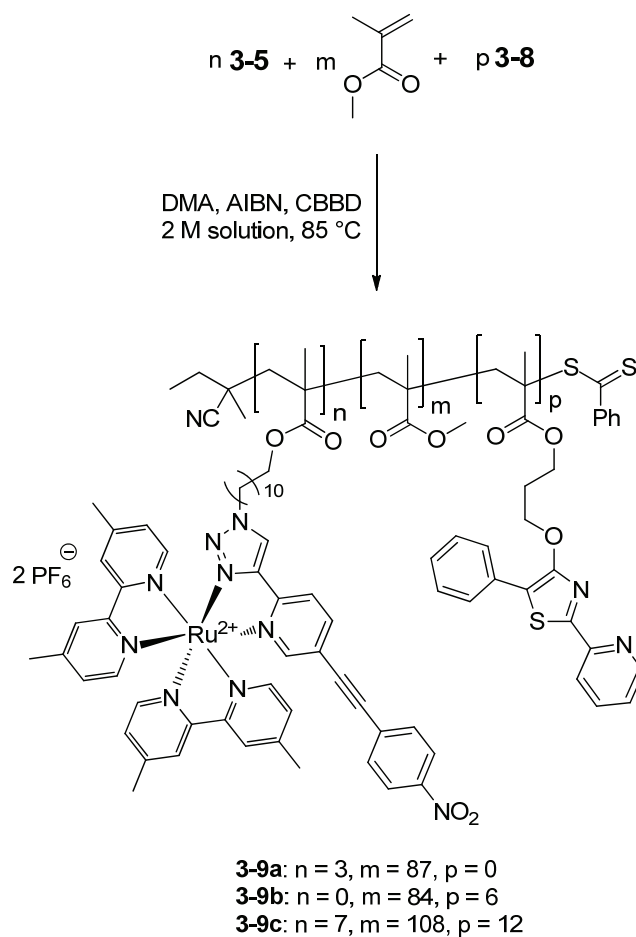
Scheme 3–4. Schematic representation of the synthesis of the statistical copolymers **3-9**.

Because of the insolubility of **3-5** in commonly utilized solvents for radical polymerization processes (*i.e.* toluene, ethanol) the RAFT polymerizations were

performed in DMA. After the reaction, **3-9b** was precipitated into cold diethyl ether yielding the desired donor-type copolymer. The polymers **3-9a,c** were further purified by preparative SEC due to remaining monomer **3-5**. It was found after optimization of the reaction conditions that initiation of the polymerization only occurred if the molar content of **3-5** did not exceed 5 mol%. This observation was attributed to the retardation nature of the NO_2 group.[88] Consequently, the ruthenium(II) content of the terpolymer **3-9c** was kept below 5 mol% to ensure sufficient initiation probability of the reaction.

In order to verify a potential energy transfer in polymer **3-9c**, firstly, excitation spectra were recorded of the donor-type polymer **3-9b**, the acceptor-type polymer **3-9a** and the donor–acceptor polymer **3-9c** (Figure 3–1a). For recording the luminescence excitation spectra of the Ru^{II} subunit the emission was monitored at 620 nm, where no donor fluorescence appeared. A difference in the luminescence excitation spectra of **3-9a** and **3-9c** indicated contributions from the thiazole excitation to the luminescence of the ruthenium(II) unit as it can be seen in the increase of intensity around 380 nm for **3-9c**. These findings point toward an energy transfer, since the excitation of the donor between 325 and 425 nm led to amplified luminescence of the acceptor (Figure 3–1a, red line).

Time-resolved measurements of the donor emission lifetime in **3-9b** and **3-9c** revealed that the donor emission decayed more rapidly in the presence of the Ru^{II} acceptor, since the interaction between the donor and the acceptor quenches the donor emission (Figure 3–1b). Based on temporal emission profiles the FRET efficiency was calculated to be 70%. Although there are many possibilities for excitation quenching in polymers, for instance energy migration, exciton–exciton annihilation,[89] and excimer formation,[90] it was assumed that this shortening of the donor decay time in the donor–acceptor polymer is dominated by FRET by comparing the results to analogous work.[91-93] Mostly, these events cause a reduction of the emission quantum yield and a non-exponential emission decay. Neither of these effects were observed in the reference polymer **3-9b** probably caused by the low concentration of donor units in the polymer backbone. Additionally, Figure 3–1b shows a non-exponential decay trace of the donor emission in presence of acceptor units in the terpolymer because no fixed donor–acceptor distances exist within the polymer. Consequently, different energy transfer rates for individual donor–acceptor pairs occur leading to different decay rates for individual photo-excited donors.
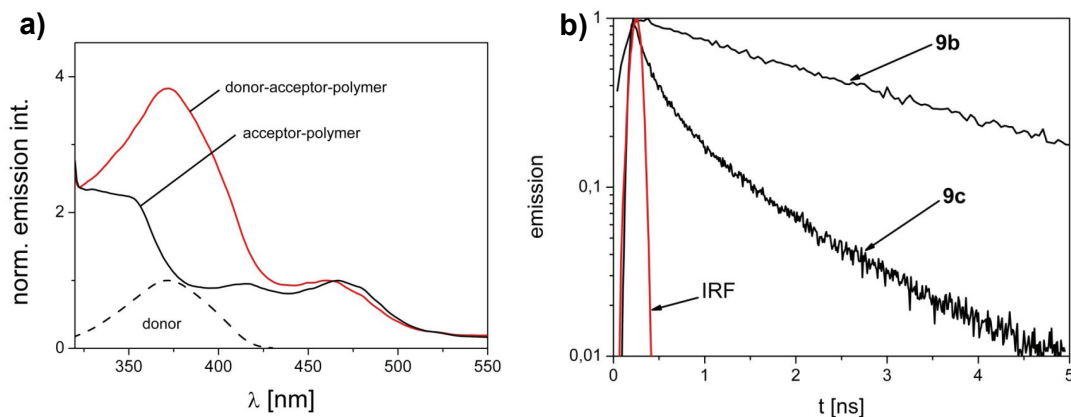
Figure 3–1. a) Excitation spectra (in CH_2Cl_2, 25 °C) of **3-9c** (red) and **3-9a** (black) recorded at the Ru^{II} complex luminescence (620 nm). The fluorescence excitation spectrum of **3-9b** recorded at 450 nm (dashed) was normalized to the maximum emission intensity. b) Donor decay profile (in CH_2Cl_2, 25 °C) of the reference polymer **3-9b** and the donor–acceptor polymer **3-9c** excited at 290 nm. The instrument response function (IRF) was measured by scattered light.

Secondly, the excitation of the thiazole unit in polymer **3-9c** evoked a reduction of the donor-based emission quantum yield by one order of magnitude compared to that of **3-9b** (see Publication A4, Table 3 for details). The quantum yield measurement in the donor–acceptor polymer **3-9c** required adequate care due to the overlap of donor and acceptor absorption bands (Figure 3–1a). It was impossible to excite donor molecules within the terpolymer exclusively. Taking into account these overlapping absorptions, the molar extinction coefficients of donor and acceptor at the excitation wavelength had to be considered as well as the ratio of donor and acceptor units attached to the polymer chain. Considering these properties, the quantum yield measurement in **3-9c** followed the same procedure as the emission quantum yield measurements of **3-8** and **3-9b**.

The description of the energy transfer process (donor quenching in the donor–acceptor polymer) would be incomplete when considering Förster's theory only. Dexter-type energy transfer can also occur at donor–acceptor distances smaller than 10 Å, when donor emission and acceptor absorption spectrally overlap and, furthermore, an overlap of wavefunctions exists so that electrons of the donor and the acceptor, respectively, can occupy the other's molecular orbitals.[94]

Above all, translational diffusion can cause an enhancement of the FRET efficiency at considerable high diffusion coefficients of an individual donor–acceptor pair, which is mainly ruled by the viscosity of the used solvent and the intrinsic viscosity of the donor

and acceptor.[95-96] However, this effect can be neglected due to the static donors and acceptors within the polymer.

Regardless of a possibly incomplete description of the excitation energy transfer only by FRET, the donor−acceptor polymers designed for efficient FRET allow enhanced light harvesting in a Ru[II] complex, whereupon energy is focused into the [1]MLCT band. By considering the charge-separating character of the MLCT states, this process increased the accessibility of Ru[II] complexes as primary electron donors in photocatalytic systems.

In summary, polymers containing a 1,3-thiazole dye (energy donor) and a ruthenium(II) chromophore (energy acceptor) were synthesized using a controlled RAFT polymerization procedure. A terpolymer, which consists of an energy donor and acceptor, was able to relay the absorbed energy by resonance energy transfer from the thiazole donor to the ruthenium(II) acceptor unit. The ruthenium(II) content in the macromolecules was limited to 5 mol% at the most, since for higher metal content the polymerization could not be initiated. The donor−acceptor functionalized terpolymer displayed a reasonable energy transfer efficiency of over 70%. Such polymeric systems might be used for the synthesis of artificial photosynthetic systems, in which they can act as light-harvesting antenna.

4 Self-assembly by d¹⁰-configurated metal ions

N-Heterocyclic polytopic ligand scaffolds can be used as driving force for the formation of polynuclear self-assembled grid-based aggregates. The desired molecular architecture strongly depends on the specific ligand design and, thereby, encodes definite coordination information. The crucial element of ligand design is the establishment of a specific number of coordination pockets with particular donor atom arrangements that match to the employed metal ions and coordination sphere, respectively. This includes the atom identity, the constitution of the atoms, and their orientation, so that a metal is easily adjusted into a ligand pocket. Ideally, the metal ion possesses elementary coordination geometries (tetrahedral, octahedral) with a coordination number of 4 and 6, respectively, and predefines the complexation mode of the ligand. The number and configuration of the coordinating pockets of the ligand then fix the number and environment of the metal ions in the resulting supramolecular assembly. Two-dimensional [n×n] grid-like coordination complexes have a well-defined 2D disposition with an exact number of ligands and metal ions. A ligand with n coordination pockets generates a homoleptic [n×n] assembly, which is composed of 2n organic ligands and n^2 metal ions. The formation of the grid-aggregate is accompanied by the competition of other types of structures, *e.g.* coordination oligomers and polymers, whereby the distinct grid-like array is preferred by entropic factors and further stabilization by non-covalent interactions (hydrogen bonding, π-π stacking).[97-99]

Basically, five- and six-membered chelating rings enable relatively strong coordinative bonds based on favorable bite angles. Those ligands based on nitrogen donor atoms are by far the most extensively studied class, as 3,6-di(2-pyridyl)pyridazines (dppn) and its derivatives are a well-studied class of compounds with respect to polynuclear coordination assemblies including self-assembled grids,[98, 100-102] metallocryptand cages,[103-104] and helices.[105-106] The nitrogen atoms afford versatile coordination sites and their attachment to a variety of metal centers, *e.g.* Cu^I, Zn^{II}, Ni^{II}, and Ag^I ions, triggered investigations of the resulting photophysical, magnetic, and electrochemical properties.[105, 107-108] However, the synthetic access is limited for the

dppn systems, as they can only be synthesized indirectly by an inverse electron-demand Diels-Alder reaction between 1,2,4,5-tetrazines and acetylenes, whereby the 1,2,4,5-tetrazine acts as the electron-deficient diene.[109] In the last decade, several groups have shown that the 1*H*-1,2,3-triazole ring has the potential to replace pyridine as a nitrogen-donor ligand for transition-metal ion complexation.[110-113] As a consequence, dppn-analogous structures were synthesized by replacing the pyridine rings with 1,2,3-triazole rings, while maintaining the ditopic scaffold. The direct synthesis of the 3,6-*bis*(1*H*-1,2,3-triazol-4-yl)pyridazine system (dtpn) was accomplished by starting with the ethynylation of 3,6-dibromopyridazine followed by the CuAAC (Scheme 4–1).

3,6-*bis*(2-pyridyl)pyridazine   **3,6-*bis*(4-triazolyl)pyridazine**
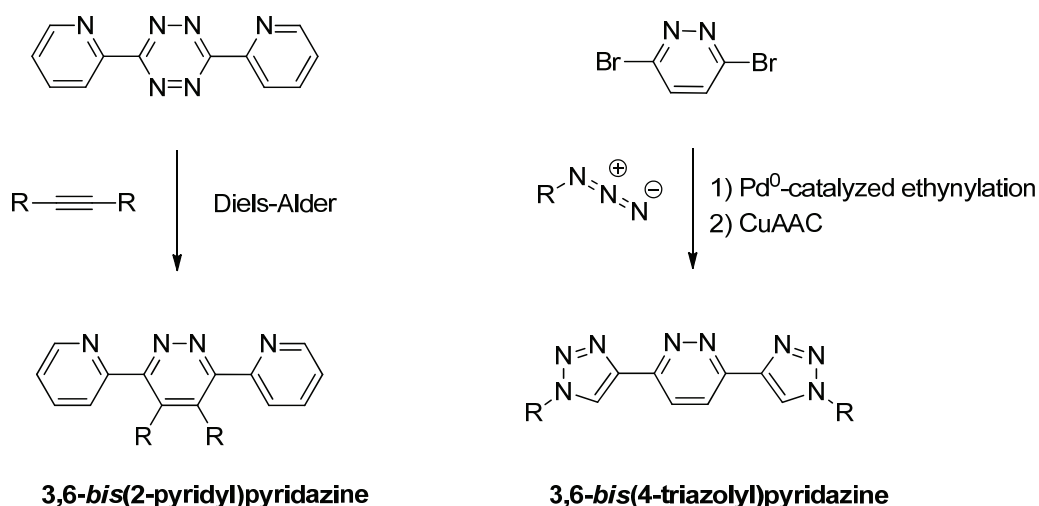
Scheme 4–1. Schematic representation of the structural analogy and general synthesis of 2-pyridyl and 4-triazolyl pyridazines, respectively.

By utilizing the CuAAC as the final step, the substitution of the triazole ring could be controlled. The following study contains the synthesis and characterization of dtpn systems bearing an aromatic and a polymeric moiety. These organic ligands have the capability to complex d[10]-configurated transition-metal ions, such as Cu[I] and Ag[I], expecting the formation of a [2×2] grid-like structure (Scheme 4–2). The verification of the structure of the metal complexes was examined by 1D and 2D NMR spectroscopy, high-resolution ESI-TOF mass spectrometry as well as analytical ultracentrifugation experiments.

4-4: Cuᴵ complex
4-5: Agᴵ complex
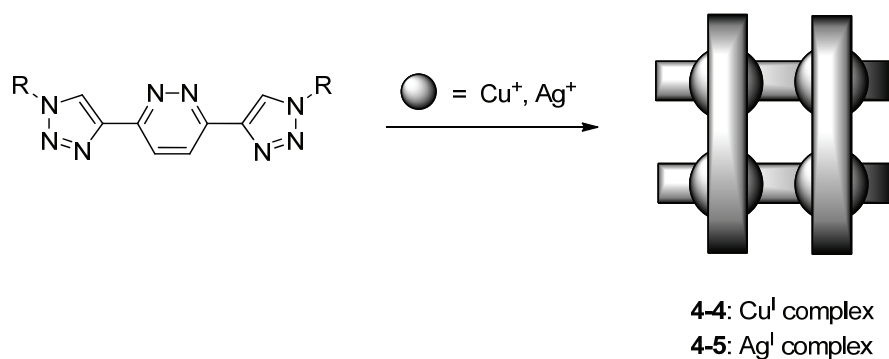
Scheme 4–2. Schematic representation of the expected self-assembly of 3,6-*bis*(1*H*-1,2,3-triazol-4-yl)pyridazines using copper(I) and silver(I) ions.

The synthesis of the ditopic ligands **4-2** and **4-3** is outlined in Scheme 4–3. Maleic hydrazide was brominated to 3,6-dibromopyridazine and subsequent Sonogashira cross-coupling as well as deprotection of the TMS-group with potassium fluoride provided the desired intermediate **4-1** in moderate yield. The following CuAAC reaction of **4-1** with mesitylazide, utilizing copper(II) sulphate and sodium ascorbate as copper(I) source, yielded the desired product **4-2** in a one-pot reaction. Consequently, the dtpn system **4-3** was synthesized by *in situ* deprotection of the TMS-groups and subsequent CuAAC reaction with the monodisperse *O*-(2-Azidoethyl)-*O'*-methyl-undecaethylene glycol, which yielded the final product **4-3** bearing an oligomeric moiety.

4-1

4-2: R = ---- 45%

4-3: R = ---- 49%
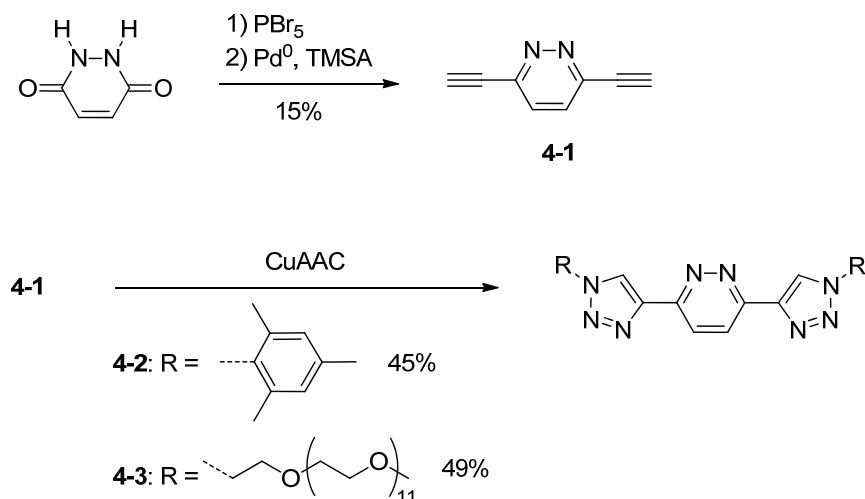
Scheme 4–3. Schematic representation of the synthesis of 3,6-*bis*(4-triazolyl)pyridazines **4-2** and **4-3**.

NMR spectroscopy was used to retrieve first information about the complexation. The ^{1}H NMR spectrum for the obtained grids **4-4** and **4-5** revealed three aromatic signals, which expresses a high symmetry of the formed complexes. The proton signals of the pyridazine ring and the triazole ring of **4-4** were significantly downfield shifted upon complexation compared to the free ligand, which is a confirmation of successful complexation. The appearance of three definite aromatic proton singlets indicates the formation of defined grid-like architectures rather than polymeric species. UV/vis spectra in methanol were recorded for **4-4** and a new absorption maximum arose at 380 nm upon complexation with copper(I) ions. The dilution of the UV/vis solution by two orders of magnitude resulted in a successive decrease in the molar extinction coefficient at 380 nm, which was attributed to a metastable nature of **4-4** in solution. The instability was investigated in more detail by ^{1}H NMR spectroscopy.

In order to gain further confirmation of the integrity of the supramolecular structure of the metal complexes **4-4** and **4-5**, analytical ultracentrifugation experiments were carried out in solution. Figure 4–1 represents the comparison of the differential distribution of the initial ligand **4-2** and the supramolecular systems *versus* the intrinsic sedimentation coefficient. Sedimentation velocity experiments of **4-4** and **4-5** in acetone clearly showed single species in solution (Figure 4–1) and illustrate that the assembly of the initial ligand with metal ions occurred. The distributions were normalized on the values of the maximal peak ordinates. By estimation, the obtained values were close to the theoretical ones of the [2×2] Cu[I] and [2×2] Ag[I] grid-like structure.
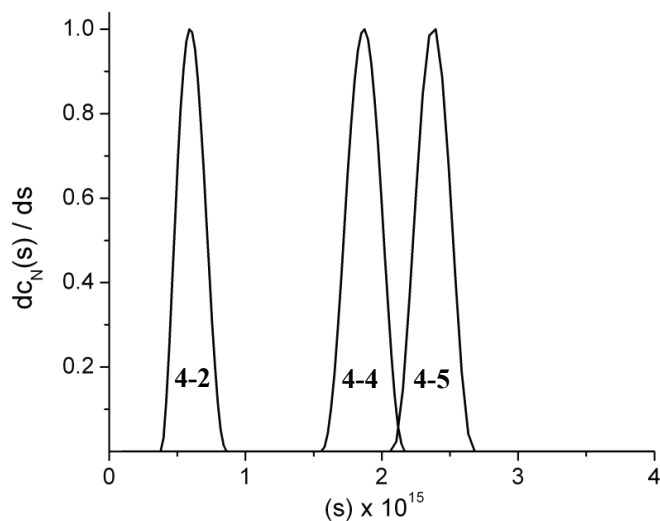
Figure 4–1. Normalized differential distributions dc(s)/ds of sedimentation coefficients obtained with a regularization procedure and a confidence level of 0.90.

Time-dependant 1D (^{1}H) and 2D (^{1}H-NOESY) NMR spectroscopy was used to gain more insight into the metastable solution behavior in solution of copper(I) complex **4-4**. The ^{1}H NOESY spectrum of **4-4** in deuterated acetone, which was recorded after one day standing in the NMR glass tube, is depicted in Figure 4–2. A correlation between the pyrimidine ring proton C and the triazole ring proton B indicates the successful complexation with copper(I) ions. A second correlation arose between proton B and a broadened signal next to it at 8.72 ppm. The latter correlation suggests the presence of at least one more copper(I) complex species.
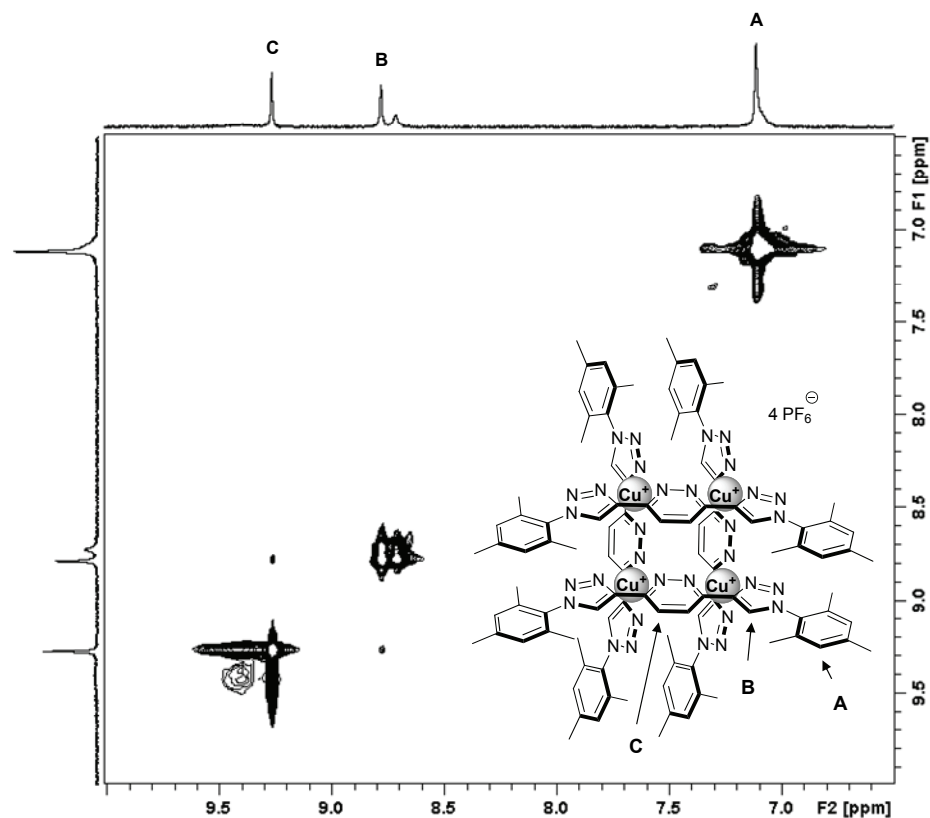
Figure 4–2. ^{1}H NOESY spectrum (400 MHz, 25 °C, (CD$_3$)$_2$CO) of copper(I) complex **4-4** after one day.

Figure 4–3 displays seven ^{1}H NMR spectra of **4-4** (compare Figure 4–2 for the assignment of the protons of the top spectrum), which have been recorded within a period of two and a half weeks. After 17 days, the three primary signals had completely vanished and three broadened signals were mainly present. The ^{1}H NMR spectrum did not transform anymore at this stage. This leads to the conclusion that the initial red material is only metastable in acetone solution. The new species formed are assumed to be

symmetrical copper(I) complexes, as the symmetry in the ^{1}H NMR spectrum is retained similar to the former spectrum and the NMR solution was still orange-colored after 17 days.
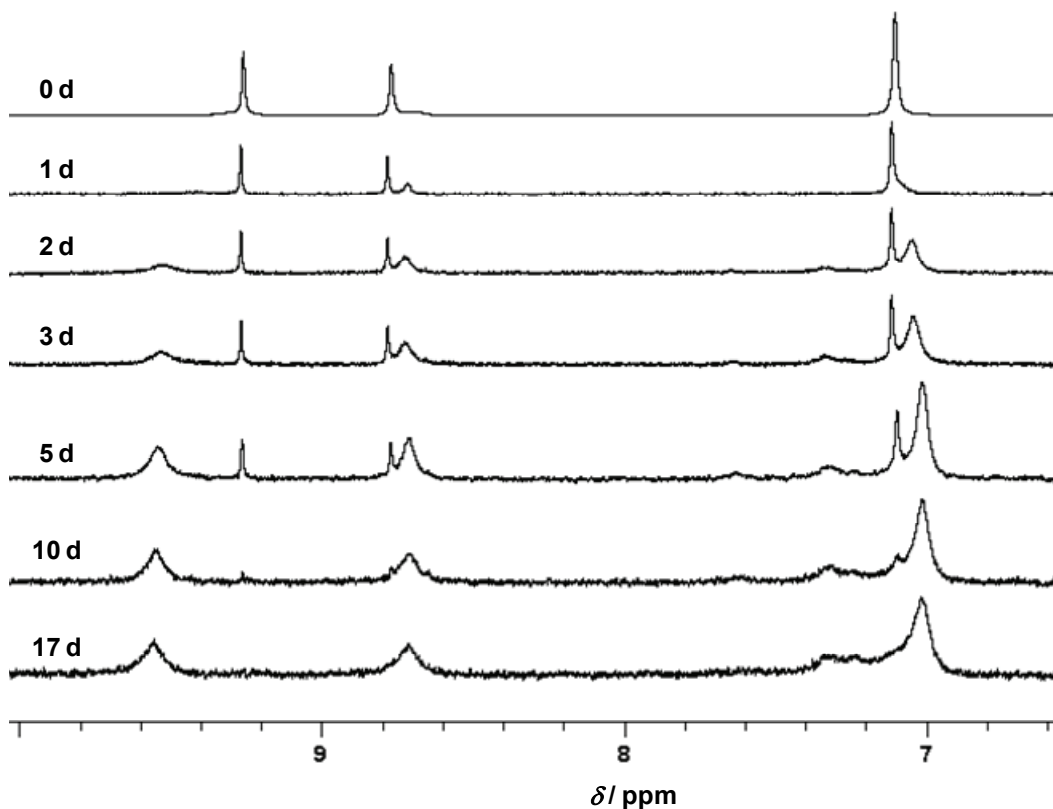
Figure 4–3. ^{1}H NMR spectra (250 MHz, $(CD_3)_2CO$) of copper(I) complex **4-4** followed over time.

Furthermore, ligand **4-3** was coordinated to copper(I) ions by adding its dichloromethane solution (1 equiv.) to a solution of $[Cu(CH_3CN)_4]PF_6$ (1 equiv.). The pure, oily product was obtained after purification by using preparative size-exclusion chromatography. ESI-QToF-MS spectrometry was used to clarify the structure of the latter purified compound and the mass spectrum revealed the existence of the complete [2×2] copper(I) grids (Figure 4–4). Peaks corresponding to fragments with four copper centers, such as $[Cu_4L_4X_2]^{2+}$ and $[Cu_4L_4X]^{3+}$ (X = PF_6^-), were observed. The isotopic pattern is accurately consistent with the simulated one and HR-ESI mass spectrometry further confirmed the stoichiometry of the fragments. Moreover, the long-term durability of the absorption maximum of 380 nm as well as the aromatic proton NMR signals demonstrated the structural stability in contrast to **4-4**. In the case of **4-4** and **4-5**, the ESI-

QToF-MS spectra did not reveal signals of the entire grid. Fragments corresponding to the successive loss of one bar of the presupposed [2×2]-grid structure were observed, namely, $[Cu_2L_3X]^+$ (X = PF_6^-) and $[Ag_2L_3X]^+$ (X = SbF_6^-) as well as $[Cu_2L_2X]^+$ (X = PF_6^-) and $[Ag_2L_2X]^+$ (X = SbF_6^-), respectively.
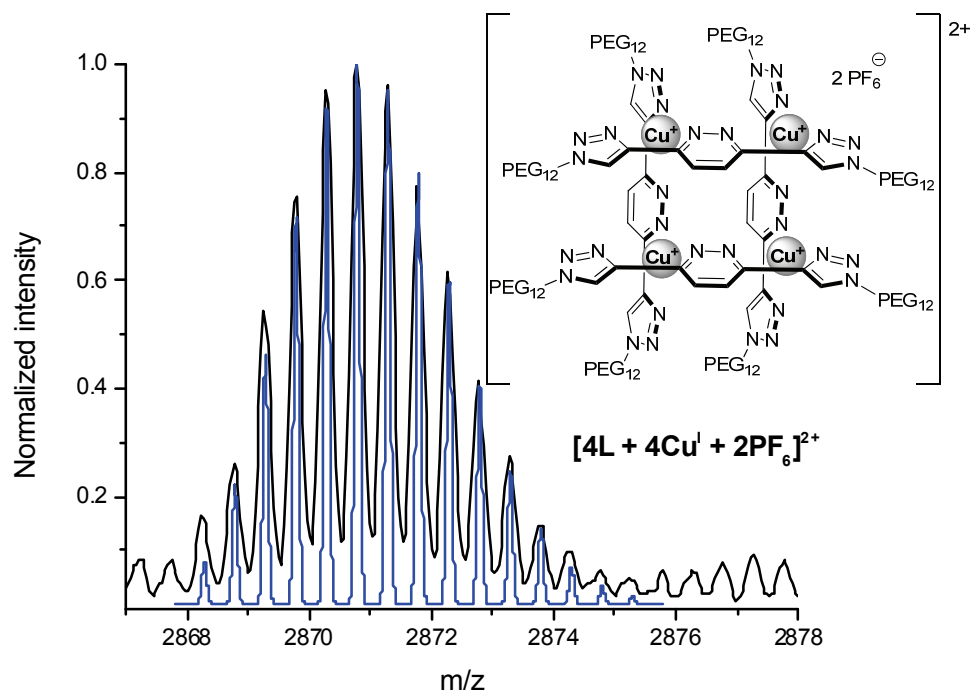
Figure 4–4. ESI-QToF-MS spectrum of the purified copper(I) complex of ligand **4-3** (black) superimposed with the calculated spectrum (blue) indicating the existence of a [2x2] grid-like species.

In summary, the synthesis of 3,6-bis(1*H*-1,2,3-triazol-4-yl)pyridazine systems was described using the Pd[0]-catalyzed Sonogashira coupling as well as the CuAAC reaction. The ditopic *N*-heterocyclic ligands **4-2** and **4-3** were investigated with respect to their complexation capability of singly charged d^{10} metal ions (copper and silver). In this context, ¹H NMR spectroscopy and ESI-QToF-MS of the copper(I) complex of ligand **4-3** indicated the existence of a stable [2×2] grid-like structure. The copper complex **4-4** turned out to be metastable in solution as confirmed by time-dependant 1D (¹H) and 2D (¹H-NOESY) NMR spectroscopy experiments. The latter experiments suggested the presence of at least one more copper(I) complex species.

5 Crosslinking assay of trzpy-based copolymers

More than three decades ago, the pioneering work amongst others by Charles U. Pittman and Charles E. Carraher has evoked a particular approach in current polymer chemistry that is phasing covalent linked polymer species with non-covalent interactions in order to establish new polymeric systems.[114-116] For this purpose, supramolecular polymers containing reversible metal-ligand interactions have been widely studied with plenty of applications that range from catalysis to light-emitting devices to sensory materials.[117] Metal-containing polymers (MCP) are macromolecules usually comprising dynamic metal–ligand coordination units. They can be classified in three categories: (i) linear, one-dimensional macromolecules that may aggregate into higher dimensional nano-sized structures, (ii) three-dimensional networks that possess ordered structures and are usually insoluble, and (iii) three-dimensional networks that are able to incorporate external components, *e.g.* hydrogels. MCPs reveal advantageous features including the capability to transfer magnetic, optical, electronic and catalytic properties of the metal complex into a polymer. Second, the weaker coordinative bond enables reversibility in the design of materials that can be triggered by an external impact, such as pH changes, solvents, light and mechanical forces. The latter feature has channeled the research to the development of advanced materials with addressable properties enclosing switchable adhesives and self-healing materials.[9, 118-120]

The following section describes the complexation and decomplexation behavior of trzpy-containing copolymers by Fe^{II} and Co^{II} ions. The macromolecules were treated with Fe^{II} and Co^{II} salts and the coordination performance was studied by means of UV/vis spectroscopy and titration experiments. Viscosity measurements and detailed analytical ultracentrifugation experiments were executed to study the intra- and intermolecular complexation behavior of the Co^{II} ion in solution. A strong competitive ligand was used to examine the reversibility of the metal complexation in low concentrated solutions by means of UV/vis spectroscopy.

The CuAAC of 2-ethynylpyridine and 11-azidoundecan-1-ol provided the alcohol-functionalized trzpy ligand **5-1**, which was subsequently esterified in good yield (87%) with methacryloyl chloride to monomer **5-2** (Scheme 5–1). The RAFT radical

copolymerization was performed to incorporate the bidentate ligand **5-2** covalently into two different polymer backbones, whereby MMA and BMA were used as comonomers. The RAFT polymerization technique was utilized due to its tolerance to a great number of functional groups. The polymerizations were performed in concentrated solutions (~2 M) to assure a controlled proceeding of the reaction. 2-Cyanobutan-2-yl benzodithioate (CBBD) was utilized as RAFT agent, since it is known to provide a narrow molar mass distribution and AIBN has been applied as initiator.[121] A reaction time of 16 h was chosen in order to drive the conversion of the reaction to approximately 80%. The obtained copolymers **5-3** and **5-4** were purified by preparative SEC and characterized by ^{1}H NMR spectroscopy, UV/vis titration experiments as well as SEC. The SEC coupled with a photodiode array detector revealed a typical UV/vis absorption spectrum of the *N*-heterocyclic trzpy ligand (λ_{max} = 286 nm), which confirmed the incorporation into the backbone of copolymers **5-3** and **5-4** (Figure 5–1). The molar masses were estimated by SEC using a linear PMMA calibration and the molar fraction (x) of trzpy-ligands was determined by both ^{1}H NMR spectroscopy and UV/vis titration experiments. The molar fraction did not significantly deviate from the theoretical values and both characterization techniques revealed comparable results.
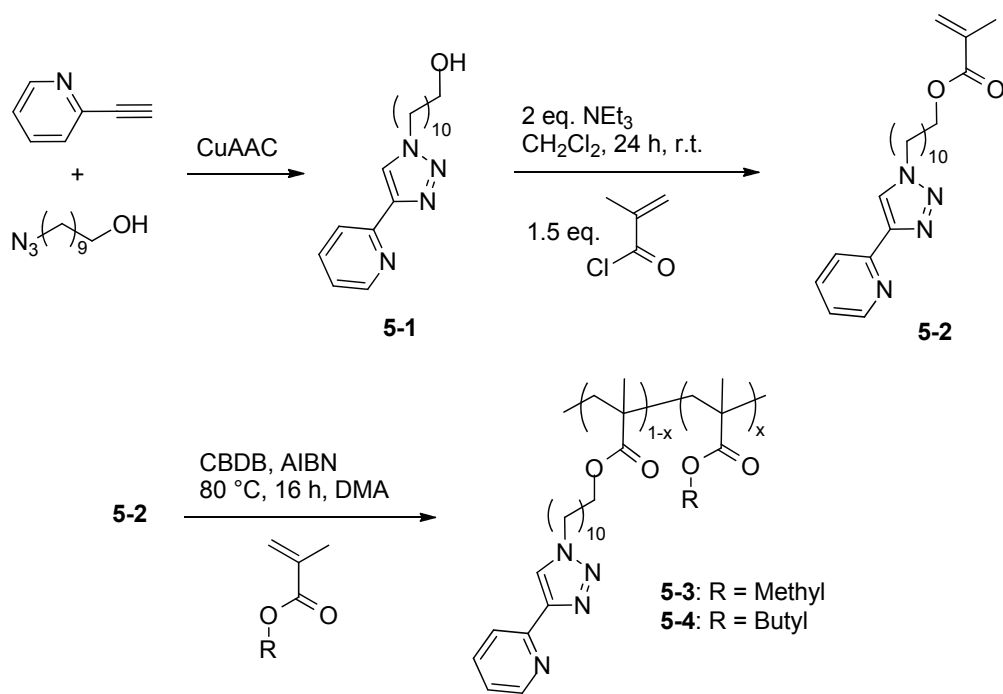
Scheme 5–1. Schematic representation of the synthesis of macromolecules **5-3** and **5-4**.
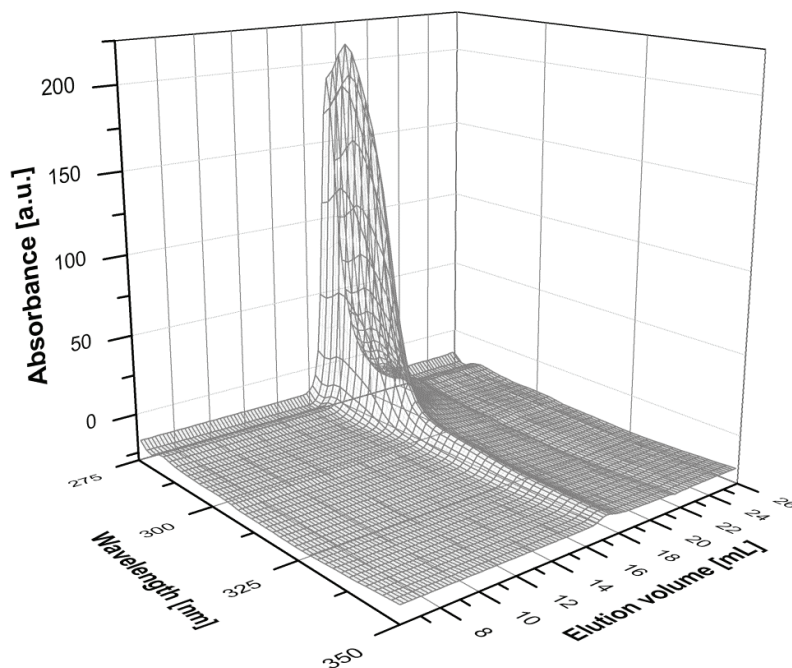
Figure 5–1. SEC coupled with a photodiode array detector of the purified copolymer **5-4** (eluent: DMA with 0.08% NH_4PF_6).

In a preliminary experiment, a concentrated dichloromethane solution of copolymers **5-3** or **5-4** (c > 10 mg·mL^{-1}) was prepared and subjected to gelation *via* metal coordination using a methanolic Fe^{II} or Co^{II} solution. In the case of Fe^{II}, a red solid was obtained upon cross-linking each with three trzpy units. The crosslinking procedure with Co^{II} ions led to a highly viscous solution, which was fluid yet. The reversibility of the crosslinking was examined by UV/vis spectroscopy experiments utilizing a strong competitive chelating agent (Scheme 5–2). At first, a UV/vis absorption spectrum of a dichloromethane solution of copolymer **5-3** was measured as a blank. The absorption spectrum exhibited a maximum at 286 nm, which can be assigned to electronic transitions of the trzpy moiety of the copolymer. Subsequently, the appropriate amount of metal salt, as methanolic Fe^{II} or Co^{II} solution, was added to obtain a ligand-to-metal stoichiometry of 3 : 1. The UV/vis spectrum was remeasured and the appearance of the MLCT bands at 433 nm (Fe^{II} *tris*-homoleptic complex) and 320 nm (Co^{II} *tris*-homoleptic complex), respectively, verified the complexation of the bidentate ligands by the metal ions (Figure 5–2). The subsequent addition of 10 equivalents of a methanolic HEEDTA solution led to a vanishing of the MLCT absorption bands for both metal ions upon decomplexation.
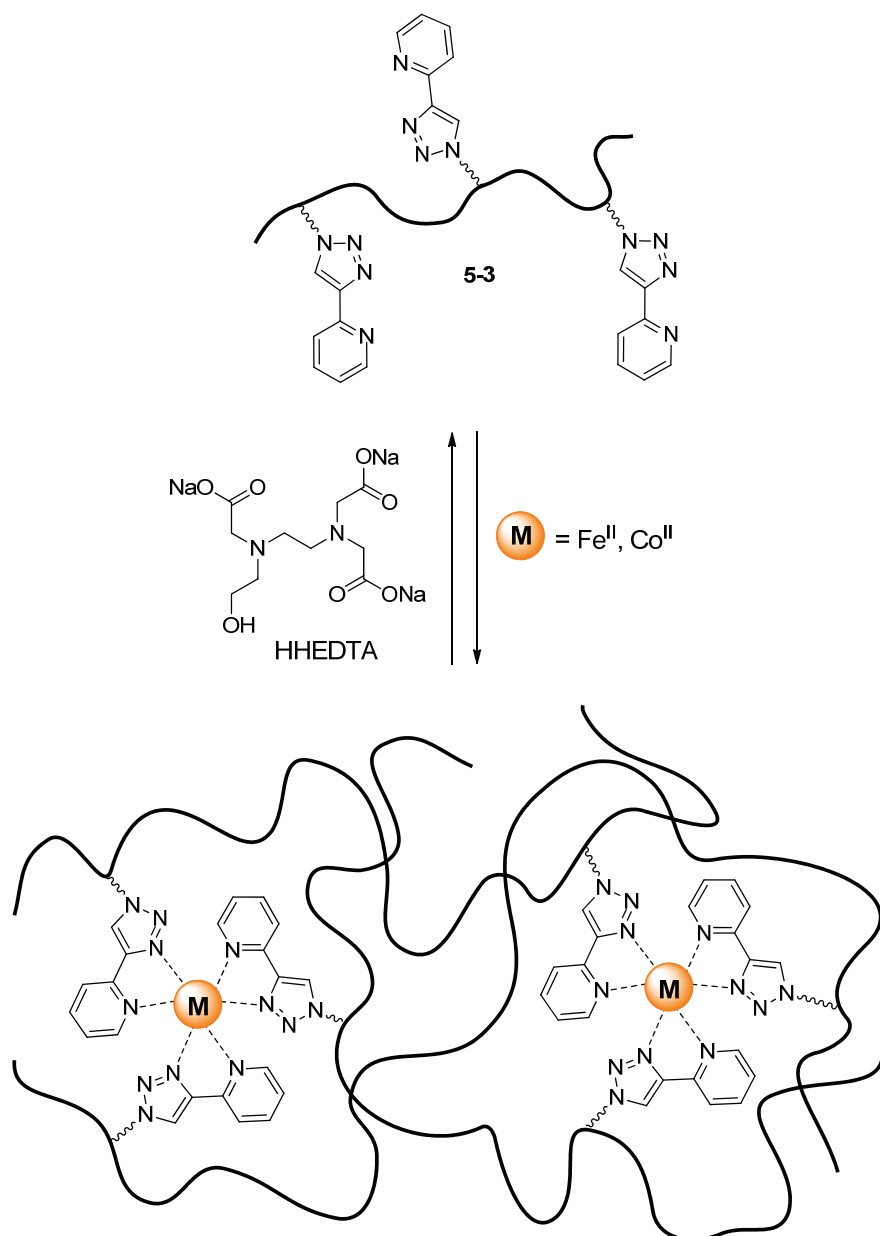
Scheme 5–2. Complexation of the copolymers with Fe^{II} and Co^{II} ions and decomplexation with HEEDTA.

In order to gain detailed insights into the crosslinking process and the metal complexation, respectively, viscosity titration experiments at different concentrations of copolymer **5-4** and Co^{II} ions were performed in acetone. Fe^{II} as metal ion could not be investigated by this method, since the acetone solution of iron(II) chloride was not stable yielding an off-white precipitate after a few minutes. The $Co(BF_4)_2 \times 6\ H_2O$ salt was dissolved in acetone and added in stepwise portions to a solution of the polymer with known concentration (c_{poly}^{init}).
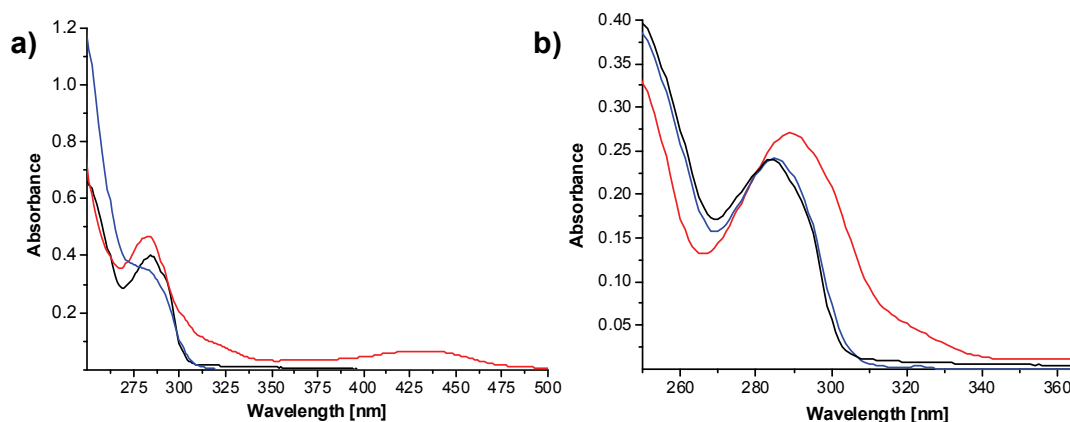
Figure 5–2. a) UV/vis spectra (solvent: CH_2Cl_2) of the blank copolymer **5-3** (black), complexation with Fe^{II} ions (red) and decomplexation with methanolic HEEDTA solution (blue). b) UV/vis spectra (solvent: CH_2Cl_2) of the blank copolymer **5-3** (black), complexation with Co^{II} ions (red) and decomplexation with methanolic HEEDTA solution (blue).

The dynamic viscosity (η) was measured after each step and after the addition of the metal salt the final solutions were shaken for a sufficient time to enable homogenization. The polymer concentration was kept constant by the addition of the corresponding amount of the polymer solution with the concentration $c = 2 \cdot c_{poly}^{init}$. The results of this study are presented in Figure 5–3. The dynamic viscosity of the solutions containing the Co^{II} salts strongly depended on the initial polymer concentration. For concentrated solutions, where the degree of dilution (product of intrinsic viscosity of the polymer and its concentration ($[\eta] \cdot c$)) was higher than 0.5 (50% of the volume is occupied by macromolecules), an exponential increase of the dynamic viscosity value was observed with increasing Co^{II} concentration. For $[\eta] \cdot c \approx 0.8$ the dynamic viscosity value increased approximately 20-fold compared to the initial one at a molar cobalt(II) concentration of $c(Co^{II}) = 3.66$ mM (Figure 5–3, line 1). When the degree of dilution was low ($[\eta] \cdot c \leq 0.25$) the dynamic viscosity value increased only about three times and after further addition of Co^{II} ions a declining tendency of the η value was observed. The remarkable large increase of the dynamic viscosity in a concentrated copolymer solution with increasing Co^{II} concentration was attributed to the formation of crosslinked structures (intermolecular complexation) in which Co^{II} metal ions are linked to several different copolymer chains. The average molar mass of a crosslinked macromolecule can be estimated from the dynamic viscosity value.
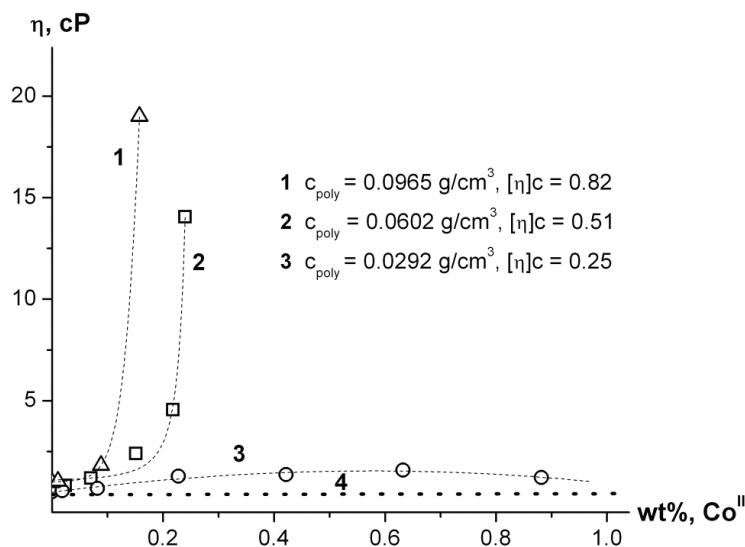
Figure 5–3. Dynamic viscosity of the acetone solutions of **5-4** in dependence on the weight fraction (wt.%) of $Co(BF_4)_2 \times 6 H_2O$. The dotted line 4 corresponds to the polymer solutions without the cobalt(II) salt.

It is known that the dynamic viscosity of various polymer-solvent systems at high concentrations above some critical molar mass (M_{cr}) is related to the molar mass by the equation $\eta = K_h \cdot M_w^{3.4}$.[122] Below M_{cr}, the value of the dynamic viscosity is directly proportional to the molar mass. Considering the latter two extremes the following estimation was obtained for the solute with $c_{poly} = 0.096$ g·cm^{-3} and $c(Co^{II}) = 3.66$ mM: $70 < M_w \times 10^{-3}$ g·mol$^{-1} < 500$. Along the intermolecular crosslinking also intramolecular complexation occurred at a higher degree of dilution (Figure 5–3, line 3).

The intramolecular complexation of such kind of copolymers with multivalent ions may be observed and studied in the regime of very dilute solutions. The velocity sedimentation of the solutions with the polymer concentration c = (0.070 ± 0.005) × 10^{-2} g·cm^{-3} was studied as function of the concentration of the $Co(BF_4)_2 \times 6 H_2O$ salt. This polymer concentration corresponds to a very high degree of dilution of 0.006, where only 0.6% of the solution volume is occupied by macromolecules. Hence, the macromolecules are separated by the distance larger than their hydrodynamic size and the information obtained at this condition virtually concern the properties of individual macromolecules.

When the solution of the $Co(BF_4)_2 \times 6 H_2O$ salt is added into a diluted polymer solution first a significant decrease of the velocity sedimentation coefficient was observed (Figure 5–4a, region 1). This experimental fact can be explained by an increase of the

proportion of Co^{II} ions bound to ligands of the polymeric chain. This leads to an increase of the number of electrical charges on individual macromolecules and, consequently, allows the raise of the translational friction coefficient due to the additional friction losses resulting from the electrostatic expansion of the chains and from the electrostatic interactions between distant macromolecules (Figure 5–5). The increase in the translational friction coefficient f results in a decrease in the velocity sedimentation coefficient, as s ~ $M_w \cdot f^{-1}$. In the range of a Co^{II} salt concentration of 0.2 mM the minimum of the velocity sedimentation coefficient was observed. The argument to prove that the decrease of the velocity sedimentation coefficient is related with the charge effect of the coordinated Co^{II} ions was supported by the addition of a one-to-one ion salt NH_4PF_6 (0.05 M) to the cobalt-containing solution. The velocity sedimentation coefficients take values close to that obtained for pure acetone without Co^{II} salt (Figure 5–4b).
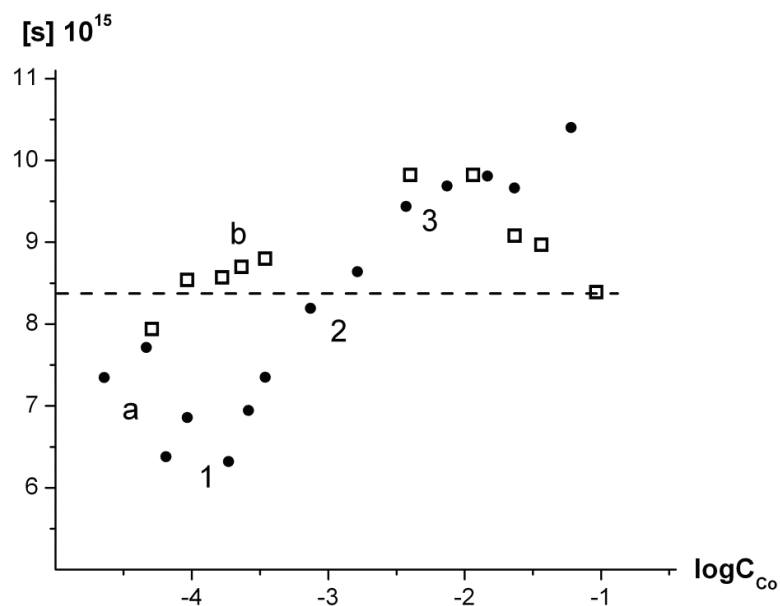
Figure 5–4. Dependence of the intrinsic velocity sedimentation coefficient measured for the copolymer **5-4** ($c_{poly} = 7 \times 10^{-4}$ g·cm^{-3} in acetone) on different molar concentrations of cobalt salt without (●) and with 0.05 M NH_4PF_6 (□) using a semi logarithmic scale.

After reaching a minimum, the value of the velocity sedimentation coefficient begins to increase as a function of the concentration of cobalt salt. Presumably, in this case the main effect is the screening of charges on the polymer chains by additional charges appearing in solution and a large part of the new added ions are not bound by the polymer chains anymore.
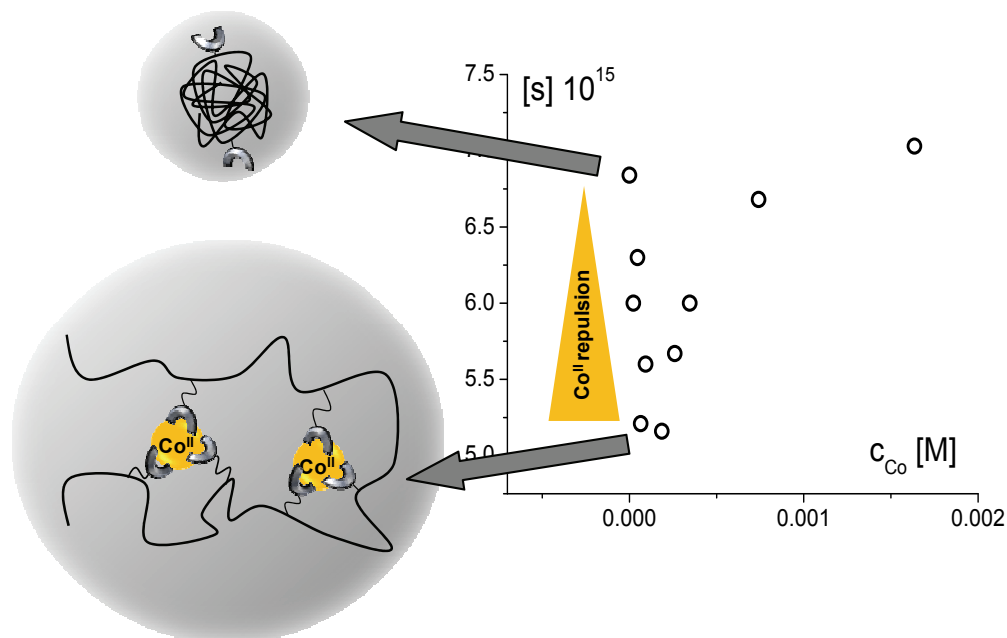
Figure 5–5. Enlargement of region 1 of the previous Figure which reveals a significant decrease in the velocity sedimentation coefficient upon metal complexation of copolymer **5-4**.

In summary, the copolymers were investigated towards their gelation properties against Fe^{II} and Co^{II} ions on a molecular level. Both metal salts showed a crosslinking ability in concentrated solution ($c > 10$ mg·mL^{-1}), whereby in the case of cobalt a highly viscous fluid was observed. The differentiation between intermolecular and intramolecular complexation, respectively, was achieved by viscosity titration experiments at different concentrations of the copolymer in acetone using Co^{II} ions. In concentrated solutions, *i.e.* with a degree of dilution higher than 0.5 of the polymer, intermolecular complexation of the Co^{II} ion with different macromolecule chains was deduced from the latter experiments. The complexes were destroyed during the dilution of the solutions. The intramolecular complexation with Co^{II} ions was studied in highly diluted acetone solution of the trzpy-containing copolymer by means of different analytical ultracentrifuge experiments. The addition of a small amount of Co^{II} ions resulted in a significant decrease of the intrinsic sedimentation coefficient, which could be related to the elongation of the individual polymer coils upon the electrostatic repulsion of the coordinated Co^{II} ions.

6 Summary

This thesis compiles construction, metal coordination chemistry and macromolecular chemistry of 2-(1*H*-1,2,3-triazol-4-yl)pyridine (trzpy) ligands (Scheme 6–1). The regioselective copper(I)-catalyzed 1,3-dipolar cycloaddition between organic azides and terminal alkynes (CuAAC) represented the key step for the preparation of the trzpy-based chelators. The use of the triazole entity provided a facile access to bidentate chelates that can be regarded as analogs to 2,2´-bipyridines. Using the CuAAC as a synthetic tool enabled a convenient functionalization of the trzpy ligands: Reactive functional groups can be directly introduced by designing the organic azide and allow subsequent chemical transformations, such as the application of radical polymerization methods. Furthermore, the CuAAC is able to support the introduction of additional functional moieties at the triazole (providing solubility, introducing substituents) due to its high tolerance to a wide range of reaction conditions and to a large independence on the electronic configuration of the deployed reactants.
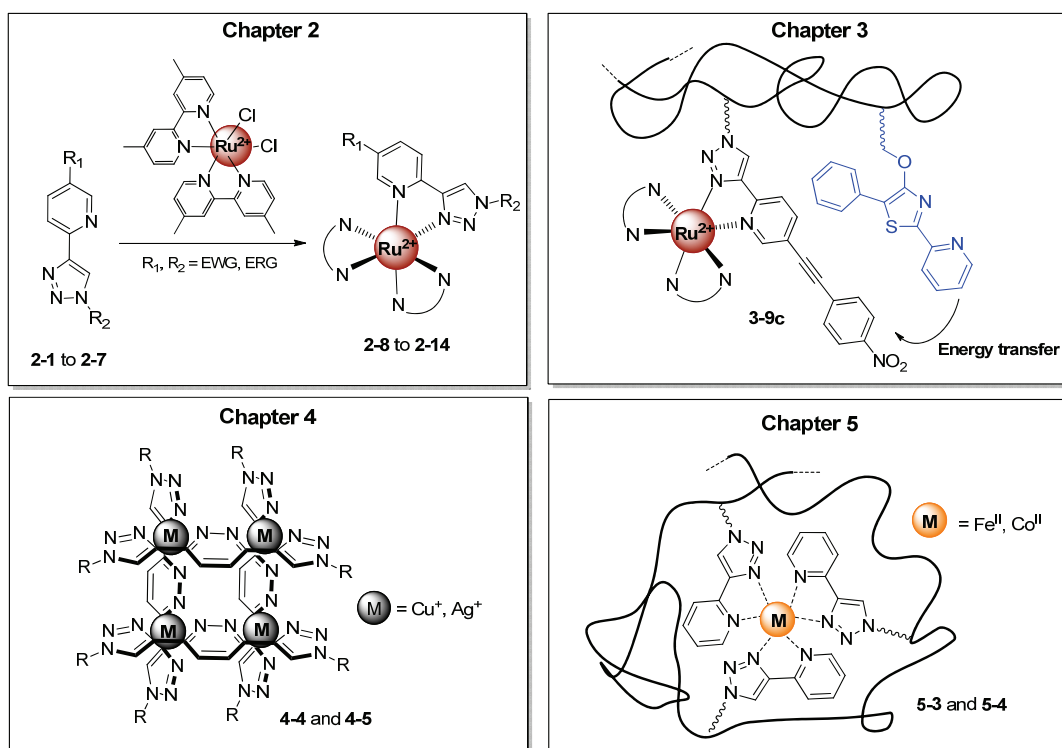
Scheme 6–1. Schematic representation of the chemistry of 2-(1*H*-1,2,3-triazol-4-yl)pyridine ligands.

It reconsiders the synthesis of trzpy ligands bearing different donor- and acceptor-type phenylacetylene moieties on the 5-position of the pyridine unit and their coordination to ruthenium(II) metal ions using $Ru(dmbpy)_2Cl_2$ as precursor. The various substituents of the phenylacetylene moieties showed a crucial influence on the photophysical properties of the ligands and their corresponding ruthenium(II) complexes. The donor or acceptor capability of the trzpy ligands determined the emission quantum yield of the resulting Ru^{II} complexes significantly, whereby the highest quantum yield was found for the Ru^{II} complex that has a nitro group attached in *para*-position of the phenylacetylene subunit. DFT ground state calculations for the donor-type ruthenium complex exhibited a π-localized HOMO on the trzpy entity unlike the acceptor-type complex possessing a t_{2g}-localized HOMO on the central Ru^{II} atom. Consequently, the HOMO–LUMO transition upon light excitation has considerable LLCT character in the case of the donor-type complex. Above all, radiative rate constants (k_r) were calculated using a mixed TD-DFT/CASSCF approach for both complexes explaining the observed drop of the luminescence quantum yield for the donor-type complex.

The reversible addition-fragmentation transfer (RAFT) copolymerization of a 1,3-thiazole dye (energy donor) and a trzpy-based Ru^{II} chromophore (energy acceptor) was highlighted with respect to the ability to transfer energy from the donor to the acceptor. It turned out during the synthesis of donor- and acceptor-alone copolymers that only a maximum content of 5 mol% of the $[Ru(dmbpy)_2(trzpy)]^{2+}$ chromophore could be embedded into the macromolecules caused by its nitro-functionalization. Several photophysical measurements (excitation spectra, lifetime) suggested successful relay of the absorbed energy by Förster resonance energy transfer (FRET) from the thiazole donor to the Ru^{II} acceptor. The donor–acceptor functionalized terpolymer displayed a reasonable energy transfer efficiency of over 70% and will therefore be practical to act as light-harvesting antennas.

The synthesis of two 3,6-*bis*(R-1*H*-1,2,3-triazol-4-yl)pyridazine systems (R = mesityl, monodisperse –$(CH_2-CH_2O)_{12}CH_3$) was carried out using a combination of Pd^0-catalyzed Sonogashira coupling and the CuAAC. The ditopic N-heterocyclic ligands were investigated with respect to their complexation capability of singly charged d^{10} metal ions (Cu^I and Ag^I). The obtained copper(I) complexes were thoroughly characterized by time-dependent 1D [^1H, ^{13}C] and 2D [^1H NOESY] NMR spectroscopy, elemental analysis, HR ESI-ToF mass spectrometry, and analytical ultracentrifugation. The latter characterization

methods indicated the formation of a self-assembled supramolecular [2×2] grid in the case of the oligomeric PEG-functionalized ligand. The mesityl-functionalized ligand yielded a red-colored Cu^I complex, which turned out to be metastable in solution. This behavior was studied by ^1H NMR spectroscopy in acetone solution over two weeks and the experiments verified the irreversible transformation of the Cu^I complex into at least one different copper complex species.

The synthesis of trzpy-containing copolymers and the subsequent characterization was described after complexation with Fe^{II} and Co^{II} ions. The reversibility of the resulting crosslinking process was demonstrated by UV/vis spectroscopy experiments utilizing a strong competitive ligand. A differentiation between intermolecular and intramolecular complexation, respectively, was achieved by viscosity titration experiments at different concentrations of the copolymer in acetone using Co^{II} ions. The intramolecular complexation with Co^{II} ions was studied in highly diluted acetone solution of the trzpy-containing copolymer by means of different analytical ultracentrifuge experiments. The addition of Co^{II} ions led to a significant decrease of the intrinsic sedimentation coefficient, which can be explained by the elongation of individual polymer coils upon the electrostatic repulsion of coordinated Co^{II} ions.

This thesis highlights the versatility of trzpy ligands. Beyond basic investigations of this topic it would be interesting to explore potential applied properties in subsequent research activities. In particular, the further development of the polymer-based donor−acceptor light-harvesting unit might be a promising scope with respect to the light-induced water-splitting.

7 Zusammenfassung

Diese Arbeit beschäftigt sich mit der Synthese, Koordinationschemie und der makromolekularen Chemie von substituierten 2-(1*H*-1,2,3-Triazol-4-yl)Pyridin (trzpy) Liganden (Scheme 7–1). Die entscheidende Reaktion zur Synthese dieser Liganden war die regioselektive Kupfer(I)-katalysierte 1,3-dipolare Cycloaddition (CuAAC) zwischen organischen Aziden und terminalen Alkinen. Diese Art von Liganden stellen ein Pendant zu 2,2´-Bipyridinen dar, jedoch ermöglicht die Verwendung des Triazolrings einen bequemeren synthetischen Zugang. Zusätzlich konnten die zweizähnigen Chelatoren – unter Zuhilfenahme der CuAAC – einfach durch die Variation des Azids funktionalisiert werden. Durch ein gezieltes Design des Azides können verschiedenste funktionelle Gruppen eingeführt werden, die anschließend weitere chemische Umsetzungen zulassen (Polymerisationen etc.) oder intrinsische Eigenschaften, wie z.B. Löslichkeit, entscheidend beeinflussen. Darüber hinaus toleriert die CuAAC ein sehr breites Spektrum an Edukten und gelingt in vielen Fällen unabhängig von den Reaktionsbedingungen sowie den elektronischen Konfigurationen der Reaktanden.
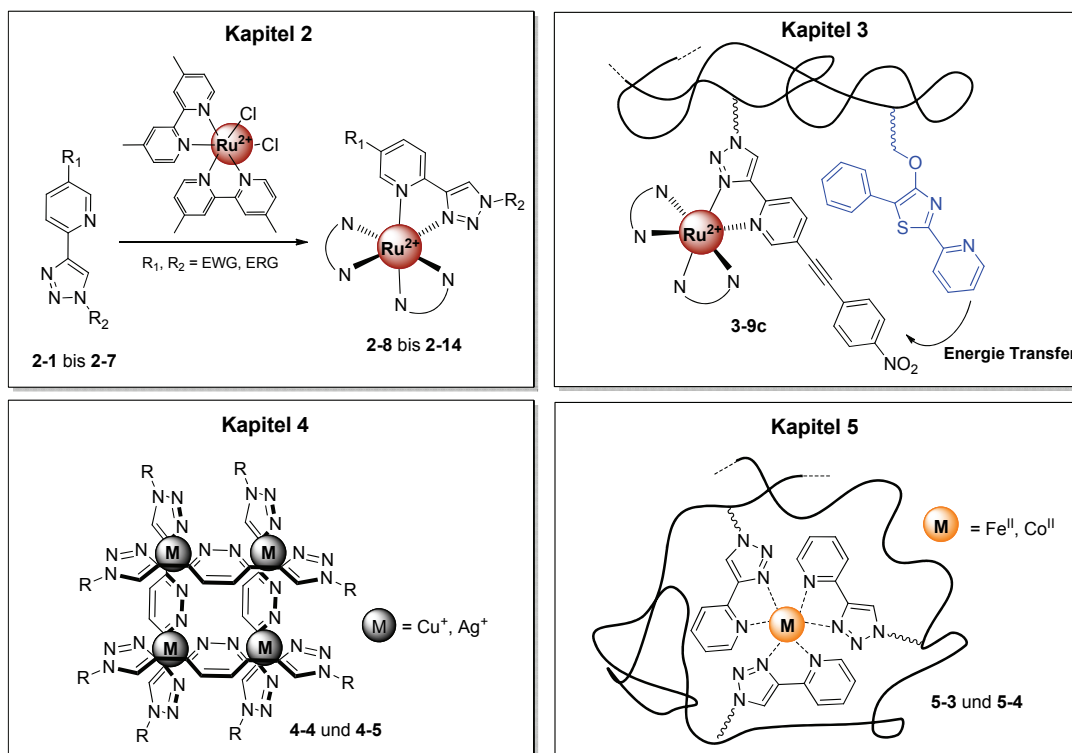
Scheme 7–1. Die Chemie der 2-(1*H*-1,2,3-Triazol-4-yl)Pyridin Liganden.

Zunächst wird die Synthese von trzpy Systemen und die anschließende Koordination an Ru^{II} Ionen mit Hilfe des Ru(dmbpy)$_2$Cl$_2$ Precursors erörtert, wobei Donor- und Akzeptor-basierte Phenylacetyleneinheiten an der 5-Position des Pyridinrings angebracht wurden. Dabei stellte sich heraus, dass diese Substituenten einen entscheidenden Einfluss auf die photophysikalischen Eigenschaften der Liganden und Metallkomplexe haben. Insbesondere die Lumineszenzquantenausbeuten der Rutheniumkomplexe hingen stark von der Elektronenkonfiguration der Substituenten ab. Der Rutheniumkomplex, der mit einer Nitro-Gruppe an der Phenylacetyleneinheit in *para*-Position funktionalisiert war, besaß die größte Lumineszenzquantenausbeute. In Folge dessen wurden DFT Berechnungen im Grundzustand und zeitabhängige DFT Berechnungen stellvertretend für einen Donor- und einen Akzeptor-basierten Rutheniumkomplex durchgeführt. Dabei zeigten die Grundzustandsberechnungen des Donor-basierten Rutheniumkomplexes, dass das HOMO am trzpy Liganden lokalisiert ist, während sich das HOMO der Akzeptor-basierten Koordinationsverbindung eher am Ruthenium befindet. Infolgedessen besitzt die langwelligste Absorptionsbande (HOMO–LUMO Übergang) des ersteren Komplexes einen erheblichen LLCT Charakter. Weiterhin haben zeitabhängige DFT/CASSCF Berechnungen dazu beigetragen, radiative Geschwindigkeitskonstanten beider Komplexe zu berechnen und so die erhebliche Auswirkung der Substituenten auf die Emissionsquantenausbeute zu erklären.

Darüber hinaus beschäftigt sich diese Arbeit mit der kontrollierten RAFT Copolymerisation eines 1,3-Thiazol-Farbstoffs (Donor) und eines trzpy-funktionalisierten Rutheniumkomplexes (Akzeptor) um den gerichteten Energietransfer vom Donor zum Akzeptor zu studieren. Jedoch fungierte der Rutheniumkomplex auf Grund seiner NO$_2$-Funktionalisierung während der Polymerisation als Inhibitor. Folglich musste für eine erfolgreiche Copolymerisation ein Anteil kleiner als 5 mol% verwendet werden. Verschiedene photophysikalische Messungen (Anregungsspektren, Lebenszeit) haben gezeigt, dass das Donor–Akzeptor Terpolymer in der Lage ist, Energie über einen Förster-Mechanismus mit einer Effizienz von ca. 70% vom Donor hin zum Akzeptor zu transportieren.

Des Weiteren wird die Synthese von 3,6-*bis*(R-1*H*-1,2,3-Triazol-4-yl)pyridazinen (R = Mesityl, monodisperses –(CH$_2$–CH$_2$O)$_{12}$CH$_3$), die als ditopische Liganden zur Komplexierung von d^{10}-konfigurierten Metallen (Cu^I und Ag^I) verwendet wurden, beschrieben. Die so erhaltenen Kupferkomplexe wurden bezüglich der Selbstorganisation

zu [2×2] Gitterstrukturen mittels zeitabhängiger 1D [^{1}H, ^{13}C] und 2D [^{1}H-NOESY] NMR- und analytischer Ultrazentrifugations-Messungen sowie HR ESI-ToF Massenspektrometrie detailliert charakterisiert. Letztere Methoden verifizierten die Bildung eines stabilen [2×2] Gitters im Falle des oligomeren Ethylenglykol-funktionalisierten Liganden. ^{1}H NMR Messungen über zwei Wochen zeigten, dass der mehrkernige Kupferkomplex des Mesityl-funktionalisierten Liganden in Aceton metastabil ist und sich irreversibel in mindestens eine neue Kupferspezies umwandelt.

Die Synthese von trzpy-basierten Copolymeren und deren Charakterisierung wurde nach der Komplexierung mit Fe^{II} bzw. Co^{II} Ionen untersucht. Die reversible Vernetzung unter Zuhilfenahme eines starken Chelatliganden konnte mittels UV/vis Spektroskopie nachgewiesen werden. Darüber hinaus wurde ein Copolymer bei verschiedenen Konzentrationen mit Co^{II} Ionen titriert. Anschließende Viskositätsmessungen ermöglichten eine Differenzierung zwischen intermolekularer und intramolekularer Komplexierung. Außerdem wurde der Einfluss der Co^{II} Ionen auf die Konformation des Copolymers in hochverdünnter Lösung untersucht. Eine geringe Zugabe an Metallionen führte zu einer Ausdehnung des Polymerknäuels, welche durch die elektrostatische Abstoßung der koordinierten Metallionen verursacht wurde.

Diese Arbeit belegt die vielfältigen Einsatzmöglichkeiten von trzpy Liganden. In weiterführenden Arbeiten dieses Themengebietes wäre es unter anderem interessant, neben der Grundlagenforschung auch anwendungsbezogene Eigenschaften dieser Ligandensysteme zu untersuchen. Insbesondere die Weiterentwicklung der polymerbasierten Donor−Akzeptor Lichtsammeleinheit könnte im Hinblick auf die lichtgetriebene Wasserspaltung ein vielversprechendes Anwendungsfeld sein.

8 References

[1]   J.-M. Lehn, *Supramolecular Chemistry, Concepts and Perspectives*, Wiley-VCH, **1995**.

[2]   J.-M. Lehn, *Angew. Chem. Int. Ed.* **1988**, *27*, 89–112.

[3]   D. J. Cram, *Angew. Chem. Int. Ed.* **1988**, *27*, 1009–1020.

[4]   U. S. Schubert, G. R. Newkome, I. Manners, *Metal-Containing and Metallosupramolecular Polymers and Materials,* Vol. 928, ACS, Washington D.C., **2006**.

[5]   U. S. Schubert, C. Eschbaumer, *Angew. Chem. Int. Ed.* **2002**, *41*, 2893–2926.

[6]   G. R. Newkome, E. He, C. N. Moorefield, *Chem. Rev.* **1999**, *99*, 1689–1746.

[7]   G. R. Whittell, I. Manners, *Adv. Mater.* **2007**, *19*, 3439–3468.

[8]   I. Manners, *Synthetic Metal-Containing Polymers*, Wiley-VCH, Weinheim, **2004**.

[9]   G. R. Whittell, M. D. Hager, U. S. Schubert, I. Manners, *Nat. Mater.* **2011**, *10*, 176–188.

[10]   M. Kirch, J.-M. Lehn, J.-P. Sauvage, *Helv. Chim. Acta* **1979**, *62*, 1345–1384.

[11]   V. Balzani, A. Juris, M. Venturi, S. Campagna, S. Serroni, *Chem. Rev.* **1996**, *96*, 759–833.

[12]   K. Kalyanasundaram, M. Grätzel, *Coord. Chem. Rev.* **1998**, *177*, 347–414.

[13]   D. Astruc, *Organometallic Chemistry and Catalysis*, Springer-Verlag, New York, **2007**.

[14]   S. Diez-Gonzalez, N. Marion, S. P. Nolan, *Chem. Rev.* **2009**, *109*, 3612–3676.

[15]   J. N. Demas, B. A. DeGraff, *Coord. Chem. Rev.* **2001**, *211*, 317–351.

[16]   Q. Zhao, F. Li, C. Huang, *Chem. Soc. Rev.* **2010**, *39*.

[17]   V. Balzani, G. Bergamini, S. Campagna, F. Puntoriero, in *Photochemistry and Photophysics of Coordination Compounds I,* Vol. 280 (Eds.: V. Balzani, S. Campagna), Springer-Verlag, Berlin, **2007**, pp. 1–36.

[18]   S. Campagna, F. Puntoriero, F. Nastasi, G. Bergamini, V. Balzani, in *Photochemistry and Photophysics of Coordination Compounds I,* Vol. 280 (Eds.: V. Balzani, S. Campagna), Springer-Verlag, Berlin, **2007**, pp. 117–214.

[19]   L. Flamigni, A. Barbieri, C. Sabatini, B. Ventura, F. Barigelletti, in *Photochemistry and Photophysics of Coordination Compounds II,* Vol. 281 (Eds.: V. Balzani, S. Campagna), Springer-Verlag, Berlin, **2007**, pp. 143–203.

[20]   R. A. Kirgan, B. P. Sullivan, D. P. Rillema, in *Photochemistry and Photophysics of Coordination Compounds II,* Vol. 281 (Eds.: V. Balzani, S. Campagna), Springer-Verlag, Berlin, **2007**, pp. 45–100.

[21]   D. Kumaresan, K. Shankar, S. Vaidya, R. H. Schmehl, in *Photochemistry and Photophysics of Coordination Compounds II,* Vol. 281 (Eds.: V. Balzani, S. Campagna), Springer-Verlag, Berlin, **2007**, pp. 101–142.

[22]   X.-Y. Wang, A. Del Guerzo, R. H. Schmehl, *J. Photochem. Photobiol. C: Photochem. Rev.* **2004**, *5*, 55–77.

[23]   G. B. Porter, *J. Chem. Educ.* **1983**, *60*, 785–790.

[24]   G. A. Crosby, *J. Chem. Educ.* **1983**, *60*, 791–796.

[25]   A. W. Adamson, *J. Chem. Educ.* **1983**, *60*, 797–802.

[26]   J. N. Demas, *J. Chem. Educ.* **1983**, *60*, 803–808.

[27]   N. Sutin, C. Creutz, *J. Chem. Educ.* **1983**, *60*, 809–813.

[28]   F. Scandola, V. Balzani, *J. Chem. Educ.* **1983**, *60*, 814–823.

[29]   J. F. Endicott, *J. Chem. Educ.* **1983**, *60*, 824–828.

[30] H. C. Kolb, M. G. Finn, K. B. Sharpless, *Angew. Chem. Int. Ed.* **2001**, *40*, 2004–2021.

[31] V. V. Rostovtsev, L. G. Green, V. V. Fokin, K. B. Sharpless, *Angew. Chem. Int. Ed.* **2002**, *41*, 2596–2599.

[32] C. W. Tornøe, C. Christensen, M. Meldal, *J. Org. Chem.* **2002**, *67*, 3057–3064.

[33] R. Huisgen, *Angew. Chem. Int. Ed.* **1963**, *2*, 565–598.

[34] F. Himo, T. Lovell, R. Hilgraf, V. V. Rostovtsev, L. Noodleman, K. B. Sharpless, V. V. Fokin, *J. Am. Chem. Soc.* **2005**, *127*, 210–216.

[35] M. Meldal, C. W. Tornøe, *Chem. Rev.* **2008**, *108*, 2952–3015.

[36] W. H. Binder, R. Sachsenhofer, *Macromol. Rapid Commun.* **2007**, *28*, 15–54.

[37] W. H. Binder, R. Sachsenhofer, *Macromol. Rapid Commun.* **2008**, *29*, 952–981.

[38] H. Struthers, T. L. Mindt, R. Schibli, *Dalton Trans.* **2010**, *39*, 675–696.

[39] J. E. Moses, A. D. Moorhouse, *Chem. Soc. Rev.* **2007**, *36*, 1249–1262.

[40] H. Nandivada, X. Jiang, J. Lahann, *Adv. Mater.* **2007**, *19*, 2197–2208.

[41] H. C. Kolb, K. B. Sharpless, *Drug Discov. Today* **2003**, *8*, 1128–1137.

[42] E. M. Sletten, C. R. Bertozzi, *Angew. Chem. Int. Ed.* **2009**, *48*, 6974–6998.

[43] F. Amblard, J. H. Cho, R. F. Schinazi, *Chem. Rev.* **2009**, *109*, 4207–4220.

[44] G. C. Tron, T. Pirali, R. A. Billington, P. L. Canonico, G. Sorba, A. A. Genazzani, *Med. Res. Rev.* **2008**, *28*, 278–308.

[45] J. E. Hein, V. V. Fokin, *Chem. Soc. Rev.* **2010**, *39*, 1302–1315.

[46] B. Eistert, E. Endres, *Justus Liebigs Ann. Chem.* **1970**, *734*, 56–69.

[47] D. Seebach, D. Enders, R. Dach, R. Pieter, *Chem. Ber.* **1977**, *110*, 1879–1886.

[48] J. T. Fletcher, B. J. Bumgarner, N. D. Engels, D. A. Skoglund, *Organometallics* **2008**, *27*, 5430–5433.

[49] C. Richardson, C. M. Fitchett, F. R. Keene, P. J. Steel, *Dalton Trans.* **2008**, 2534–2537.

[50] B. Happ, C. Friebe, A. Winter, M. D. Hager, R. Hoogenboom, U. S. Schubert, *Chem. Asian J.* **2009**, *4*, 154–163.

[51] B. Happ, D. Escudero, M. D. Hager, C. Friebe, A. Winter, H. Görls, E. Altuntas, L. Gonzalez, U. S. Schubert, *J. Org. Chem.* **2010**, *75*, 4025–4038.

[52] M. Juricek, M. Felici, P. Contreras-Carballada, J. Lauko, S. R. Bou, P. H. J. Kouwer, A. M. Brouwer, A. E. Rowan, *J. Mater. Chem.* **2011**, *21*, 2104–2111.

[53] S. Ladouceur, D. Fortin, E. Zysman-Colman, *Inorg. Chem.* **2011**, *50*, 11514–11526.

[54] D. Sykes, M. D. Ward, *Chem. Commun.* **2011**, *47*, 2279–2281.

[55] M. Obata, A. Kitamura, A. Mori, C. Kameyama, J. A. Czaplewska, R. Tanaka, I. Kinoshita, T. Kusumoto, H. Hashimoto, M. Harada, Y. Mikata, T. Funabiki, S. Yano, *Dalton Trans.* **2008**, 3292–3300.

[56] A. Boulay, A. Seridi, C. Zedde, S. Ladeira, C. Picard, L. Maron, E. Benoist, *Eur. J. Inorg. Chem.* **2010**, *2010*, 5058–5062.

[57] D. Schweinfurth, R. Pattacini, S. Strobel, B. Sarkar, *Dalton Trans.* **2009**, 9291–9297.

[58] D. Schweinfurth, S. Strobel, B. Sarkar, *Inorg. Chim. Acta* **2011**, *374*, 253–260.

[59] K. J. Kilpin, E. L. Gavey, C. J. McAdam, C. B. Anderson, S. J. Lind, C. C. Keep, K. C. Gordon, J. D. Crowley, *Inorg. Chem.* **2011**, *50*, 6334–6346.

[60] O. Fleischel, N. Wu, A. Petitjean, *Chem. Commun.* **2010**, *46*, 8454–8456.

[61] B. Happ, G. M. Pavlov, E. Altuntas, C. Friebe, M. D. Hager, A. Winter, H. Görls, W. Günther, U. S. Schubert, *Chem. Asian J.* **2011**, *6*, 873–880.

[62] J. D. Crowley, P. H. Bandeen, L. R. Hanton, *Polyhedron* **2010**, *29*, 70–83.

[63] J. D. Crowley, P. H. Bandeen, *Dalton Trans.* **2010**, *39*, 612–623.

[64]   M. L. Gower, J. D. Crowley, *Dalton Trans.* **2010**, *39*, 2371–2378.

[65]   T. Romero, R. l. A. Orenes, A. Espinosa, A. Tárraga, P. Molina, *Inorg. Chem.* **2011**, *50*, 8214–8224.

[66]   I. Stengel, A. Mishra, N. Pootrakulchote, S.-J. Moon, S. M. Zakeeruddin, M. Gratzel, P. Bauerle, *J. Mater. Chem.* **2011**, *21*, 3726–3734.

[67]   N. Mourtzis, P. C. Carballada, M. Felici, R. J. M. Nolte, R. M. Williams, L. de Cola, M. C. Feiters, *Phys. Chem. Chem. Phys.* **2011**, *13*, 7903–7909.

[68]   D. Schweinfurth, K. I. Hardcastle, U. H. F. Bunz, *Chem. Commun.* **2008**, 2203–2205.

[69]   R. Lalrempuia, N. D. McDaniel, H. Müller-Bunz, S. Bernhard, M. Albrecht, *Angew. Chem. Int. Ed.* **2010**, *49*, 9765–9768.

[70]   D. Urankar, A. Pevec, I. Turel, J. Košmrlj, *Cryst. Growth Des.* **2010**, *10*, 4920–4927.

[71]   Y. Hua, A. H. Flood, *Chem. Soc. Rev.* **2010**, *39*, 1262–1271.

[72]   Y. Li, A. H. Flood, *Angew. Chem. Int. Ed.* **2008**, *47*, 2649–2652.

[73]   M. G. Fisher, P. A. Gale, J. R. Hiscock, M. B. Hursthouse, M. E. Light, F. P. Schmidtchen, C. C. Tong, *Chem. Commun.* **2009**, 3017–3019.

[74]   O. Schuster, L. Yang, H. G. Raubenheimer, M. Albrecht, *Chem. Rev.* **2009**, *109*, 3445–3478.

[75]   H. Hofmeier, U. S. Schubert, *Chem. Soc. Rev.* **2004**, *33*, 373–399.

[76]   V. Marin, E. Holder, R. Hoogenboom, U. S. Schubert, *Chem. Soc. Rev.* **2007**, *36*, 618–635.

[77]   E. C. Constable, *Chem. Soc. Rev.* **2007**, *36*, 246–253.

[78]   K. Kalyanasundaram, *Coord. Chem. Rev.* **1982**, *46*, 159–244.

[79]   A. Juris, V. Balzani, F. Barigelletti, S. Campagna, P. Belser, A. von Zelewsky, *Coord. Chem. Rev.* **1988**, *84*, 85–277.

[80]   R. J. Watts, *Comments Inorg. Chem.* **1991**, *11*, 303–337.

[81]   D. A. M. Egbe, C. Bader, J. Nowotny, W. Guenther, E. Klemm, *Macromolecules* **2003**, *36*, 5459–5469.

[82]   R. B. Nair, B. M. Cullum, C. J. Murphy, *Inorg. Chem.* **1997**, *36*, 962–965.

[83]   Y. Sun, C. Turro, *Inorg. Chem.* **2010**, *49*, 5025–5032.

[84]   M. Kasha, *Discuss. Faraday Soc.* **1950**, *9*, 14–19.

[85]   M. Sykora, K. A. Maxwell, J. M. DeSimone, T. J. Meyer, *Proc. Natl. Acad. Sci. U.S.A.* **2000**, *97*, 7687–7691.

[86]   U. S. Schubert, A. Winter, G. R. Newkome, *Terpyridine-based Materials*, Wiley-VCH, Weinheim, **2011**.

[87]   C. R. K. Glasson, L. F. Lindoy, G. V. Meehan, *Coord. Chem. Rev.* **2008**, *252*, 940–963.

[88]   G. Odian, in *Principles of Polymerization*, 4th ed., John Wiley & Sons, New Jersey, **2004**, pp. 255–263.

[89]   S. Ozcelik, *J. Phys. Chem. B* **1997**, *5647*, 3021–3024.

[90]   K. P. Ghiggino, T. A. Smith, *Prog. Reaction Kinetics,* **1993**, *18*, 375–436.

[91]   A. Adronov, S. L. Gilat, J. M. J. Frechet, K. Ohta, F. V. R. Neuwahl, G. R. Fleming, *J. Am. Chem. Soc* **2000**, *122*, 1175–1185.

[92]   K. P. Ghiggino, T. a. Smith, D. J. Haines, G. J. Wilson, *Can. J. Chem.* **1995**, *73*, 2015–2020.

[93]   A. Adronov, D. R. Robello, J. M. J. Fréchet, *J. Polym. Sci., Part A: Polym. Chem.* **2001**, *39*, 1366–1373.

[94]   N. J. Turro, V. Ramamurthy, J. C. Scaiano, in *Principles of Molecular Photochemistry*, University Science Books, Sausalito, California, **2009**, pp. 383–479.

[95]   D. D. Thomas, W. F. Carlsen, L. Stryer, *Proc. Natl. Acad. Sci. U.S.A.* **1978**, *75*, 5746–5750.

[96]   J. R. Lakowicz, H. Szmacinski, I. Gryczynski, W. Wiczk, M. L. Johnson, *J. Phys. Chem.* **1990**, *94*, 8413–8416.

[97]   S. De, K. Mahata, M. Schmittel, *Chem. Soc. Rev.* **2010**, *39*, 1555–1575.

[98]   L. K. Thompson, *Coord. Chem. Rev.* **2002**, *233–234*, 193–206.

[99]   E. Pardo, R. Ruiz-Garcia, J. Cano, X. Ottenwaelder, R. Lescouezec, Y. Journaux, F. Lloret, M. Julve, *Dalton Trans.* **2008**, 2780–2805.

[100]   W. Kaim, *Coord. Chem. Rev.* **2002**, *230*, 127–139.

[101]   L. N. Dawe, K. V. Shuvaev, L. K. Thompson, *Chem. Soc. Rev.* **2009**, *38*, 2334–2359.

[102]   M. Ruben, J. Rojo, F. J. Romero-Salguero, L. H. Uppadine, J.-M. Lehn, *Angew. Chem. Int. Ed.* **2004**, *43*, 3644–3662.

[103]   V. J. Catalano, B. L. Bennett, M. A. Malwitz, R. L. Yson, H. M. Kar, S. Muratidis, S. J. Horner, *Comments Inorg. Chem.* **2003**, *24*, 39–68.

[104]   V. J. Catalano, M. A. Malwitz, S. J. Horner, J. Vasquez, *Inorg. Chem.* **2003**, *42*, 2141–2148.

[105]   S. Achelle, N. Ple, A. Turck, *RSC Adv.* **2011**, *1*, 364–388.

[106]   A. N. Khlobystov, A. J. Blake, N. R. Champness, D. A. Lemenovskii, A. G. Majouga, N. V. Zyk, M. Schröder, *Coord. Chem. Rev.* **2001**, *222*, 155–192.

[107]   B. L. Schottel, H. T. Chifotides, M. Shatruk, A. Chouai, L. M. Pérez, J. Bacsa, K. R. Dunbar, *J. Am. Chem. Soc.* **2006**, *128*, 5895–5912.

[108]   M.-T. Youinou, N. Rahmouni, J. Fischer, J. A. Osborn, *Angew. Chem. Int. Ed.* **1992**, *31*, 733–735.

[109]   J. Sauer, in *Comprehensive Heterocyclic Chemistry II,* Vol. 6 (Eds.: R. K. Alan, W. R. Charles, E. F. V. Scriven), Pergamon, Oxford, **1996**, pp. 901–955.

[110]   R. M. Meudtner, M. Ostermeier, R. Goddard, C. Limberg, S. Hecht, *Chem. Eur. J.* **2007**, *13*, 9834–9840.

[111]   Y. Li, J. C. Huffman, A. H. Flood, *Chem. Commun.* **2007**, 2692–2694.

[112]   B. Beyer, C. Ulbricht, D. Escudero, C. Friebe, A. Winter, L. González, U. S. Schubert, *Organometallics* **2009**, *28*, 5478–5488.

[113]   B. Schulze, C. Friebe, M. D. Hager, A. Winter, R. Hoogenboom, H. Görls, U. S. Schubert, *Dalton Trans.* **2009**, 787–794.

[114]   C. E. Carraher, *J. Macromol. Sci., Chem.* **1982**, *A17*, 1293–1356.

[115]   C. U. Pittman, L. R. Smith, R. M. Hanes, *J. Am. Chem. Soc.* **1975**, *97*, 1742–1748.

[116]   C. Pittman, *J. Inorg. Organomet. Polym. Mater.* **2005**, *15*, 33–55.

[117]   A. S. Abd-El-Aziz, I. Manners, *Frontiers in Transition Metal-Containing Polymers*, John Wiley & Sons, New Jersey, **2006**.

[118]   A. W. Bosman, R. Vestberg, A. Heumann, J. M. J. Fréchet, C. J. Hawker, *J. Am. Chem. Soc.* **2002**, *125*, 715–728.

[119]   M. D. Hager, P. Greil, C. Leyens, S. van der Zwaag, U. S. Schubert, *Adv. Mater.* **2010**, *22*, 5424–5430.

[120]   I. Luzinov, S. Minko, V. V. Tsukruk, *Prog. Polym. Sci.* **2004**, *29*, 635–698.

[121]   E. Rizzardo, M. Chen, B. Chong, G. Moad, M. Skidmore, S. H. Thang, *Macromol. Symp.* **2007**, *248*, 104–116.

[122]   R. H. Colby, L. J. Fetters, W. W. Graessley, *Macromolecules* **1987**, *20*, 2226–2237.

Curriculum Vitae

02.05.1984	born in Suhl
1990 – 1994	school education in Benshausen
1994 – 2002	school education in Zella-Mehlis
10/2003 – 08/2008	study of chemistry at the Friedrich-Schiller-Universität Jena
09/2006	"Vordiplom" (equivalence to bachelor)
10/2007 – 06/2008	Diploma thesis at the University of Technology Eindhoven in the group of Prof. Dr. Ulrich S. Schubert
25.08.2008	acquisition of academic degree "Diplom-Chemiker" at the Friedrich-Schiller University Jena (equivalence to M. Sc.)
since 10/2008	scientific coworker at the Friedrich-Schiller University Jena (Institute of Organic Chemistry and Macromolecular Chemistry, group of Prof. Dr. Ulrich S. Schubert)

Jena, den

_____

(Bobby Happ)

Publication list

Refereed publications

1)   Bobby Happ, Christian Friebe, Andreas Winter, Martin D. Hager, Richard Hoogenboom, Ulrich S. Schubert. "2-(1*H*-1,2,3-Triazol-4-yl)-pyridine ligands as alternatives to 2,2´-bipyridines in ruthenium(II) complexes", *Chem. Asian J.* **2009**, *4*, 154−163.

2)   Bobby Happ, Richard Hoogenboom, Andreas Winter, Martin D. Hager, Stefan O. Baumann, Guido Kickelbick, Ulrich S. Schubert. "2-[1-(1-Naphthyl)-1*H*-1,2,3-triazol-4-yl]pyridine", *Acta Cryst.* **2009**, *E65*, o1146.

3)   Bobby Happ, Christian Friebe, Andreas Winter, Martin D. Hager, Ulrich S. Schubert. "Click chemistry meets polymerization: Controlled incorporation of an easily accessible ruthenium(II) complex into a PMMA backbone *via* RAFT copolymerization", *Eur. Polym. J.* **2009**, *45*, 3433−3441.

4)   Bobby Happ, Daniel Escudero, Martin D. Hager, Christian Friebe, Andreas Winter, Helmar Görls, Esra Altuntas, Leticia González, Ulrich S. Schubert. "*N*-Heterocyclic donor- and acceptor-type ligands based on 2-(1*H*-[1,2,3]triazol-4-yl)pyridines and their ruthenium(II) complexes", *J. Org. Chem.* **2010**, *75*, 4025−4038.

5)   Bobby Happ, Johann Schäfer, Roberto Menzel, Martin D. Hager, Andreas Winter, Jürgen Popp, Rainer Beckert, Benjamin Dietzek, Ulrich S. Schubert. "Synthesis and resonance energy transfer study on a random terpolymer containing a 2-(pyridine-2-yl)thiazole donor-type ligand and a luminescent [Ru(bpy)$_2$(2-(triazol-4-yl)pyridine)]$^{2+}$ chromophores", *Macromolecules* **2011**, *44*, 6277−6287.

6)   Bobby Happ, Georges M. Pavlov, Esra Altuntas, Christian Friebe, Martin D. Hager, Andreas Winter, Helmar Görls, Wolfgang Günther, Ulrich S. Schubert. "Self-assembly of 3,6-bis(4-triazolyl)pyridazine ligands with copper(I) and silver(I) ions: Time-dependant 2D-NOESY and ultracentrifuge measurements", *Chem. Asian J.* **2011**, *6*, 873−880.

7)   Daniel Escudero, <u>Bobby Happ</u>, Andreas Winter, Martin D. Hager, Ulrich S. Schubert, Leticia González. "The radiative decay rates tune the emissive properties of Ru(II)polypyridyl complexes. A computational study", *Chem. Asian J.* **2012**, *7*, 667−671.

8)   <u>Bobby Happ</u>, Andreas Winter, Martin D. Hager, Ulrich S. Schubert. "Photogenerated avenues in macromolecules containing Re(I), Ru(II), Os(II), and Ir(III) metal complexes of pyridine-based ligands", *Chem. Soc. Rev.* **2012**, *41*, 2222–2255.

9)   <u>Bobby Happ</u>, Johann Schäfer, Christian Friebe, Helmar Görls, Andreas Winter, Martin D. Hager, Benjamin Dietzek, Jürgen Popp, Ulrich S. Schubert. "Chelating fluorene dyes as mono- and ditopic 2-(1*H*-[1,2,3]-triazol-4-yl)pyridine ligands and their corresponding Ru(II) complexes", *Synthesis* **2012**, 44, 2287–2294.

10)   <u>Bobby Happ</u>, Georges M. Pavlov, Igor Perevyazko, Martin D. Hager, Andreas Winter, Ulrich S. Schubert. "Induced charge effect by Co^{II}-complexation on the conformation of a copolymer containing a bidentate 2-(1,2,3-triazol-4-yl)pyridine chelating unit". *Macromol. Chem. Phys.* **2012**, 213, 1339−1348.

Non-refereed publications

1)   Ulrich S. Schubert, Beatrice Beyer, <u>Bobby Happ</u>, Benjamin Schulze, Martin D. Hager, Andreas Winter, Christoph Ulbricht, Richard Hoogenboom. "Utilizing the Huisgen 1,3-dipolar cycloaddition to synthesize new 1*H*-[1,2,3]-triazole based ligands", *Abs. Pap. Am. Chem. Soc.* **2009**, *238*, 569-ORGN.

2)   <u>Bobby Happ</u>, Martin D. Hager, Andreas Winter, Christian Friebe, Richard Hoogenboom, Ulrich S. Schubert. " Alternative bipyridines analogs *via* click chemistry", *Abs. Pap. Am. Chem. Soc.* **2009**, *238*, 72-POLY.

3)   <u>Bobby Happ</u>, Martin D. Hager, Andreas Winter, Ulrich S. Schubert. "Click chemistry meets polymerization: Controlled incorporation of an easily accessible ruthenium(II)-complex into a PMMA backbone *via* RAFT copolymerization", *Abs. Pap. Am. Chem. Soc.* **2009**, *238*, 331-POLY.

4)   Bobby Happ, Johann Schäfer, Roberto Menzel, Martin D. Hager, Andreas Winter, Jürgen Popp, Rainer Beckert, Benjamin Dietzek, Ulrich S. Schubert. "Resonance energy transfer study on a random terpolymer containing a 2-(pyridine-2-yl) thiazole donor-type ligand and a luminescent [Ru(bpy)(2)(2-(triazol-4-yl) pyridine)]$^{2+}$ chromophores", *Abs. Pap. Am. Chem. Soc.* **2011**, *242*, 399-POLY.

5)   Bobby Happ, Johann Schäfer, Roberto Menzel, Martin D. Hager, Andreas Winter, Jürgen Popp, Rainer Beckert, Benjamin Dietzek, Ulrich S. Schubert. "Toward photoactive architectures composed of light-harvesting units and metal colloids: Energy transfer study of multifunctional terpolymers containing thiazole and ruthenium chromophores and coating studies of colloids", *Abs. Pap. Am. Chem. Soc.* **2011**, *242*, 68-FUEL.

6)   Bobby Happ, Georges M. Pavlov, Esra Altuntas, Christian Friebe, Martin D. Hager, Andreas Winter, Helmar Görls, Wolfgang Günther, Ulrich S. Schubert. "Self-assembly of 3,6-bis(4-triazolyl)pyridazines ligands with Cu(I) and Ag(I) ions: Time-dependant 2D-NOESY and ultracentrifuge measurements", *Abs. Pap. Am. Chem. Soc.* **2011**, *242*, 594-INOR.

Posters

1)   Bobby Happ, Martin D. Hager, Andreas Winter, Ulrich S. Schubert. "Alternative bipyridines analogs *via* click chemistry", ORCHEM, Weimar, Germany, **2008**.

2)   Bobby Happ, Andreas Winter, Martin D. Hager, Christian Friebe, Ulrich S. Schubert. "Click-chemistry meets polymerization", 238th ACS National Meeting, Washington D.C., USA, **2009**.

3)   Beatrice Beyer, Bobby Happ, Benjamin Schulze, Andreas Winter, Martin D. Hager, Christian Friebe, Ulrich S. Schubert. "1*H*-[1,2,3]-Triazole based ligands", 238th ACS National Meeting, Washington D.C., USA, **2009**.

4)   Bobby Happ, Daniel Escudero, Martin D. Hager, Christian Friebe, Andreas Winter, Helmar Görls, Leticia González, Ulrich S. Schubert. "*N*-Heterocyclic donor- and acceptor-type ligands based on 2-(1*H*-[1,2,3]triazol-4-yl)pyridines", ORCHEM, Weimar, Germany, **2010**.

5)   Bobby Happ, Georges M. Pavlov, Martin D. Hager, Andreas Winter, Helmar Görls, Ulrich S. Schubert. "Self-assembly of 3,6-bis(4-triazolyl)pyridazines ligands with Cu(I) and Ag(I) ions", 242th ACS National Meeting, Denver, USA, **2011**.

6)   Bobby Happ, Georges M. Pavlov, Igor Perevyazko, Martin D. Hager, Andreas Winter, Ulrich S. Schubert. "Induced charge effect of Co(II) ions on the conformation of a ligand-functionalized copolymer", 4th EuCheMS Chemistry Congress, Prague, Czech Republic, **2012**.

Oral presentations

1)   Bobby Happ, Andreas Winter, Martin D. Hager, Christian Friebe, Ulrich S. Schubert. "1*H*-1,2,3-Triazolpyridine systems as alternative bipyridines and their ruthenium(II) complexes", 238th ACS National Meeting, Washington D.C., USA, **2009**.

2)   Bobby Happ, Johann Schäfer, Roberto Menzel, Martin D. Hager, Andreas Winter, Ulrich S. Schubert. "Resonance energy transfer study on a random terpolymer containing a 2-(pyridine-2-yl)thiazole donor-type ligand and a luminescent [Ru(bpy)$_2$(2-(triazol-4-yl)pyridine)]$^{2+}$ chromophores", 242th ACS National Meeting, Denver, USA, **2011**.

Acknowledgement

Declaration of Autorship/
Selbstständigkeitserklärung

Hiermit erkläre ich, dass ich die vorliegende Arbeit selbständig angefertigt, nicht anderweitig zu Prüfungszwecken vorgelegt und keine anderen als die angegebenen Hilfsmittel verwendet habe. Sämtliche wissentlich verwendete Textausschnitte, Zitate oder Inhalte anderer Verfasser wurden ausdrücklich als solche gekennzeichnet.

I hereby certify that the work disclosed here is, to the best of my knowledge, original and the result of my own investigations, except as acknowledged, and has not been submitted, either in part or whole, for a degree at this or any other university.

_____   Jena, den

Bobby Happ

Abbreviations

abs	absorption
AIBN	2,2´-azo*bis*(*iso*-butyronitrile)
BMA	butyl methacrylate
bpy	2,2´-bipyridine
CBBD	2-cyanobutan-2-yl benzodithioate
CuAAC	copper(I)-catalyzed azide–alkyne cycloaddition
CV	cyclic voltammetry
DAD	diode array detector
DFT	density functional theory
DMA	*N,N*-dimethylacetamide
dmbpy	4,4´-dimethyl-2,2´-bipyridine
DMF	*N,N*-dimethylformamide
DMSO	dimethyl sulfoxide
DP	degree of polymerization
EDTA	ethylenediaminetetraacetic acid
em	emission
ESI	electron spray ionization
f	translational friction coefficient
Φ	quantum yield
Fc	ferrocene
FRET	Förster resonance energy transfer
η	dynamic viscosity
HEEDTA	trisodium *N*-(2-hydroxyethyl)ethylenediamine triacetate
HOMO	highest occupied molecular orbital
HR-ESI MS	high-resolution electron spray ionization mass spectrum
IC	internal conversion
IL	intra-ligand
IRF	instrument response function
ISC	inter-system crossing
J	overlap integral
k_r	radiative rate constant

LLCT	ligand-to-ligand charge transfer
LUMO	lowest occupied molecular orbital
M	$mol \cdot L^{-1}$
M_n	number average molar mass
M_w	weight average molar mass
MALDI	matrix-assisted laser desorption ionization
MC	metal-centered
MCP	metal-containing polymer
Mes	mesityl
MLCT	metal-to-ligand charge transfer
MMA	methyl methacrylate
NMR	nuclear magnetic resonance
NOESY	nuclear Overhauser effect spectroscopy
PDI	polydispersity index
PEG	poly(ethylene glycol)
PL	photoluminescence
PMMA	poly(methyl methacrylate)
RAFT	reversible addition-fragmentation transfer
s	velocity sedimentation coefficient
SEC	size exclusion chromatography
SOC	spin-orbit coupling
τ	luminescence lifetime
TD-DFT	time-dependent density functional theory
TEA	triethylamine
THF	tetrahydrofurane
TMSA	trimethylsilylacetylene
trzpy	2-(1H-1,2,3-triazol-4-yl)pyridine
UV/vis	ultraviolet-visible

Publications A1–A7

Publication A1

N-HETEROCYCLIC DONOR- AND ACCEPTOR-TYPE LIGANDS BASED ON 2-(1H-[1,2,3]TRIAZOL-4-YL)PYRIDINES AND THEIR RUTHENIUM(II) COMPLEXES

Bobby Happ, Daniel Escudero, Martin D. Hager, Christian Friebe, Andreas Winter, Helmar Görls, Esra Altuntas, Leticia González,* Ulrich S. Schubert*

JOC Article

N-Heterocyclic Donor- and Acceptor-Type Ligands Based on 2-(1H-[1,2,3]Triazol-4-yl)pyridines and Their Ruthenium(II) Complexes

Bobby Happ,[†,‡] Daniel Escudero,[§] Martin D. Hager,[†,‡] Christian Friebe,[†]
Andreas Winter,[†,‡,⊥] Helmar Görls,[¶] Esra Altuntaş,[†] Leticia González,*,[§] and
Ulrich S. Schubert*,[†,‡,⊥]

[†]Laboratory of Organic and Macromolecular Chemistry, Friedrich-Schiller-University Jena, Humboldtstrasse
10, 07743 Jena, Germany, [‡]Dutch Polymer Institute (DPI), P.O. Box 902, 5600 AX Eindhoven,
The Netherlands, [§]Laboratory of Physical Chemistry, Friedrich-Schiller-University Jena, Helmholtzweg 4,
07743 Jena, Germany, [⊥]Laboratory of Macromolecular Chemistry and Nanoscience, Eindhoven University of
Technology, P.O. Box 513, 5600 MB Eindhoven, The Netherlands, and [¶]Laboratory of Inorganic and
Analytical Chemistry, Friedrich-Schiller-University Jena, Lessingstrasse 8, 07743 Jena, Germany

*To whom correspondence should be addressed. L.G.: fax +49 (0)3641 948302 and e-mail leticia.
gonzalez@uni-jena.de. U.S.S.: fax: +49 (0)3641 948202, e-mail ulrich.schubert@uni-jena.de, and internet
www.schubert-group.com.
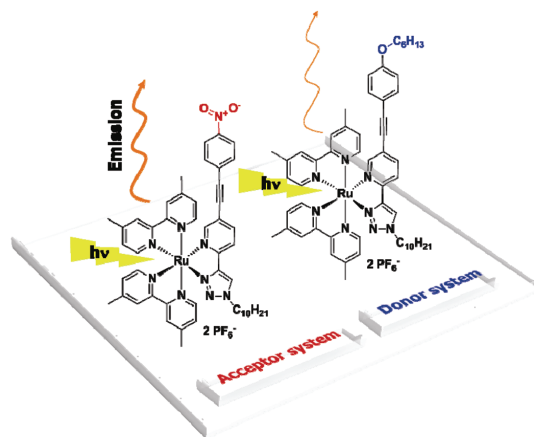
New 2-(1H-[1,2,3]triazol-4-yl)pyridine bidentate ligands were synthesized as bipyridine analogs, whereas different phenylacetylene moieties of donor and acceptor nature were attached at the 5-position of the pyridine unit. The latter moieties featured a crucial influence on the electronic properties of those ligands. The N-heterocyclic ligands were coordinated to ruthenium(II) metal ions by using a bis(4,4'-dimethyl-2,2'-bipyridine)ruthenium(II) precursor. The donor or acceptor capability of the 2-(1H-[1,2,3]triazol-4-yl)pyridine ligands determined the quantum yield of the resulting ruthenium(II) complexes remarkably. Separately, 2-([1,2,3]triazol-4-yl)pyridine ligands are known to be potential quenchers, but using these new ligand systems led to room temperature emission of the corresponding ruthenium(II) complexes. The compounds have been fully characterized by elemental analysis, high-resolution ESI mass spectrometry, ^{1}H and ^{13}C NMR spectroscopy, and X-ray crystallography. Theoretical calculations for two ruthenium(II) complexes bearing a donor and acceptor unit, respectively, were performed to gain a deeper understanding of the photophysical behavior.

Introduction

The well-known N-heterocycles 2,2'-bipyridine (bpy) and 2,2':6',2''-terpyridine (tpy) have been widely studied owing to their predictable coordination behavior and the interesting photophysical and electrochemical properties that can result from their corresponding metal complexes. Such distinctiveness can be utilized for supramolecular self-assembly, molecular electronics, and catalysis applications.[1] Because functionalization

JOC Article
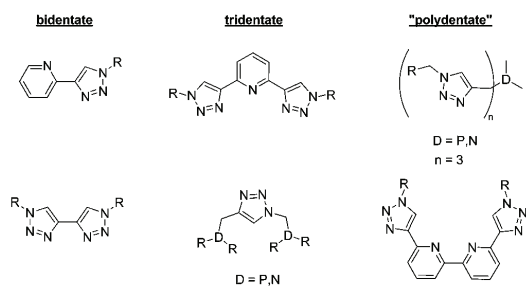
FIGURE 1. Schematic representation of 1*H*-[1,2,3]triazole-containing ligand architectures.

of polypyridine-based chelators can be synthetically troublesome,[2] it remains important to search for new approaches in the preparation of analogous bidentate chelating ligands that also possess well-defined coordination properties and can be prepared and modified with high effectiveness. In this respect the Cu[I]-catalyzed 1,3-cycloaddition of organic azides with terminal alkynes (the CuAAC reaction) has a great potential due to its mild reaction conditions and wide range of usable substrates.[3] The latter features have directed its application in the synthesis of functional molecules for biological and material sciences.[4] Furthermore, the development of the CuAAC reaction resulted in an increased interest toward the coordination chemistry of 1,4-functionalized 1*H*-[1,2,3]triazoles due to their potential as *N*-donor ligands. A variety of new bi-,[5,6] tri-,[7] and polydentate[6] 1*H*-[1,2,3]-triazole-containing ligands have been synthesized and their coordination properties were investigated (Figure 1).

(1) (a) Balzani, V.; Juris, A.; Venturi, M.; Campagna, S.; Serroni, S. *Chem. Rev.* **1996**, *96*, 759–833. (b) Schubert, U. S.; Eschbaumer, C. *Angew. Chem., Int. Ed.* **2002**, *41*, 2892–2926. (c) Hofmeier, H.; Schubert, U. S. *Chem. Soc. Rev.* **2004**, *33*, 373–399. (d) Sauvage, J.-P.; Collin, J.-P.; Chambron, J.-C.; Guillerez, S.; Coudret, C. *Chem. Rev.* **1994**, *94*, 993–1019. (e) Amabilino, D. B.; Stoddart, J. F. *Chem. Rev.* **1995**, *95*, 2725–2828.

(2) (a) Newkome, G. R.; Patri, A. K.; Holder, E.; Schubert, U. S. *Eur. J. Org. Chem.* **2004**, 235–254. (b) Heller, M.; Schubert, U. S. *Eur. J. Org. Chem.* **2003**, 947–961. (c) Marin, V.; Holder, E.; Schubert, U. S. *J. Polym. Sci., Part A: Polym. Chem.* **2004**, *42*, 374–385.

(3) (a) Kolb, H. C.; Finn, M. G.; Sharpless, K. B. *Angew. Chem., Int. Ed.* **2001**, *40*, 2004–2021. (b) Tornoe, C. W.; Christensen, C.; Meldal, M. *J. Org. Chem.* **2002**, *67*, 3057–3064. (c) Rostovtsev, V. V.; Green, L. G.; Fokin, V. V.; Sharpless, K. B. *Angew. Chem., Int. Ed.* **2002**, *41*, 2596–2599.

(4) (a) Lutz, J.-F. *Angew. Chem., Int. Ed.* **2007**, *46*, 1018–1025. (b) Bock, V. D.; Hiemstra, H.; van Maarseveen, J. H. *Eur. J. Org. Chem.* **2005**, 51–68. (c) Meldal, M.; Tornoe, C. W. *Chem. Rev.* **2008**, *108*, 2952–3015. (d) Kolb, H. C.; Sharpless, K. B. *Drug Discovery Today* **2003**, *8*, 1128–1137. (e) Angell, Y. L.; Burgess, K. *Chem. Soc. Rev.* **2007**, *36*, 1674–1689. (f) Becer, C. R.; Hoogenboom, R.; Schubert, U. S. *Angew. Chem., Int. Ed.* **2009**, *48*, 4900–4908.

(5) (a) Schweinfurth, D.; Hardcastle, K. I.; Bunz, U. H. F. *Chem. Commun.* **2008**, 2203–2205. (b) Monkowius, U.; Ritter, S.; Koenig, B.; Zabel, M.; Yersin, H. *Eur. J. Inorg. Chem.* **2007**, 4597–4606. (c) Richardson, C.; Fitchett, C. M.; Keene, F. R.; Steel, P. J. *Dalton Trans.* **2008**, 2534–2537.

(6) (a) Rodionov, V. O.; Fokin, V. V.; Finn, M. G. *Angew. Chem., Int. Ed.* **2005**, *44*, 2210–2215. (b) Huang, S.; Clark, R. J.; Zhu, L. *Org. Lett.* **2007**, *9*, 4999–5002. (c) Donnelly, P. S.; Zanatta, S. D.; Zammit, S. C.; White, J. M.; Williams, S. J. *Chem. Commun.* **2008**, 2459–2461.

(7) (a) Li, Y.; Huffman, J. C.; Flood, A. H. *Chem. Commun.* **2007**, 2692–2694. (b) Meudtner, R. M.; Ostermeier, M.; Goddard, R.; Limberg, C.; Hecht, S. *Chem.—Eur. J.* **2007**, *13*, 9834–9840. (c) Schuster, E. M.; Botoshansky, M.; Gandelman, M. *Angew. Chem., Int. Ed.* **2008**, *47*, 4555–4558. (d) Fletcher, J. T.; Bumgarner, B. J.; Engels, N. D.; Skoglund, D. A. *Organometallics* **2008**, *27*, 5430–5433. (e) Schulze, B.; Friebe, C.; Hager, M. D.; Winter, A.; Hoogenboom, R.; Goerls, H.; Schubert, U. S. *Dalton Trans.* **2009**, 787–794.

Our interest was to tune in particular the electronic properties of the bidentate 2-(1*H*-[1,2,3]triazol-4-yl)pyridine ligands. This was accomplished by introducing electron-donating and electron-withdrawing units on the 5-position of the pyridine ring with a 2-(1*H*-[1,2,3]triazol-4-yl)pyridine system (trzpy) as central structural motive (Scheme 1). In the present study the synthesis and the characterization of new 2-(1*H*-[1,2,3]triazol-4-yl)pyridine ligand systems with donor and acceptor nature are described by using the efficient Sonogashira coupling and the versatile copper(I)-catalyzed azide−alkyne 1,3-cycloaddition intended for the ligand synthesis as well as the subsequent coordination onto a bis-(4,4′-dimethyl-2,2′-bipyridine)ruthenium(II) precursor complex. The photophysical properties were studied by UV-vis and emission spectroscopy, cyclic voltammetry and analyzed in detail by theoretical calculations.

The coordination to the ruthenium(II) metal ion by using bis(4,4′-dimethyl-2,2′-bipyridine) as ancillary ligand revealed two interesting features. First, 2-(1*H*-[1,2,3]triazol-4-yl)-pyridine systems are known to be potential luminescence quenchers at room temperature as soon as they are attached to a ruthenium(II) metal ion[8] and, unexpectedly, the here-in described heteroleptic ruthenium(II) complexes bearing a 2-(1*H*-[1,2,3]triazol-4-yl)pyridine ligand furnished with an acceptor unit overcame this luminescence quenching and yielded in room temperature emission. Second, by replacing the latter acceptor system with a donor structure the luminescence at room temperature decreased considerably. Therefore, time-dependent density functional theory calculations (TD-DFT) were done to gain a deeper insight into the photophysical processes.

Results and Discussion

Synthesis. The general procedure for the synthesis of donor-type 2-(1*H*-[1,2,3]triazol-4-yl)pyridine **5** is outlined in Scheme 2. The Sonogashira cross-coupling[9] and the CuAAC[3b,c] reaction were the key reaction types for the construction of the targeted ligand. Consecutive Sonogashira reactions with 2 mol % of Pd[0] catalyst were carried out to synthesize intermediate **3**. Subsequently, deprotection of the trimethylsilyl group (TMS) utilizing fluoride ions afforded **4** in good yield (75%). The subsequent CuAAC reaction provided the final product **5** (67% yield) by using 5 mol % CuSO₄ and 25 mol % sodium ascorbate as the catalytic system. The purity of **5** was proven by NMR spectroscopy, mass spectrometry, and elemental analysis.

The synthesis of the acceptor systems **10a−d** also involved the Sonogashira cross-coupling and the CuAAC reaction as synthetic tools; however, a different synthetic approach had to be used. The synthesis of a precursor compound similar to **3** with electron-withdrawing substituents could not be performed. As a result, two alternative routes were applied to synthesize precursor compound **9** (Scheme 3). Though the first route consisted of one step less, both routes gave comparable overall yields (route 1: 61%; route 2: 51%). The reason for this observation might be the efficient cleavage of the TMS group[10] affording **6**

(8) Happ, B.; Friebe, C.; Winter, A.; Hager, M. D.; Hoogenboom, R.; Schubert, U. S. *Chem.−Asian J.* **2009**, *4*, 154–163.

(9) Analogue procedure: Bianchini, C.; Giambastiani, G.; Rios, I. G.; Meli, A.; Oberhauser, W.; Sorace, L.; Toti, A. *Organometallics* **2007**, *26*, 5066–5078.

(10) Nakano, Y.; Ishizuka, K.; Muraoka, K.; Ohtani, H.; Takayama, Y.; Sato, F. *Org. Lett.* **2004**, *6*, 2373–2376.

SCHEME 1. Schematic Representation of the Synthesis of the *N*-Heterocyclic Ligands and Their Corresponding Heteroleptic Ruthenium(II) Complexes
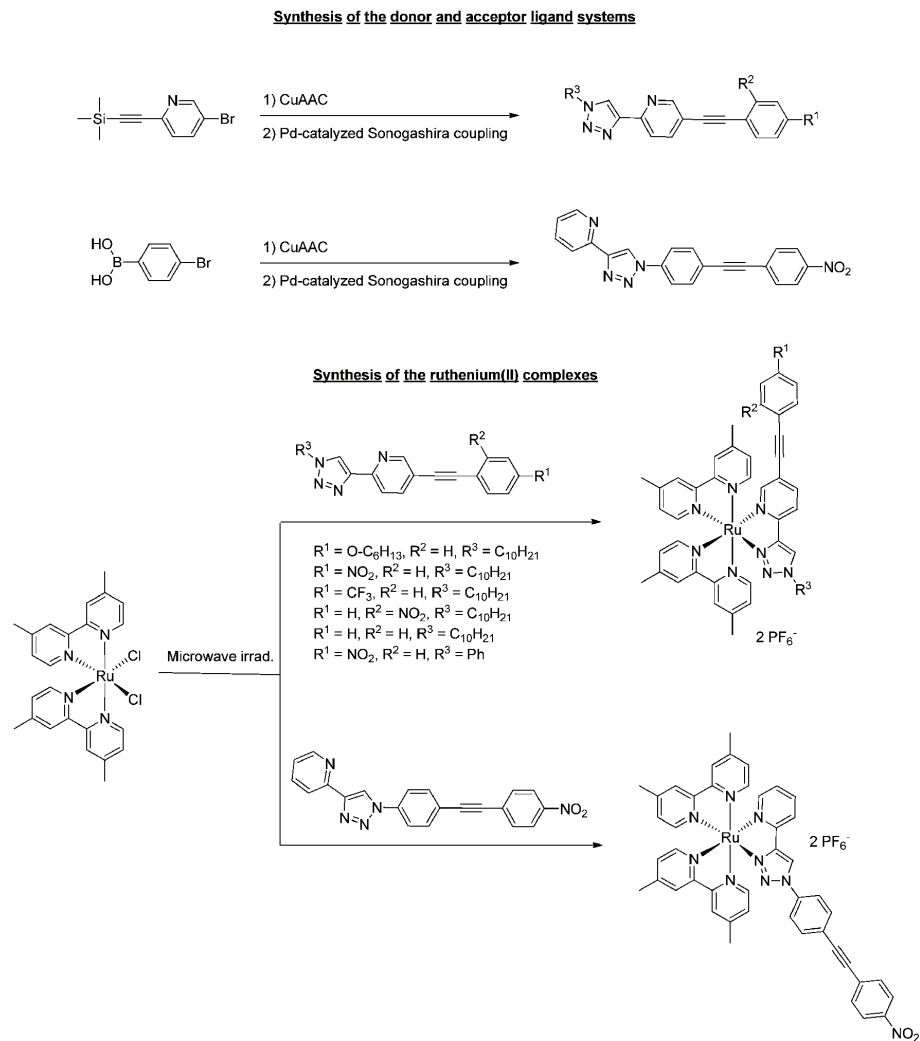
in quantitative yield. Subsequently, the ligands **10a−d** were obtained in good to high yields (70−93%) utilizing the straight-forward Sonogashira cross-coupling with 2−4 mol % of the palladium(0) catalyst. All final products were purified by column chromatography on silica and the purity was confirmed by elemental analysis, high-resolution mass spectrometry (HR-ESI-MS), as well as ^{1}H and ^{13}C NMR spectroscopy.

The second route turned out to be also a versatile way to introduce an aromatic substituent in the N^1-position of the triazole as an alternative to the decyl-moiety in **10** (Scheme 4). Substitution of the flexible alkyl-chain by a more rigid phenyl ring should enhance the growth of single crystals, in particular of the targeted heteroleptic Ru^{II} complexes. For this purpose, **6** was allowed to react with phenylazide[8] using the CuAAC reaction

yielding compound **11** (45%) after cleavage of the isopropanol protection group (Scheme 4). Finally, the N^1-phenyl-substituted compound **12** was obtained by Sonogashira cross-coupling reaction in good yield (77%).

Besides the systems featuring donor or acceptor units attached to the pyridine ring (**5**, **10**, and **12**), also derivatives with similar substituents in the N^1-position of the 1*H*-[1,2,3]tri-azole subunit were in the focus (Scheme 5). For this purpose, (1-azidophenyl)boronic acid[8] and 2-ethynylpyridine were conjugated by using the CuAAC reaction yielding **13**. The purification steps, i.e. simple filtration and recrystallization from ethanol, fully met the criteria of a "click reaction" as defined by Sharpless et al.[3a] Following two times the standard protocol for the Sonogashira cross-coupling reaction, the final

JOC*Article*

SCHEME 2. **Schematic Representation of the Synthesis of the Donor-Type Ligand 5**
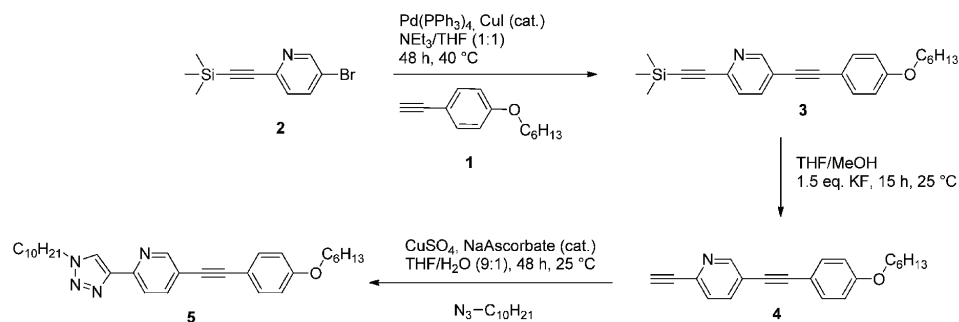
SCHEME 3. **Schematic Representation of the Synthesis of the Acceptor-Type Ligands 10**

10a, R^1 = NO$_2$, R^2 = H
10b, R^1 = H, R^2 = NO$_2$
10c, R^1 = CF$_3$, R^2 = H
10d, R^1 = H, R^2 = H

Happ et al.

JOC Article
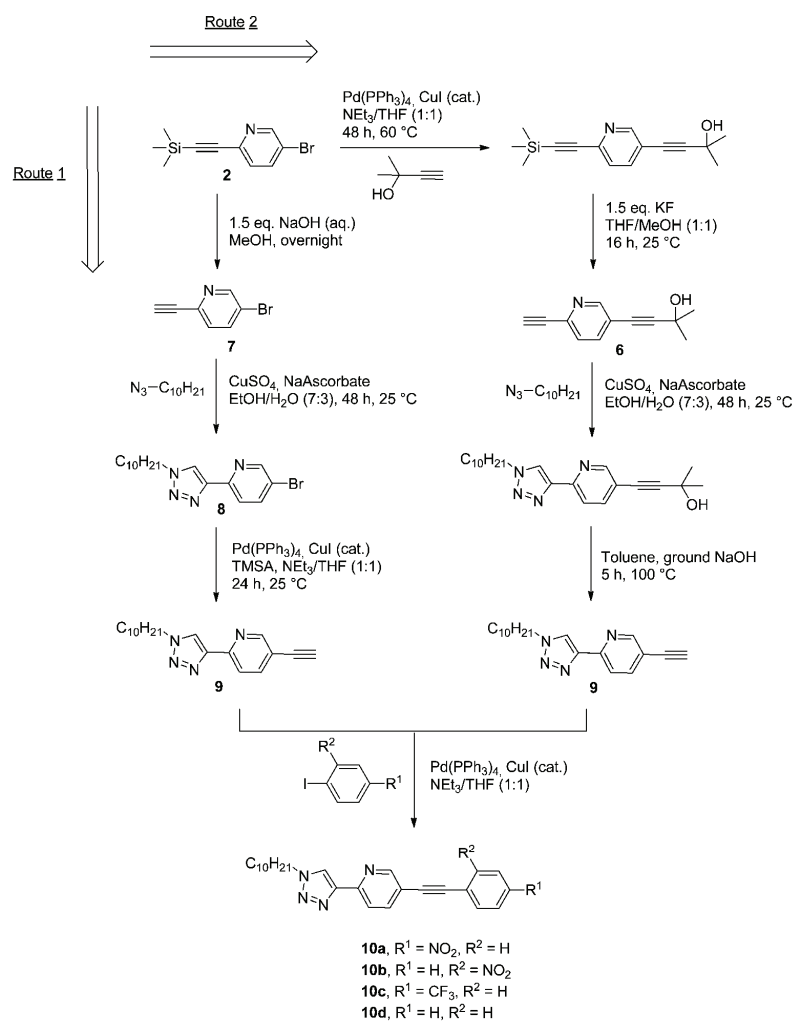
SCHEME 4. Schematic Representation of the Synthesis of the Acceptor-Type Ligand 12 Bearing an Aromatic Moiety
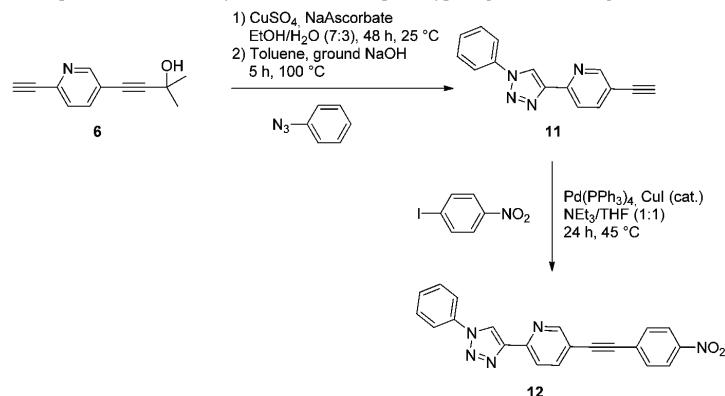
SCHEME 5. Schematic Representation of the Synthesis of a 2-(1*H*-[1,2,3]Triazol-4-yl)pyridyl Ligand with an Acceptor-Unit Attached on the Triazole Ring
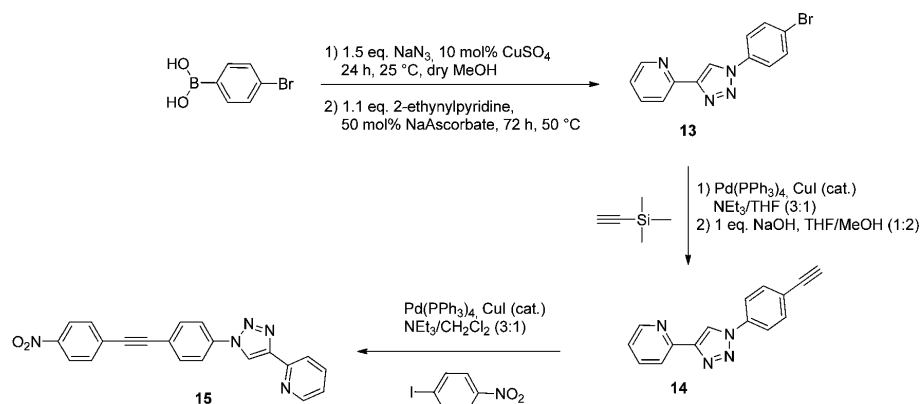
acceptor-functionalized compound **15** was synthesized in moderate yield (50%). However, the implementation of the *O*-alkyl donor system in analogy to **5** was not yet successful.

The heteroleptic ruthenium(II) complexes **16** to **18** of the general structure [(dmbpy)$_2$RuL](PF$_6$)$_2$ (dmbpy = 4,4'-dimethyl-2,2'-bipyridine) were synthesized by heating Ru-(dmbpy)$_2$Cl$_2$[8,11] and the appropriate ligands (L = **5, 10, 12, 15**) under microwave irradiation (Table 1). After 2 h the reactions were completed and a 10-fold excess of NH$_4$PF$_6$ was added to precipitate the products. In most cases, precipitation occurred after 15 min and the pure complex was isolated after washing with ethanol and diethyl ether in moderate to very good yields (Table 1). Only **16c** and **17** had to be recrystallized from ethanol/water. The latter fact may explain the moderate yields obtained for these complexes. The verification of the structures of **16−18** was carried out by ^{1}H and ^{13}C NMR spectroscopy as well as HR-ESI mass spectrometry.

Crystallographic Analysis. For the heteroleptic Ru^{II} complex **17** single crystals suitable for X-ray crystallographic analysis were obtained by slow diethyl ether diffusion revealing the coordination of the two 4,4'-dimethyl-2,2'-bipyridine and the 2-(1*H*-[1,2,3]triazol-4-yl)pyridine ligand **12** to the Ru^{II} core. The molecule crystallizes in a triclinic system with $P\bar{1}$ symmetry (for ORTEP see the Supporting Information). The structural parameters observed from **17** were compared to the corresponding structurally related homoleptic complex [Ru(bpy)$_3$](PF$_6$)$_2$[12] (Figure 2).

It is noteworthy that the interligand angle of the nitrogen atoms in the square plane were similar for both complexes (**17**: 170.40° and 174.40°; [Ru(bpy)$_3$](PF$_6$)$_2$: 172.3°; see Figure 2) resulting in a comparable distortion of the ideal octahedral geometry. The bond length from ruthenium to the coordinating nitrogen atom of the triazole ring (N': 2.028(2), Figure 2) was shortened significantly compared

(11) Rau, S.; Ruben, M.; Büttner, T.; Temme, C.; Dautz, S.; Görls, H.; Rudolph, M.; Walther, D.; Vos, J. G. *J. Chem. Soc., Dalton Trans.* **2000**, 3649–3657.

(12) Biner, M.; Buergi, H. B.; Ludi, A.; Roehr, C. *J. Am. Chem. Soc.* **1992**, *114*, 5197–5203.

(13) Egbe, D. A. M.; Bader, C.; Nowotny, J.; Günther, W.; Klemm, E. *Macromolecules* **2003**, *36*, 5459–5469.

Happ et al.

TABLE 1.   Synthesis of the Heteroleptic Ruthenium(II) Complexes
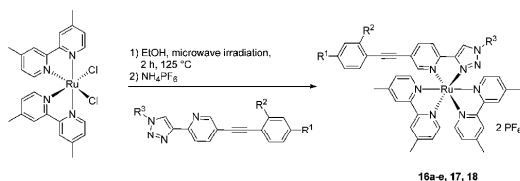
Entry	Compound	Product	Yield (%)
1	**16a**	$R^1 = OC_6H_{13}$ $R^2 = H$ $R^3 = n\text{-}C_{10}H_{21}$	81
2	**16b**	$R^1 = NO_2$ $R^2 = H$ $R^3 = n\text{-}C_{10}H_{21}$	88
3	**16c**	$R^1 = CF_3$ $R^2 = H$ $R^3 = n\text{-}C_{10}H_{21}$	48
4	**16d**	$R^1 = H$ $R^2 = NO_2$ $R^3 = n\text{-}C_{10}H_{21}$	90
5	**16e**	$R^1 = H$ $R^2 = H$ $R^3 = C_{10}H_{21}$	75
6	**17**	$R^1 = NO_2$ $R^2 = H$ $R^3 = phenyl$	63
7	**18**		77

FIGURE 2. A comparison of bond angles and bond lengths derived from the crystallographic analysis. Left: Ru^{II} complex **17**. Right: $Ru(bpy)_3(PF_6)_2$.[12]
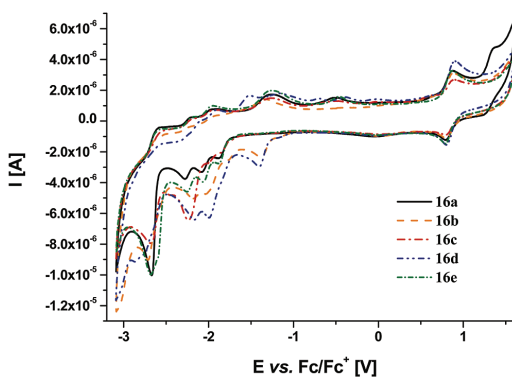
FIGURE 3. Cyclic voltammograms of ruthenium(II) complexes **16a** to **16e** (10^{-4} M, CH_3CN containing 0.1 M TBAPF$_6$).

to that of the adjacent coordinating nitrogen atom of the bipyridine ring (N: 2.052(1), Figure 2). In contrast, the bond length of the opposed coordinating nitrogen to the triazole nitrogen was not reduced but comparable to that of bipyridine. This observation could be rationalized by the expected higher π-acceptor strength of the triazole ring and, consequently, the increased π-back-bonding resulting in a reduced bond length. Additionally, the distance between the ruthenium center and the nitrogen atom of the pyridine moiety of **12** was elongated considerably (N: 2.102(1), Figure 2). This fact derives from a reduction of electron density of this bond in concert with an increased π-back-bonding toward the triazole ring.

Electrochemical Properties. The complexes **16a−e** were subsequently characterized by cyclic voltammetry (CV). The electrochemical properties are presented in Table 2 and Figure 3.

In all cases a first reversible oxidation wave occurred at around 0.85 V (vs Fc/Fc$^+$) that can be assigned to a Ru^{II}/Ru^{III} oxidation process. Furthermore, compound **16a** showed a second oxidation process at 1.28 V, probably originating from an oxidation process of the triazole ligand. Due to the absence of electron-donating substituents at the triazole ligand, the respective ligand-centered π-orbitals are more stabilized for complexes **16b−e** and, therefore, no such oxidation processes were visible in the CV spectrum.

In contrast to the other systems, the nitro-containing complexes **16b** and **16d** featured a single reversible reduction wave at around −1.35 V vs Fc/Fc$^+$ that could be assigned to a triazole ligand-based reduction process. Both complexes provided a strongly electron-withdrawing substituent causing a stabilization of the triazole-ligand-located antibonding

TABLE 2.   Electrochemical Data of Selected Ru^{II} Complexes

complex	$E_{1/2,\text{ox}}$ [V][a]	$E_{1/2,\text{red}}$ [V][a]	E_g^{opt} [eV][b]	E^{HOMO} [eV][c]	E^{LUMO} [eV][c]
16a	0.82, 1.28	−1.85, −2.06, −2.23	2.48	−5.62	−3.18
16b	0.88	−1.34, −1.97, −2.18	2.43	−5.67	−3.70
16c	0.84	−1.89, −2.13	2.44	−5.69	−3.21
16d	0.88	−1.36, −1.98, −2.11	2.43	−5.64	−3.62
16e	0.84	−1.85, −2.03, −2.18	2.49	−5.64	−3.17

[a]Measurements were performed in CH_3CN containing 0.1 M TBAPF$_6$. The potentials are given vs ferrocene/ferricinium (Fc/Fc$^+$) couple. [b]Estimated from the UV−vis spectra at 10% of the maximum of the longest-wavelength absorption band on the low-energy side. [c]Determined using $E^{\text{HOMO}} = -[(E_{\text{onset,ox}} - E_{\text{onset,Fc/Fc+}}) - 4.8]$eV and $E^{\text{LUMO}} = -[(E_{\text{onset,red}} - E_{\text{onset,Fc/Fc+}}) - 4.8]$eV, respectively.[13]

Happ et al.

TABLE 3. Photophysical Data of the Donor- and Acceptor-Type Ligands

compound	λ_{abs} [nm] (ε [10^3 L·mol^{-1}·cm^{-1}])^a	λ_{em} [nm]^a
5	250 (2), 323 (32), 338 (30)	378
10a	273 (26), 343 (47)	—^{b}
10b	271 (30), 315 (33), 338 (21)	—^{b}
10c	297 (24), 315 (32), 329 (26)	363
10d	297 (24), 315 (29), 329 (25)	358
12	270 (18), 342 (25)	—^{b}

^{a}For all measurements: 10^{-6} M solution (CH$_2$Cl$_2$). For emission measurements: excitation at longest absorption wavelength. ^{b}No emission detectable at room temperature.

π^*-orbitals (*q.v.* results of the DFT calculations). Starting at −1.8 V all five complexes showed additional reduction waves deriving from ligand-based (dmbpy and triazole ligand) π^*-orbitals.

Photophysical Properties. The UV−vis absorption and emission data of the donor- and acceptor-type systems are depicted in Table 3. As expected, ligand 10a (nitro-moiety in the para-position) revealed the largest bathochromic shift in the absorption spectrum, but did not show fluorescence at room temperature. In contrast to 10a, the donor-system 5 as well as the acceptor ligands without nitro groups (10c/d) revealed room temperature emission. Compound 5 showed the largest Stokes shift of 3130 cm^{-1} whereas 10c and 10d featured remarkably small Stokes shifts (10c: 1220 cm^{-1}; 10d: 1240 cm^{-1}). The reason for the large Stokes shift of 5 was probably caused by the charge transfer nature of the electronic transition.

The optical properties of the heteroleptic ruthenium(II) complexes are summarized in Table 4. A common feature of all complexes was a broad absorption band at around 400 to 500 nm, which could be assigned mainly to various metal-to-ligand charge-transfer (MLCT) transitions between the ruthenium metal center and either the 4,4′-dimethyl-2,2′-bipyridine or the triazole ligand (see DFT calculations). All complexes possessed extinction coefficients of about 20 000 M^{-1}·cm^{-1}, whereas the alkoxy and the unsubstituted systems showed slightly higher values (24 000 and 21 000 M^{-1}·cm^{-1}) than their trifluoromethyl (18 000 M^{-1}·cm^{-1}) or even nitro counterparts (12 000 and 13 000 M^{-1}·cm^{-1}). Between 300 and 400 nm, the complexes investigated herein exhibited different absorption behavior concerning their wavelength maxima and band shape. Therefore, this region seemed to be dominated by intraligand (IL) transitions, namely located at the triazole ligand. A comparison with the respective absorption spectra of triazole ligands (Table 3) supported this assumption. At 286 nm a strong absorption (65 000 to 135 000 M^{-1}·cm^{-1}) could be observed for all complexes, most likely originating from a dmbpy-located IL

transition. More bands were present below 280 nm that arose from further MLCT, ligand-to-ligand charge transfer (LLCT) and metal-centered (MC) d−d transitions, respectively.

The observed emission energies (Table 4) showed a clear dependency on the used substituent. Starting at 602 nm in the case of the alkoxy-containing system, the emission was strongly red-shifted to 621 nm for the unsubstituted triazole ligand and to 640 and even 674 nm in the case of the complexes possessing an *o*- and *p*-nitrophenyl moiety, respectively. This trend was most likely caused by the stabilization of the π^*-orbitals located at the triazole ligand via introduction of electron-withdrawing groups. These orbitals are, at least in case of electron-acceptor substituents, supposed to be involved in the emissive ^{3}MLCT state, so that a lower energy level led to decreased emission energy.

Also depicted in Table 4 are the photoluminescence quantum yields (Φ_{PL}) of the ruthenium(II) systems. At least in aerated acetonitrile, the Φ_{PL} values were rather low (around 0.1% for 16a−e, nearly no emission in the case of phenyl-substituted 17 and about 0.3% for the "inverse" system 18). When changing to dichloromethane as solvent, the emission efficiencies rose and a significant difference between the donor- (16a) and the acceptor-substituted complex (16b) became obvious (0.5% and 2.2%, respectively).

DFT Calculations. To gain a more detailed insight into the photophysical properties of the acceptor- and donor-based complexes, density functional theory (DFT) and time-depended (TD) DFT (B3LYP/6-31G*) calculations were performed. DFT/TD-DFT studies on Ru(II) polypyridyl complexes have been successfully used to understand and rationalize the experimental photophysical features of these complexes.[15] Figure 4 shows the obtained Kohn−Sham frontier orbitals and energy level schemes of the ground state optimized geometries of complexes 16a and 16b. In complex 16b the highest occupied molecular orbitals (HOMOs) were the set t$_{2g}$ of the central Ru^{II} atom. A π-orbital localized in the 2-(1*H*-[1,2,3]triazol-4-yl)-pyridine ligand (π_L) was lower in energy corresponding to the HOMO-3. These orbitals were in different order in the complex 16a: The π_L corresponded to the HOMO orbital and the set t$_{2g}$ of orbitals was found lower in energy. Both complexes 16a and 16b also differed in the order of the lowest unoccupied molecular orbitals (LUMO). In the case of the acceptor-type compound the LUMO orbital corresponded to a π-antibonding orbital located in the 2-(1*H*-[1,2,3]triazol-4-yl)-pyridine ligand (π^*_L), while this orbital was shifted to the LUMO+2 in complex 16a. In 16a the LUMO possessed π-antibonding character and was located on the dmbpy ligand (π^*_{dmbpy}). Substitution of the 2-(1*H*-[1,2,3]triazol-4-yl)pyridine ligand with an electron-donating or -withdrawing group,

TABLE 4. Photophysical Data Recorded for the Ru^{II} Complexes

complex	λ_{abs} [nm] (ε [10^3 L·mol^{-1}·cm^{-1}])^{a,b}	λ_{em} [nm]^a	Φ_{PL}^{a,c}
16a	206 (145.6), 286 (133.1), 333 (59.8), 435 (23.6)	602	0.001 [0.005^d]
16b	209 (58.4), 286 (63.4), 328 (38.6), 441 (11.6)	674	0.001 [0.022^d]
16c	209 (88.1), 286 (103.9), 312s (51.6), 440 (18.3)	620	0.002
16d	208 (66.6), 286 (74.7), 341s (22.6), 442 (12.4)	640	0.001
16e	205 (131.1), 286 (125.6), 315s (60.9), 438 (20.6)	621	0.001
17	206 (83.7), 286 (76.9), 326 (52.5), 440 (12.8)	642	<0.001
18	195 (102.9), 286 (83.1), 316s (40.5), 442s (12.5)	610	0.003

^{a}For all measurements: 10^{-6} M solution in aerated CH$_3$CN at room temperature. For emission measurements: excitation at longest absorption wavelength. ^{b}"s" signifies absorption shoulder. ^{c}Photoluminescence quantum yields determined with [Ru(bpy)$_3$](PF$_6$)$_2$ (Φ_{PL} = 0.062) as standard.[14] ^{d}Measured in aerated CH$_2$Cl$_2$ solution at room temperature (10^{-6} M).
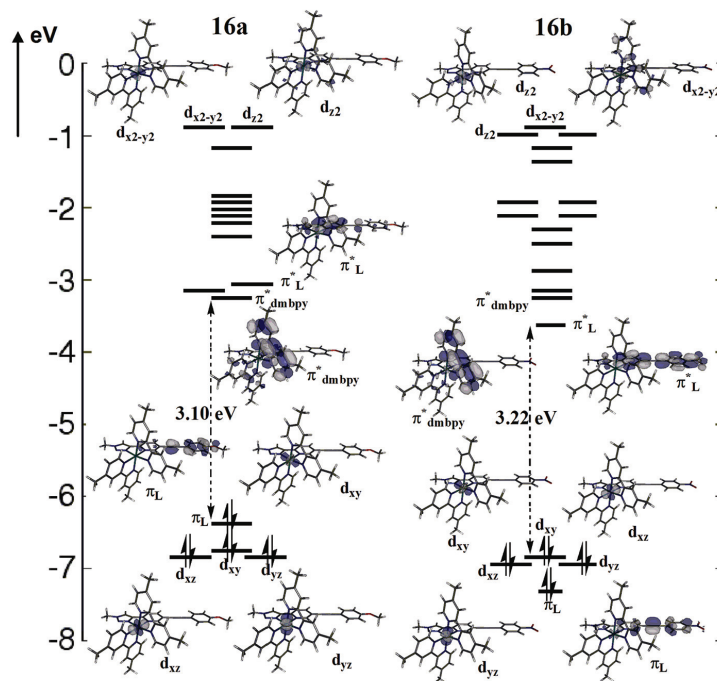
FIGURE 4. Energy level scheme for the Kohn–Sham orbitals of complexes **16a** and **16b**, including the most relevant Kohn–Sham orbitals and the HOMO–LUMO gaps calculated with B3LYP/6-31G*.

respectively, had therefore an important influence on the energy level and ordering of the molecular orbitals.

The set e_g of Ru^{II} orbitals was, as shown in Figure 4, strongly destabilized. Thus, the d_{z^2} and $d_{x^2-y^2}$ orbitals corresponded to LUMO+10 and LUMO+11 in complex **16a**, respectively, while in complex **16b** they related to the orbitals LUMO+12 and LUMO+14. The energetic gaps between the HOMO and LUMO levels are also shown in Figure 4. We obtained theoretical HOMO–LUMO gaps of 3.10 and 3.22 eV for **16a** and **16b**, respectively.

Figure 5 shows the theoretical UV–vis spectra of complexes **16a** and **16b** vs the experimental ones. Table 5 collects the main TD-DFT electronic excitations recorded in the presence of solvent (i.e., CH_2Cl_2). A fairly good agreement between experiment and theory was observed, notwithstanding that TD-DFT generally tends to underestimate the energy of the charge-transfer states,[16] even if it is well-established that hybrid functionals, such as B3LYP, are less affected by this problem.[17] However, the combination of a

hybrid functional and the consideration of solvent effects on the electronic excitations seemed to be a reasonable approach to reproduce the photophysical properties of the ruthenium(II) complexes (with errors amounting to approximately 0.3 eV). The main features of the experimental spectra were reproduced. Three main bands were obtained for both complexes **16a** and **16b**. As seen in Figure 5, no absorption for both compounds was theoretically predicted beyond 470 nm. Experimentally, absorption was recorded up to 500 nm. The tail between 470 and 520 nm, where singlet–singlet excitations are dark or do not exist, should then be attributed to singlet–triplet excitations (due to non-negligible spin–orbit coupling for the ruthenium atom).

The effect of substitution with an acceptor or a donor unit attached in the 5-position of the pyridine ring had a significant influence on the nature as well as on the position of the UV–vis bands. Thus, in the case of **16a**, the low-energy broad band centered around 440 nm could be assigned to different singlet–singlet electronic excitations of MLCT character (see S_4, S_8, and S_9 in Table 5) as well as LLCT character (see S_3 and S_7 in Table 5). Although a very similar broad band was obtained in the case of compound **16b**, the character of the underlying transitions was different. In complex **16b** this band was mainly composed of MLCT states (see S_4, S_5, S_6, and S_8 in Table 5).

The explanation of the different character of the low-energy bands of **16a** and **16b** could be found by analyzing the orbitals involved in these transitions. For instance, the LLCT states (S_3 and S_7) of compound **16b**, which involved

(14) (a) Demas, J. N.; Crosby, G. A. *J. Phys. Chem.* **1971**, *75*, 991–1024. (b) Juris, A.; Balzani, V.; Barigelletti, F.; Campagna, S.; Belser, B.; von Zelewsky, A. *Coord. Chem. Rev.* **1988**, *84*, 85–277.

(15) (a) Vlcek, A., Jr.; Zalis, S. *Coord. Chem. Rev.* **2007**, *251*, 258–287. (b) Charlot, M.-F.; Aukauloo, A. *J. Phys. Chem. A* **2007**, *111*, 11661–11672. (c) Abbotto, A.; Barolo, C.; Bellotto, L.; De Angelis, F.; Grätzel, M.; Manfredi, N.; Marinzi, C.; Fantacci, S.; Yum, J.-H.; Nazeeruddin, M. K. *Chem. Commun.* **2008**, 5318–5320.

(16) Dreuw, A.; Head-Gordon, M. *Chem. Rev.* **2005**, *105*, 4009–4037.

(17) Dreuw, A.; Weisman, J. L.; Head-Gordon, M. *J. Chem. Phys.* **2003**, *119*, 2943–2946.

Happ et al.

TABLE 5. Main Theoretical Electronic Transition Energies (ΔE) with Corresponding Oscillator Strengths (f) and Assignment for Complexes 16a and 16b

16a				16b			
state	ΔE (nm)	f	assignment	state	ΔE (nm)	f	assignment
S_1	477	0.003	$d_{xy} \rightarrow \pi^*_{dmbpy}$ (0.53) MLCT	S_1	479	0.010	$d_{xy} \rightarrow \pi^*_L$ (0.66) MLCT
S_2	462	0.003	$d_{xy} \rightarrow \pi^*_{dmbpy}$ (0.59) MLCT	S_2	466	0.011	$d_{xy} \rightarrow \pi^*_{dmbpy}$ (0.65) MLCT
S_3	453	0.056	$\pi_L \rightarrow \pi^*_{dmbpy}$ (0.53) LLCT	S_4	448	0.023	$d_{xy} \rightarrow \pi^*_L$ (0.66) MLCT
S_4	441	0.162	$d_{xy} \rightarrow \pi^*_L$ (0.51) MLCT	S_5	439	0.065	$d_{yz} \rightarrow \pi^*_L$ (0.54) MLCT
S_7	430	0.180	$\pi_L \rightarrow \pi^*_{dmbpy}$ (0.54) LLCT	S_6	433	0.030	$d_{xz} \rightarrow \pi^*_{dmbpy}$ (0.49) MLCT
S_8	425	0.191	$d_{xy} \rightarrow \pi^*_{dmbpy}$ (−0.35) MLCT; $\pi_L \rightarrow \pi^*_L$ (0.35) IL	S_8	414	0.136	$d_{yz} \rightarrow \pi^*_{dmbpy}$ (0.40) MLCT; $d_{xz} \rightarrow \pi^*_{dmbpy}$ (0.43) MLCT
S_9	420	0.313	$d_{xz} \rightarrow \pi^*_{dmbpy}$ (0.44) MLCT	S_9	395	0.124	$d_{xz} \rightarrow \pi^*_{dmbpy}$ (0.54) MLCT
S_{10}	407	0.104	$d_{xz} \rightarrow \pi^*_L$ (0.63) MLCT	S_{11}	371	1.262	$\pi_L \rightarrow \pi^*_L$ (0.63) IL
S_{11}	401	0.243	$d_{xz} \rightarrow \pi^*_{dmbpy}$ (0.45) MLCT	S_{13}	348	0.039	$d_{yz} \rightarrow \pi^*_L$ (0.54) MLCT
S_{13}	360	0.192	$\pi_L \rightarrow \pi^*_L$ (0.61) IL	S_{27}	312	0.071	$d_{yz} \rightarrow \pi^*_{dmbpy}$ (−0.29) MLCT; $d_{xz} \rightarrow \pi^*_{dmbpy}$ (0.30) MLCT; $d_{yz} \rightarrow \pi^*_{dmbpy}$ (0.32) MLCT
S_{30}	307	0.094	$d_{yz} \rightarrow \pi^*_{dmbpy}$ (0.51) MLCT	S_{32}	305	0.116	$d_{yz} \rightarrow \pi^*_{dmbpy}$ (0.44) MLCT; $d_{xy} \rightarrow \pi^*_{dmbpy}$ (−0.38) MLCT
S_{32}	306	0.034	$d_{xy} \rightarrow \pi^*_{dmbpy}$ (0.37) MLCT	S_{42}	294	0.066	$d_{yz} \rightarrow \pi^*_L$ (0.47) MLCT
S_{47}	282	0.234	$\pi_L \rightarrow \pi^*_L$ (0.52) IL	S_{49}	276	0.284	$\pi_{dmbpy} \rightarrow \pi^*_{dmbpy}$ (0.41) IL
S_{52}	276	0.177	$\pi_{dmbpy} \rightarrow \pi^*_L$ (0.54) LLCT	S_{50}	274	0.419	$\pi_{dmbpy} \rightarrow \pi^*_{dmbpy}$ (0.33) IL
S_{54}	273	0.286	$\pi_{dmbpy} \rightarrow \pi^*_{dmbpy}$ (0.25) LLCT; $d_{xz} \rightarrow d_{x^2-y^2}$ (0.24) MC	S_{51}	273	0.286	$\pi_{dmbpy} \rightarrow \pi^*_{dmbpy}$ (0.23) IL; $\pi_{dmbpy} \rightarrow \pi^*_{dmbpy}$ (−0.22) IL
S_{55}	273	0.509	$\pi_{dmbpy} \rightarrow \pi^*_L$ (0.27) LLCT; $\pi_{dmbpy} \rightarrow \pi^*_{dmbpy}$ (−0.23) IL; $\pi_{dmbpy} \rightarrow \pi^*_{dmbpy}$ (0.23) IL	S_{54}	265	0.146	$\pi_L \rightarrow \pi^*_L$ (0.54) IL

FIGURE 5. Experimental spectra of complexes 16a (top) and 16b (bottom) in solid lines superimposed to the TD-DFT (B3LYP/6-31G* in CH$_2$Cl$_2$) vertical excitations. The main electronic states are highlighted (see Table 5 for assignments).

electronic transitions from the same π-orbital localized in the 2-(1H-[1,2,3]triazol-4-yl)pyridine ligand (π_L) to different π-antibonding orbitals located on the dmbpy ligands (π^*_{dmbpy}), appeared lower in energy in 16a. This fact was due to the destabilization of the π_L orbital in the donor-based compound as compared to the same orbital in the acceptor-based compound (recall that the π_L orbital is the HOMO in compound 16a but the HOMO-3 in 16b, see Figure 4). The

second band, located experimentally around 360 and 340 nm in complexes 16a and 16b, respectively, was characterized by the same electronic excitations (S_{13} and S_{11} for compounds 16a and 16b, respectively). These corresponded to intra-ligand (IL) states, which involved local $\pi_L \rightarrow \pi^*_L$ electronic excitations within the 2-(1H-[1,2,3]triazol-4-yl)pyridine ligand. Finally, the most intense peak centered at 286 nm in both complexes was mainly due to IL states in 16b and states of IL and LLCT character in the case of 16a (see Table 5). In the case of 16a, one of these states (S_{54}) was mixed with a MC transition, involving an electronic excitation from the d_{xz} orbital to the unoccupied $d_{x^2-y^2}$ orbital.

Concerning the emission behavior, the trzpy-type ligand systems are known to be potential luminescence quenchers and the ruthenium(II) complexes reported previously did not show any luminescence at room temperature.[7e,8] Also the complexes presented in this contribution showed only very weak emission intensities (see Table 4). For excited Ru^{II} polypyridyl complexes it is well-known that the triplet excited states are populated rapidly via efficient intersystem crossings (ISC) from the singlet photoexcited states[18] (due to the strong spin−orbit coupling of the ruthenium center). Afterward, relaxation to the lowest triplet excited state (T$_1$) follows. Obviously, the nature of the low-lying singlets and triplets excited states should determine the effectiveness of the ISC. As revealed, different singlet excited states were obtained for complexes 16a and 16b and, consequently, a different emission behavior was expected. We are currently developing a methodology to estimate the phosphorescence rates and the quantum yields, based on accurate estimation of the spin−orbit couplings between the singlet and triplet manifolds which, in turn, determine the ISC rates.

Conclusions

New 2-(1H-[1,2,3]triazol-4-yl)pyridine bidentate ligands were synthesized as bipyridine analogs, whereas different

(18) Bhasikuttan, A. C.; Suzuki, M.; Nakashima, S.; Okada, T. J. Am. Chem. Soc. 2002, 124, 8398–8345.

phenylacetylene moieties of donor and acceptor nature, respectively, were attached at the 5-position of the pyridine unit. The moieties featured a crucial influence on the electronic properties of these ligands. In addition, the *N*-heterocyclic ligands were coordinated to the ruthenium(II) metal ion by using the bis(4,4'-dimethyl-2,2'-bipyridine)ruthenium(II) precursor. The Ru^{II} complex with electron-donor nature revealed considerable weaker luminescence intensity at room temperature in contrast to the one with acceptor capability revealing remarkable luminescence at room temperature in CH$_2$Cl$_2$. Furthermore, 2-(1*H*-[1,2,3]triazol-4-yl)pyridine systems are known to be potential luminescence quenchers at room temperature as soon as they are attached to a ruthenium(II) metal ion. All herein described heteroleptic ruthenium(II) complexes overcame this luminescence quenching and led to room temperature emission in acetonitrile. The highest quantum yield could be found for the Ru^{II} complex **16b** (Φ = 0.02) bearing a nitro group in the para-position of the phenylacetylene subunit.

Experimental Section

Materials and Instrumentation. Unless noted otherwise, all reagents were acquired from commercial sources and used without further purification. Solvents were dried and distilled according to standard procedures and stored under argon. If not specified otherwise solvents were degassed by bubbling with argon 1 h before use. All reactions were performed in air-dried flasks under an argon atmosphere unless stated otherwise. Purification of reaction products was carried out by column chromatography with 40–63 μm silica gel. Analytical thin layer chromatography (TLC) was performed on silica sheets precoated with silica gel 60 F254 and visualization was accomplished with UV light (254 nm). The heteroleptic ruthenium(II) complexes were synthesized by microwave-assisted reactions, using a Biotage Initiator ExpEU (maximum power: 400 W; working frequency: 2450 MHz) with closed reaction vials. During the experiments the temperature and the pressure profiles were detected. 1D-(^{1}H and ^{13}C) and 2D-(^{1}H–^{1}H gCOSY) nuclear magnetic resonance spectra were recorded at 298 K. Chemical shifts are reported in parts per million (ppm, δ scale) relative to the signal of the applied solvent. Coupling constants are given in hertz. Data are reported as follows: multiplicity (ap = apparent, br = broad, s = singlet, d = doublet, t = triplet, q = quartet, m = multiplet).

Computational Details. The geometries of **16a** and **16b** were optimized in the electronic singlet ground state using density functional theory (DFT) with the hybrid functional B3LYP[19,20] and the 6-31G* basis set for all atoms. Relativistic effects were included in the Ru atom, using the ECP-28-mwb Stuttgart/Dresden pseudopotential.[21] For computational ease the structures were reduced by substitution of the decyl chain attached to the triazole ring by a methyl group and in the case of compound **16b**, additionally the hexyloxy group of **16a** was replaced by a methoxy group. The lowest-lying 55 vertical singlet electronic excitation energies were obtained by using TD-DFT at the S$_0$ optimized geometries. This calculation was performed in solution with CH$_2$Cl$_2$ as solvent with the polarization continuum

model,[22,23] (ε = 8.93). All the calculations were performed with the Gaussian03 program package.[24]

1-Ethynyl-4-(hexyloxy)benzene (1).[25] 1-Iodo-4-(hexyloxy)-benzene (1.5 g, 4.93 mmol), tetrakis(triphenylphosphine)-palladium(0) (114 mg, 0.1 mmol), and CuI (20 mg, 0.1 mmol) were dissolved in a degassed NEt$_3$/THF mixture (3:7 ratio, 35 mL) at room temperature. After trimethylsilylacetylene (0.7 mL, 4.93 mmol) was added quickly through a syringe, the solution was stirred for 24 h at room temperature. The salts formed were filtered off, and the solution was evaporated under reduced pressure. The yellow oil was purified by a chromatographic filtration over a silica gel pad (toluene as eluent) yielding pure 1-(trimethylsilyl)ethynyl-4-(hexyloxy)benzene. Subsequently, the silylated compound was dissolved in a mixture of THF and methanol and aq NaOH (5 M, 1 mL) was added. The reaction mixture was stirred overnight at room temperature and then extracted with dichloromethane after adding brine (50 mL). The organic extract was dried over anhydrous MgSO$_4$ and subsequent gel filtration (silica, toluene) afforded the pure, colorless product (0.91 g, 91%).

5-Bromo-2-((trimethylsilyl)ethynyl)pyridine (2).[26] 2,5-Dibromopyridine (3.5 g, 14.8 mmol), tetrakis(triphenylphosphine)-palladium(0) (347 mg, 0.3 mmol), and CuI (57 mg, 0.3 mmol) were dissolved in a degassed NEt$_3$/THF mixture (3:7 ratio, 50 mL) at 0 °C. After trimethylsilylacetylene (2.09 mL, 14.8 mmol) was added quickly through a syringe, the solution was stirred for 2 h at 0 °C and was then allowed to stir at room temperature overnight. The salts formed were filtered off, and the solution was evaporated under reduced pressure. The dark orange oil was purified by a chromatographic filtration over a silica gel pad (toluene as eluent) providing the product as yellow oil, which solidifies upon standing at room temperature after one week. Finally, purification by gentle sublimation (3.3×10^{-2} mbar, 60 °C) afforded the pure product as a white powder (3.25 g, 86%).

2-Ethynyl-5-((4-(hexyloxy)phenyl)ethynyl)pyridine (4). 5-Bromo-2-((trimethylsilyl)ethynyl)pyridine (**2**, 1.0 g, 4 mmol), 1-ethynyl-4-(hexyloxy)benzene (**1**, 0.8 g, 4 mmol), tetrakis(triphenylphosphine)palladium(0) (90 mg, 0.08 mmol), and CuI (16 mg, 0.08 mmol) were dissolved in a degassed NEt$_3$/THF mixture (3:7 ratio, 35 mL) at room temperature and the solution was stirred for 48 h at room temperature. The salts formed were filtered off, and the solution was evaporated under reduced pressure. The dark red oil was purified by a gel filtration over silica (toluene as eluent). The obtained 2-(trimethylsilyl)-ethynyl-5-((4-(hexyloxy)phenyl)ethynyl)pyridine was desilylated by dissolving in THF/MeOH (1:2 ratio, 30 mL) and treating with an equimolar amount of potassium fluoride. The red solution was stirred overnight under an argon atmosphere. After that the reaction mixture was concentrated under vacuum and

(19) Becke, A. D. *J. Chem. Phys.* **1993**, *98*, 5648–5652.
(20) Lee, C. T.; Yang, W. T.; Parr, R. G. *Phys. Rev. B* **1988**, *37*, 785–789.
(21) Andrae, D.; Häusermann, U.; Dolg, M.; Stoll, H.; Preuss, H. *Theor. Chim. Acta* **1990**, *77*, 123–141.
(22) Cossi, M.; Barone, V.; Menucci, B.; Tomasi, J. *Chem. Phys. Lett.* **1998**, *286*, 253–260.
(23) Menucci, B.; Tomasi, J. *J. Chem. Phys.* **1997**, *106*, 5151–5158.

(24) Frisch, M. J.; Trucks, G. W.; Schlegel, H. B.; Scuseria, G. E.; Robb, M. A.; Cheeseman, J. R.; Montgomery, J. A., Jr.; Vreven, T.; Kudin, K. N.; Burant, J. C.; Millam, J. M.; Iyengar, S. S.; Tomasi, J.; Barone, V.; Mennucci, B.; Cossi, M.; Scalmani, G.; Rega, N.; Petersson, G. A.; Nakatsuji, H.; Hada, M.; Ehara, M.; Toyota, K.; Fukuda, R.; Hasegawa, J.; Ishida, M.; Nakajima, T.; Honda, Y.; Kitao, O.; Nakai, H.; Klene, M.; Li, X.; Knox, J. E.; Hratchian, H. P.; Cross, J. B.; Bakken, V.; Adamo, C.; Jaramillo, J.; Gomperts, R.; Stratmann, R. E.; Yazyev, O.; Austin, A. J.; Cammi, R.; Pomelli, C.; Ochterski, J. W.; Ayala, P. Y.; Morokuma, K.; Voth, G. A.; Salvador, P.; Dannenberg, J. J.; Zakrzewski, V. G.; Dapprich, S.; Daniels, A. D.; Strain, M. C.; Farkas, O.; Malick, D. K.; Rabuck, A. D.; Raghavachari, K.; Foresman, J. B.; Ortiz, J. V.; Cui, Q.; Baboul, A. G.; Clifford, S.; Cioslowski, J.; Stefanov, B. B.; Liu, G.; Liashenko, A.; Piskorz, P.; Komaromi, I.; Martin, R. L.; Fox, D. J.; Keith, T.; Al-Laham, M. A.; Peng, C. Y.; Nanayakkara, A.; Challacombe, M.; Gill, P. M. W.; Johnson, B.; Chen, W.; Wong, M. W.; Gonzalez, C.; Pople, J. A. *Gaussian-03*, Revision C.02; Gaussian, Inc., Wallingford, CT, 2004.
(25) Chang, J. Y.; Yeon, J. R.; Shru, Y. S.; Han, M. J.; Hong, S.-K. *Chem. Mater.* **2000**, *12*, 1076–1082.
(26) Bianchini, C.; Giambastiani, G.; Rios, I. G.; Meli, A.; Oberhauser, W.; Sorace, L.; Toti, A. *Organometallics* **2007**, *26*, 5066–5078.

purified by means of gel filtration on silica gel yielding the desired product as a slight yellow powder (1.06 g, 87%). ^{1}H NMR (CDCl$_3$, 300 MHz) δ 8.62 (d, J = 1.3 Hz, 1H), 7.73 (dd, J = 8.1 Hz, J = 2.1 Hz, 1H), 7.49–7.42 (m, 3H), 6.91–6.85 (m, 2H), 3.97 (t, ^3J = 6.6 Hz, 2H), 3.25 (s, 1H), 1.79–1.74 (m, 2H), 1.49–1.30 (m, 6H), 0.91 (t, J = 6.8 Hz, 3H). ^{13}C NMR (CDCl$_3$, 75 MHz) δ 159.8, 152.2, 140.3, 138.1, 133.2, 126.71, 120.7, 114.7, 114.0, 94.9, 84.5, 82.6, 78.6, 68.1, 31.5, 29.1, 25.7, 22.6, 14.0. Anal. Calcd for C$_{21}$H$_{21}$NO: C 83.13, H 6.98, N 4.62. Found: C 82.78, H 7.08, N 4.92.

2-(1-Decyl-1H-[1,2,3]triazol-4-yl)-5-((4-(hexyloxy)phenyl)-ethynyl)pyridine (5). A sealed microwave vial with 1-bromode-cane (91 mg, 0.41 mmol) and 1.5 equiv of sodium azide (40 mg) in DMSO (5 mL) was heated under microwave irradiation for 1 h at 100 °C. Water was then added to quench the reaction and the product was extracted into diethyl ether, washed with brine, and dried over Na$_2$SO$_4$. The solution was subsequently reduced in vacuo to yield 1-azidodecane (95%). The organic azide, 2-ethynyl-5-((4-(hexyloxy)phenyl)ethynyl)pyridine (4, 127 mg, 0.42 mmol), CuSO$_4$ (7 mg, 0.042 mmol, dissolved in 0.5 mL water), and sodium ascorbate (42 mg, 0.21 mmol, dissolved in 1 mL water) were dissolved in THF (15 mL) and the reaction mixture was stirred for 24 h at room temperature. Subsequently, ethylenediaminetetraacetic acid-containing water (60 mL) was added to the reaction mixture and the product was extracted with CH$_2$Cl$_2$. Gel filtration on silica (CHCl$_3$/EtOAc 1:1 ratio) and subsequent column chromatography (silica, CHCl$_3$/EtOAc 20:1 ratio) provided the pure product as white powder (134 mg, 67%). ^{1}H NMR (CDCl$_3$, 300 MHz) δ 8.68 (s, 1H), 8.13–8.11 (m, 2H), 7.86 (dd, J = 8.2 Hz, J = 2.1 Hz, 1H), 7.46–7.42 (m, 2H), 6.86–6.82 (m, 2H), 4.4 (t, J = 7.2 Hz, 2H), 3.97 (t, J = 6.5 Hz, 2H), 1.94–1.88 (m, 2H), 1.79–1.76 (m, 2H), 1.48–1.22 (m, 20H), 0.87–0.81 (m, 6H). ^{13}C NMR (CDCl$_3$, 75 MHz) δ 159.5, 151.6, 148.7, 147.8, 139.0, 133.0, 122.0, 119.6, 119.3, 114.5, 114.3, 93.1, 84.8, 68.0, 50.4, 31.7, 31.5, 30.1, 29.3, 29.2, 29.1, 29.0, 28.9, 26.3, 25.6, 22.5, 22.5, 14.0, 13.9. Anal. Calcd for C$_{31}$H$_{42}$N$_4$O: C 76.50, H 8.70, N 11.51. Found: C 76.52, H 8.79, N 11.71.

4-(6-Ethynylpyridin-3-yl)-2-methylbut-3-yn-2-ol (6).[27] To a degassed solution of 5-bromo-2-[(trimethylsilyl)ethynyl]pyridine (2, 1.5 g, 5.9 mmol), CuI (23 mg, 0.12 mmol), and Pd(PPh$_3$)$_4$ (140 mg, 0.12 mmol) in triethylamine (50 mL) was added 2-methyl-3-butyn-2-ol (0.58 mL, 5.9 mmol) and the reaction mixture was stirred for 24 h at 55 °C. The mixture was diluted with diethyl ether, washed once with brine, and dried over MgSO$_4$. Concentration in vacuo yielded the crude product, which was purified by chromatography on silica gel (chloroform/ethyl acetate 4:1) to afford 5-(3-hydroxy-3-methyl-1-butynyl)-2-[(triisopropylsilyl)-ethynyl]pyridine. To a stirred solution of the latter product in methanol (50 mL) was added solid potassium fluoride (1.5 equiv), and the mixture was stirred at room temperature overnight under an argon atmosphere. Subsequently, the reaction mixture was filtered by means of gel filtration on silica gel (chloroform/ethyl acetate 4:1) and concentrated in vacuo yielding the desired product as an orange powder (670 mg, 61%).

5-Bromo-2-ethynylpyridine (7).[28] To a solution of 2,5-dibromo-pyridine (7 g, 30 mmol), CuI (70 mg, 0.37 mmol), and Pd-(PPh$_3$)$_4$ (260 mg, 0.37 mmol) in degassed NEt$_3$/THF (1:1 ratio, 100 mL) was added trimethylsilylacetylene (4.2 mL, 30 mmol). The mixture was stirred at room temperature overnight under argon atmosphere. After removal of the solvent under reduced pressure, the residue was purified by gel filtration on silica (CHCl$_3$) to yield 2-(trimethylsilyl)ethynyl-5-bromopyridine as off-white powder (6.95 g, 92%). Subsequently, the compound was dissolved in

methanol (80 mL) and treated with aq NaOH (5 M, 12 mL). The yellow solution was stirred overnight, whereupon the solution turned black. Subsequent gel filtration on silica (CHCl$_3$) yielded the product as white powder (3.79 g, 69%).

5-Bromo-2-(1-decyl-1H-[1,2,3]triazol-4-yl)pyridine (8). 5-Bromo-2-ethynylpyridine (7, 1.04 g, 5.45 mmol) and 1-azidodecane (see synthesis of 5, 1.0 g, 5.45 mmol) were dissolved in an ethanol/water mixture (7:1 ratio, 70 mL), using a round-bottomed flask (100 mL). Then copper(II) sulfate (80 mg, 0.5 mmol, dissolved in 3 mL of water) and sodium ascorbate (490 mg, 2.5 mmol, dissolved in 4 mL of water) were added. The reaction mixture turned yellow after a while and was stirred for 72 h at 25 °C. The yellow precipitate was filtered and washed with ethanol. After recrystallization from ethanol the pure product was obtained as colorless crystals (1.35 g, 67%). ^{1}H NMR (CDCl$_3$, 300 MHz) δ 8.61 (s, 1H), 8.09–8.07 (m, 2H), 7.89–7.86 (m, 1H), 4.40 (t, J = 7.2 Hz, 2H), 1.94–1.89 (m, 2H), 1.34–1.24 (m, 14H), 0.87–0.81 (m, 3H). ^{13}C NMR (CDCl$_3$, 75 MHz) δ 150.3, 148.9, 147.4, 139.4, 121.9, 121.3, 119.3, 50.5, 31.8, 30.2, 29.4, 29.3, 29.2, 28.9, 26.4, 22.6, 14.0. Anal. Calcd for C$_{17}$H$_{25}$BrN$_4$: C 55.89, H 6.90, N 15.34. Found: C 56.22, H 7.23, N 14.98.

2-(1-Decyl-1H-[1,2,3]triazol-4-yl)-5-ethynylpyridine (9, Route 1). 4-(6-Ethynylpyridin-3-yl)-2-methylbut-3-yn-2-ol (6, 300 mg, 1.58 mmol) and 1-azidodecane (see synthesis of 5, 275 mg, 1.5 mmol) were dissolved in an ethanol/water mixture (7:3 ratio, 30 mL), using a round-bottomed flask (100 mL). Then copper(II) sulfate (24 mg, 0.15 mmol, dissolved in 1 mL of water) and sodium ascorbate (150 mg, 0.75 mmol, dissolved in 1 mL of water) were added. The reaction mixture turned green after a while and was stirred for 72 h at 50 °C. Subsequently, an excess of water was poured into the reaction mixture (100 mL) and the crude product precipitated and was filtered off. Gel filtration on silica (CHCl$_3$/EtOAc 1:1) provided 4-(6-(1-decyl-1H-[1,2,3]triazole-4-yl)pyridin-3-yl)-2-methylbut-3-yn-2-ol as white powder (490 mg, 85%). This intermediate was dissolved in dry toluene (30 mL). After adding ground NaOH (200 mg, 5 mmol) and KOH (150 mg, 2.6 mmol) the reaction mixture was refluxed for 5 h. Subsequent column chromatography on silica (CHCl$_3$/EtOAc 2:1 ratio) yielded 2-(1-decyl-1H-[1,2,3]-triazole-4-yl)-5-ethynylpyridine as transparent crystals (303 mg, 74%). ^{1}H NMR (CDCl$_3$, 300 MHz) δ 8.67 (d, J = 1.6 Hz, 1H), 8.20–8.14 (m, 2H), 7.89–7.83 (m, 1H), 4.41 (t, J = 7.2 Hz, 2H), 3.25 (s, 1H), 1.95–1.89 (m, 2H), 1.34–1.25 (m, 14H), 0.87 (t, J = 6.5 Hz, 3H). ^{13}C NMR (CDCl$_3$, 75 MHz) δ 152.4, 149.7, 147.7, 139.9, 122.2, 119.3, 118.0, 80.8, 80.5, 50.5, 31.8, 30.2, 29.4, 29.3, 29.2, 28.9, 26.4, 22.6, 14.0. Anal. Calcd for C$_{19}$H$_{26}$N$_4$: C 73.51, H 8.44, N 18.05. Found: C 73.50, H 8.24, N 18.38.

2-(1-Decyl-1H-[1,2,3]triazol-4-yl)-5-ethynylpyridine (9, Route 2). To a solution of 5-bromo-2-(1-decyl-1H-[1,2,3]triazol-4-yl)-pyridine (8, 1.0 g, 2.74 mmol), CuI (13 mg, 0.07 mmol), and Pd(PPh$_3$)$_4$ (80 mg, 0.07 mmol) in degassed NEt$_3$/CH$_2$Cl$_2$ (3:1 ratio, 500 mL) was added trimethylsilylacetylene (280 mg, 2.8 mmol). The mixture was stirred 48 h at room temperature under argon atmosphere. After removal of the solvent under reduced pressure, the residue was purified by gel filtration on silica (chloroform). Afterward, the trimethylsilyl-protected product was dissolved in methanol (40 mL) and treated with aq NaOH (5 M, 1 mL). After 5 h the solvent was removed and the crude product was finally purified by gradient column chromatography on silica (CHCl$_3$, CHCl$_3$/EtOAc 3:1 ratio) yielding the product as white powder (470 mg, 55%).

General Procedure of the Sonogashira Reaction. 2-(1-Decyl-1H-[1,2,3]triazol-4-yl)-5-ethynylpyridine (0.32 mmol), nitro-substituted 1-iodobenzene (0.32 mmol), tetrakis(triphenylphos-phine)palladium(0) (16 mg, 0.012 mmol), and CuI (8 mg, 0.012 mmol) were dissolved in a degassed NEt$_3$/THF mixture (1:1, 10 mL). The solution was stirred for 48 h at 40 °C under argon atmosphere. The salts formed were filtered off, and the solution

(27) Nakano, Y.; Ishizuka, K.; Muraoka, K.; Ohtani, H.; Takayama, Y.; Sato, F. *Org. Lett.* **2004**, *6*, 2373–2376.
(28) Tilley, J. W.; Zawoiski, S. *J. Org. Chem.* **1988**, *53*, 386–390.

was evaporated under reduced pressure. The pure product was isolated by column chromatography over silica.

2-(1-Decyl-1H-[1,2,3]triazol-4-yl)-5-((4-nitrophenyl)ethynyl)-pyridine (10a). According to the general procedure the product was synthesized and purified by column chromatography over silica (CHCl$_3$, R_f 0.6) yielding **10a** as a slight yellow powder (128 mg, 93%). ^{1}H NMR (CDCl$_3$, 300 MHz) δ 8.76 (s, 1H), 8.26–8.16 (m, 4H), 7.94–7.90 (m, 1H), 7.71–7.68 (m, 2H), 4.4 (t, J = 7.2 Hz, 2H), 1.99–1.91 (m, 2H), 1.35–1.25 (m, 14H), 0.87–0.81 (m, 3H). ^{13}C NMR (CDCl$_3$, 75 MHz) δ 152.1, 150.0, 147.6, 147.3, 139.5, 132.4, 129.5, 123.7, 122.4, 119.6, 118.1, 91.3, 90.9, 50.6, 31.8, 30.2, 29.4, 29.3, 29.2, 29.0, 26.5, 22.6, 14.1. ESI-TOF MS: m/z 432.24 ([M + H]$^+$). Anal. Calcd for C$_{25}$H$_{29}$N$_5$O$_2$: C 69.58, H 6.77, N 16.23. Found: C 69.21, H 6.72, N 16.58.

2-(1-Decyl-1H-[1,2,3]triazol-4-yl)-5-((2-nitrophenyl)ethynyl)-pyridine (10b). According to the general procedure the product was synthesized and purified by column chromatography over silica (CHCl$_3$/EtOAc, 5:1 ratio) yielding **10b** as off-white powder (63 mg, 69%). ^{1}H NMR (CDCl$_3$, 300 MHz) δ 8.76 (s, 1H), 8.21–8.10 (m, 3H), 7.97–7.91 (m, 1H), 7.73–7.69 (m, 1H), 7.63–7.60 (m, 1H), 7.53–7.49 (m, 1H), 4.42 (t, J = 7.2 Hz, 2H), 1.99–1.91 (m, 2H), 1.34–1.24 (m, 14H), 0.88 (t, J = 6.7 Hz, 3H). ^{13}C NMR (CDCl$_3$, 75 MHz) δ 152.2, 150.0, 149.5, 147.7, 139.7, 134.6, 132.9, 129.0, 124.8, 122.4, 119.5, 118.1, 93.8, 88.2, 50.6, 31.8, 30.2, 29.4, 29.3, 29.2, 29.0, 26.4, 22.6, 14.1. ESI-HRMS calcd for C$_{25}$H$_{30}$N$_5$O$_2$ ([M + H]$^+$) 432.2394, found 432.2390.

2-(1-Decyl-1H-[1,2,3]triazol-4-yl)-5-((4-trifluoromethyl)phe-nyl)ethynyl)pyridine (10c). According to the general procedure, the product was synthesized and purified by column chromatography over silica (CHCl$_3$, R_f 0.5) yielding **10d** as white powder (81 mg, 94%). ^{1}H NMR (CDCl$_3$, 300 MHz) δ 8.72 (s, 1H), 8.21–8.17 (m, 2H), 7.92–7.88 (m, 1H), 7.68–7.61 (m, 4H), 4.42 (t, J = 7.2 Hz, 2H), 1.96–1.90 (m, 2H), 1.34–1.24 (m, 14H), 0.88 (t, J = 6.7 Hz, 3H). ^{13}C NMR (CDCl$_3$, 75 MHz) δ 152.0, 139.5, 131.9, 126.4, 125.6, 125.5, 125.4, 125.4, 125.3, 122.4, 119.5, 118.5, 91.4, 88.5, 50.6, 31.8, 30.2, 29.5, 29.4, 29.2, 29.0, 26.5, 22.7, 14.1. ESI-HRMS calcd for C$_{26}$H$_{30}$F$_3$N$_4$ ([M + H]$^+$) 455.2417, found 455.2408.

5-((4-Phenyl)ethynyl)-2-(1-phenyl-1H-[1,2,3]triazol-4-yl)pyr-idine (10d). According to the general procedure the product was synthesized and purified by column chromatography over silica (CHCl$_3$/EtOAc, 5:1 ratio) as off-white powder (44 mg, 61%). ^{1}H NMR (CDCl$_3$, 300 MHz) δ 8.74 (s, 1H), 8.16–8.11 (m, 2H), 7.90–7.84 (m, 1H), 7.58–7.54 (m, 2H), 7.39–7.35 (m, 3H), 4.42 (t, J = 7.2 Hz, 2H), 1.96–1.89 (m, 2H), 1.34–1.24 (m, 14H), 0.88 (t, J = 6.7 Hz, 3H). ^{13}C NMR (CDCl$_3$, 75 MHz) δ 151.8, 139.3, 131.7, 128.8, 128.4, 122.6, 122.2, 119.5, 119.4, 93.1, 86.1, 50.6, 31.8, 30.2, 29.4, 29.3, 29.2, 29.0, 26.4, 22.6, 14.1. ESI-HRMS calcd for C$_{25}$H$_{30}$N$_4$Na ([M + Na]$^+$) 409.2363, found 409.2334.

5-Ethynyl-2-(1-phenyl-1H-[1,2,3]triazol-4-yl)pyridine (11). Sodium azide (330 mg, 5.1 mmol) and anhydrous CuSO$_4$ (54 mg, 0.34 mmol) were dissolved in abs methanol (30 mL). Phenylboronic acid (414 mg, 3.4 mmol) was added to the brown solution and the reaction mixture was stirred for 48 h at room temperature. The conversion was controlled by TLC on silica (CHCl$_3$). The slightly green solution was concentrated to 10 mL in vacuum and, subsequently, THF (20 mL), sodium ascorbate (336 mg, 1.7 mmol, in 1 mL of water), 4-(6-ethynylpyridin-3-yl)-2-methylbut-3-yn-2-ol (600 mg, 3.24 mmol), and water (4 mL) were added. The reaction was stirred for 72 h at 50 °C. After that, an excess of water was added to the reaction mixture and the precipitate was filtered off. The filtrate was cautiously extracted with CHCl$_3$ and the organic extract was combined with the precipitate. The CHCl$_3$ solution was dried over NaSO$_4$ and filtered. Column chromatography on silica (CHCl$_3$/EtOAc, 2:1 ratio) provided the (2-methylbut-3-yn-2-ol)-protected product as a white powder. The deprotection was accomplished by refluxing overnight in toluene with ground NaOH

(1.5 equiv). The toluene solution was washed with water and subsequent gel filtration on silica provided the pure desired product (360 mg, 45%). ^{1}H NMR (CDCl$_3$, 300 MHz) δ 8.71 (s, 1H), 8.61 (s, 1H), 8.23 (d, J = 8.2 Hz, 1H), 7.90 (dd, J = 8.2 Hz, J = 2.0 Hz, 1H), 7.83–7.80 (m, 2H), 7.59–7.44 (m, 3H), 3.28 (s, 1H, CH). ^{13}C NMR (CDCl$_3$, 75 MHz) δ 152.5, 149.2, 148.3, 140.0, 136.8, 129.9, 128.9, 120.4, 119.6, 118.3, 81.0, 80.5. Anal. Calcd for C$_{15}$H$_{10}$N$_4$: C 73.16, H 4.09, N 22.75. Found: C 73.49, H 3.78, N 22.50.

5-((4-Nitrophenyl)ethynyl)-2-(1-phenyl-1H-[1,2,3]triazol-4-yl)-pyridine (12). 5-Ethynyl-2-(1-phenyl-1H-[1,2,3]triazol-4-yl)pyr-idine (**11**, 75 mg, 0.3 mmol), 1-iodo-4-nitrobenzene (76 mg, 0.3 mmol), tetrakis(triphenylphosphine)palladium(0) (8 mg, 0.006 mmol), and CuI (2 mg, 0.006 mmol) were dissolved in a degassed NEt$_3$/THF mixture (3:1 ratio, 10 mL) and the solution was stirred for 48 h at 40 °C under argon atmosphere. The solvent was evaporated under reduced pressure. The pure product was isolated by column chromatography over silica (CHCl$_3$) as slightly yellow powder (85 mg, 77%). ^{1}H NMR (CDCl$_3$, 300 MHz) δ 8.80 (s, 1H), 8.65 (s, 1H), 8.32–8.25 (m, 3H), 7.98–7.96. (m, 1H), 7.85–7.82 (m, 2H), 7.74–7.71 (m, 2H), 7.61–7.47 (m, 3H). ^{13}C NMR (CDCl$_3$, 75 MHz) δ 147.3, 143.3, 139.6, 136.9, 132.4, 129.9, 129.1, 123.7, 120.5, 91.2, 91.1 (some carbon signals are missing due to the low solubility of the compound). ESI-HRMS calcd for C$_{21}$H$_{13}$N$_5$O$_2$Na ([M + Na]$^+$) 390.0961, found 390.0940.

2-(1-(4-Bromophenyl)-1H-[1,2,3]triazol-4-yl)pyridine (13). Sodium azide (480 mg, 7.5 mmol) and anhydrous CuSO$_4$ (80 mg, 0.5 mmol) were dissolved in abs methanol (40 mL). (4-Bromo-phenyl)boronic acid (1 g, 5 mmol) was added to the brown solution and the reaction mixture was stirred for 48 h at room temperature. The conversion was controlled by TLC on silica (ethyl acetate). Sodium ascorbate (400 mg, 2 mmol, in 1 mL of water), 2-ethynylpyridine (515 mg, 5 mmol), and water (5 mL) were added. The reaction was stirred for 5 days at 40 °C. After that, an excess of water was added to the reaction mixture and the precipitate was filtered off. The filtrate was cautiously extracted with CHCl$_3$ and the organic extract was combined with the precipitate. The CHCl$_3$ solution was dried over NaSO$_4$ and filtered and the solvent was evaporated. Subsequent recrystallization from ethanol provided the pure product as colorless crystals (905 mg, 61%). ^{1}H NMR (CDCl$_3$, 300 MHz) δ 8.62–8.60 (m, 1H), 8.59 (s, 1H), 8.24–8.21 (m, 1H), 7.83–7.80 (m, 1H), 7.75–7.67 (m, 4H), 7.29–7.26 (m, 1H). ^{13}C NMR (CDCl$_3$, 75 MHz) δ 149.5, 137.0, 133.0, 123.2, 121.8, 120.5, 119.8. Anal. Calcd for C$_{13}$H$_9$BrN$_4$: C 51.85, H 3.01, N 18.60. Found: C 51.76, H 3.09, N 18.69.

2-(1-(4-Ethynylphenyl)-1H-[1,2,3]triazol-4-yl)pyridine (14). 2-(1-(4-Bromophenyl)-1H-[1,2,3]triazol-4-yl)pyridine (**13**, 600 mg, 2 mmol), trimethylsilylacetylene (0.3 mL, 2.05 mmol), tetrakis-(triphenylphosphine)palladium(0) (95 mg, 0.08 mmol) and CuI (18 mg, 0.08 mmol) were dissolved in a degassed NEt$_3$/THF mixture (2:1 ratio, 10 mL) and the reaction mixture was stirred for 24 h at 40 °C under argon atmosphere. The solution was evaporated under reduced pressure. The trimethylsilyl-protected product was isolated by column chromatography over silica (CHCl$_3$). The product was dissolved in a MeOH/THF solvent mixture (2:1 ratio, 30 mL) and treated with aq NaOH (200 mg of NaOH in 3 mL of water). After stirring overnight under an argon atmosphere the final product was purified by column chromatography over silica (CHCl$_3$) and obtained as white powder (340 mg, 69%). ^{1}H NMR (CDCl$_3$, 300 MHz) δ 8.63–8.60 (m, 2H), 8.23–8.20 (m, 1H), 7.84–7.78 (m, 3H), 7.67–7.63 (m, 2H), 7.26–7.21 (m, 1H), 3.19 (s, 1H). ^{13}C NMR (CDCl$_3$, 75 MHz) δ 149.7, 149.5, 136.9, 133.5, 123.1, 122.8, 120.4, 120.0, 119.6, 82.2, 79.0. Anal. Calcd for C$_{15}$H$_{10}$N$_4$: C 73.16, H 4.09, N 22.75. Found: C 73.34, H 4.12, N 23.04.

2-(1-(4-(4-Nitrophenyl)ethynyl)phenyl)-1H-[1,2,3]triazol-4-yl)pyridine (15). 2-(1-(4-Ethynylphenyl)-1H-[1,2,3]triazol-4-yl)-pyridine (**14**, 65 mg, 0.26 mmol), 1-iodo-4-nitrobenzene (68 mg,

Happ et al.

0.27 mmol), tetrakis(triphenylphosphine)palladium(0) (16 mg, 0.006 mmol), and CuI (3 mg, 0.006 mmol) were dissolved in a degassed NEt₃/THF mixture (10:1 ratio, 25 mL) and the solution was stirred for 24 h at 50 °C under argon atmosphere. The solvents were evaporated under reduced pressure and the pure product was obtained by crystallization from chloroform at 5 °C (48 mg, 50%). ¹H NMR (CDCl₃, 300 MHz) δ 8.66–8.62 (m, 2H), 8.25–8.22 (m, 3H), 7.88–7.70 (m, 7H), 7.30–7.26 (m, 1H). ¹³C NMR (CDCl₃, 75 MHz) δ 147.3, 133.4, 132.4, 129.6, 123.7, 122.8, 120.2, 119.6, 93.1 (some carbon signals are missing due to the low solubility of the compound). ESI-TOF MS: *m/z* 368.12 ([M + H]⁺). Anal. Calcd for C₂₁H₁₃N₅O₂: C 68.66, H 3.57, N 19.06. Found: C 68.32, H 3.74, N 19.31.

General Procedure for Complexing the (1*H*-1,2,3-Triazole)-pyridine Ligand to Ru(dmbpy)₂Cl₂. *cis*-Dichlorobis(4,4'-dimethyl-2,2'-bipyridine)ruthenium(II)¹¹ (43 mg, 0.08 mmol) and the respective 1*H*-[1,2,3]triazole ligand (0.08 mmol) were suspended in degassed ethanol (8 mL). After heating under microwave irradiation at 125 °C for 2 h, the red solution was treated with a 10-fold excess of NH₄PF₆ and subsequently stirred until precipitation occurred (10 min to 2 h). The colored precipitate was filtered off and purified by washing twice with ethanol and diethyl ether providing the pure product. In the cases where the ¹H NMR spectrum indicated any impurities, the compound was further purified by recrystallization from ethanol.

Bis(4,4'-dimethyl-2,2'-bipyridine)-{2-(1-decyl-1*H*-[1,2,3]tri-azol-4-yl)-5-((4(hexyloxy)phenyl)ethynyl)pyridine}ruthenium(II) Hexafluorophosphate (16a). According to the above standing general procedure *cis*-dichlorobis(4,4'-dimethyl-2,2'-bipyridine)-ruthenium(II) (30 mg, 0.056 mmol) and 2-(1-decyl-1*H*-[1,2,3]-triazol-4-yl)-5-((4-(hexyloxy)phenyl)ethynyl)pyridine (**5**, 27 mg, 0.056 mmol) were reacted to yield the complex as an orange powder after washing twice with ethanol and diethyl ether (55 mg, 81%). ¹H NMR (CD₃CN, 300 MHz) δ 8.68 (s, 1H), 8.38 (s, 2H), 8.31 (s, 1H), 8.28 (s, 1H), 8.10–8.0 (m, 2H), 7.73–7.61 (m, 4H), 7.50 (d, *J* = 5.8 Hz, 1H), 7.43–7.38 (m, 2H), 7.28–7.22 (m, 3H), 7.17–7.14 (m, 1H), 6.94–6.87 (m, 2H), 4.34 (t, *J* = 7.0 Hz, 2H), 4.0 (t, *J* = 6.5 Hz, 2H), 2.56–2.52 (m, 12H), 1.95–1.92 (m, 4H), 1.83–1.69 (m, 4H), 1.47–1.08 (m, 20H), 0.93–0.86 (m, 6H). ¹³C NMR (CD₃CN, 75 MHz) δ 161.3, 158.1, 157.8, 157.7, 157.5, 153.8, 152.2, 152.1, 152.0, 151.9, 151.21, 151.2, 151.1, 150.9, 150.6, 148.1, 140.5, 134.2, 129.2, 129.0, 128.4, 126.6, 125.9, 125.8, 125.4, 125.0, 123.3, 122.9, 115.8, 113.9, 96.6, 83.8, 69.1, 53.0, 32.6, 32.2, 30.1, 30.0, 29.9, 29.7, 29.3, 26.6, 26.3, 23.3, 23.2, 21.22, 21.2, 21.1, 14.3, 14.2. ESI-TOF MS *m/z* 1101.40 ([M − PF₆]⁺), 478.22 ([M − 2PF₆]²⁺). ESI-HRMS calcd for C₅₅H₆₆N₈ORu [M − 2PF₆]²⁺ 478.2203, found 478.2199.

Bis(4,4'-dimethyl-2,2'-bipyridine)-{2-(1-decyl-1*H*-[1,2,3]triazol-4-yl)-5-((4-nitrophenyl)ethynyl)pyridine}ruthenium(II) Hexafluorophosphate (16b). According to the above standing general procedure *cis*-dichlorobis(4,4'-dimethyl-2,2'-bipyridine)ruthe-nium(II) (35 mg, 0.065 mmol) and 2-(1-decyl-1*H*-[1,2,3]triazol-4-yl)-5-((4-nitrophenyl)ethynyl)pyridine (**10a**, 28 mg, 0.065 mmol) were reacted to yield the pure complex as an orange powder after washing twice with ethanol and diethyl ether (68 mg, 88%). ¹H NMR ((CD₃)₂CO, 300 MHz) δ 9.23 (s, 1H), 8.67–8.60 (m, 4H), 8.42–8.39 (m, 1H), 8.30–8.25 (m, 3H), 8.12–8.08 (m, 2H), 7.96 (d, 1H), 7.87 (d, 1H), 7.78–7.70 (m, 3H), 7.44–7.32 (m, 4H), 4.52 (t, *J* = 7.1 Hz, 2H), 2.58–2.52 (m, 12H), 2.05–2.01 (m, 2H), 1.89–1.79 (m, 2H), 1.25–1.07 (m, 12H), 0.87–0.81 (m, 3H). ¹³C NMR ((CD₃)₂CO, 75 MHz) δ 158.1, 158.0, 157.8, 154.5, 152.4, 152.21, 152.2, 151.2, 151.1, 148.9, 148.2, 141.4, 133.6, 129.4, 129.0, 128.7, 126.0, 125.5, 125.2, 124.7, 123.1, 121.9, 95.6, 89.3, 52.1, 32.6, 26.7, 23.3, 21.2, 14.3. ESI-TOF MS *m/z* 1046.3 ([M − PF₆]⁺), 450.67 ([M − 2PF₆]²⁺). ESI-HRMS calcd for C₄₉H₅₃N₉O₂Ru ([M − 2PF₆]²⁺): 450.6684, found 450.6685.

Bis(4,4'-dimethyl-2,2'-bipyridine)-{2-(1-decyl-1*H*-[1,2,3]tri-azol-4-yl)-5-((4-(trifluoromethyl)phenyl)ethynyl)pyridine}ruthenium-(II) Hexafluorophosphate (16c). According to the above standing general procedure *cis*-dichlorobis(4,4'-dimethyl-2,2'-bipyridine)-ruthenium(II) (30 mg, 0.056 mmol) and 2-(1-decyl-1*H*-[1,2,3]tri-azol-4-yl)-5-((4-(trifluoromethyl)phenyl)ethynyl)pyridine (**10c**, 25 mg, 0.056 mmol) were reacted to yield the pure complex as red powder after recrystallization from ethanol (32 mg, 48%). ¹H NMR (CD₃CN, 300 MHz) δ 8.71 (s, 1H), 8.38 (s, 2H), 8.31–8.27 (m, 2H), 8.11–8.08 (m, 2H), 7.79–7.60 (m, 8H), 7.49–7.46 (m, 1H), 7.28–7.23 (m, 3H), 7.18–7.16 (m, 1H), 4.35 (t, *J* = 7.0 Hz, 2H), 2.56–2.51 (m, 12H), 1.80–1.72 (m, 2H), 1.37–1.07 (m, 14H), 0.89 (t, *J* = 6.7 Hz, 3H). ¹³C NMR (CD₃CN, 75 MHz) δ 157.2, 156.9, 156.7, 156.6, 153.4, 151.3, 151.2, 151.1, 151.0, 150.7, 150.3, 150.3, 150.2, 150.0, 147.1, 140.1, 132.2, 128.2, 128.0, 127.5, 126.0, 125.7, 125.6, 125.0, 124.9, 124.5, 124.1, 122.1, 121.3, 93.2, 86.1, 52.1, 31.6, 29.2, 29.2, 29.1, 29.0, 28.4, 25.6, 22.4, 20.4, 20.3, 20.2, 13.4. ESI-TOF MS *m/z* 1069.30 ([M − PF₆]⁺), 462.17 ([M − 2PF₆]²⁺). ESI-HRMS calcd for C₅₀H₅₃F₉N₈PRu ([M − PF₆]⁺) 1069.3025, found 1069.2993.

Bis(4,4'-dimethyl-2,2'-bipyridine)-{2-(1-decyl-1*H*-[1,2,3]tri-azol-4-yl)-5-((2-nitrophenyl)ethynyl)pyridine}ruthenium(II) Hexafluorophosphate (16d). According to the above standing general procedure *cis*-dichlorobis(4,4'-dimethyl-2,2'-bipyridine)ruthenium-(II) (30 mg, 0.056 mmol) and 2-(1-decyl-1*H*-[1,2,3]triazol-4-yl)-5-((2-nitrophenyl)ethynyl)pyridine (**10b**, 24 mg, 0.056 mmol) were reacted to yield the pure complex as red powder after washing twice with ethanol and diethyl ether (59 mg, 90%). ¹H NMR (CD₃CN, 300 MHz) δ 8.71 (s, 1H), 8.38–8.29 (m, 4H), 8.13–8.09 (m, 3H), 7.74–7.53 (m, 8H), 7.27–7.23 (m, 3H), 7.17–7.15 (m, 1H), 4.35 (t, *J* = 7.0 Hz, 2H), 2.58–2.52 (m, 12H), 1.80–1.72 (m, 2H), 1.37–1.07 (m, 14H), 0.89 (t, *J* = 6.7 Hz, 3H). ¹³C NMR (CD₃-CN, 75 MHz) δ 158.1, 157.8, 157.7, 157.5, 154.5, 152.2, 152.2, 152.0, 151.8, 151.6, 151.3, 151.2, 150.9, 147.9, 140.5, 135.5, 134.6, 131.5, 129.2, 129.0, 128.4, 127.0, 126.0, 125.9, 125.8, 125.4, 125.1, 123.0, 122.1, 91.4, 91.2, 53.1, 32.6, 30.1, 30.1, 30.0, 29.9, 29.3, 26.6, 23.3, 21.3, 21.2, 21.1, 14.3. ESI-TOF MS *m/z* 1046.30 ([M − PF₆]⁺), 450.67 ([M − 2PF₆]²⁺). ESI-HRMS calcd for C₄₉H₅₃F₆N₉O₂PRu ([M − PF₆]⁺) 1046.3002, found 1046.2997.

Bis(4,4'-dimethyl-2,2'-bipyridine)-{5-((4-phenyl)ethynyl)-2-(1-phenyl-1*H*-[1,2,3]triazol-4-yl)pyridine}ruthenium(II) Hexafluoro-phosphate (16e). According to the above-mentioned general procedure *cis*-dichlorobis(4,4'-dimethyl-2,2'-bipyridine)ruthenium(II) (30 mg, 0.056 mmol) and 5-((4-phenyl)ethynyl)-2-(1-phenyl-1*H*-[1,2,3]triazol-4-yl)pyridine (**10d**, 23 mg, 0.056 mmol) were reacted to yield the pure complex as red powder after washing twice with ethanol and diethyl ether (48 mg, 75%). ¹H NMR (CD₃CN, 300 MHz) δ 8.69 (s, 1H), 8.37–8.27 (m, 4H), 8.11–8.05 (m, 2H), 7.75–7.72 (m, 2H), 7.66–7.62 (m, 2H), 7.50–7.39 (m, 6H), 7.27–7.24 (m, 3H), 7.18–7.16 (m, 1H), 4.34 (t, *J* = 7.0 Hz, 2H), 2.56–2.51 (m, 12H), 1.79–1.71 (m, 2H), 1.37–1.06 (m, 14H), 0.89 (t, *J* = 6.7 Hz, 3H). ¹³C NMR (CD₃CN, 75 MHz) δ 157.2, 156.9, 156.7, 156.6, 153.2, 151.3, 151.2, 151.1, 151.0, 150.3, 150.3, 150.2, 150.2, 150.0, 147.1, 139.9, 131.6, 129.7, 128.8, 128.2, 128.0, 127.5, 125.8, 125.0, 124.9, 124.5, 124.1, 122.0, 121.9, 121.4, 95.0, 83.9, 52.1, 31.6, 29.2, 29.1, 29.0, 28.4, 25.6, 22.4, 20.3, 20.2, 13.4. ESI-TOF MS *m/z* 1001.32 ([M − PF₆]⁺), 428.18 ([M − 2PF₆]²⁺). ESI-HRMS calcd for C₄₉H₅₄F₆N₈PRu [M − PF₆]⁺ 1001.3151, found 1001.3168.

Bis(4,4'-dimethyl-2,2'-bipyridine)-{5-((4-nitrophenyl)ethynyl)-2-(1-phenyl-1*H*-[1,2,3]triazol-4-yl)pyridine}ruthenium(II) Hexafluorophosphate (17). According to the above standing general procedure Ru(dmbpy)₂Cl₂ (35 mg, 0.065 mmol) and 5-((4-nitrophenyl)ethynyl)-2-(1-phenyl-1*H*-[1,2,3]triazol-4-yl)pyridine (**12**, 24 mg, 0.065 mmol) were reacted to yield the pure complex as red powder after washing twice with ethanol and diethyl ether (45 mg, 63%). ¹H NMR (CD₃CN, 300 MHz) δ 9.24 (s, 1H), 8.39 (s, 2H), 8.33–8.18 (m, 6H), 7.86 (s, 1H), 7.79–7.76 (m, 2H),

7.71–7.53 (m, 9H), 7.29–7.25 (m, 3H), 7.17 (m, 1H), 2.56–2.53 (m, 12H). ^{13}C NMR (CD$_3$CN, 75 MHz) δ 157.1, 156.8, 156.7, 156.5, 153.7, 151.5, 151.4, 151.0, 150.9, 150.5, 150.5, 150.4, 150.4, 150.2, 148.0, 140.4, 136.1, 132.7, 130.3, 130.1, 128.3, 128.2, 128.0, 127.5, 125.0, 124.9, 124.6, 124.2, 123.9, 122.2, 121.4, 120.7, 92.9, 88.2, 20.3, 20.3, 20.2. ESI-TOF MS *m/z* 982.17 ([M − PF$_6$]$^+$). ESI-HRMS calcd for C$_{45}$H$_{37}$F$_6$N$_9$O$_2$PRu ([M − PF$_6$]$^+$) 982.1750, found 982.1776.

Bis(4,4′-dimethyl-2,2′-bipyridine)-{2-(1-(4-((4-nitrophenyl)-ethynyl)phenyl)-1*H*-[1,2,3]triazol-4-yl)pyridine}ruthenium(II) Hexa-fluorophosphate (18). According to the above standing general procedure Ru(dmbpy)$_2$Cl$_2$ (25 mg, 0.046 mmol) and 2-(1-(4-((4-nitrophenyl)ethynyl)phenyl)-1*H*-[1,2,3]triazol-4-yl)pyridine (15, 17 mg, 0.046 mmol) were reacted 2.5 h to yield the pure complex as red powder after washing twice with ethanol and diethyl ether (40 mg, 77%). ^{1}H NMR (CD$_3$CN, 300 MHz) δ 9.25 (s, 1H), 8.38–8.32 (m, 4H), 8.25–8.21 (m, 2H), 8.17–8.15 (m, 1H), 8.03–8.0 (m, 1H), 7.83–7.73 (m, 7H), 7.71–7.58 (m, 4H), 7.36–7.19 (m, 5H), 2.55–2.51 (m, 12H). ^{13}C NMR (CD$_3$CN, 75 MHz) δ 157.2, 156.8, 156.8, 156.5, 151.7, 151.3, 151.1, 151.1, 150.8, 150.6, 150.4, 150.3, 150.1, 148.7, 147.6, 138.1, 136.1, 133.4, 132.5, 129.0, 128.3, 128.2, 127.5, 126.2, 124.9, 124.8, 124.6, 124.2, 123.9, 123.8, 123.4, 122.7, 120.8, 92.1, 89.4, 20.3, 20.3. ESI-TOF MS *m/z* 982.17 ([M − PF$_6$]$^+$). ESI-HRMS calcd for C$_{45}$H$_{37}$F$_6$N$_9$O$_2$PRu ([M − PF$_6$]$^+$) 982.1750, found 982.1759.

Supporting Information Available: UV−vis absorption and emission spectra for the ligands and corresponding ruthenium complexes, crystallographic data for **17**, computational details of **16a** and **16b** (Cartesian coordinates and total energies), and ^{1}H and ^{13}C NMR spectra of all new compounds. This material is available free of charge via the Internet at http://pubs.acs.org.

Publication A2

THE RADIATIVE DECAY RATES TUNE THE EMISSIVE PROPERTIES OF
RU(II)POLYPYRIDYL COMPLEXES. A COMPUTATIONAL STUDY

Daniel Escudero, Bobby Happ, Andreas Winter, Martin D. Hager, Ulrich S. Schubert,
Leticia González*

The Radiative Decay Rates Tune the Emissive Properties of Ruthenium(II) Polypyridyl Complexes: A Computational Study

Daniel Escudero,[a] Bobby Happ,[b, c] Andreas Winter,[b, c] Martin D. Hager,[b, c] Ulrich S. Schubert,[b, c] and Leticia González*[a]

Ru[II] polypyridyl complexes are promising candidates for use as light harvesting antennas in, e.g., artificial photosynthesis,[1–3] light-driven catalysis,[4–5] and dye-sensitized solar cells (DSSCs),[6–7] due to a combination of optimal chemical, electrochemical, and photophysical properties. The rationalization of the photophysical processes, that is, absorption and emission properties and of the excited-state lifetimes of the radiative and nonradiative processes, is fundamental to achieve an optimal behavior of photochemical devices.[8–9] For instance, to avoid recombination processes in DSSCs and artificial photosynthesis devices, long lifetimes of the excited states of Ru[II] polypyridyl complexes are desired. For the well-known $[Ru(bpy)_3]^{2+}$ (bpy = bipyridine) complex, femtosecond transient absorption experiments have shown that, upon excitation to the first singlet excited states (absorption maximum around 450 nm), ultrafast intersystem crossing (ISC) occurs in less than 100 fs,[10–11] leading to the formation of triplet states with near-unity quantum yield, and hence demonstrated that relaxation processes are dominated by the decay of the triplets rather than by spin-allowed fluorescence from the excited single states.[10] Still, fluorescence bands are often detected and evidence is increasing that intramolecular energy redistribution occurs within the manifold of singlet states, prior to the ISC, as it has been demonstrated for $[Fe^{II}(bpy)_3]^{2+}$.[12] Both singlet and triplet excited states have been theoretically assigned as singlet and triplet

metal-to-ligand charge transfer states (^{1}MLCT and ^{3}MLCT, respectively) by using time-dependent density functional theory (TD-DFT) calculations.[13] The ultrafast nature of the ISC processes is thus not surprising, as strong spin-orbit couplings (SOC) are expected in states with participation of the metal ion. The ^{3}MLCT manifold then decays to the lowest triplet excited state because lifetimes of hundreds of nanoseconds are obtained—rates, which, in turn, depend on the sample conditions (i.e., the solvent and room temperature).[10]

In this contribution, we investigate the emissive properties of the heteroleptic Ru[II] polypyridyl complexes shown in Scheme 1 from the computational viewpoint. Both complexes bear two 4,4-dimethyl-2,2′-bipyridine ligands (dmbpy) and a bidentate 2-(1H-1,2,3-triazol-4-yl)pyridine ligand (L). The electron-donating ($-OC_6H_{13}$) or electron-withdrawing ($-NO_2$) peripheral substitution on the phenylacetylene moiety attached to the ligand L yields complexes **1** and **2**, respectively.
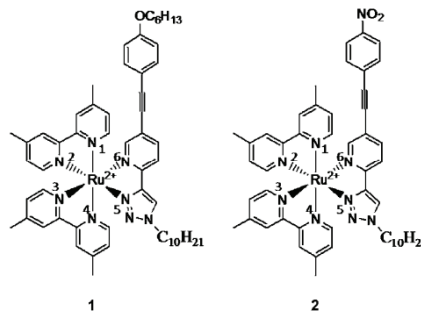
Scheme 1. Chemical structure of complexes **1** and **2**.

In a recent manuscript, the synthesis and spectroscopic and electrochemical properties of these complexes were experimentally presented.[14] Table 1 collects the emission data of complexes **1** and **2** recorded in dichloromethane and acetonitrile (the emission spectra are presented in Figure S1 in the Supporting Information). Astonishingly, the measured emissive behavior reveals a clear dependency on the electronic character of the peripheral substitution as well as on the polarity of the solvent. The nitro-substituted compound

[a] Dr. D. Escudero,# Prof. Dr. L. González+
Institute of Physical Chemistry (IPC)
Friedrich-Schiller-University Jena
Helmholtzweg 4, 07743 Jena (Germany)

[b] B. Happ, A. Winter, M. D. Hager, Prof. Dr. U. S. Schubert
Laboratory of Organic and Macromolecular Chemistry (IOMC)
Friedrich-Schiller-University Jena
Humboldtstraße 10, 07743 Jena (Germany)

[c] B. Happ, A. Winter, M. D. Hager, Prof. Dr. U. S. Schubert
Jena Center for Soft Matter (JCSM)
Friedrich-Schiller-University Jena
Humboldtstraße 10, 07743 Jena (Germany)

[+] Present address:
Institute of Theoretical Chemistry University of Vienna
Währinger St. 17, 1090 Vienna (Austria)
E-mail: leticia.gonzalez@univie.ac.at

[#] Present address:
Max-Planck Institut für Kohlenforschung Kaiser-Wilhelm-Platz 1
45470 Mülheim an der Ruhr (Germany)

Supporting information for this article is available on the WWW under http://dx.doi.org/10.1002/asia.201100864.

COMMUNICATION

Table 1. Emission data of complexes **1** and **2**.

Compd.	λ_{ems} [nm (eV)][a]	Φ_P[a]	λ_{ems} [nm (eV)][b]	Φ_P[b]	Solvent shift λ_{ems} [eV]
1	594 (2.089)	<0.005	602 (2.061)	0.001	0.028
2	647 (1.918)	0.022	674 (1.841)	0.001	0.077

[a] Measured in CH_2Cl_2. [b] Measured in MeCN.

2 shows an almost one order of magnitude higher phosphorescence quantum yield (Φ_P) in dichloromethane than the electron-donor-substituted compound **1**. On the contrary, in a more polar solvent, similar Φ_P values are registered for both complexes. A similar solvent-dependent luminescence has been reported recently by Turro et al.[15–16] for similar Ru^{II} polypyridyl complexes, thereby illustrating that the solvent plays a crucial role not only in determining the phosphorescence quantum yield but also in biasing the emission profile. Although the phosphorescence quantum yields Φ_P are a subtle balance between radiative and nonradiative decay rates [k_r and k_{nr}, respectively; see Eq. (1)], it is generally assumed that the nonradiative rate constant dominates. The calculation of the nonradiative decay rates k_{nr} is complicated and, therefore, they are usually empirically estimated from the energy gap law.[17] According to Equation (2), the k_{nr} values increase exponentially with decreasing T_1–S_0 gaps.

$$\Phi_P = \frac{k_r}{k_r + k_{nr}} \tag{1}$$

$$k_{nr}(T_1 \rightarrow S_0) \propto \exp\{-\beta[\Delta E(T_1 - S_0)]\} \tag{2}$$

The parameter β depends on the structural distortion undergone by the S_0 minimum when relaxing to the emitting T_1 equilibrium geometry. The larger the distortions are, the higher k_{nr} values become. The exponential dependence of k_{nr} on the T_1–S_0 energy gap was shown to hold true for related Ru^{II} and Os^{II} polypyridyl complexes[18–19]; thus, similar β values could be assumed for complexes **1** and **2**.

Puzzling enough, the phosphorescence behavior of complexes **1** and **2** cannot be explained solely by the energy gap rule. Since complex **2** has—regardless of the solvent—lower emission maxima (lower T_1–S_0 gap) than complex **1**, a larger k_{nr} value for complex **2** is expected. Excluding the k_r values, smaller Φ_P yields should then be expected for complex **2**. However, as seen in Table 1, an almost one order of magnitude higher Φ_P is obtained in CH_2Cl_2, thus providing evidence that rates k_r are also mandatory to estimate Φ_P.

In contrast to k_{nr}, the radiative rates k_r from a triplet excited state (T_m) to the ground state (S_0) can be computed with Equation (3), an expression effectively employed for other transition metal complexes.[20–22]

$$k_r^\alpha(T_m \rightarrow S_0) = \frac{\eta^2}{1.5} \left\{ \sum_n \frac{|\langle T_m^\alpha | H_{SOC} | S_n \rangle|}{\chi_n^{1/2} |(\chi_n - 1)|} \cdot f_n^{1/2} \right\}^2 \tag{3}$$

In this expression χ_n is defined as $E(S_n)/E(T_m)$, f_n denotes the associated oscillator strengths of the $S_n \rightarrow S_0$ transitions,

and η is the refractive index of the medium. As one can see, the rates are directly proportional to the SOC and to the f_n values. Furthermore, k_r values depend strongly on the energy difference between the manifold of singlet and triplet excited states; hence, an efficient transfer of the population to the triplet emissive states requires the interacting states lying close in energy. The calculation of SOCs in transition metal complexes is nevertheless not routine. In recent papers they have been estimated from TD-DFT[20–22] as well as from quadratic response TD-DFT calculations;[23] in part because the excitation energies and the f_n values of Ru^{II} polypyridyl complexes calculated with hybrid functionals in the presence of solvent effects are in very good agreement with the experiment,[14,24–27] and in part because multiconfigurational calculations are extraordinarily demanding in these cases.[28] In this work we applied a mixed PCM-TD-DFT/CASSCF (PCM, polarizable continuum model; CASSCF, complete active space self-consistent field) methodology to compute the k_r values. The SOCs are evaluated with accurate CASSCF(8,7) multiconfigurational wavefunctions whilst the energies of the electronic states as well as the associated f_n are evaluated with the PCM-TD-B3LYP protocol (further details are given in the Supporting Information). Note that individual phosphorescence rates for the three possible spin sublevels (T_m^x, T_m^y and T_m^z) can be only experimentally determined in the limit of large fine-structure splittings and at low temperatures. At the high temperature limit, spin relaxation is usually fast and the triplet levels are almost equally populated. As a consequence, only weighted phosphorescence rates can be measured under experimental conditions. Here, these will be calculated according to Equation (4).

$$k_r = \frac{1}{3} \sum_\alpha k_r^\alpha \tag{4}$$

In the computation of the k_r values, the following further assumptions have been made: 1) Because of the ultrafast nature of the ISC process, the relative energies, oscillator strengths, and SOCs have been computed at the S_0 geometry. Indeed, there is direct experimental evidence that the actual excited state geometries are only slightly distorted with respect to the ground state geometries.[29] 2) The photophysical picture is restricted below the λ_{exp} of the photoluminescence experiments (443 nm).

The Jablonski diagrams computed for complexes **1** and **2** help rationalizing the larger Φ_P measured in complex **2** in CH_2Cl_2. The main singlet–singlet and singlet–triplet electronic excitations computed in CH_2Cl_2 at the S_0 geometry as well as some important triplet excited states at the T_1 geometry are depicted in Figure 1a and 1b for complexes **1** and **2**, respectively. The corresponding assignment and oscillator strengths of the singlet and triplet states are shown in Tables S1 and S2 in the Supporting Information. The main absolute SOC matrix elements at the CASSCF(8,7) level of theory between the manifold of singlet and triplet excited states for the three possible spin sublevels (T_m^x, T_m^y and

Emissive Properties of Ruthenium(II) Polypyridyl Complexes
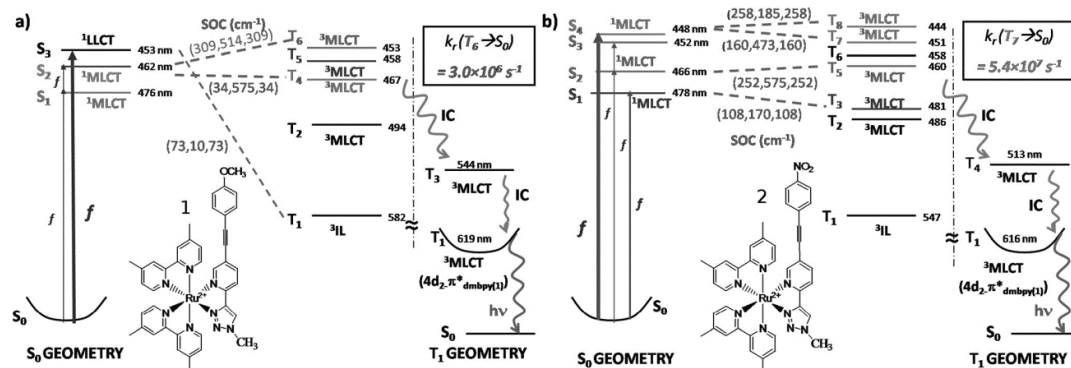
Figure 1. Jablonski diagrams of a) complex **1** and b) complex **2**, with PCM(CH$_2$Cl$_2$)-TD-B3LYP singlet–singlet and singlet–triplet vertical excitations (in nm). The main absolute SOC (cm^{-1}) and the main k_r values (s^{-1}) are highlighted. The magnitude of the oscillator strengths at the S$_0$ geometry is pictorially indicated by the width of the vertical transition.

$T_m{}^z$) are also included in Figure 1 (the description of the CASSCF states and involved orbitals are collected in Table S3 and Figure S2 in the Supporting Information). Not surprisingly, the biggest SOC elements are obtained between ^{1}MLCT and ^{3}MLCT states, particularly those possessing the same π^* orbital but with participation of different 4d orbitals (the case of S$_2$ interacting with T$_6$ in complex **1** or with T$_5$ in complex **2**, see Figure 1).

Only the largest k_r obtained for each complex is shown in Figure 1; the remaining k_r values are collected in Table 2. Noteworthy, in general the k_r values for complex **2** are approximately one order of magnitude larger than for complex **1**. The highest k_r value for complex **1** amounts to k_r(T$_6 \rightarrow$ S$_0$)$=3.0\times10^6$ s^{-1} while that for complex **2** is k_r(T$_7 \rightarrow$S$_0$)$= 5.4\times10^7$ s^{-1}. A detailed analysis reveals that in complex **1** the largest radiative rate is due to the interaction of T$_6$ and S$_2$, both states of MLCT character at the S$_0$ geometry. From T$_6$, internal conversion (IC) processes lead to the lowest T$_1$, which is the emissive state as stated by Kasha's rule.[30] In the case of complex **2**, the ISC is due to the interaction of T$_7$ with S$_4$ at the Franck–Condon geometry and further IC to T$_1$ follows. In both complexes, the T$_1$ state is a ^{3}MLCT state with 4d$_{2-} \rightarrow \pi^*_{dmbpy}$ character, as reflected by both the spin-density analysis (Figure S3 in the Supporting Informa-

tion) and the TD-DFT calculations at the T$_1$ geometry (Table S2 in the Supporting Information). The reason behind the different orders of magnitude in the radiative rates can be directly correlated with the electronic nature of the substituent.

Electron-rich substituents on the ligand L (complex **1**) stabilize and destabilize the related π_L and π^*_L orbitals, respectively. As a consequence, less ^{1}MLCT states are excited below the λ_{exp}. Moreover, in complex **2**, CT transitions to the ligand L with high oscillator strengths (Table S1 in the Supporting Information) are additionally present below the experimental excitation wavelength. The presence of these states is vital to provide smaller ^{1}MLCT–^{3}MLCT gaps that contribute to a more efficient horizontal ISC and thus a larger radiative rate constant in complex **2** in comparison to complex **1**.

In summary: Since higher k_r values imply higher Φ_P, as deduced from Equation 1, the increase in the expected k_{nr} values for complex **2**, as compared to complex **1**, is overcompensated. Therefore, the combination of both effects finally leads to higher Φ_P values for complex **2**.

In the following, we address the influence of solvent effects. As already pointed out, the emissive behavior of complexes **1** and **2** is highly solvent-dependent. Not only the Φ_P values are different but also the emission maxima show a remarkable dependency on the environment. The emission maximum of **1** shifts from 594 nm in CH$_2$Cl$_2$ to 602 nm in CH$_3$CN (a red-shift of ca. 0.03 eV, see Table 1). The change of the solvent also shifts the emission in complex **2** by approximately 0.08 eV to the red. Similar red-shifts in the emission maximum of other Ru^{II} polypyridyl complexes when going from CH$_2$Cl$_2$ to CH$_3$CN have been previously reported.[15–16,31] Interestingly, in CH$_3$CN, a similar weak phosphorescence ($\Phi_P=0.001$) is observed regardless of the lateral substitution on L. In principle, the diminished Φ_P values in CH$_3$CN when compared to those in CH$_2$Cl$_2$ could be correlated with the observed red-shifts of the emission

Table 2. Computed phosphorescence k_r(T$_m \rightarrow$S$_0$) (s^{-1}) for the Ru^{II} complexes **1** and **2**. T$_m$ stands for the mth singlet–triplet excitation at the S$_0$ geometry.

	1 (CH$_2$Cl$_2$)	**1** (CH$_3$CN)	**2** (CH$_2$Cl$_2$)	**2** (CH$_3$CN)
k_r(T$_1 \rightarrow$S$_0$)	2.77×10^3	3.07×10^2	6.64×10^3	1.51×10^4
k_r(T$_2 \rightarrow$S$_0$)	1.84×10^4	8.10×10^5	2.10×10^4	4.46×10^5
k_r(T$_3 \rightarrow$S$_0$)	4.09×10^4	6.88×10^5	2.86×10^5	3.75×10^7
k_r(T$_4 \rightarrow$S$_0$)	2.30×10^6	1.19×10^6	6.84×10^6	3.46×10^5
k_r(T$_5 \rightarrow$S$_0$)	8.48×10^5	6.75×10^5	1.02×10^6	7.98×10^6
k_r(T$_6 \rightarrow$S$_0$)	2.99×10^6	1.31×10^7	1.15×10^5	4.36×10^5
k_r(T$_7 \rightarrow$S$_0$)	9.29×10^4	2.84×10^7	5.38×10^7	2.76×10^8
k_r(T$_8 \rightarrow$S$_0$)	–	–	2.94×10^7	3.56×10^8

COMMUNICATION

maximum and their concomitant repercussion from the energy gap law. In complex **2**, where the red-shift is more pronounced than in complex **1**, the decrease in Φ_P is more remarkable: Φ_P is 22 times lower in **2** in CH_3CN but only 5 times lower in **1**. Apparently, this behavior is, contrary to substitution on the ligand, mainly governed by the energy gap law. Solvent effects are typically more complicated to rationalize than substitution effects. For example, temperature-dependent emission experiments and ultrafast transient spectroscopy have recently shown that a solvent-induced light-switch between competitive emissive states that possess different emissive properties might be operative for several Ru^{II} polypyridyl complexes.[32–33] It is therefore concluded that solvent polarity affects the competition between triplet states, favoring or disfavoring the interconversion between them, and, hence, biasing the emissive properties. Additionally, Chergui et. al have observed a solvent dependence on the relaxation dynamics of several $Re(bpy)(CO)_n$ complexes.[34] It was concluded that solvent molecules are close to the metal center in these complexes and therefore actively participate in the intramolecular charge separation. Such processes are very likely not to occur on Ru^{II} polypyridyl complexes because the interaction of the solvent molecules with the shielded metal centers is expected to be poor.

To gain some insight into the underlying reasons for the large decrease in Φ_P, especially in the case of complex **2**, TD-DFT calculations in the presence of CH_3CN have also been performed. The corresponding lowest-lying PCM-(CH_3CN)-TD-B3LYP singlet–singlet and singlet–triplet electronic excitations computed at the S_0 and T_1 geometries are also presented in Tables S1 and S2 in the Supporting Information. In both complexes the emissive state (T_1) is also the ^{3}MLCT of $4d_{2-} \rightarrow \pi^*_{dmbpy}$ character. The photophysical picture of the lowest-lying triplet excited states at the T_1 geometry is globally maintained when going from CH_2Cl_2 to CH_3CN (Table S2 in the Supporting Information). There are negligible changes in the ordering of the lowest-lying triplet excited states (e.g., the T_2 state of $\pi_L \rightarrow \pi^*_L$ character is ca. 30 and 60 nm below the T_1 state for complexes **1** and **2**, respectively, irrespective of the solvent) due to changes in solvent polarity. Therefore, the hypothesis of solvent light-switch of the emissive state appears less plausible for complexes **1** and **2**. Intrigued by these results we have also computed the k_r values in CH_3CN solution (Table 2). The largest k_r values are $k_r(T_7 \rightarrow S_0) = 2.8 \times 10^7$ s^{-1} and $k_r(T_8 \rightarrow S_0) = 3.6 \times 10^8$ s^{-1}, for complexes **1** and **2**, respectively. Interestingly, the radiative rate constants are higher for both complexes in CH_3CN than in CH_2Cl_2, a trend that is more enhanced in complex **1** than in **2**. Despite the higher k_r values in CH_3CN, the decrease in the phosphorescence quantum yield Φ_P is still in accord with the energy gap law. Both facts—a more enhanced k_{nr} value and a less enhanced k_r value for complex **2** as compared to complex **1**—are the underlying reasons that finally lead to similar quantum yields for both complexes in CH_3CN.

Summarizing, the present communication addresses experimentally and computationally the effect of ligand substitution and the nature of the solvent on the emissive properties of two Ru^{II} polypyridyl complexes. Radiative rate constants have been computed using a mixed TD-DFT/CASSCF approach. While it is generally believed that the phosphorescence quantum yields of Ru^{II} polypyridyl complexes are mainly governed by the nonradiative k_{nr} values, that is, by the energy gap law, here we demonstrate that the radiative k_r rate constants also need to be considered. The rationalization of the emissive properties of complexes **1** and **2** is only possible after computing the corresponding k_r values. This change of paradigm should be useful to understand the underlying ultrafast excited state processes after light excitation of other Ru^{II} polypyridyl complexes. Linking theory and experiment can contribute to the design of new ruthenium complexes with optimized photophysical properties for potential applications, such as solar energy conversion.

Acknowledgements

[1] D. Gust, T. A. Moore, A. L. Moore, *Acc. Chem. Res.* **2009**, *42*, 1890–1898.

[2] S. Rau, B. Schäfer, D. Gleich, E. Anders, M. Rudolph, M. Friedrich, H. Görls, W. Henry, J. G. Vos, *Angew. Chem.* **2006**, *118*, 6361–6364; *Angew. Chem. Int. Ed.* **2006**, *45*, 6215–6218.

[3] S. Tschierlei, M. Karnahl, M. Presselt, B. Dietzek, J. Guthmuller, L. González, M. Schmitt, S. Rau, J. Popp, *Angew. Chem.* **2010**, *122*, 4073–4076; *Angew. Chem. Int. Ed.* **2010**, *49*, 3981–3984.

[4] J. J. Concepcion, J. W. Jurss, M. K. Brennaman, P. G. Hoertz, A. O. T. Patrocinio, N. Y. M. Iha, J. L. Templeton, T. J. Meyer, *Acc. Chem. Res.* **2009**, *42*, 1954–1965.

[5] S. Romain, L. Vigara, A. Llobet, *Acc. Chem. Res.* **2009**, *42*, 1944–1953.

[6] M. Grätzel, *Nature* **2001**, *414*, 338–344.

[7] A. Hagfeldt, M. Grätzel, *Acc. Chem. Res.* **2000**, *33*, 269–277.

[8] V. Balzani, A. Credi, M. Venturi, *ChemSusChem* **2008**, *1*, 26–58.

[9] V. Balzani, A. Juris, M. Venturi, S. Campagna, S. Serroni, *Chem. Rev.* **1996**, *96*, 759–834.

[10] A. Cannizzo, F. van Mourik, W. Gawelda, G. Zgrablic, C. Bressler, M. Chergui, *Angew. Chem.* **2006**, *118*, 3246–3248; *Angew. Chem. Int. Ed.* **2006**, *45*, 3174–3176.

[11] A. C. Bhasikuttan, M. Suzuki, S. Nakashima, T. Okada, *J. Am. Chem. Soc.* **2002**, *124*, 8398–8405.

[12] W. Gawelda, A. Canizzo, V.-T. Pham, F. van Mourik, C. Bressler, M. Chergui, *J. Am. Chem. Soc.* **2007**, *129*, 8199–8206.

[13] M. F. Charlot, Y. Pellegrin, A. Quaranta, W. Leibl, A. Aukauloo, *Chem. Eur. J.* **2006**, *12*, 796–812.

[14] B. Happ, D. Escudero, M. D. Hager, C. Friebe, A. Winter, H. Görls, E. Altuntaş, L. González, U. S. Schubert, *J. Org. Chem.* **2010**, *75*, 4025–4038.

[15] Y. Sun, C. Turro, *Inorg. Chem.* **2010**, *49*, 5025–5032.

[16] R. B. Nair, B. M. Cullum, C. J. Murphy, *Inorg. Chem.* **1997**, *36*, 962–965.

Emissive Properties of Ruthenium(II) Polypyridyl Complexes

[17] J. S. Wilson, N. Chawdhury, M. R. A. Al-Mandhary, M. Younus, M. S. Khan, P. R. Raithby, A. Köhler, R. H. Friend, *J. Am. Chem. Soc.* **2001**, *123*, 9412–9417.

[18] J. A. Treadway, B. Loeb, R. Lopez, P. A. Anderson, F. R. Keene, T. J. Meyer, *Inorg. Chem.* **1996**, *35*, 2242–2246.

[19] E. M. Kober, J. V. Caspar, R. S. Lumpkin, T. J. Meyer, *J. Phys. Chem.* **1986**, *90*, 3722–3734.

[20] G. S.-M. Tong, C.-M. Che, *Chem. Eur. J.* **2009**, *15*, 7225–7237.

[21] G. S. M. Tong, P. K. Chow, C.-M. Che, *Angew. Chem.* **2010**, *122*, 9392–9395; *Angew. Chem. Int. Ed.* **2010**, *49*, 9206–9209.

[22] Z. A. Siddique, Y. Yamamoto, T. Ohno, K. Nozaki, *Inorg. Chem.* **2003**, *42*, 6366–6378.

[23] B. Minaev, H. Ågren, F. D. Angelis, *Chem. Phys.* **2009**, *358*, 245–257.

[24] A. Vlček Jr, S. Záliš, *Coord. Chem. Rev.* **2007**, *251*, 258–287.

[25] M.-F. Charlot, A. Aukauloo, *J. Phys. Chem. A* **2007**, *111*, 11661–11672.

[26] A. Abbotto, C. Barolo, L. Bellotto, F. D. Angelis, M. Grätzel, N. Manfredi, C. Marinzi, S. Fantacci, J.-H. Yum, M. K. Nazeeruddin, *Chem. Commun.* **2008**, 5318–5320.

[27] B. Schulze, D. Escudero, C. Friebe, R. Siebert, H. Görls, U. Köhn, E. Altuntas, A. Baumgaertel, M. D. Hager, A. Winter, B. Dietzek, J. Popp, L. González, U. S. Schubert, *Chem. Eur. J.* **2011**, *17*, 5494–5498.

[28] a) E. Gindensperger, H. Koppel, C. Daniel, *Chem. Commun.* **2010**, *46*, 8225–8227; b) L. González, D. Escudero, L. Serrano-Andrés, *ChemPhysChem* **2012**, *13*, 28—51; c) D. Escudero, L. González, *J. Chem. Theory Comput.* **2012**, *8*, 203—213.

[29] W. Gawelda, M. Johnson, F. M. F. de Groot, R. Abela, C. Bressler, M. Chergui, *J. Am. Chem. Soc.* **2006**, *128*, 5001–5009.

[30] M. Kasha, *Discuss. Faraday Soc.* **1950**, *9*, 14–19.

[31] D. A. Lutterman, A. Chouai, Y. Liu, Y. Sun, C. D. Stewart, K. R. Dunbar, C. Turro, *J. Am. Chem. Soc.* **2008**, *130*, 1163–1170.

[32] Y. Sun, Y. Liu, C. Turro, *J. Am. Chem. Soc.* **2010**, *132*, 5594–5595.

[33] B. R. Spencer, B. J. Kraft, C. G. Hughes, M. Pink, J. M. Zaleski, *Inorg. Chem.* **2010**, *49*, 11333–11345.

[34] A. El Nahhas, A. Cannizzo, F. van Mourik, A. M. Blanco-Rodríguez, S. Záliš, A. Vlček Jr, M. Chergui, *J. Phys. Chem. A* **2010**, *114*, 6361–6369.

Publication A3

PHOTOGENERATED AVENUES IN MACROMOLECULES CONTAINING RE(I),
RU(II), OS(II), AND IR(III) METAL COMPLEXES OF PYRIDINE-BASED LIGANDS

Bobby Happ, Andreas Winter, Martin D. Hager, Ulrich S. Schubert*

Chem Soc Rev

Dynamic Article Links ▶

CRITICAL REVIEW

Photogenerated avenues in macromolecules containing Re(I), Ru(II), Os(II), and Ir(III) metal complexes of pyridine-based ligands

Bobby Happ,[abc] Andreas Winter,[ab] Martin D. Hager[abc] and Ulrich S. Schubert*[abc]

Pyridine-based ligands, such as 2,2′-bipyridine and 1,10-phenanthroline, have gained much interest in the fields of supramolecular chemistry as well as materials science. The appealing optoelectronic properties of their complexes with heavy d^6 transition metal ions, such as Ru(II), Os(II), Re(I) and Ir(III), primarily based on the metal-to-ligand charge-transfer (MLCT) nature featuring access to charge-separated states, have provided the starting point for many studies in the field of dye-sensitized solar cells (DSSCs), organic light emitting diodes (OLEDs), artificial photosynthesis and photogenerated electron as well as energy transfer processes. This *critical review* provides a comprehensive survey over central advances in the field of soluble metal-containing macromolecules in the last few decades. The synthesis and properties of functionalized 2,2′-bipyridyine- and 1,10-phenanthroline-based d^6 metal complexes, in particular, their introduction into different prevailing polymeric structures are highlighted. In the most part of the review metal complexes which have been attached as pendant groups on the polymer side chain are covered. Selected applications of the herein discussed metal-containing macromolecules are addressed, particularly, with respect to photogenerated electron/energy transfer processes. In order to enable a deeper understanding of the properties of the ligands and metal complexes, the fundamentals of selected photophysical processes will be discussed (223 references).

[a] *Laboratory of Organic and Macromolecular Chemistry (IOMC), Friedrich-Schiller-University Jena, Humboldtstraße 10, 07743 Jena, Germany. E-mail: ulrich.schubert@uni-jena.de; Fax: +49 (0)3641 9482 02; Tel: +49 (0)3641 9482 00*
[b] *Jena Center for Soft Matter (JCSM), Friedrich-Schiller-Universität Jena, Humboldtstraße 10, 07743 Jena, Germany*
[c] *Dutch Polymer Institute (DPI), P.O. Box 902, 5600 AX Eindhoven, The Netherlands*

Introduction

In the last few decades, polymers containing phosphorescent heavy d^6 transition metal ion complexes have attracted much attention, since the utility of these metal complexes, in particular of Ru(II), Ir(III), Os(II) and Re(I) ions, led to important applications in materials science. By embedding metal complexes into a

Bobby Happ was born in Suhl (Germany) and studied chemistry at the Friedrich-Schiller-University Jena (Germany). He graduated in chemistry in 2008 and is since then a PhD student in the group of Prof. Ulrich S. Schubert at the Friedrich-Schiller-University Jena, where he works on the design of metallo-supramolecular systems based on 2-(1H-[1,2,3]-triazol-4-yl)pyridines.

Bobby Happ

Andreas Winter was born in Herne (Germany) and studied chemistry at the University of Dortmund (Germany) where he graduated in organic chemistry in 1999. In 2003 he received his PhD in chemistry (University of Paderborn, Germany) for work on applications of the Mannich reaction in the synthesis of pyridine derivatives under the supervision of Professor N. Risch, and stayed on as a postdoc. Subsequently, in 2005 he joined the group of Prof.

Andreas Winter

U. S. Schubert (Eindhoven University of Technology, The Netherlands and Friedrich-Schiller University Jena, Germany). His research is focused on the synthesis of emissive and luminescent metallo-supramolecular assemblies.

This journal is © The Royal Society of Chemistry 2012

polymeric structure, the photophysical and electrochemical properties of the resulting material can be tuned by the nature of the metal complexes, while the properties attributed to the polymer, *e.g.* processability and film forming ability, can be maintained at the same time. Metal-containing polymers are the topic of different areas of scientific research: supramolecular chemistry,[1–7] fundamental electron and energy transfer investigations,[8–14] metal ion sensors[15–18] as well as electronic devices.[19–24] Wong and co-workers have also extensively studied the photovoltaic and optical power limiting applications of metallopolymers containing transition metal elements.[25–35] The d^6 configured metal ions [*i.e.* Ru(II), Ir(III), Os(II) and Re(I)] were and are the transition metal ions of choice, because of their exceptional spectroscopic properties featuring photostability and a broad absorption in the visible region. A unique coherence of chemical stability, redox properties, luminescence, excited-state lifetime and excited-state reactivity was the trigger for the synthesis of hundreds of derivatives. The relatively long-lived excited states of the late d^6 metal complexes, which are of metal-to-ligand charge transfer (MLCT) character, established comprehensive photophysical and photochemical studies leading to a nowadays well-understood field of chemistry.[24,36–42] Due to the rapid development in the field of polymers that contain metal complexes,[5,11,19,43–49] only selected examples will be discussed in this contribution. Scheme 1 depicts metal complex subunits which were frequently incorporated into macromolecular structures and display the main focus of this review.

In general, a metal complex can be incorporated into a polymer as part of the main chain or as a pendant group. It is also possible to prepare materials in which the metal complex is present in both the side and main chains (*e.g.* in dendrimers). Based on a categorization by W. K. Chan, there are three different types of metal-containing polymers (Fig. 1).[50] The metal ions/complexes are attached to the polymer backbone at the side chain or as an end group by electrostatic interaction, metal–ligand coordination or covalent bonds (Type Ia-c, Fig. 1). In Type II, the metal complexes are part of the polymer main chain (coordination or covalent connection); in the case of Type III, the metal ions are embedded in the polymer matrix by physical interaction.

From the synthesis point of view, two primary procedures were applied to prepare the metal-containing polymers in the course of the article (Scheme 2): (i) the transition metal complex was attached to a polymer backbone after the polymerization process (grafting), and (ii) the metal complex served as a monomer itself and was incorporated into the polymer by (co)polymerzation. In general, there are two possibilities to graft a transition metal complex onto a polymer (Scheme 2): suitable combinations of matching functionalities connected to the polymer and complex, respectively, are applied (a) or the polymer bears appropriate ligand units that can be reacted with a proper precursor complex (b). Further polymerization techniques are described in detail elsewhere.[22]

Martin D. Hager

Martin D. Hager was born in Coburg (Germany) and studied chemistry at the Friedrich-Schiller-University Jena (Germany) where he graduated in organic and macro-molecular chemistry in 2005. In 2007, he received his PhD in chemistry (Friedrich-Schiller-University Jena, Germany) for work on conjugated rod–coil polymers under the supervision of Prof. E. Klemm (scholarship of the Fonds der Chemischen Industrie). Subsequently, in 2007 he joined the group of Prof. U. S. Schubert (Eindhoven University of Technology, the Netherlands and then Friedrich-Schiller University Jena, Germany). His research is focused on conjugated polymers for solar-cell applications and self-healing materials.

Ulrich S. Schubert

Ulrich S. Schubert was born in Tübingen (Germany) in 1969. He studied chemistry at the Universities of Frankfurt and Bayreuth (both Germany) and the Virginia Commonwealth University, Richmond (USA). His PhD work was performed under the supervision of Prof. C. D. Eisenbach (Bayreuth, Germany) and Prof. G. R. Newkome (Florida, USA). After a postdoctoral training with Prof. J.-M. Lehn at the Université Strasbourg (France), he moved to the Munich University of Technology (Germany) to obtain his habilitation in 1999 (with Prof. O. Nuyken). From 1999 to spring 2000, he held a temporary position as a professor at the Center for NanoScience (CeNS) at the LMU Munich (Germany). From June 2000 to March 2007, he was Full-Professor at the Eindhoven University of Technology (Chair for Macromolecular Chemistry and Nanoscience), the Netherlands. Since April 2007, he is Full-Professor at the Friedrich-Schiller-University Jena (Chair of Organic and Macromolecular Chemistry), Germany. He has published over 500 papers, 18 patents, and edited/written 5 scientific books. His awards include the Bayerischen Habilitations-Förderpreis, the Habilitandenpreis of the GDCh (Makromolekulare Chemie), the Heisenberg-Stipendium of the DFG, the Dozenten-Stipendium of the Fonds der Chemischen Industrie, the VICI award of the NWO, the Piet-Lemstra innovation award of the DPI and the BPG biannual international award.
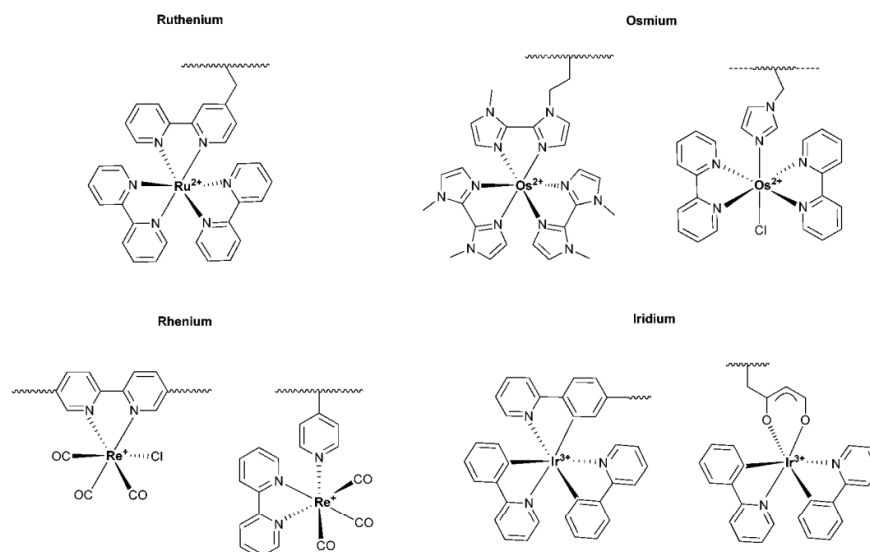
Scheme 1 Schematic representation of the main metal subunits used and examined in polymeric structures (the counter ions are omitted for clarity).

Type I: Metal ions/complexes linked to a chain or surface of a polymer molecule

(a) metal ions attached to the polymer by localized electrostatic attraction

(b) metal complex linked to the polymer by coordination

(c) metal complex linked to the polymer as pendant group
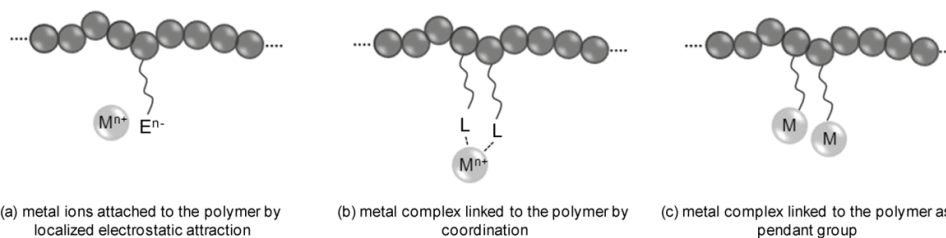
Type II: Metal complexes as a part of the polymer chain

(a) metal complexes form part of the polymer main chain by covalent linkage

(b) metal ligand coordination forms part of the polymer main chain
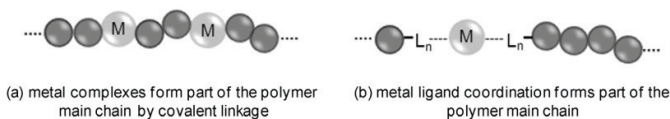
Type III: Metal ions/complexes interact with polymer physically
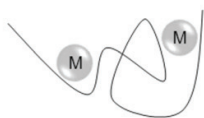
Fig. 1 Various approaches in preparing metal-containing polymers (the counter ions are omitted for clarity).[50]

The first section recalls some basic concepts on photophysics and photochemistry in d^6 metal complexes, since these optical properties are retained in the metal containing polymers and, thus, this knowledge is required to understand the scope of the materials reviewed. Subsequently, selected pyridine-based d^6 metal complexes encircling Ru(II), Os(II), Re(I) and Ir(III) ions,

Grafting

1) anchorage of a complex to a polymer   2) coordination at a polymer

(Co)polymerization

3) (co)polymerization of a complex functionalized with a polymerizable group
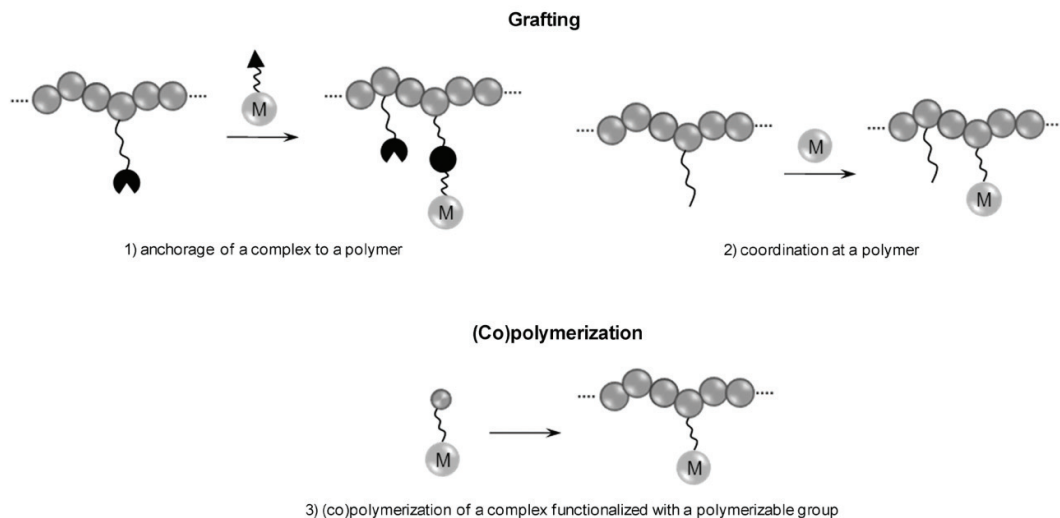
Scheme 2   Schematic representation of the primarily used polymerization techniques.

which were incorporated into polymeric structures, are discussed that have developed or emerged during the last two decades. The different materials are highlighted with respect to design principles, synthetic strategies, structure–property relationships, and applications in their respective subject area. Since there is a broad range of recent review articles and monographs dealing with 2,2′:2,6′-terpyridine-based materials,[5,51–59] this field of research will not be part of this review.

Theoretical aspects of relevant photophysical and photochemical processes

Excited states in d^6 transition metal ion complexes

The photophysical behavior of d^6 transition metal ions coordinated to one or more N-heterocyclic organic ligands has been intensively investigated.[36–38,60–62] The used N-heterocycles cover a broad range of structures and the excited states of the derived complexes strongly differ in energy for both singlet and triplet states. Without considering symmetry, the complexes of second and third row d^6 transition metal ions, in particular Ru(II), Os(II), Re(I) and Ir(III), have low spin ground states ($S = 0$), when ligands which establish a strong ligand field are considered (*e.g.* 2,2′-bipyridine, carbon monoxide, *etc.*). Polypyridine ligands are usually colorless molecules possessing σ-donor orbitals localized on the nitrogen atoms and π-donor and π*-acceptor orbitals delocalized to some extent on the aromatic rings. Following a single-configuration one-electron description of the excited state, the promotion of an electron from a π(M) metal orbital to the π*(L) ligand orbitals gives rise to MLCT excited states, whereas promotion of an electron from π(M) to σ*(M) orbitals gives rise to metal-centered (MC) excited states (Δ = ligand field splitting). Ligand-centered (LC) excited states can be obtained by promoting an electron from π(L) to π*(L) (Fig. 2).[36,37]
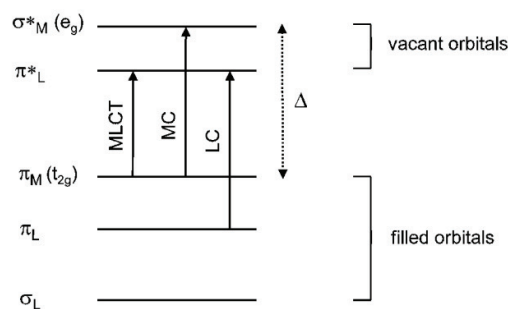
Fig. 2   Simplified molecular orbital diagram for d^6 metal complexes in octahedral symmetry showing the three types of electronic transitions without metal–ligand π-bonding interaction.[8]

The MC state energy can be controlled by varying either the ligands or the central metal ion (both affecting Δ). The strength of the ligand field increases in the order:

Cl < pyridine ≪ 2,2′-bipyridine, 1,10-phenanthroline < CN < CO.
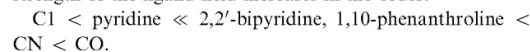
For a central metal ion, Δ increases when going down a column of the periodic table. Charge transfer state energies are mainly affected by the ease of oxidation/reduction of the ligands and the metal ion, respectively. For MLCT transitions, more easily reducible ligands and more easily oxidizable metal ions lower the MLCT states. The π–π* state energies are basically dictated by the ligand itself. The energies and intensities of the LC transitions can be tuned by changing either the substituents on the ligand, the heteroatoms in the aromatic ring or the extent of π-conjugation. The degree of spin–orbit coupling is most effectively increased by using higher atomic number metals.[8]

The thermally equilibrated excited states of these complexes, observed on longer time scales (>ns), are usually assigned to

be either MLCT (d–π*) in the case of $Ru(bpy)_3^{2+}$ and $Os(bpy)_3^{2+}$ or intraligand (IL, π–π*) states of $Ir(bpy)_3^{3+}$ with varying degrees of triplet character.[63] By contrast, numerous Re(I) complexes having N-heterocyclic ligands with relatively low energy ^3IL states exhibit both types of excited states and usually their mixing can be observed in the form of metal-to-ligand–ligand charge transfer (MLLCT) states. These complexes are often luminescent in solution and, in most cases, the observed emission arises entirely from the lowest triplet energy state. Strong spin–orbit coupling induced by the heavy atoms leads to efficient intersystem crossing (ISC) from the singlet excited state to the triplet state. Mixing singlet and triplet states *via* spin–orbit coupling eliminates the spin-forbidden nature of the $T_1 \rightarrow S_0$ radiative transition yielding relatively high phosphorescence quantum yields. Some relevant parameters are summarized in Table 1 for different d^6 metal complexes.[36,64]

Despite the apparent similarities of these d^6 complexes, the excited-state properties have significant differences with respect to their lowest MC, MLCT, and LC triplet states. While keeping the ligands the same, Δ increases while going from Fe(II) over Ru(II) to Os(II). Thus, the MC state energies rise from Fe(II) over Ru(II) to Os(II). The MLCT state energies are in the order Os < Fe < Ru, which reflects the ease of the metal oxidation. Since the MLCT state of Ru(II) complexes is commonly well above the ground state, inefficient radiationless deactivation with a consequential luminescence is usually observed for such complexes. In contrast, Os(II) complexes reveal much shorter emission lifetimes than the Ru(II) analogs (compare Table 1), since the energy of their MLCT state is lower and, consequently, quenching to the ground state is more efficient, as expected by the energy gap law (Fig. 3, left).[64]

Photochemistry and deactivation *via* MC states may be an issue considering photostability, if the MC states are thermally

accessible from the excited MLCT state. For example, $Ru(bpy)_3^{2+}$ is partially deactivated *via* an upper MC state. Due to the higher Δ value, the gap to the MC state is larger and the deactivation is less efficient than for the pyridine complex. Furthermore, if the deactivating MC state is thermally activated, there is a significant increase in the deactivation rate as the temperature is raised. Hence, $Ru(bpy)_3^{2+}$ shows a strong change in the luminescence lifetime over temperature, which limits its use at elevated temperatures regarding luminescence applications.[8,9] A widely accepted model is shown schematically in Fig. 3 (right).

The temperature dependence of the lifetime is given by

$$\frac{1}{\tau} = k_r + k_{nr} + k' e^{\frac{\Delta E}{kT}} \tag{1}$$

where k_r and k_{nr} are the radiative and nonradiative decay constants, respectively, ΔE is the energy gap between the MC state and emitting state (^3MLCT), and k' is the Arrhenius preexponential factor for the thermal activation of the MC state. This model assumes that the deactivation from the MC state is much faster than the return to the MLCT state ($k_2 \gg k_{-1}$), and, therefore, no thermal equilibrium can be established between the states (*e.g.* for $Ru(bpy)_3^{2+}$ at room temperature). Hence, the correlation of $1/\tau$ with temperature represents a reasonable starting model for calculating the energy gap between the MLCT and MC states over a limited temperature range (~ 50 K).[8,64]

Photophysical and photochemical processes

Any photophysical or photochemical process is initiated by the absorption of a photon by a molecule (Scheme 3). The excited state of the molecule (M*) is higher in energy than the ground state (M). As shown in Scheme 3, the unstable species M* may pass one of the available types of deactivation

Table 1 Photophysical properties of some representative d^6 metal complexes in MeCN[a]

Complex	$\lambda_{abs,max}$/nm	$\lambda_{em,max}$/nm	ϕ_{lum}	τ/μs	Ref.
$Ru(bpy)_3^{2+}$	451	606	0.075	0.87	8
$Ru(phen)_3^{2+}$	442	604	0.028	0.46	8
$Os(bpy)_3^{2+}$	640	740	0.005	0.049	65
$Os(phen)_3^{2+}$	650	690	n.d.	0.08	65
$Re(phen)(CO)_3Cl$	380	573	0.017	0.183	66
$Ir(bpy)_3^{3+}$	344	441	n.d.	2.4	61

[a] Photophysical properties in solution at room temperature.

Fig. 3 Left: lowest triplet state energy ordering for different d^6 metal complexes showing the relative positions of the LC, MC and MLCT states. Right: general state diagram illustrating the loss of excitation energy *via* radiationless decay through the MC state.[64]

Scheme 3 Representation of possible deactivation channels of excited states (M: molecule, Q: quencher).[8]
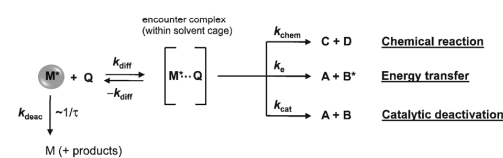
Scheme 4 Representation of various bimolecular processes in the presence of a quencher.[8]

channels: (i) vanishing of the original molecule (photochemical reaction), (ii) emission of light (luminescence), (iii) losing the excess energy (radiationless deactivation), and (iv) some kind of interaction with another species present in the environment (quenching process).[8]

Each of the intramolecular decay steps is characterized by its own rate constant and each excited state is characterized by its lifetime (τ) and is defined by

$$\tau = \frac{1}{\sum_i k_i} \qquad (2)$$

where k is the first order rate constant for a generic unimolecular process that causes the disappearance of the excited state. An important quantity for transition metal complexes is the quantum yield of emission from the lowest spin-forbidden excited state (phosphorescence quantum yield ϕ_P) which is

$$\phi_P = \eta_{ISC} k_P \tau_P \qquad (3)$$

where η_{ISC} is the efficiency of the population of the emitting excited state with

$$\eta_{ISC} = \frac{k_{ISC}}{(k_{ISC} + k_{IC} + k_f)} \qquad (4)$$

and τ_P is the lifetime of the emitting state:

$$\tau_P = \frac{1}{k_P + k'_{ISC}} \qquad (5)$$

If the lifetime of the excited state is sufficiently long, there is a high probability that the excited molecule comes across another quencher molecule Q (Scheme 4). In this case, a specific interaction can occur, where kinetic investigations have shown that only those excited states that live longer than $ca.$ 10^{-9} s have a chance to be involved in an interaction with other molecules. For transition metal complexes, only the lowest spin-forbidden excited state (^{3}MLCT) meets this requirement.[67,68] However, there is also the chance that the excited molecule M cannot interact with the quencher due to its diffusion out of the encounter complex cage (Scheme 4, $-k_{diff}$). The cage escape yield, $e.g.$ for energy transfer (ϕ_{ce}), is defined by

$$\phi_{ce} = \frac{k_e}{k_e + k_{-diff}} \qquad (6)$$

which describes the extent of the escape of the excited molecule by diffusion and can be determined by transient absorption spectroscopy.[69–71]

The two most important processes are energy transfer[9,10,68] and electron transfer,[9,10,67,71] where the latter denotes either the oxidation or the reduction of the excited state.

$$A^* + B \rightarrow A + B^* \text{ energy transfer}$$

$$A^* + B \rightarrow A^+ + B^- \text{ oxidative electron transfer}$$

$$A^* + B \rightarrow A^- + B^+ \text{ reductive electron transfer}$$
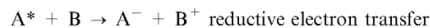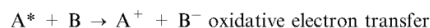
Electron and energy transfer processes are important, since they can be utilized to quench an excited state, for instance, avoiding intramolecular deactivation. Secondly, these processes are able to sensitize other species, for example, inducing

chemical changes or luminescence from species that do not absorb light.

The kinetic aspects of energy and electron transfer processes are discussed in detail elsewhere.[39,67,71] However, one important aspect is worth to mention: a molecule in its electronically excited state is a species with rather different properties compared with the ground-state molecule. The ability of an excited state to participate in energy transfer processes is related to its zero–zero spectroscopic energy (E^{0-0}). For the electron transfer the relevant thermodynamic parameters are the oxidation and reduction potentials of the *A/A$^+$ and *A/A$^-$ couples (eqn (7) and (8)). Because of its higher energy content, an excited state is both a stronger reductant and a stronger oxidant than the corresponding ground state. The redox potentials for the excited state couples can be calculated in a first approximation from the potentials of the ground state couples and the zero–zero excitation energy E^{0-0}:

$$E(A^+/A^*) = E(A^+/A) - E^{0-0} \qquad (7)$$

$$E(A^*/A^-) = E(A/A^-) + E^{0-0} \qquad (8)$$

Scheme 5 summarizes some important molecular quantities that describe the relationship between ground and excited state parameters.

Transition d^6 polypyridine metal complexes have strongly contributed to the development of electron transfer processes. When light is used, as a reactant, and one considers the following situations,

$$A + h\nu \rightarrow A^*$$

$$A^* + B \rightarrow A^+ + B^-$$
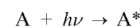
there are two thermodynamic pathways for electron transfer reactions (Scheme 6). Firstly, an exergonic reaction, which is slow for kinetic reasons (due to the high activation energy), is considered (Scheme 6, left side): upon light excitation the reductant A is converted into the much stronger reductant A*, thus the reaction between A* and B is much more exergonic than between A and B. The reaction of the excited state is generally much faster than the ground state
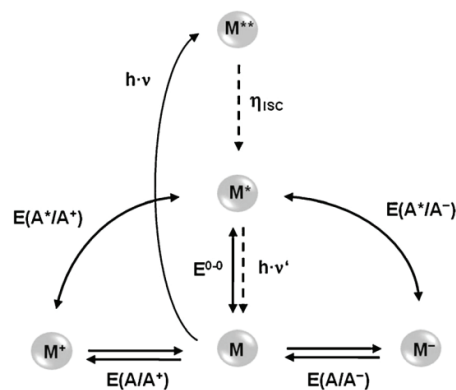
Scheme 5 Representation of important molecular quantities.[8]
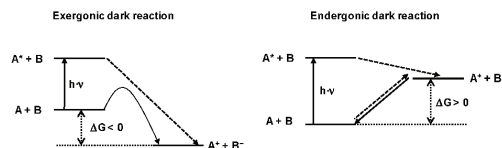
Scheme 6 Representation of the two possible energetic situations for electron transfer reactions involving an excited state reactant.[8]

reaction, since the activation energy usually decreases with increasing exergonicity.

Here, light is simply used to overcome a kinetic barrier and acts as a catalyst. The second is an endergonic dark reaction (Scheme 6, right side): the charge separation reaction ($A + B \rightarrow A^+ + B^-$) cannot take place for thermodynamic reasons. However, the latter reaction becomes thermodynamically allowed if A is excited to A* and the portion of light energy implied to the reaction is converted into chemical energy of the products. The converted energy is discharged when A^+ and B^- undergo an electron back-transfer reaction leading to $A + B$.[8]

Sensitization by light

Many d^6 metal polypyridine compounds are also involved as mediators in photochemical processes.[10,68] There are reactions that do not occur because the reactants are not able to absorb light and/or the excited state, responsible for the specific photochemical reaction, has too short of a lifetime. As discussed in the previous section, a chemical reaction $A + B \rightarrow A^+ + B^-$ cannot occur because of its endergonic nature. By excitation with light the process would be thermodynamically allowed (Scheme 6). Nevertheless, if neither A nor B is able to absorb the exciting light, still the reaction cannot take place. This is the case if the reaction is sensitized by a species which has specific electrospectroscopic properties; such compounds are called light absorption sensitizers (LASs) and perform as shown in Fig. 4. The LAS has to absorb the light resulting in an excited state and this excited state must be able to oxidize (or reduce) one of the reactants. Finally, if the reduced (or oxidized) LAS is able to reduce (or oxidize) the second reactant the redox process cycle is closed by regenerating the LAS. For an ideal LAS some requirements can be proposed: a reversible redox behavior, suitable ground and excited state potentials, stability towards thermal and photochemical decomposition, as high as possible absorption in a suitable spectral region, a small energy gap between the appropriate excited states, high quantum yield of
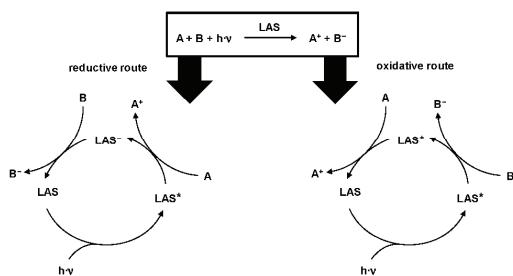
Fig. 4 General photosensitized electron transfer processes by light absorption.[8]

the reactive excited state, a proper lifetime of the reactive excited state and a high energy content of the reactive excited state.[8]

Concerning the redox behavior of d^6 metal pyridine-based complexes there are fundamental dissimilarities, for instance, when comparing Ru(II) and Ir(III). Cyclic voltammetric studies of Ru(II) polypyridine complexes have shown that they undergo a reversible oxidation associated with the metal-centered Ru(II)/Ru(III) couple as well as a reversible ligand-centered py/py− (py = polypyridine ligand) reduction to form Ru(I). The existence of an oxidizable Ru(II) center and a reducible ligand, in general, establishes a relatively long-lived (10^{-6} to 10^{-7} s) low energy MLCT-associated excited state.[8,72] When it comes to charged Ir(III) polypyridine complexes cyclic voltammetric studies indicated that oxidation of Ir(III) to Ir(IV) is often irreversible, which was attributed to the preference of oxidation at the ligand rather than at the metal center. As expected from charge considerations, reduction of Ir(III) occurs at a much less negative potential than it does in the corresponding Ru(II) complexes (this process is a reversible one related to reduction at the ligand). In contrast to Ru(II), the oxidation and reduction potentials of Ir(III) complexes suggest a relatively high energy MLCT excited state. As a consequence, Ir(III) is a far stronger oxidizing agent than Ru(II), but a weaker reducing agent.[73]

Furthermore, LASs can drive some interesting and useful processes:[9,11,15,16,74,75] for example, hydrogen evolution has been observed for a number of polypyridine complex sensitized systems.[9,67,74,76,77] As the result discussed in the previous
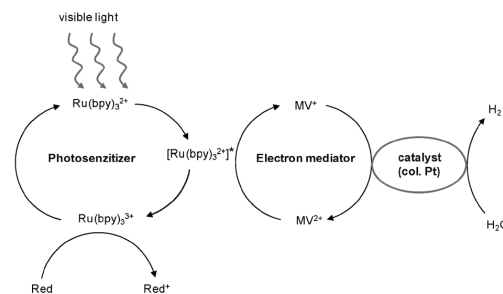
Fig. 5 Overview of the photoinduced reduction of water (Red = reductant, bpy = 2,2′-bipyridine, MV = methyl viologen).[11]

Table 2 Systems for the photochemical generation of molecular hydrogen

Sensitizer	Electron donor	Quencher or catalyst	Quantum yield $H_2{}^a$ [mol einstein^{-1}]	Ref.
*Ru(bpy)$_3^{2+}$	EDTA or TEOA	MV^{2+}, colloidal Pt	0.13	74
*Ru(bpy)$_3^{2+}$	TEOA	MV^{2+}	0.01	74
*Ru(bpy)$_3^{2+}$	TEOA	Colloidal Ru or Os	0.001	74
*Ru(bpy)$_3^{2+}$	TEOA	Rh(bpy)$_3^{3+}$, Pt^0	0.11	76
*Ru(bpy)$_3^{2+}$	EDTA	*Rh(bpy)$_3^{3+}$	0.04	76
*Ru(bpy)$_3^{2+}$	TEA	PtO$_2$ (suspended)	0.53	76
*Ru(bpy)$_3^{2+}$	Ascorbate	Co^{II}	0.0005	9
*Ru(bpy)$_3^{2+}$	Ascorbate	Co(bpy)$_n^{2+}$ (in situ)	0.13	9
*Cr(bpy)$_3^{3+}$	EDTA	Colloidal Pt	0.08	9

^{a} For quantum yield determination of molecular hydrogen see ref. 80 and 81.

2228 | *Chem. Soc. Rev.*, 2012, **41**, 2222–2255

This journal is © The Royal Society of Chemistry 2012
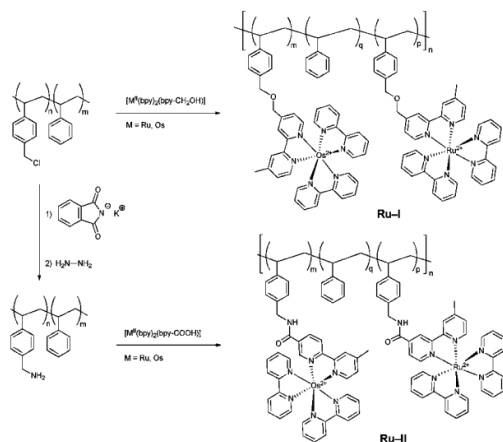
Scheme 7 Schematic representation of the synthesis of ether- and amide-linked copolymers (the counter ions are omitted for clarity) synthesized by the group of Meyer.

Table 3 Structural details of the metallopolymers synthesized by the Meyer group

Polymer	m	q	p	n	$M_n{}^a$/g mol^{-1}	PDI^a	Ref.
Ru-Ia	0	0.5	0.5	54	7000	1.54	92
Ru-Ib	0.5	0.5	0	54	7000	1.54	92
Ru-Ic	0.1	0.5	0.4	54	7000	1.54	92
Ru-Id	0	0.5	0.5	60	7700	2.4	93
Ru-IIa	0	0.5	0.5	32	4200	1.53	94
Ru-IIb	0.5	0.5	0	32	4200	1.53	94
Ru-IIc	0.1	0.5	0.4	32	4200	1.53	94
Ru-IId	0.15	0.5	0.35	32	4200	1.53	95
Ru-IIe	0	0.8	0.2	20	4200	1.53	94
Ru-IIf	0.2	0.8	0	20	4200	1.53	94

^{a} Determined by size exclusion chromatography.
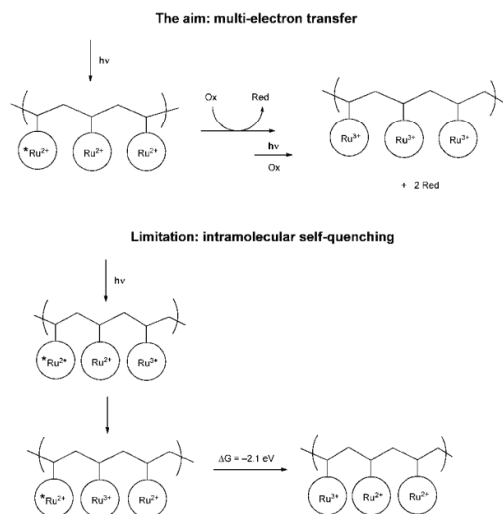
Fig. 6 Intramolecular electron transfer quenching of the highly metal-loaded polymer **Ru-Id**.[96]

$R = H$
$R = CONEt_2$
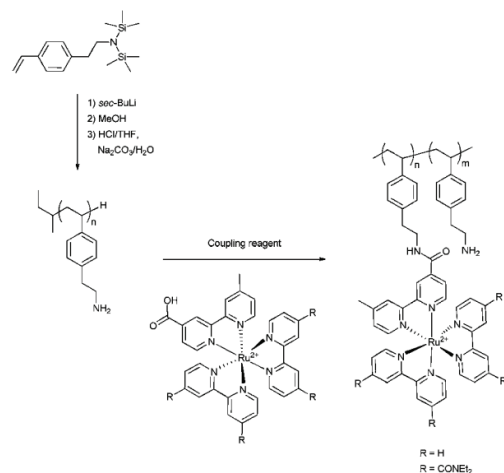
Scheme 8 Schematic representation of the synthesis of amide-linked Ru(II)-containing polymers by living anionic polymerization (the counter ions are omitted for clarity).

Ru-III; M = Ru and/or Os
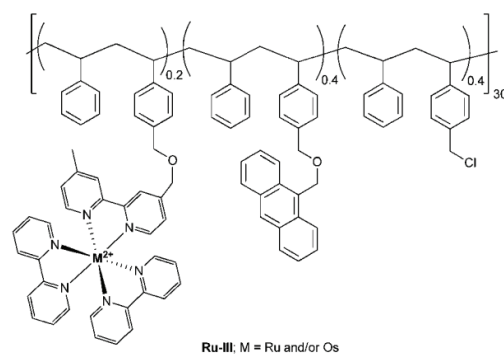
Scheme 9 Triply functionalized polymer containing a Ru(II) complex, an Os(II) complex and anthracene (the counter ions are omitted for clarity).
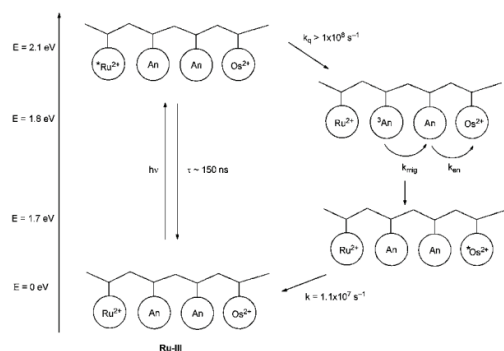
Fig. 7 Intrapolymeric energy transfer in 1,2-dichloroethane at 298 K (the counter ions are omitted for clarity).[100]

paragraph, $Ru(bpy)_3{}^{2+}$ was widely applied as a prototype of a light absorption sensitizer due to the unique photoredox behavior of the Ru(II) metal ion. The splitting of water into hydrogen and oxygen by visible light

$$2H_2O + h\nu \rightarrow 2H_2 + O_2$$
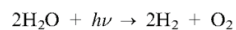
is endergonic in the dark by 1.23 eV for each of the four electrons involved. This four-electron process requires the following redox potentials:

$$2H_2O \rightarrow 4H^+ + 4e^- + O_2 \quad E^0 = +0.82 \text{ eV}$$

$$2H^+ + 2e^- \rightarrow H_2 \quad E^0 = -0.41 \text{ eV}$$
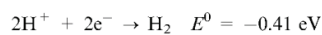
In principle, $Ru(bpy)_3{}^{2+}$ can act as a LAS and the energetics of the relevant step is as follows (pH = 7):[78]

$$2*Ru(bpy)_3{}^{2+} + 2H^+ \rightarrow 2Ru(bpy)_3{}^{3+} + H_2 \quad \Delta G = -0.44 \text{ eV}$$
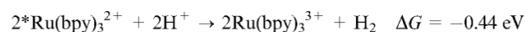
In practice, the first step is too slow to compete with the excited state deactivation. A reducing agent (Red) is
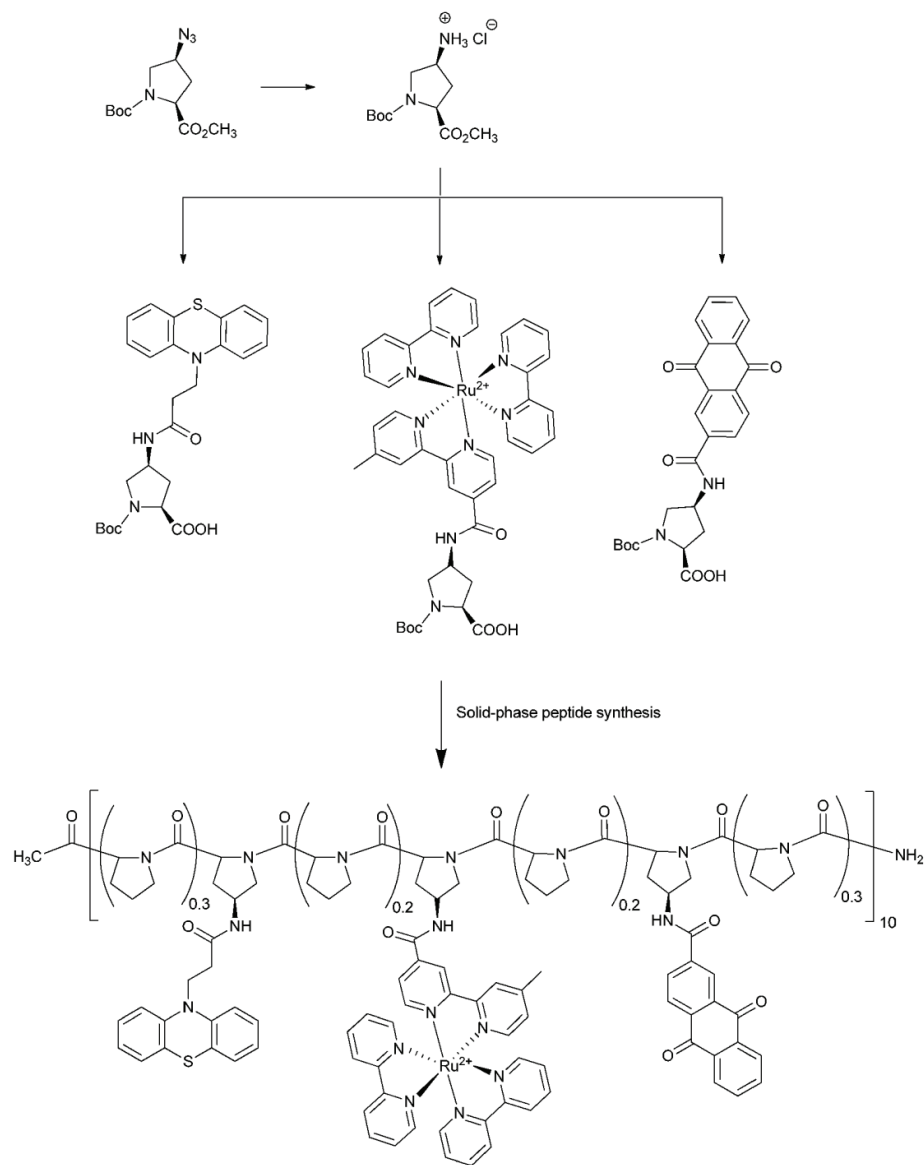
Scheme 10 Schematic representation of the structure and the synthesis of an oligoproline assembly (the counter ions are omitted for clarity).

added, as electron donor, to trap the $Ru(bpy)_3^{3+}$ produced in the quenching reaction and suppresses back-electron transfer processes. Additionally, methyl viologen (1,1'-dimethyl-4,4'-bipyridinium, MV^{2+}), as an electron mediator, was found to be necessary to transport electrons to the multielectron redox catalyst (e.g. colloidal platinum), which combines two protons and electrons to afford molecular hydrogen (Fig. 5).[8]

$$*Ru(bpy)_3^{2+} \ + \ MV^{2+} \ \rightarrow \ Ru(bpy)_3^{3+} \ + \ MV^+$$

$$Ru(bpy)_3^{3+} \ + \ Red \ \rightarrow \ Ru(bpy)_3^{2+} \ + \ Red^+$$

$$2MV^+ \ + \ 2H_2O \ + \ cat. \ \rightarrow \ 2MV^{2+} \ + \ H_2 \ + \ 2OH^-$$

The best characterized systems are those where the reducing agents are triethylamine (TEA), triethanolamine (TEOA) or ethylene diamine tetraacetic acid (EDTA), respectively.[11,74,76,77,79] Hydrogen evolution rates in the $Ru(bpy)_3^{2+}$/EDTA system were used, as the standard, for comparing the efficiencies of different catalysts, including colloidal Pt [stabilized with poly(vinyl alcohol)] and suspensions of PtO_2 (Table 2). In general, the colloidal metals and the metal oxide suspensions were the most efficient systems. The investigation of the effect of the particle size and catalyst concentration in the colloidal
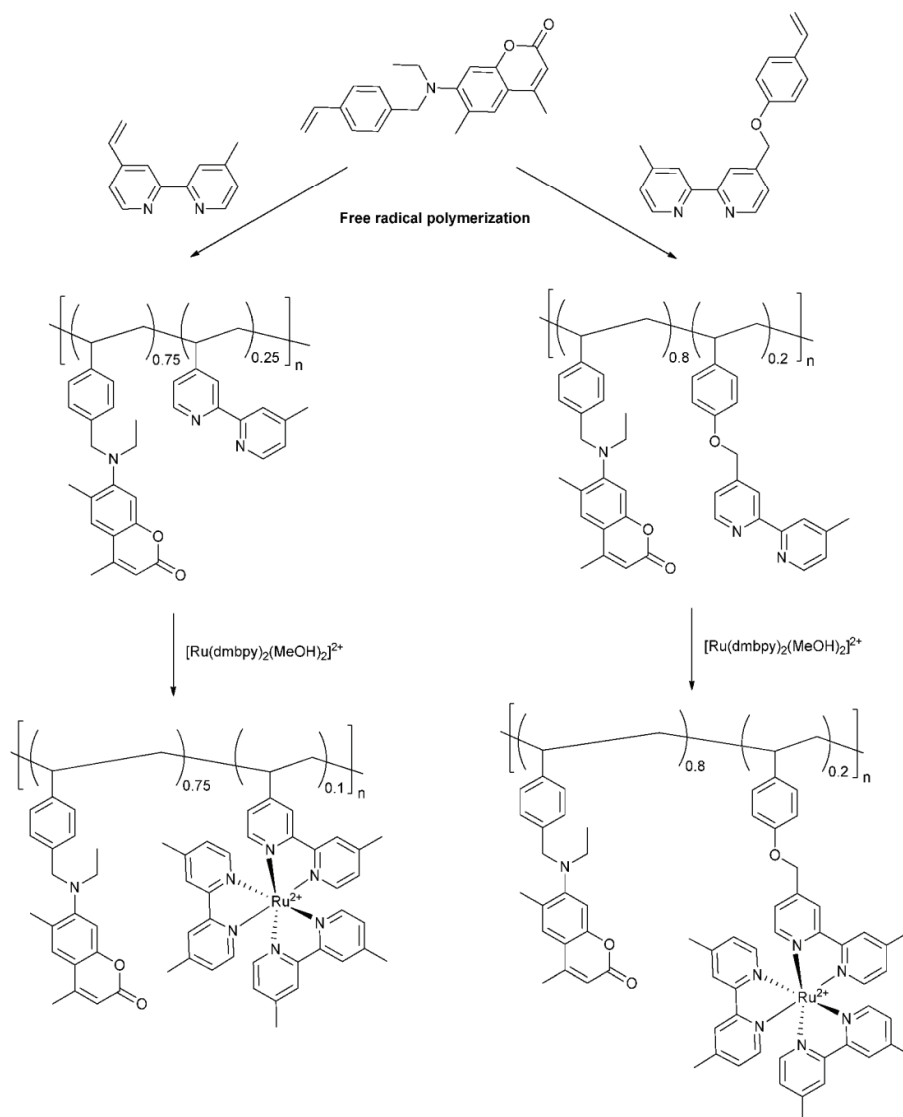
Scheme 11 Schematic representation of the synthesis of different antenna copolymers (the counter ions are omitted for clarity).[112,113]

Pt system showed that the rate of hydrogen evolution increases six-fold upon decreasing the radius of the colloidal particles from 50 to 10 nm. For particles of 10 nm radius, the hydrogen generation rate also increased six-fold upon increasing the Pt concentration from 8 mgL^{-1} to 120 mgL^{-1}.[76]

In a very recent assay, it was demonstrated that upon arranging the platinum catalyst and the Ru(bpy)$_3^{2+}$ sensitizer closely into a gel network, the electronic transmitting reaction to generate hydrogen proceeded more efficiently than in the solution-based systems.[82] The system with an immobilized platinum catalyst and the copolymerized sensitizer [Ru(bpy)$_3^{2+}$] as well as the mediator (MV) revealed two orders of magnitude higher H$_2$ gas generation rates than the solution systems.

Macromolecules containing pyridine-based Ru(II)/Os(II) complexes

In the early 1980s, chemists faced a time where chemical systems were screened in order to provide the basis for new families of devices, such as solar energy storage systems and light-emitting arrays. One extensively studied example was artificial photosynthesis where solar energy is utilized for the formation of high energy chemicals. A number of molecular features, within a single structure, had to be combined when aiming for applications of those materials including light absorption, direct electron transfer by the utilization of free energy gradients, and the delivery of the photochemically produced oxidative and reductive equivalents to catalytic sites.
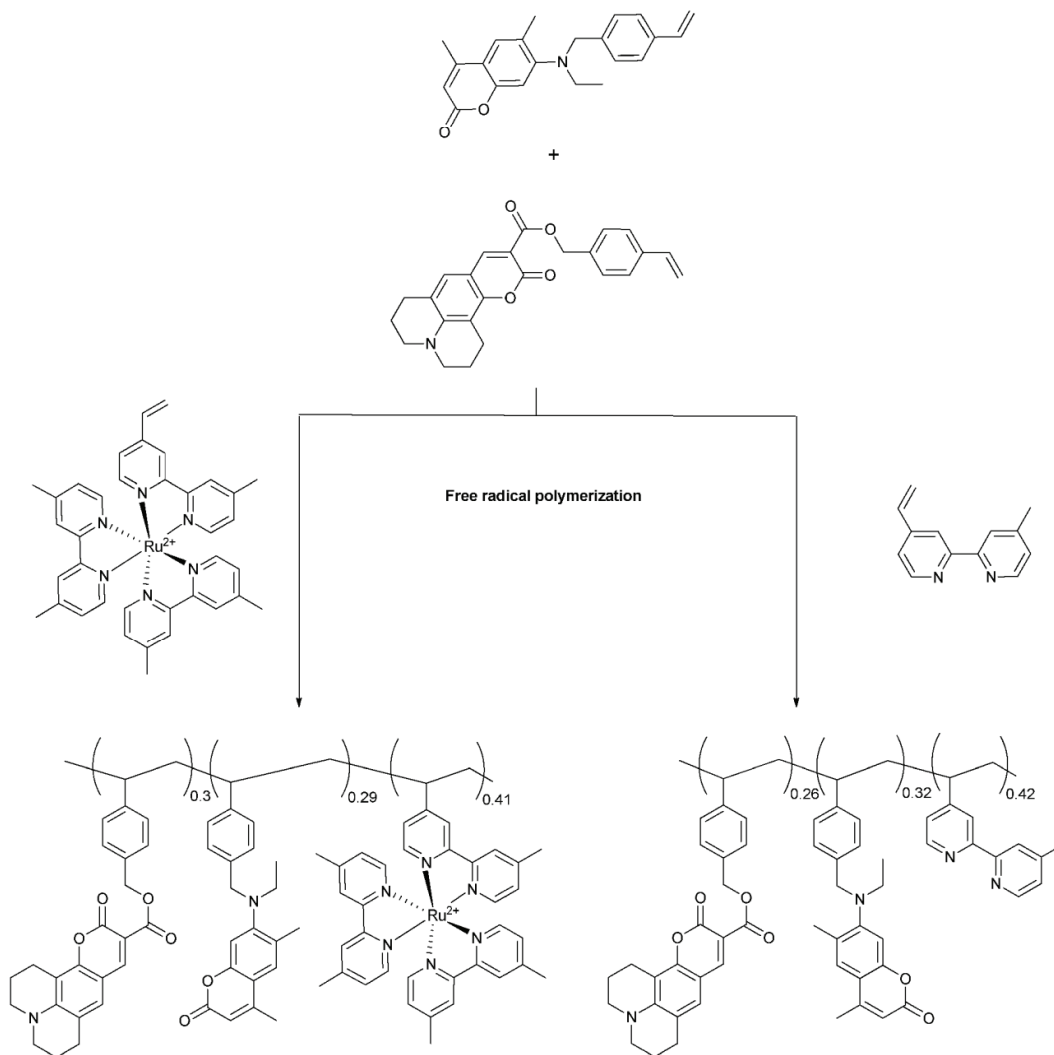
Scheme 12 Schematic representation of the synthesis of different terpolymers (the counter ions are omitted for clarity).[113]

For this purpose, a number of approaches were explored at the molecular level for creating molecular assemblies for artificial photosynthesis.[11,77,83–89]

Meyer et al. used polystyrene (PS) as polymer backbone because the molecular structure of the styrene repeating units ensured relatively high inertness toward electron or energy transfer processes. There are no low-lying excited states and oxidation or reduction only occurred either at high oxidative or low reductive potentials. In initial experiments, the copolymerization of styrene and (chloromethyl)styrene (as a mixture of *meta*, *para* isomers) *via* free radical polymerization (FRP) gave atactic polymer samples of varying molar masses and polydispersity index values (PDI) depending on the reaction conditions.[90,91] In subsequent investigations only polymers containing the *para*-isomer were utilized yielding chloro-functionalized copolymers by FRP ($M_n \approx 7000$ g mol^{-1}, PDI: 1.6–2.5).[92]

For the functionalization of these polymers, a new linkage chemistry was developed: nucleophilic chloride displacement by hydroxymethyl-substituted polypyridyl complexes $[M(bpy)_2(bpyCH_2OH)]^{2+}$ (M = Ru or Os; bpyCH$_2$OH = 4-methyl-4′-hydroxymethyl-2,2′-bipyridine) in the presence of CsOH, as base, in DMSO gave the metal-containing copolymers **Ru-I** (Scheme 7, see structural details in Table 3).[90,92] By using an excess of the metal complex, quantitative substitution at the available chloromethylated sites on the polymer was achieved yielding macromolecules with a high degree-of-metal-loading (Scheme 7, **Ru-Ia**, **Ru-Ib**).

The mixed Ru(II)–Os(II) polymer **Ru-Ic** was investigated by means of different photophysical techniques with respect to intra-strand electron and energy transfer—stemmed by the issue of concentrating redox equivalents to a particular spot—where the desired photon-driven transformation is

PMMA-Ru

PNAA-Ru

R =

x = 0.90, y = 0.10   x = 0.93, y = 0.07

x = 0.96, y = 0.04
x = 0.88, y = 0.12
x = 0.82, y = 0.18

P(CM-Ru)

PCMA-Ru
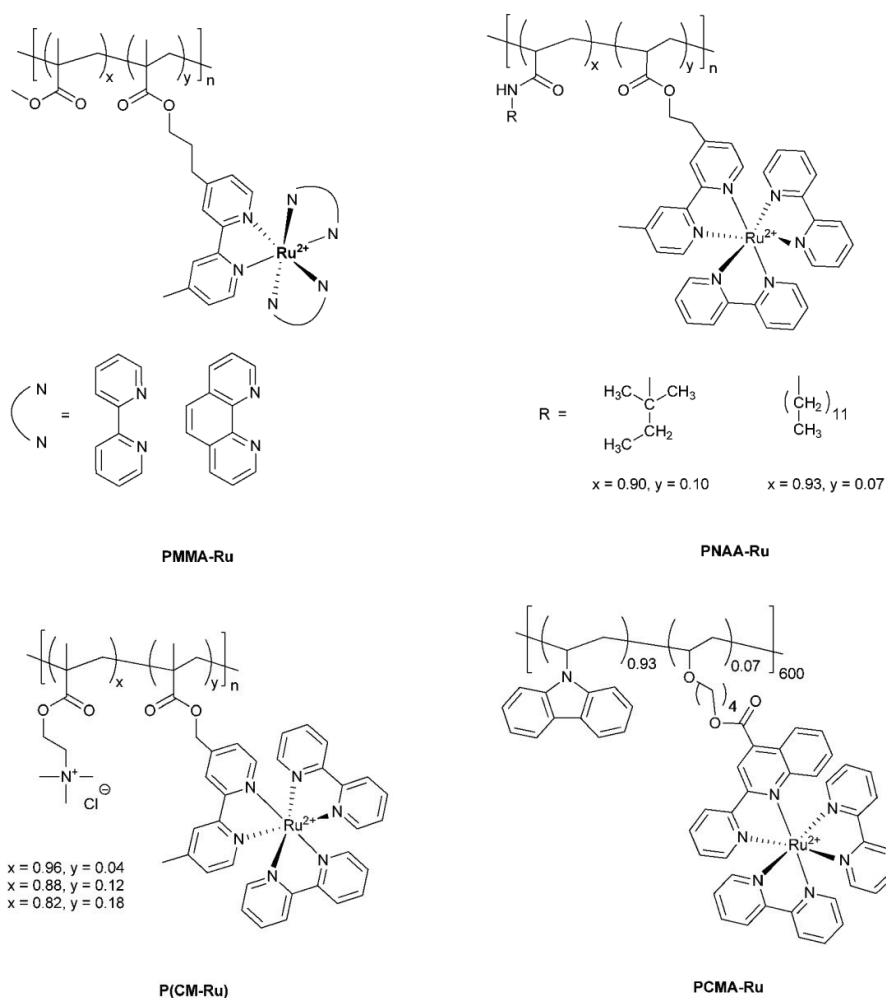
Scheme 13   Schematic representation of Ru(II) complexes attached to a polyacrylate backbone (the counter ions are omitted for clarity).

supposed to occur. The Os(II) units acted as a trap, whereas energy transfer *via* *Ru(II) → Os(II) was favored by $\Delta G = -0.36$ eV. Transient emission measurements in MeCN showed that rapid energy transfer ($k > 2 \times 10^8$ s^{-1}) occurred only at Ru(II) sites adjacent to Os(II) complexes.[92] In later experiments, it was shown by laser flash photolysis at high irradiances that multiphoton excitation in the presence of high concentrations of phenothiazine (PTZ), as reductive quencher, led to individual polymeric strands that were reduced by up to seven electrons:[93]

$$[co\text{-PS–CH}_2\text{OCH}_2\text{–(Ru}^{II})_{30}]^{60+} + 7h\nu + 7\text{PTZ}$$
$$\rightarrow [co\text{-PS–CH}_2\text{OCH}_2\text{–(Ru}^{II})_{23}(\text{Ru}^I)_7]^{53+} 7\text{PTZ}^{\bullet+}$$
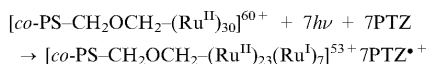
A problem occurred concerning the storage of multiple redox equivalents, which is illustrated in Fig. 6 for a polymer with a high loading of [Ru(bpy)₃]$^{2+}$ units: upon excitation and electron transfer quenching, oxidative equivalents, such as Ru(III), were observed on the polymeric strands. The second excitation occurred at a Ru(II) site adjacent to Ru(III) and electron transfer from *Ru(II) to Ru(III) was favored by a free energy change of -2.1 eV and led thereby to unproductive self-quenching of the excited state.[96,97]

The utilization of ether-linked polymers for the study of photochemical electron and energy transfer was limited due to the failure of facile intra-strand energy transfer. Consequently, amide-based linkage chemistry was used by the same group by applying the well-developed coupling chemistry between amines and carboxylic acids. The acid-derivatized complexes [M(bpy)₂(bpyCO₂H)]$^{2+}$ (M = Ru or Os; bpyCO₂H = 4-methyl-(2,2′-bipyridine)-4′-carboxylic acid) were added in different stoichiometric amounts to polystyrene-based polymers by amide coupling in DMF/CH₂Cl₂ solvent mixtures providing metallopolymers **Ru-II** (Scheme 7, see details in Table 3).[94,98] Spectroscopic and electrochemical measurements showed that the properties of the polymer-bound complexes were similar to those of the isolated monomers, and evidence for multi-photon effects in fully loaded polymers was found. There was also a striking difference between the ether- and amide-linked polymers in their abilities to enable intra-strand energy transfer: the amide-linked polymers **Ru-II** revealed two orders of magnitude higher energy migration rates which was attributed to the differences in orientation of the excited-state dipoles.[98–100] A comprehensive insight in the excited-state dynamics of **Ru-IId** was gained by time-correlated single photon counting with pico-seconds time resolution in MeCN at room temperature. In these experiments, the *Ru(II) emission decay at $\lambda_{max} = 640$ nm as well as the growth and decay, respectively, of *Os(II) emission at $\lambda_{max} = 780$ nm was monitored. Average rate constants for nearest neighbor *Ru(II) → Os(II) quenching ($k = 2 \times 10^8$ s^{-1}) and for *Ru(II) → Ru(II) migration ($k = 5 \times 10^7$ s^{-1}) were obtained, which explained the efficient *Ru(II) quenching.[95]

In order to achieve better control over the polymerization, amide-linked polymers were synthesized by living anionic polymerization later on (Scheme 8).[101–104] Trimethylsilyl-protected (aminoethyl)styrene was polymerized using *sec*-BuLi
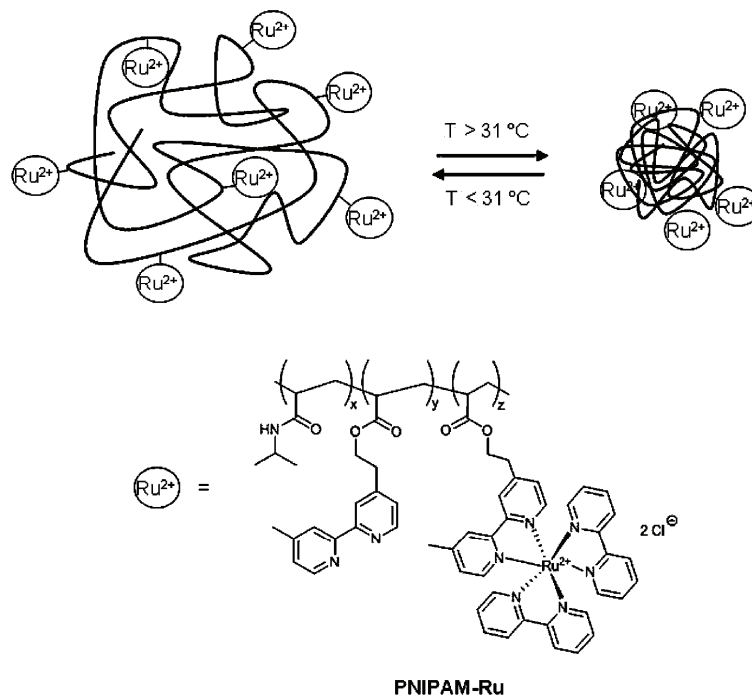
PNIPAM-Ru

Fig. 8 Structure change of **PNIPAM–Ru** at the LCST by phase transition.[117]

Ru-IV

Ru-Va: n:m = 30:140   **Ru-Vd:** n:m = 14:10
Ru-Vb: n:m = 20:40   **Ru-Ve:** n:m = 67:11
Ru-Vc: n:m = 10:8   **Ru-Vf:** n:m = 20:20
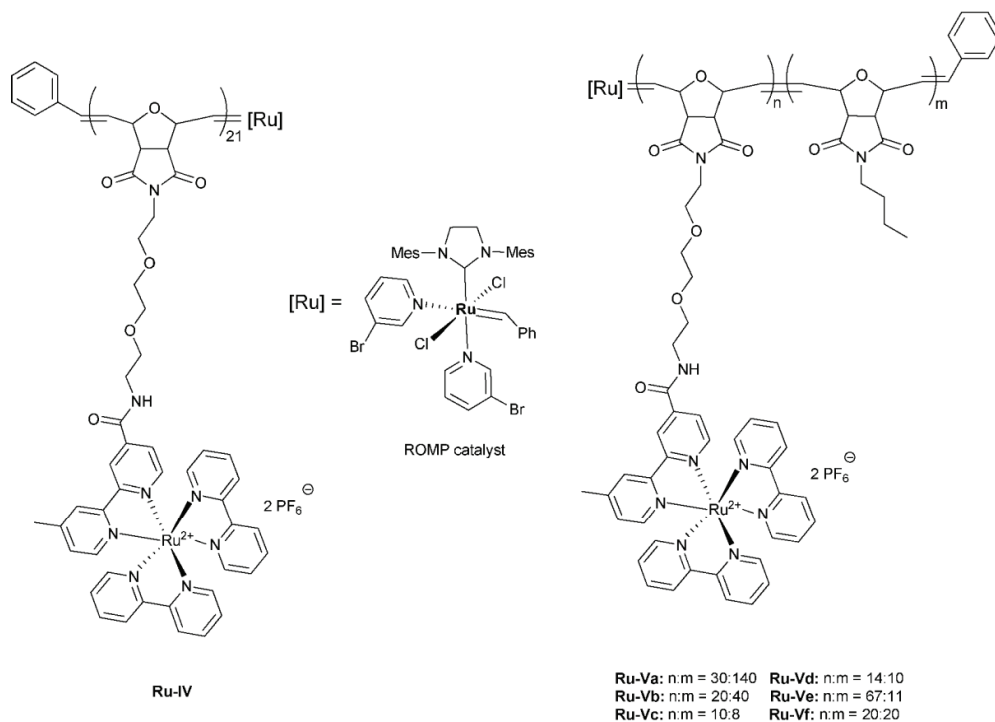
Scheme 14 Schematic representation of Ru(II)-containing polymers and copolymers, respectively, synthesized by ring-opening metathesis polymerization.

as initiator and yielded polymers with PDI values between 1.08–1.18 characteristic for a "living" polymerization procedure.[104] Subsequently, the amino-functionalized polymer was linked to carboxy-functionalized metal complexes, such as $[Ru^{II}(R\text{-}bpy)_2(bpyCO_2H)]^{2+}$ and/or $[Os^{II}(bpy)_2(bpyCO_2H)]^{2+}$. Time-resolved emission decay dynamics were analyzed in rigid media [using poly(methyl methacrylate) as matrix] and a direct evidence for Ru(II)* → Ru(II) migration and Ru(II)* → Os(II) energy transfer was obtained by time-correlated single photon counting, as discussed for **Ru-IId**.[99,103,105]

Intra-strand energy migration and transfer were shown by Meyer *et al.* to occur in a trifold functionalized polymer containing Ru(II) and Os(II) complexes as well as 9-hydroxy-methyl-anthracene (Scheme 9).[10,91,100] The functionalized 1 : 1 copolymer **Ru-III** of styrene and *p*-(chloromethyl)-styrene that contained: (i) a polypyridyl complex of Ru(II), which upon excitation resulted in a high-energy MLCT excited state, (ii) a polypyridyl complex of Os(II), which had a lower energy MLCT excited state, and (iii) an anthryl derivative, which had a triplet state of intermediate energy. The metal subunits and the 9-anthracenemethanol were sequentially attached by nucleophilic substitution of the randomly located chloride atoms. It was demonstrated that upon excitation of the Ru(II) chromophores, rapid long-range energy transfer ($k > 1 \times 10^8 \ s^{-1}$) occurred at the Os(II) centers *via* a cascade mechanism in which the internal anthryl groups acted as energy relays (Fig. 7). Laser flash photolysis and emission quantum yield measurements

showed nearly complete quenching of *Ru(II) by *Os(II), whereby the energy transfer appeared on the timescale of the laser pulse (∼5 ns). In contrast, partly loaded polymers missing the
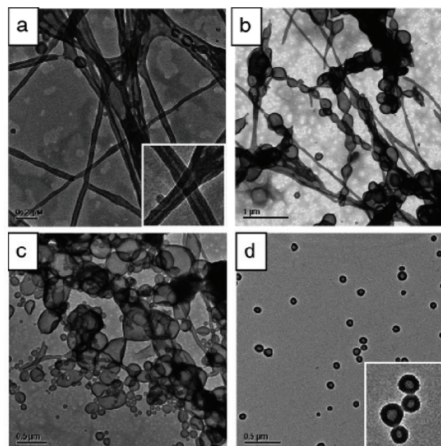
Fig. 9 TEM images of polymer **Ru-Vf** ($c = 20 \ mg \ mL^{-1}$) with increasing toluene content: (a) toluene/acetonitrile ratio 20/80, (b) toluene/acetonitrile ratio 35/65, (c) toluene/acetonitrile ratio 40/60, (d) toluene/acetonitrile ratio 70/30 (reproduced from ref. 134 with permission by the American Chemical Society).
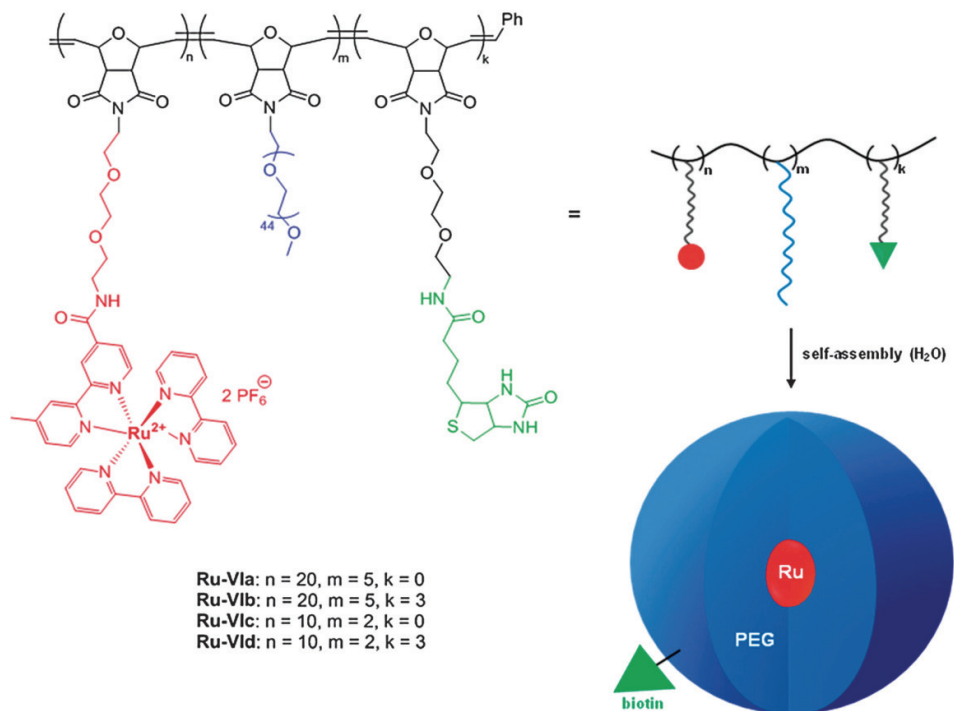
Fig. 10 Self-assembly of block copolymers into spherical aggregates containing (i) a luminescent metal unit (red), (ii) a poly(ethylene glycol) biocompatible corona (blue), and (iii) a biotin-functionalized unit on the periphery as bio-recognition component (green).[136]

anthracene residue gave no indication for such *Ru(II) → Os(II) energy transfer following excitation at Ru(II).[100]

The former investigations demonstrated the feasibility of substituted polystyrene as a framework for constructing multi-functional architectures. However, the use of pre-formed polymers suffered from the disadvantage that no control over the relative regional constitution of functional groups along the polymer could be achieved. Consequently, Meyer *et al.* explored solid phase peptide synthesis and constructed oligopeptides in a stepwise fashion as a tool to control the local array of additional functional groups.[106–109]

The aim of this approach was to prepare chromophore-electron transfer assemblies with control of both the constitution of added subunits and the 3D-structure of the resulting assembly. For synthesizing the oligoproline helical structural motif, depicted in Scheme 10, the preparation of appropriate amino acids containing the Ru(II) chromophore as well as electron transfer donors and acceptors was required. For this purpose, the L-enantiomer of azidoproline was reduced to the amine (Scheme 10). Subsequently, the amine group was *tert*-butoxycarbonyl-protected (Boc) and the proline derivative was coupled with [Ru(bpy)$_2$(bpy-COOH)]$^{2+}$ or with the carboxylic acid derivatives of PTZ, as donor, and the electron transfer acceptor anthraquinone (ANQ). Subsequent solid-state peptide synthesis yielded the 13-residue oligoproline displayed in Scheme 10, which adopted a prolin-II-type helical structure in water as confirmed by circular dichroism (CD) measurements

of the amide region.[108,109] Quenching of the MLCT excited state of the Ru(II) centers was dominated by PTZ → Ru(II)* reductive electron transfer and occurred within 10–20 ns time scale with solvent-dependent efficiencies (>0.9). It was further shown that the reductive quenching was followed by [Ru^{II}L$_2$L$^-$] → ANQ electron transfer yielding a redox-separated state: the efficiency of its formation was solvent dependent and varied from 33% (1,2-dichloroethane) to 86% (acetonitrile).[109]

Molecular assemblies, which are capable of harvesting light and convert the absorbed photon energy, were reported by the Fréchet group. However, the demanding multi-step synthesis of dendritic systems, which contain light-collecting dyes at the periphery and channel light to a different dye with extremely high energy-transfer efficiencies, limited their use for realistic applications.[110,111] In order to circumvent the troublesome synthesis of such dendrimers, Fréchet *et al.* established analogous polymers in which the donor–acceptor ratios were optimized by mimicking the dendrimer models (Schemes 11 and 12). Polymers containing coumarin and Ru(dmbpy)$_3$$^{2+}$

Table 4 Photophysical properties of diblock and triblock copolymers

Polymer	Solvent	$\lambda_{abs,max}$/nm	$\lambda_{abs,max}$/nm	ϕ_{lum}
Ru-VIc	Acetonitrile	457	626	0.064
Ru-VIc	Acetonitrile/water (1 : 5)	457	642	0.021
Ru-VId	Acetonitrile	457	626	0.060
Ru-VId	Acetonitrile/water (1 : 5)	457	642	0.021

(dmbpy = 4,4′-dimethyl-2,2′-bipyridine) chromophores were synthesized using a grafting-onto (Scheme 11) as well as a copolymerization approach (Scheme 12) utilizing FRP. It was found that the solubility of polymers derived from Ru(II)-containing monomers was higher than those obtained by grafting of the Ru(II) complexes. The resulting bichromophoric macromolecules exhibited enhanced absorption and luminescence properties compared to single Ru(II) complexes due to an efficient

(>95%) energy transfer between the coumarin donor dyes and the ruthenium subunits.[112,113] Moreover, a system in which two different donor dyes were present together with a Ru(II) complex (Scheme 12) was synthesized and found to also offer efficient energy transfer to the Ru(II) units.[113]

Various light-harvesting antennas based on acrylate monomers are depicted in Scheme 13. Schubert *et al.* utilized FRP to synthesize a methacrylate-based bipyridine pre-polymer.
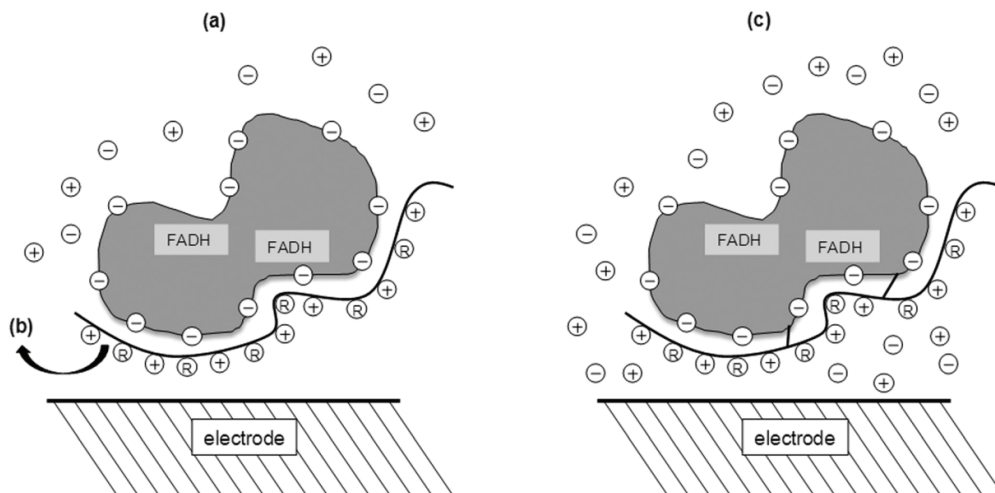
Fig. 11 Electrooxidation of glucose *via* a high molar mass polycationic redox polymer. (a) Electrostatic interaction of a polycationic redox polymer with a polyanionic enzyme brings the redox centers at a close range for the electron transfer. Electrons are transferred to the electrode *via* the polymer. (b) Charge transmission and coiling of the redox polymer lead to dissociation of the electrostatic complex, stop the electron transfer, and, thereby, electrooxidize glucose. (c) After covalent bonding of the redox polymer to the enzyme the complex does not dissociate and retains the electrooxidation of glucose.[144]
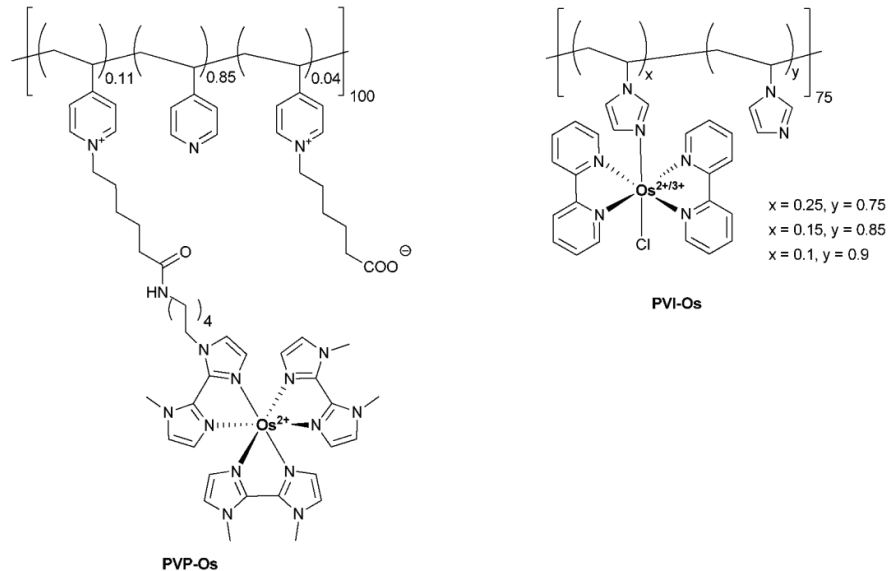
Scheme 15 Schematic representation of Os(II) complexes incorporated in redox polymers (the counter ions are omitted for clarity).

Subsequent grafting of Ru(II) polypyridyl (2,2'-bipyridine or 1,10-phenanthroline) precursor complexes onto the poly-(methyl methacrylate) (PMMA) copolymer allowed the formation of graft copolymers (Scheme 13, **PMMA–Ru**), which revealed the optical properties of the corresponding single Ru(II) complex. It was demonstrated that the PMMA backbone did not interfere with the photophysical properties, but enabled the processing of the material.[114] In a second approach, a (methyl methacrylate)-functionalized Ru(II) complex was used as comonomer in the free radical polymerization of methyl methacrylate (MMA).[115] By using different molar monomer-to-initiator ratios the metal content was varied from 1.3 to 22%. The luminescence properties of the Ru(II) subunit were not influenced indicating that self-quenching of the complexes was prevented. The graft-copolymers were processed into thin films, either by spin-coating or inkjet-printing, whereby no aggregation of the metal centers was observed even not for the polymers with higher ruthenium content.[116]

Miyashita et al. grafted Ru(bpy)$_3^{2+}$ on a pre-copolymerized system consisting of *N-tert*-pentylacrylamide and *N*-dodecyl-acrylamide, respectively, as well as an acrylate-functionalized bipyridine (Scheme 13, **PNAA–Ru**).[117] These copolymers formed stable condensed monolayers at the air/water interface. The monolayers were consecutively transformed onto solid supports, yielding Y-type polymer Langmuir–Blodgett[118] (LB) films. The UV/vis absorption spectra of the LB films indicated that the Ru(bpy)$_3^{2+}$ chromophores were incorporated into the polymer monolayer with a concentration of 3.9×10^{-11} mol cm^{-2}. The cyclic voltammograms (CVs) of the monolayers deposited on an electrode showed a well-defined symmetrical surface wave revealing reversible redox peaks of Ru(bpy)$_3^{2+}$ at different scan rates.[119] By depositing the LB films on an ITO electrode in the presence of a sacrificial electron donor (*e.g.* thiosalicylic acid), a large anodic photocurrent was observed with a rapid response to the light intensity. The conversion efficiencies of photons absorbed by the Ru(II) chromophores varied from 0.8% (dodecyl moiety) to 1.1% (*tert*-pentyl moiety). In further studies, *N*-isopropylacrylamide and an acrylate-functionalized 2,2'-bipyridine were copolymerized by FRP and, subsequently, *cis*-Ru(bpy)$_2$Cl$_2$ was grafted onto the poly(*N*-isopropylacryl-amide) (PNIPAM) copolymer, which is known to be a thermo-responsive polymer with a lower critical solution temperature (LCST) of 31 °C (Fig. 8). The electron transfer quenching of the **PNIPAM–Ru** polymer by MV^{2+} was investigated as a function of temperature. The electron transfer quenching rate constant (k_q) in the globular state (*i.e.* at a temperature above the LCST) was 5 times higher than that in the coil state (*i.e.* at a temperature below the LCST).[117]

A crucial issue concerning systems fabricated on flat substrates is the low optical density of chromophores in ultrathin films, since the thinness of active layers results in a limited number of effective photon-interacting chromophores per unit area. One approach toward obtaining a high optical density is the deposition of materials on a porous substrate with a large surface area, which greatly increased the load of chromophores.[120] Another approach is the layer-by-layer (LBL) deposition technique developed by Decher, which is a proper method for the deposition of ultrathin films on flat as well as on porous substrates.[121] Thin polymer films of **P(CM–Ru)** ($M_n \approx 1 \times 10^5$ g mol^{-1}) bearing

Ru(bpy)$_3^{2+}$ moieties (Scheme 13) were fabricated by the LBL technique at various concentrations and the light-collecting capability of the ruthenium-containing layer was demonstrated.[122] The absorption and the emission spectra were similar to those of individual Ru(bpy)$_3^{2+}$ centers and showed the match of the electronic states in the incorporated polymer. The phosphorescence of the Ru(II) moiety was quenched by ferrocene *via* energy migration between the Ru(II) moieties. The efficiency of the quenching strongly depended on the concentration of the Ru(II) moiety and exhibited its maximum for the polymer with 18 mol% of Ru(II). The diffusion coefficient for the energy migration increased by two orders of magnitude by increasing the ruthenium content from 4 mol% to 18 mol%.

Moreover, functionalized polypyridyl Ru(II) complexes were also grafted onto carbazole-based copolymers synthesized by FRP (*e.g.* Scheme 13, **PCMA–Ru**).[123] The resulting polymers were characterized in detail and the maintenance of the optical properties of the metal complex was demonstrated.[123–125] Recently, Kim et al. have applied carbazole-based polymers with Ru(II) chromophores as photosensitizers in photoconducting devices.[126]
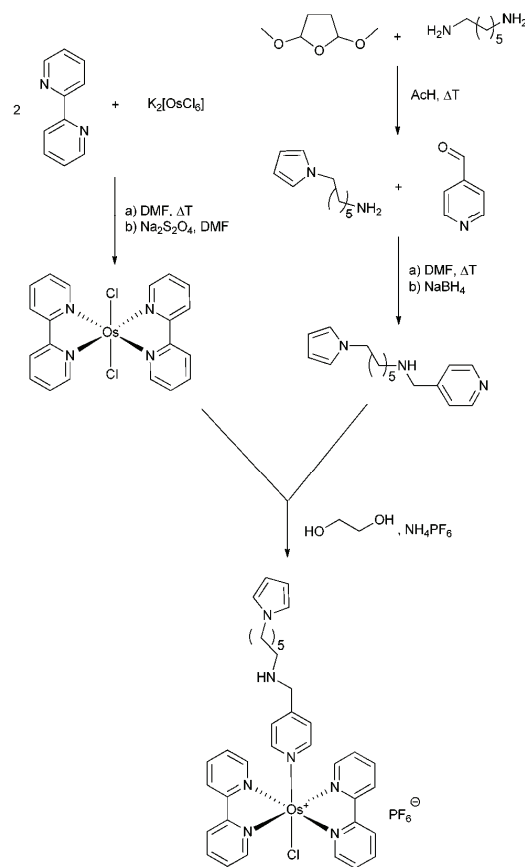
Scheme 16 Schematic representation of the synthesis of the hetero-leptic osmium complex monomer.
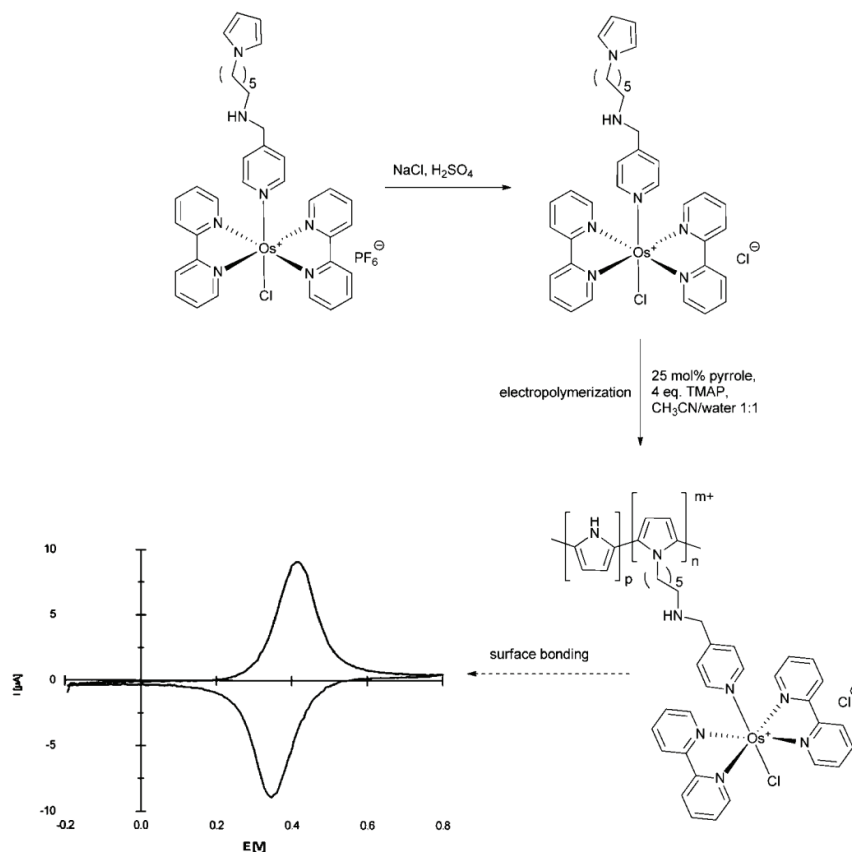
Scheme 17 Radical electropolymerization of a pyrrole-functionalized osmium complex (reproduced from ref. 152 with authorization by the American Chemical Society).

Another approach to control the construction of functional polymers was the utilization of the ring-opening metathesis polymerization (ROMP) due to its living nature and considerable functional group tolerance.[127–132] Sleiman *et al.* presented the direct and efficient synthesis of homopolymers and block copolymers bearing $Ru(bpy)_3^{2+}$ and $Ru(phen)_3^{2+}$ complexes, as pendant groups, *via* ROMP using a third generation Grubbs' catalyst.[133–135] The polymers **Ru-IV** and **Ru-V** (Scheme 14) were characterized by NMR spectroscopy, where the degree-of-polymerization (DP) of **Ru-IV** was calculated as 21. However, size exclusion chromatography (SEC) analysis could not be performed on the polymers, presumably due to strong interactions with the stationary phase. UV/vis absorbance and luminescence studies as well as CV measurements showed that the properties of the Ru(II) monomer were retained in both the homopolymers and the block copolymers. Using the controlled ROMP, the Ru(II)-containing block copolymers **Ru-V**, consisting of a Ru(II)–bipyridine-based block and a hydrophobic block, were varied with regard to their composition (*i.e.* block length, block ratio and polymer length) and, subsequently, systematically studied with respect to their
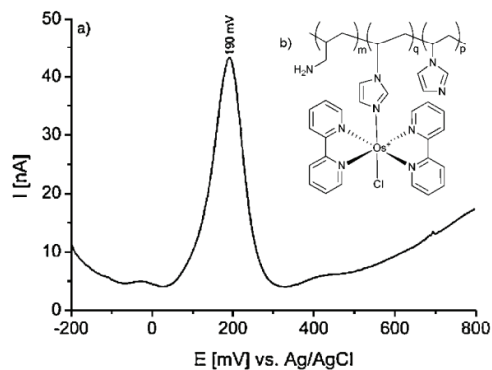
Fig. 12 (a) Differential pulse voltammograms for the osmium redox polymer (1 M aq. KCl, step potential 49.5 mV, interval time 0.2 s, modulation amplitude 150 mV, modulation time 0.06 s). (b) Structure of poly(vinyl)imidazole-Os(bpy)$_2$Cl (reproduced from ref. 159 with permission by Wiley-VCH).

self-assembly in different acetonitrile/toluene mixtures.[134] Depending on the composition of the solvent various morphologies of the micellar aggregates were observed, whereby polymer **Ru-Vf** disclosed the largest assortment including tubular structures (20 and 35% toluene, Fig. 9a and b), large spherical bilayers (40% toluene, Fig. 9c) and uniformly sized vesicles (70% toluene, Fig. 9d).

In a very recent publication, Sleiman *et al.* introduced a new class of block copolymers using ROMP for biological detection applications with signal amplification.[136] For this purpose,

three classes of ROMP monomers were synthesized: (i) luminescent metal-containing monomers, bearing Ru(II) and Ir(III) bipyridine units, (ii) biologically compatible macromonomers, containing oligoethylene glycol units, and (iii) biorecognizable monomer units, such as biotin (specific binding to avidin[137] proteins). ROMP was used to copolymerize these monomers into amphiphilic di- and triblock copolymers (Fig. 10). Since the metal-containing polymers interacted with the stationary phase of the SEC, the metal-free monomers were first employed to synthesize homopolymers in order to demonstrate the controlled
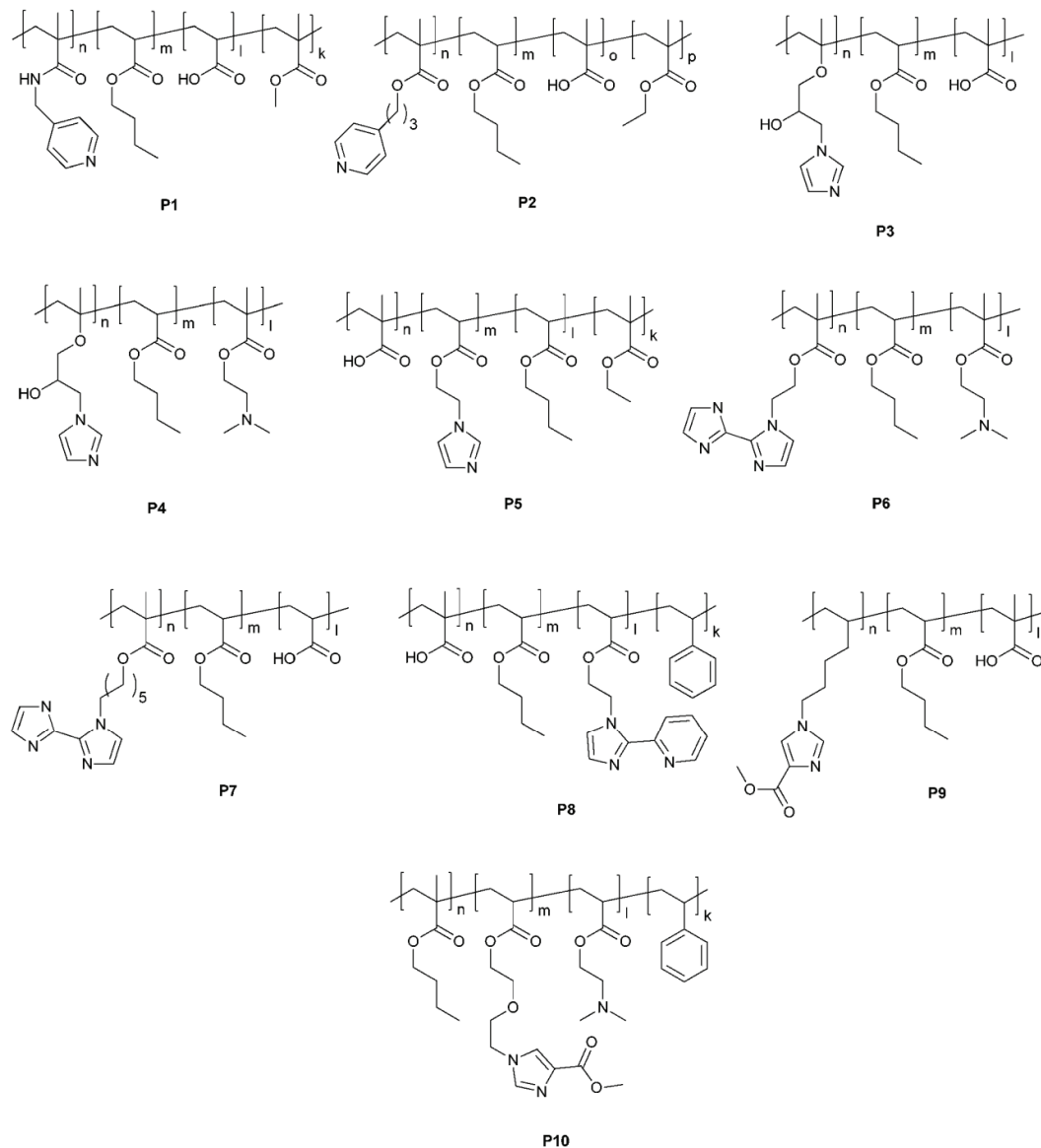
Fig. 13 Schematic representation of the molecular structures of the polymers **P1–10**.

2240 | *Chem. Soc. Rev.*, 2012, **41**, 2222–2255

This journal is © The Royal Society of Chemistry 2012

- 115 -

nature of the polymerization procedure, whereby PDI values below 1.1 were achieved. The Ru(II)-equipped di- and triblock polymers **Ru-VI** were examined in detail and formed spherical micelles upon self-assembly in aqueous media. Preliminary photophysical data were recorded for the latter ones and are summarized in Table 4 indicating that the Ru(bpy)$_3^{2+}$ units primarily acted as individual chromophores. Currently, the authors are optimizing these systems towards their potential applications as luminescent markers for biological molecules as well as drug delivery systems. Besides the examples evaluated in this section, there are a large number of studies dealing with polypyridyl Ru(II) complexes, as part of the polymer main-chain. These contributions have been reviewed lately by several authors[4,5,50,52,58,59,138–142] and will, therefore, not be discussed any further here.

Macromolecules containing pyridine-based Os(II) complexes in the side-chain

In 1990 Heller *et al.* reported the usage of hydrophilic poly-(4-vinylpyridine)s (PVPs), as macroligands, in order to complex Os(II) ions generating stable redox polymers.[16,143] These redox polymers were investigated towards their ability of biosensing, in particular, for the mediation of the electrooxidation of glucose. Electron mediators that are commonly employed in ampero-metric glucose sensors include ferrocenes, quinones, and ruthenium complexes.[144–146]

Commercial PVP (M_n = 50 000 g mol^{-1}) was partially complexed with the Os(II) precursor *cis*-Os(bpy)$_2$Cl$_2$ and, subsequently, the metal-free pyridine units were quaternized with bromoethylamine resulting in a high hydrophilicity. The same group also copolymerized *N*-methylvinylpyridinium chloride and Os(bpy)$_2$(4-vinylpyridine)Cl as well as with 1/20

of the vinylpyridine/pyridinium replaced by 4-aminostyrene.[143,144,147] It was demonstrated that these Os(II) redox polymers were able to mediate the oxidation of glucose by an electron transfer between polyanionic enzymes (*e.g.* glucose oxidase) and the polycationic redox polymers by forming a cross-linked redox hydrogel (Fig. 11). However, the complex decomposed with time and the electron transfer rate became evanescently small at high ionic strengths.[144,145]

Inner coordination sphere halides, *i.e.* chlorides, are not easily exchangeable in Os(III) complexes, since they are electro-statically strongly bound. However, they can be exchanged by *N*-heterocycles like pyridine (py), imidazole (im) or a primary amine if the complex is reduced to Os(II). Accordingly, if an electrode is covered by an adsorbed redox polymer and the Os(III) complex is electroreduced to Os(II), the chlorine ligands of the osmium complex are exchanged by the respective *N*-heterocycles of the backbone of the adsorbed strands, coordinatively linking the two strands. Thereby, the enzyme-wiring redox polymer avoids a possible phase separation. The polyanionic enzyme (glucose oxidase) forms an electrostatic adduct with the electro-deposited redox polymer and can be electro-deposited as well. Subsequently, the electro-deposited films catalyze the electrooxidation of glucose.[16,145]

In order to optimize the electrooxidation, new generations of redox polymers have been developed and investigated: crucial parameters, including the tuning of the redox potential of the osmium complex, the substrate diffusion barrier, the electron transfer properties and the optimization of the current density could be improved by employing the redox polymers depicted in Scheme 15.[148–151] 2,2'-*bis*(1-Methyl-1*H*-imidazole) (bim) and 2,2'-bipyridine, respectively, were used as ancillary ligands for the osmium complexes.

Table 5 Electrochemical potentials of the polymer-bound Os(II) complexes

	Parent Os(II) complex	$E_{1/2}{}^a$/mV	Product	Conditions
P1	[Os(bpy)$_2$Cl$_2$]	−169	[Os(bpy)$_2$(CO)Cl]$^+$	75 °C, H$_2$O/EtOH
		+60	[Os(bpy)$_2$Py(CO)]$^{2+}$	75 °C, H$_2$O/EtOH
		+340	[Os(bpy)$_2$PyCl]$^+$	75–95 °C, H$_2$O/i-PrOH
		+560	[Os(bpy)$_2$(Py)]$^{2+}$	90–95 °C, i-PrOH
P2	[Os(bpy)$_2$Cl$_2$]	+340	[Os(bpy)$_2$PyCl]$^+$	90–95 °C, i-PrOH
P3	[Os(bpy)$_2$Cl$_2$]	−15	[Os(bpy)$_2$Im(CO)]$^{2+}$	85 °C, H$_2$O/EtOH
		+115	[Os(bpy)$_2$ImCl]$^+$	85–95 °C, H$_2$O/EtOH
P4	[Os(bpy)$_2$Cl$_2$]	−155	[Os(bpy)$_2$(CO)Cl]$^{2+}$	80 °C, H$_2$O
		−6	[Os(bpy)$_2$Im(CO)]$^{2+}$	75–85 °C, H$_2$O/EtOH
		+108	[Os(bpy)$_2$ImCl]$^+$	75–85 °C, H$_2$O/EtOH
		+200	[Os(bpy)$_2$(CO)$_2$]$^{2+}$	75–85 °C, H$_2$O
		+300	[Os(bpy)$_2$(Im)$_2$]$^{2+}$	95–140 °C, H$_2$O/i-PrOH
	[Os(bim)$_2$Cl$_2$]	−430	[Os(bim)$_2$Im(CO)]$^{2+}$	85 °C, H$_2$O
		−300	[Os(bim)$_2$(Im)Cl]$^+$	90–95 °C, H$_2$O/EtOH
		−234	[Os(bim)$_2$(Im)$_2$]$^{2+}$	85 °C, H$_2$O
P5	[Os(bpy)$_2$Cl$_2$]	+105	[Os(bpy)$_2$(Im)Cl]$^+$	80 °C, EtOH
P6	[Os(bpy)$_2$Cl$_2$]	+320	[Os(bpy)$_2$(bim)]$^{2+}$	95 °C, i-PrOH
P7	[Os(bim)$_2$Cl$_2$]	−251	[Os(bim)$_2$(bim)]$^{2+}$	100 °C, i-PrOH
P8	[Os(bpy)$_2$Cl$_2$]	−165	[Os(bpy)$_2$(CO)Cl]$^+$	85 °C, H$_2$O/EtOH
		+350	[Os(bpy)$_2$(Py)Cl]$^+$	85 °C, H$_2$O/EtOH
		+470	[Os(bpy)$_2$(Py)Im]$^{2+}$	85–95 °C, H$_2$O/EtOH
	[Os(bim)$_2$Cl$_2$]	−300	[Os(bim)$_2$(CO)Cl]$^+$	85 °C, H$_2$O/i-PrOH
		−142	[Os(bim)$_2$(Py)Im]$^{2+}$	85 °C, H$_2$O/i-PrOH
		+271	[Os(bim)$_2$(CO)$_2$]$^{2+}$	85 °C, H$_2$O/i-PrOH
P9	[Os(bpy)$_2$Cl$_2$]	−10	[Os(bpy)$_2$Im(CO)]$^{2+}$	75–85 °C, H$_2$O/EtOH
P10	[Os(bpy)$_2$Cl$_2$]	−12	[Os(bpy)$_2$Im(CO)]$^{2+}$	85 °C, H$_2$O
		+180	[Os(bpy)$_2$(CO)$_2$]$^{2+}$	85 °C, H$_2$O

^{a} Measured *versus* Ag/AgCl electrode.

Schuhmann *et al.* were also interested in amperometric biosensors utilizing glucose oxidase, as a biological recognition system, whereby the enzyme-integrated prosthetic group (FADH$_2$) was reoxidized by means of an Os(II) complex containing a redox polymer mediator. Though, the related enzyme electrodes have shown distinct sensor properties, the formation of the cross-linked redox hydrogels revealed an unsolved problem regarding reproducibility (due to inhomogeneous thickness of the polymer layer). Consequently, the group of Schuhmann used a modified poly(pyrrole), which was covalently attached to the osmium complexes. In contrast to the cross-linking approach, electrochemically-induced polymerization occurred on the active surface of the working electrode. In addition, the thickness of the polymer film could be controlled *via* the charge transferred during the polymerization process.[152]

The reaction sequence yielding a mediator-modified pyrrole derivative is shown in Scheme 16. *cis*-Os(bpy)$_2$Cl$_2$ can be synthesized by a two-step reaction from K$_2$OsCl$_6$ and 2,2′-bipyridine.

The final pyrrole functionalization of the osmium complex was carried out by a ligand exchange reaction with (pyridin-4-yl-methyl)-(6-pyrrol-1-yl-hexyl)amine. The aliphatic spacer chain provided the desired flexibility.

The electrochemically-induced copolymerization of pyrrole[152,153] and the pyrrole-functionalized Os(II) complex in the presence of glucose oxidase occurred *via* intermediate radical cations and was, hence, highly dependent on the presence of molecular oxygen or nucleophilic groups, which could capture the formed radicals. For solubility reasons the counter ion of the osmium complex was changed from hexafluorophosphate to chloride prior to the polymerization process (Scheme 17). Copolymerization of the two monomers could be proven by CV measurements showing nearly symmetric oxidation and reduction waves of the polymer-integrated osmium centers, which indicated surface attached redox species.[152,154,155]

Warren *et al.* carried out the electrochemical characterization of films obtained by copolymerization of [Os(bpy)$_2$XCl]

Re-I
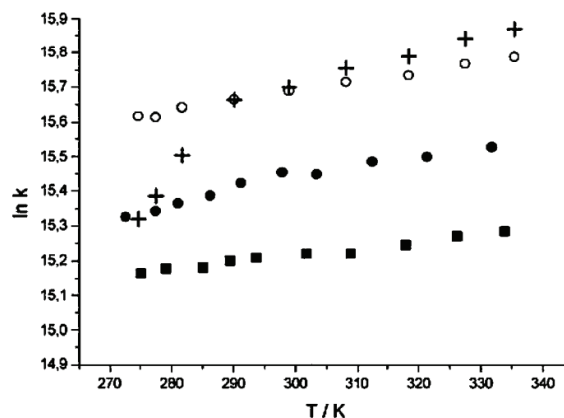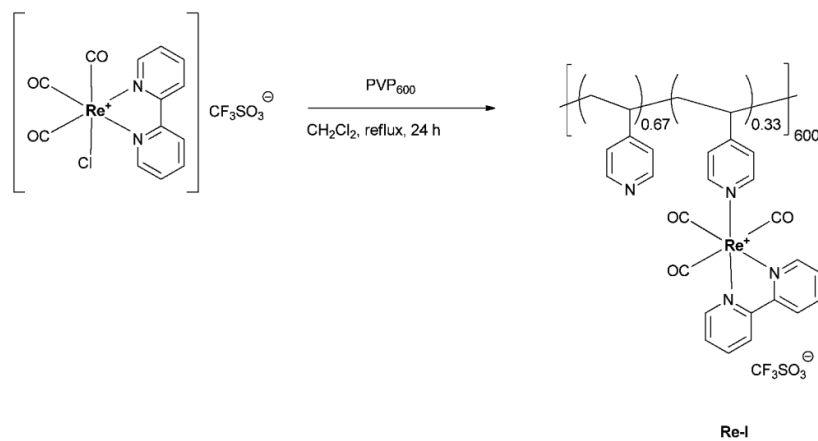
Scheme 18 Top: synthesis of a Re(I)-containing PVP ($M_n \approx 6 \times 10^4$ g mol^{-1}). Bottom: temperature dependence of the emission liftetimes for the monomer and the polymer in MeCN and MeCN/H$_2$O (1 : 4 mixture). (■)—[(py)Re(CO)$_3$bpy]$^+$ in MeCN; (●)—**Re-I** in MeCN; (○)—[(py)Re(CO)$_3$bpy]$^+$ in MeCN/H$_2$O and (+)—**Re-I** in MeCN/H$_2$O (reproduced from ref. 167 with permission by the Royal Society of Chemistry).

[Os-PMP, X = 3-(pyrrol-1-ylmethyl)pyridine] with 3-methyl thiophene or 1,2-diaminobenzene.[156] The complex was copolymerized with 3-methylthiophene utilizing CV yielding a stable redox active film. Afterwards, a copolymer based on [Os(bpy)₂PMP(Cl)]PF₆ and 1,2-diaminobenzene was synthesized electrochemically using the so-called membrane templating method.[157,158] The obtained films, formed by the latter method, revealed tubular aggregates of the copolymer on the surface and could improve the stability of the system compared to those in the absence of the tubular structures.

Schuhmann *et al.* could also demonstrate the suitability of Os(bpy)₂Cl₂-modified poly(vinyl)imidazole (PVI) redox polymers (Fig. 12b) as both immobilization matrix and electron mediator for isolated photosystem-2 (PS2) complexes leading to enhanced water oxidation.[159] PVI was synthesized by FRP using 2,2′-azo*bis*(isobutyronitrile) (AIBN), as initiator, and the resulting polymer was subsequently treated with *cis*-Os(bpy)₂Cl₂. Similarly, systems based on PVP and PVI were studied as described elsewhere.[17,160–162]

The polymer immobilized the PS2 firmly on the electrode surface, while its hydrogel-type character still allowed small molecules to diffuse almost freely through the immobilization matrix. Electrons from the PS2-driven water splitting were accepted by the redox centers of the polymer and transferred to the electrode surface. Amino functions on the polymer and on the lysine residues of the protein complex were cross-linked by means of a bifunctional molecule, such as poly(ethylene glycol)diglycidyl ether (PEGDGE), yielding a polymer network. The potential of the redox polymer was determined by differential pulse voltammetry (DPV, Fig. 12a).

The peak at 190 mV (*vs.* Ag/AgCl, 3 M aq. KCl) was attributed to the Os(II)/Os(III) redox couple. The absence of other peaks indicated that the coordination sphere was uniform for all Os(II) complexes attached to the polymer backbone. Gold electrodes modified with the cross-linked redox polymer and PS2 showed a ten times higher photocurrent (current density ≈ 45 μA cm⁻²) than the comparable redox polymer systems immobilizing PS2.[163,164]

A recent publication by Schuhmann *et al.* comprised a library of over 50 Os(II) complex-containing polymers suited for electrodeposition, which were tested with respect to their electron transfer ability in combination with enzymes, such as glucose oxidase and cellobiose dehydrogenase.[165] The redox potential of the resulting poly(acrylate)-based polymers, which were synthesized by FRP, could be tuned over a wide range by grafting different osmium complexes, such as *cis*-Os(bpy)₂Cl₂ and *cis*-Os(bim)₂Cl₂ (Fig. 13, Table 5). Furthermore, the latter complexes featured an easy exchange of the chlorine ligand by oxygen under mild conditions (at 70 to 90 °C in aqueous solution), when incorporated in acrylic acid-based polymers resulting in a low redox potential. Currently, a few examples of these polymers are investigated towards the design of biofuel cell cathodes.[166]

Macromolecules containing pyridine-based Re(I) complexes

Rhenium(I)-containing polymers have widely been studied, triggered by their interesting properties: these types of materials

combine the advantage of the tunability of the redox and photophysical properties of the Re(I) complex with the processability of an organic polymer, which is predominantly important for low-cost device manufacturing in the field of optoelectronics. The accessible excited states, which are metal-to-ligand charge transfer (MLCT), ligand-to-ligand charge transfer (LLCT) and/or intraligand (IL) excited states, are generally involved in the observed luminescence at room temperature.[38,50,62,138,141]

Rhenium(I) complexes attached on the side-chain

Wolcan *et al.* have applied ligand substitution reactions on commercial PVP using Re(I) tricarbonyl complexes. The photophysical properties of the resulting Re(I) polymer and the corresponding [(py)Re(CO)₃(bpy)]⁺ monomer were investigated in detail, where solvent, temperature and laser power effects on the distinct photophysical behavior were observed for both the monomer and the polymer (Scheme 18). It has been
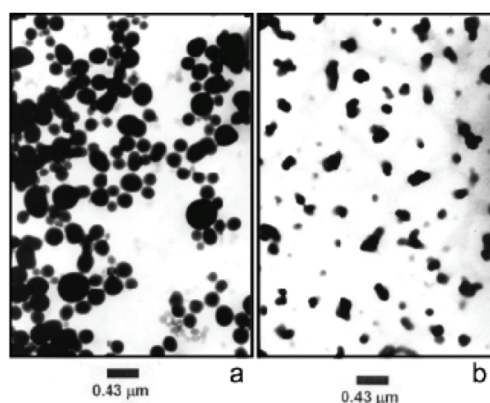
Fig. 14 Transmission electron micrographs of the solvent cast films of the polymer (a) **Re-I** and (b) **Re-I–CuCl₂** (reproduced from ref. 168 with authorization by the American Chemical Society).
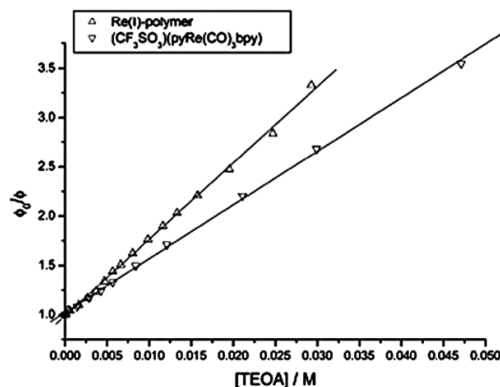
Fig. 15 Stern–Volmer plots for the luminescence quenching of **Re-I** and the monomer [(py)Re(CO)₃bpy]⁺ by TEOA (reproduced from ref. 168 with authorization by the American Chemical Society).
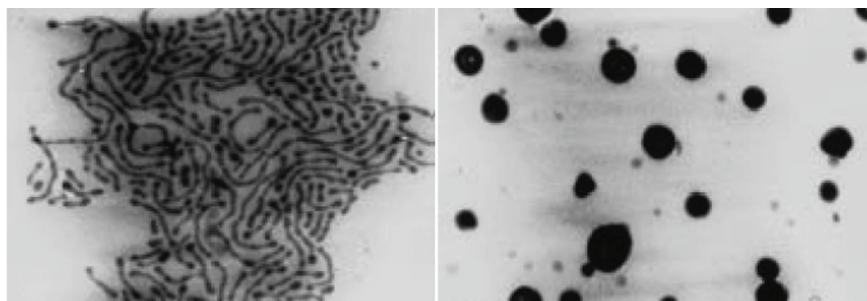
Fig. 16 Transmission electron micrographs of **Re-IIb** (left) and **Re-IIa** (right) prepared from toluene/CH_2Cl_2 (reproduced from ref. 171 with permission by Wiley-VCH).

demonstrated that the incorporation of roughly 200 $Re(CO)_3$bpy chromophores into the PVP had only little impact relative to the single monomers MLCT excited state, if these complexes were irradiated with low photonic fluxes (*i.e.* steady state irradiations with $n_{h\nu} \leq 2$ mJ pulse^{-1}).[167] The temperature dependence of the emission lifetimes (Scheme 18, bottom) in a polar solvent mixture (MeCN/water) showed a bi-exponential behavior for the polymer at temperatures below 15 °C; above this temperature its behavior was mono-exponential. Wolcan *et al.* claimed that thermal activation might be responsible for a transition between a coil and a rigid-rod structure,

whereby the coil structure dominated in highly polar (or in highly non-polar) solvents, at temperatures below 15 °C, and the rigid-rod structure in solvents like MeCN above 15 °C.

The polymer **Re-I** was later on investigated with respect to micelle formation and reductive redox quenching.[168] Transmission electron microscopy (TEM) images (Fig. 14) and DLS experiments demonstrated that the latter polymer aggregated to form mainly spherical micelles, whose dimensions were in the range of 90 to 430 nm. Subsequent to the treatment with

Re-IIa: x/y = 3.1
Re-IIb: x/y = 0.35

Scheme 19 Schematic representation of the synthesis of the Re(I)-containing block copolymers.[171]
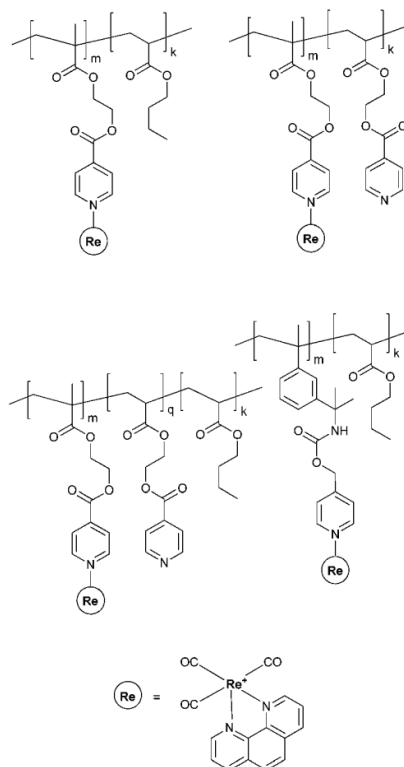
Scheme 20 Schematic representation of the structures of Re(I)-functionalized methacrylate-based polymers.

Cu(II) ions, the formed polymer **Re-I–CuCl₂** assembled into micelles that were distorted from the spherical shape, and whose dimensions were smaller than those of the micelles formed by the parent polymer (Fig. 15). Additionally, **Re-I** revealed reductive quenching by triethanolamine (TEOA) following a typical Stern–Volmer kinetics (Fig. 16). From the Stern–Volmer constant ($K_{SV} = 77$ M^{-1}) and the luminescence lifetime in acetonitrile, a bimolecular quenching constant of $k_q = 3.8 \times 10^8$ M^{-1} s^{-1} was calculated.

Similar PVP-based polymers were studied, where the Re(I) subunit bears 1,10-phenanthroline (phen) as an ancillary ligand. [Re(CO)₃(phen)]$^+$ was attached to commercial PVP₆₀₀ by ligand substitution reactions of the Re(I) complexes.[169,170] The polymer and the metal complex [(py)Re(CO)₃phen]CF₃SO₃, as model substrate, were characterized by UV/vis spectroscopy exhibiting similar features. The extinction coefficient of the polymer corresponded to approximately 200 chromophores ([Re(CO)₃phen]$^+$) per polymer chain in comparison to the extinction coefficient of the monomer. Detailed photochemical investigations by flash

photolysis and pulse radiolysis showed that the MLCT excited states in the polymer underwent a more efficient annihilation than in the monomer. Redox quenching experiments with the polymer by MV^{2+} and TEOA indicated the presence of intrastrand electron transfer processes.[170] The rate constant of the latter process was dependent on the solvent used, displaying a six-time higher rate in methanol compared to that in acetonitrile.

Chan *et al*. were interested in Re(I)-containing block copolymers derived from polystyrene-*block*-poly(4-vinylpyridine) (PS-*b*-PVP). The pyridine moieties of a PS-*b*-PVP diblock copolymer were used to coordinate [Re(CO)₃(bpy)]$^+$ yielding the Re(I)-functionalized block copolymers **Re-II**.[171] The polymers were synthesized according to Scheme 19 and selected characterization parameters are summarized in Table 6. It was assumed that the metal-containing blocks were ionic in nature and that their properties were different from the hydrophobic PS block. The PS blocks aggregated in polar as well as non-polar solvents and formed micelles of different sizes and shapes, depending on the block size and the solvent system (Table 6, Fig. 16).

Table 6 Selected properties of the Re(I)-containing block copolymers

Polymer	x/y	$M_n{}^a$/g mol^{-1}	PDI^b	Re/PVP^c	Micelle structure in CH₂Cl₂/toluene	Micelle structure in CH₂Cl₂/MeOH
Re-IIa	3.1	53 900	1.13	0.13	Disc (radius ≈ 100 nm)	Sphere (radius 20 to 80 nm)
Re-IIb	0.35	30 800	1.16	0.21	Rod (length ≈ 200 nm, radius ≈ 20 nm)	Sphere (radius ≈ 200 nm)

^{a} Number average molar mass determined by SEC. ^{b} Polydispersity index of the starting PS-*b*-PVP. ^{c} Pyridine moieties functionalized with a rhenium complex.

1: M = no metal; **Re-III**: M = Re^I(CO)₃Cl

2: M = no metal; **Re-IVa**: M = Re^I(CO)₃Cl; **Re-IVb**: M = Re^I(CO)₃NCCH₃

3: n = 1, M = no metal; **Re-Va**: M = Re^I(CO)₃Cl; **Re-Vb**: M = Re^I(CO)₃NCCH₃
4: n = 2, M = no metal; **Re-VI**: M = Re^I(CO)₃Cl
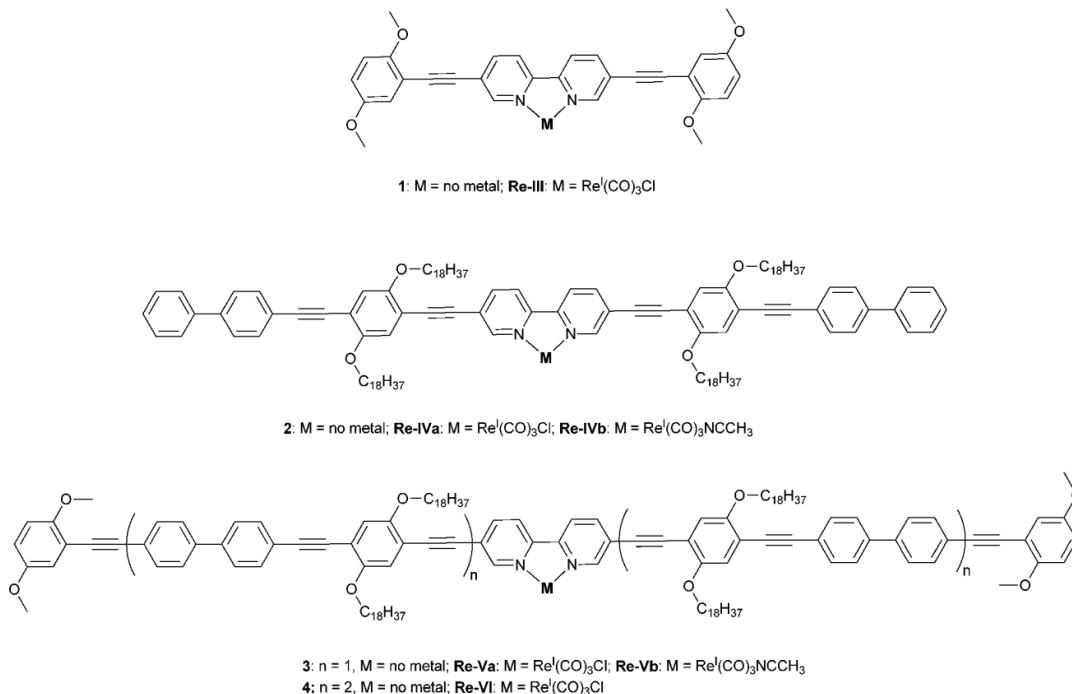
Scheme 21 Schematic representation of oligo(arylene ethynylene)s containing two different Re(I) complexes.[188]

Re-VII: x = 0, y = 1   **Re-IX**: x = 0.25, y = 0.75
Re-VIII: x = 0.1, y = 0.9   **Re-X**: x = 0.5, y = 0.5
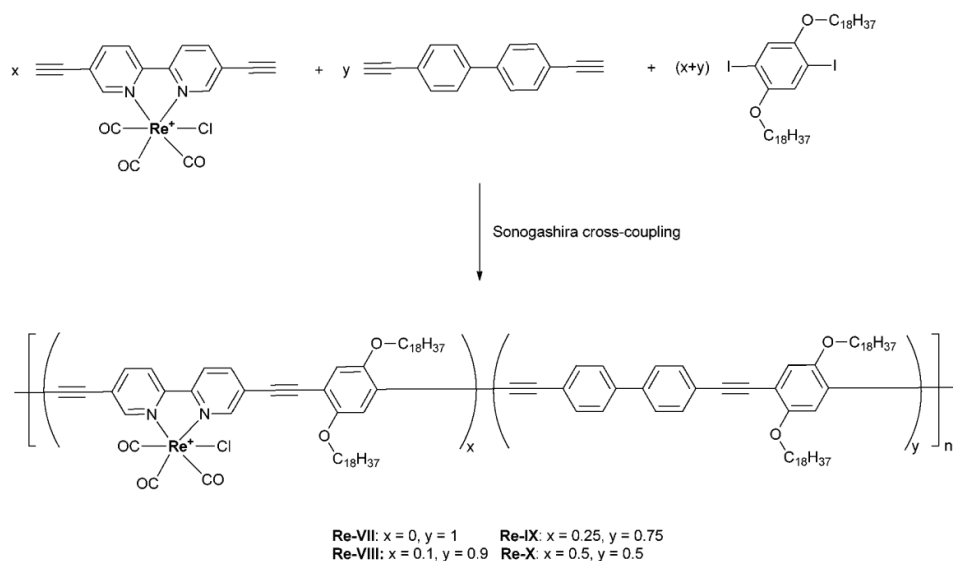
Scheme 22 Schematic representation of poly(arylene ethynylene) (PPE) architectures containing Re(I) complexes.[186]

In a mixture of toluene and CH_2Cl_2 the macromolecules possessed higher flexibility and experienced reduced charge repulsion. Steric effects between different Re(I) moieties became more important and, consequently, the micelles formed from polymer **Re-IIb** revealed a rod-like structure, which was almost 200 nm in length. By contrast, the micelles formed by polymer **Re-IIa** appeared to be spherical in shape (Fig. 16, right).

There are only a few examples, where Re(I) complexes of the general type $[Re(CO)_3L]^+$ (L = 1,10-phenanthroline, 2,2′-bipyridine, iminopyridines) were bound to methacrylate-based polymers. The preparation of the corresponding Re(I)-containing polymers was performed both by FRP and controlled copolymerization methods (in the latter case using atom transfer radical polymerization (ATRP)). In the former case, the light-emitting Re(I) complex was attached to a pre-synthesized polymer by complexation reaction between a reactive $[Re(phen)(CO)_3(acetone)]^+$ precursor and the pyridine units of the polymer side-chains.[172] All polymers reported by Bignozzi et al. (Scheme 20) were characterized by conventional experimental techniques including NMR spectroscopy, size exclusion chromatography (SEC), differential scanning calorimetry (DSC), and thermogravimetric analysis (TGA). UV/vis and emission spectroscopies were applied to investigate the optical properties of the polymers in solid-state films and in solution. The structure of the synthesized polymers was confirmed by ^{1}H NMR spectroscopy and allowed the estimation of the monomer sequences in the copolymer chains. The glass transition temperatures (T_g) for the polymers were determined by DSC. The T_g is related to the permeability of the polymeric matrix towards diffusion of gases; the relatively low T_g of the rubber-like polymers depicted in Scheme 20 and time-resolved emission quenching experiments implied an application of these polymeric materials as oxygen sensors.[11,173,174]

In the group of Chan, Re(I)-iminopyridine and 2,2′-bipyridine complexes were successfully polymerized by ATRP. The copolymerization of MMA with different Re(I) complex/MMA ratios was demonstrated as well as the synthesis of an ABA triblock copolymer with PMMA, as macroinitiator.[175]

Table 7 Selected photophysical properties of the polymers **Re-VII–Re-X**[186]

Polymer	$\lambda_{\text{abs,max}}{}^a$/nm	Assignment	$\lambda_{\text{em,max}}{}^a$/nm	$\phi^{a,b}$	$\tau^{a,c}$/ns
Re-VII	400	$\pi \to \pi^*$	435	0.28	1.1
Re-VIII	400	$\pi \to \pi^*$	435	0.16	0.78
	465(sh)	$d\pi \to \pi^*$ (MLCT)			
Re-IX	400	$\pi \to \pi^*$	435	0.11	0.48
	469(sh)	$d\pi \to \pi^*$ (MLCT)			
Re-X	388	$\pi \to \pi^*$	432	0.073	0.40
	469	$d\pi \to \pi^*$ (MLCT)			

^{a} Ambient temperature data in THF solution. ^{b} Quantum yield of π–π^* fluorescence. ^{c} Median lifetime.

Re-fluI: m = 0.8, n = 0.2
Re-fluII: m = 0.9, n = 0.1
Re-fluIII: m = 0.95, n = 0.05
Re-fluIV: m = 0.995, n = 0.005
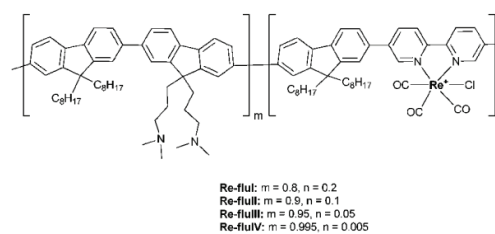
Scheme 23 Schematic representation of polyfluorene copolymers with different Re(I) complex contents.

- 121 -
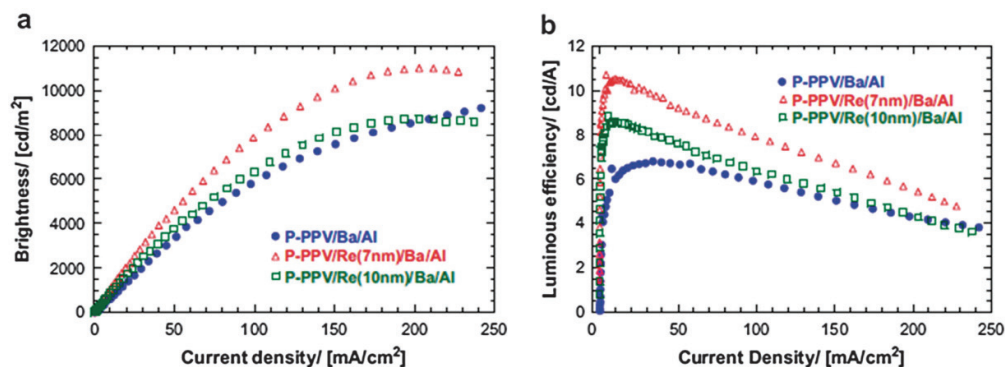
Fig. 17 The current density–brightness (a) and current density–luminance efficiency (b) curves of PPV devices with Ba/Al and **Re-fluIII**/Ba/Al as cathodes (reproduced from ref. 191 with permission by Elsevier).

The neutral Re(I) complex in the homopolymers and copolymers was further converted into an ionic form by replacing the chloride ligand by an imidazole ligand, thereby significantly enhancing the solubility of the resulting ionic polymers. The photosensitizing properties of the polymer films were investigated by the measurement of the photocurrent response under an externally applied electric field: the photoconductivity values of the polymers containing the Re(I) iminopyridine complexes were in the range of 10^{-12}–10^{-13} Ω^{-1} cm^{-1}, which were comparable to the values reported for other conjugated polymers equipped with ruthenium(I) complexes as photosensitizers.[176]

Rhenium(I) complexes in the main-chain

π-Conjugated polymers and oligomers are of interest due to their unique optical and electronic properties, which enable their use, as an active medium, in optical, electronic, optoelectronic and chemical sensing devices. Studies of organic π-conjugated materials have established the relationship between molecular structure and the properties of the materials.[177–182] Rhenium(I) diimine complexes have been incorporated into polymeric structures based on polystyrene,[183] poly(methyl methacrylate),[183] poly(p-phenylenevinylene)[20,23,184] and polyurethane.[185]

However, only a few articles deal with the structure–property relationships of conjugated Re(I)-containing polymers.[23,186,187] Schanze et al. selected, as targets, a series of oligo(arylene ethynylene)s (OAEs) that contained a central 2,2′-bipyridine metal chelating unit. A broad examination of the optical properties was carried out on a series of well-defined π-conjugated oligomers comprising a [Re(CO)$_3$L]$^+$ (L = Cl, MeCN) complex as chelating unit (Scheme 21).[186–188] The bipyridine-containing oligomers were synthesized by a stepwise sequence utilizing the Pd^0-catalyzed cross-coupling of a terminal acetylene and an aryl iodide (Sonogashira coupling) as the key step. The metalation with Re(I) complexes was conducted afterwards. The final compounds revealed a complex arrangement of excited states and, therefore, it was not possible to clearly interpret the influence of the π-conjugated electronic system on the MLCT excited states of the Re(I)-containing oligomers. The unmetalated oligomers **1–4** strongly absorbed throughout the near-UV into

the visible region and showed remarkably similar fluorescence energies around 450 nm. The metal-containing oligomers were surprisingly dominated by π–π* transitions and their luminescence was largely quenched as revealed by transient absorption and time-resolved electron paramagnetic resonance (TREPR) spectroscopy.[189] Poly(arylene ethynylene)s (PPEs) functionalized
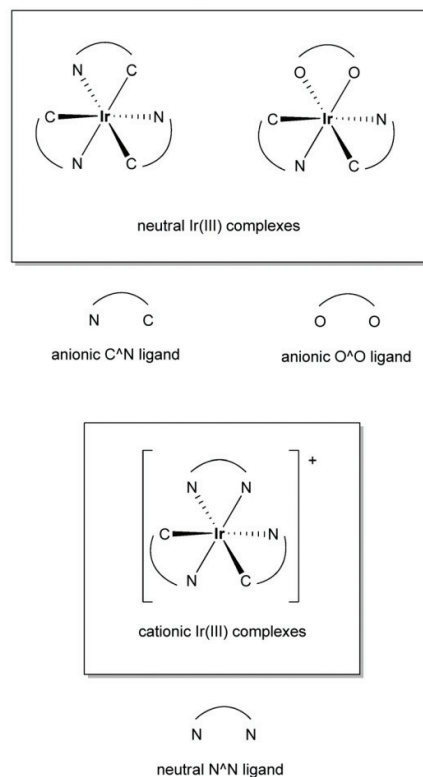
Fig. 18 General structure of frequently used neutral and ionic Ir(III) complexes.[194]

with $[Re(CO)_3Cl]^+$ were synthesized by the same group utilizing Sonogashira cross-coupling, and displayed remarkable photophysical features as well (Scheme 22, Table 7).[141,186,190] The excitation of **Re-VII–Re-X** into the π–π^* absorption band revealed a strong emission (435 nm) and a bathochromically-shifted shoulder due to vibronic coupling. Because of the small Stokes-shift the emission was assigned to be fluorescence from the π–π^* exciton state. The fluorescence lifetimes and quantum yields for **Re-VII–Re-X** decreased as the Re(I) content increased. This parallel decrease indicated that the $^1\pi$–π^* exciton was quenched by the [(bpy)Re^I(CO)$_3$Cl] subunits in the polymers.[186]

Moreover, the $[Re(CO)_3Cl]^+$ subunit was attached to 2,2′-bipyridine-based aminoalkyl-polyfluorenes yielding copolymers **Re-fluI-IV** with different contents of the Re(I) complex (Scheme 23). The polymer backbone was synthesized *via* a Suzuki cross-coupling polymerization procedure. The unmetalated aminoalkyl-polyfluorenes had good solubility in organic solvents in contrast to the Re(I)-containing copolymers, which became insoluble in most organic solvents. The optoelectronic and electroluminescent properties of these copolymers were investigated and were found to show similar performances in polymer light-emitting devices (PLEDs). Furthermore, the Re(I)-containing copolymers were used, as an electron transport layer, in a PLED leading to a general performance improvement.[191] Fig. 17 shows the current density–voltage characteristic and the light output from different device structures (*i.e.* ITO/PEDOT/PPV/Ba/Al, ITO/PEDOT/PPV/**Re-fluIII** (7 nm)/Ba/Al and ITO/PEDOT/PPV/**Re-fluIII** (10 nm)/Ba/Al; with PPV as emissive layer). By introducing a thin layer of the Re(I)-containing polymer **Re-fluIII** between the emissive layer and the cathode,

the device performance was significantly improved. The device performance with a 7 nm-thick layer of **Re-fluIII** was better than with a layer thickness of 10 nm. At the same current density, the devices with the additional Re(I) layer revealed higher brightness output and luminance efficiency than the device with a pure Ba/Al cathode.

Macromolecules containing pyridine-based Ir(III) complexes

The heavy atom effect has been used in phosphorescent Ir(III) complexes for developing materials predominantly applied in organic light-emitting diodes (OLEDs). The main motivation for the synthesis of phosphorescent Ir(III) complexes was the access to more efficient OLEDs compared to fluorescent materials, because they can gather both the singlet and the triplet excitons formed during excitation. Most studies on Ir(III) complexes have focused on small molecules, which generally require high temperature/vacuum deposition techniques during the device fabrication procedure.[61,192,193]

So far, the incorporation of Ir(III) ions into a polymeric backbone has been investigated to a minor extent compared to the isoelectronic Ru(II) species, which was mainly owed to synthetic problems in the past. Polymer light-emitting diodes (PLEDs) are very attractive compared to OLEDs, since such devices can be manufactured using low cost and efficient solution processing techniques, such as spin-coating or ink-jet printing.[19,22,116,194–196]

Polymers bearing Ir(III) complexes attached to the polymer backbone, as pendant groups, fall into two categories: the complex
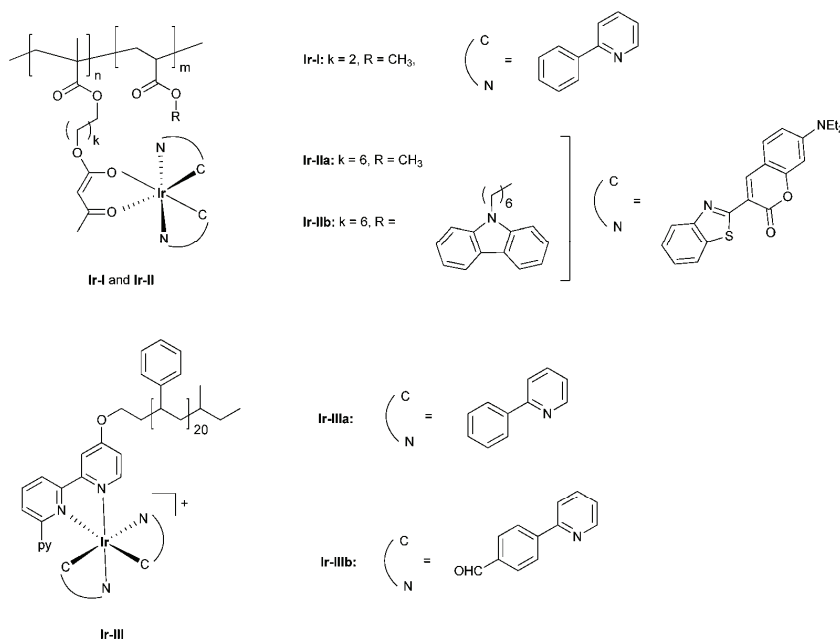
Scheme 24 Schematic representation of Ir(III)-containing polymers with polystyrene and poly(methacrylate) as backbones (the counter ions are omitted for clarity).[209–211]

is connected to a conjugated polymer [*e.g.* polyfluorene, poly-(fluorene-carbazole)], or to a polymer with a saturated, *i.e.* non-conjugated, backbone [*e.g.* poly(methacrylate), polystyrene, poly(styrene-carbazole)]. In this review, only non-conjugated polymers will be highlighted. Iridium(III) complexes attached to poly-fluorenes as pendant groups,[22,138,140,197–202] or as an integral part of a conjugated main-chain[22,138,201–208] have been comprehensively reviewed recently.

In general, Ir(III) complexes can be divided into two classes: neutral and cationic complexes (Fig. 18). Neutral Ir(III) complexes contain three anionic ligands, which have been mostly reported in the past [thereby, mono-cyclometalating ligands (C^N) are the most common representatives in this respect]. In the last few years, cationic Ir(III) complexes, containing two anionic ligands and one neutral ligand (Fig. 18), have moved

to the focus of interest, because they are able to offer emissive centers and ionic conductivity in the same molecule.

Schubert *et al.* synthesized Ir(III)-containing polymers based on polystyrene and poly(methacrylate) backbones with different *mono*-cyclometalating C^N ligands. A defined copolymer (Scheme 24) bearing an acetylacetonate-type (acac) ligand was synthesized by utilizing the controlled reversible addition–fragmentation transfer (RAFT) radical polymerization technique: a dimeric hydroxy-bridged Ir(III) precursor was used to coordinate the Ir(III) chromophore to the copolymer afterwards.[209] The successful coordination was confirmed by NMR, UV/vis absorption, and emission spectroscopy as well as SEC and enabled the preparation of Ir(III)-containing polymers as potential emitters for PLEDs. Furthermore, a methacrylate-functionalized phosphorescent Ir(III)-complex was copolymerized with MMA using
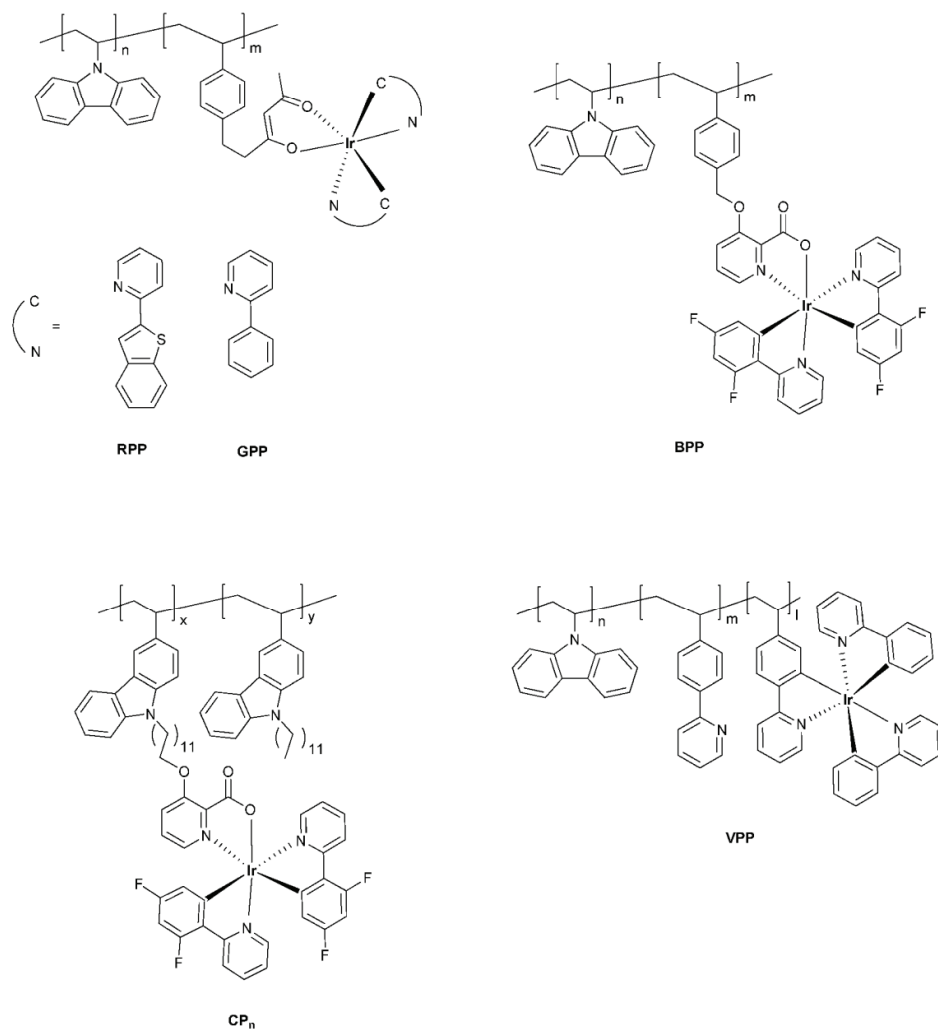
Scheme 25 Schematic representation of iridium polymers based on poly(vinylcarbazole), as host material.

FRP yielding polymer **Ir-IIa** (Scheme 24).[210] Aiming for host–guest systems the complex was further copolymerized with a methacrylate-functionalized carbazole derivative by ATRP providing copolymer **Ir-IIb**. The optical properties of the monomers and the copolymers were investigated by absorption and emission spectroscopy in solution. The emission of the carbazole-copolymer **Ir-IIb** was found to be iridium-based and indicated an intra-chain energy transfer. Cationic Ir(III)-complexes were further grafted onto terpyridine-functionalized polystyrene using 2-phenylpyridine, as cyclometalating ligand [polymers **Ir-III** (Scheme 24)].[211] Their structure and purity were investigated in detail by 1D- and 2D-NMR spectroscopy as well as SEC. The aldehyde functionality on the cyclometalating ligand created a significant change in the emission color in solution shifting to yellow-greenish, whereas the polymer without the aldehyde functionality displayed an orange emission color. The materials were inkjet-printed on glass substrates and the film forming properties were studied by atomic force microscopy (AFM) with respect to the morphology. In addition, thin films of various thicknesses of the Ir(III) copolymer **Ir-IIIa** were effectively inkjet-printed; the absorption as well as emission intensities of the copolymers declined with decreasing film thickness in a linear fashion.[116] Similar systems have been studied elsewhere[212–216] revealing the successful incorporation of phosphorescent Ir(III) complexes into a polystyrene backbone and were characterized afterwards with regard to their optical properties.

Poly(vinylcarbazole) (PVC) and its derivatives are commonly used as non-conjugated host materials, since they display a good hole-transport ability and high energy singlet excited states as well as favorable film-forming properties and durability at high temperatures.[194]

Ir-IVa: m/n/k = 1/1/1
Ir-IVb: m/n/k = 6/1/6
Ir-IVc: m/n/k = 10/1/10

Ir-IV

Ir-V
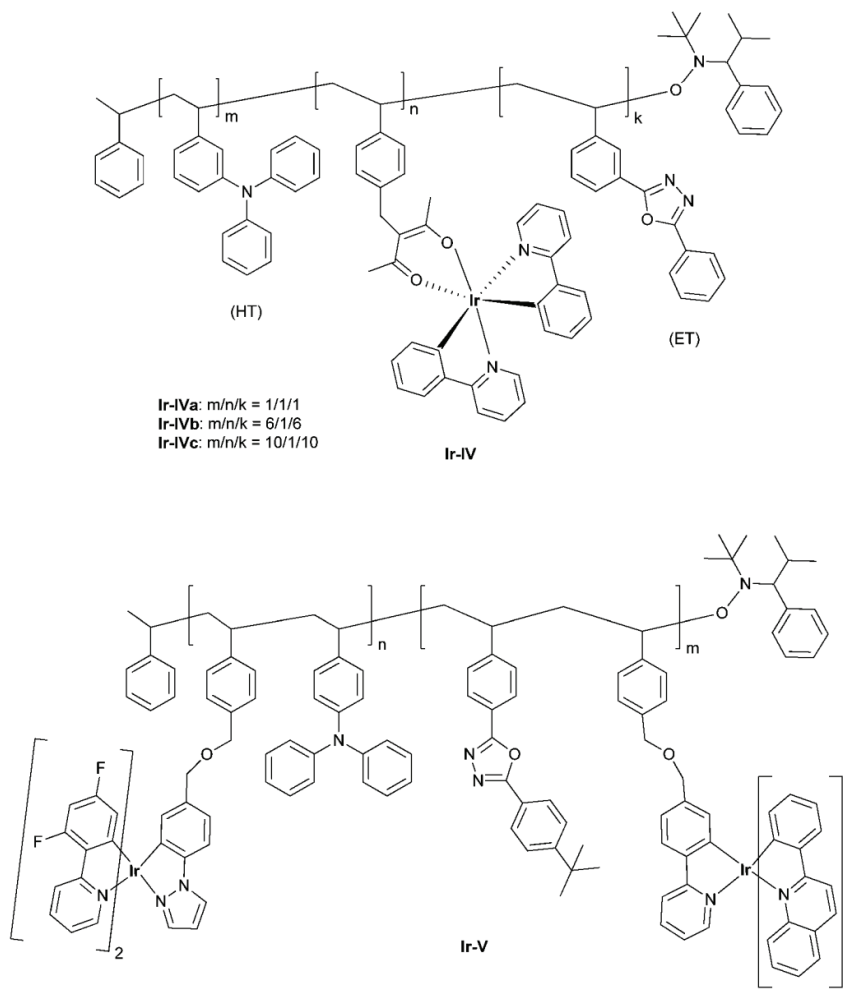
Scheme 26 Schematic representation of iridium-containing nitroxide initiated terpolymers **Ir-IV** and **Ir-V** (HT = hole transport, ET = electron transport).

Tokito *et al.* reported polymers **BPP**, **GPP**, **RPP** (Scheme 25) combining PVC, as hosts, and neutral Ir(III) complexes, as guests.[217,218] The concentration of the Ir(III) complex in the final polymer could be controlled during the copolymerization and was varied within a range of 0.1–2.0 mol%. The molar mass was determined by SEC ($M_n \approx 16\,000$ g mol^{-1}, PDI: not reported). These polymers were soluble in common organic solvents and were processed from solution into films by spin-coating. The corresponding PLEDs exhibited red, green, or blue emission depending on the electronic nature of the cyclometalating ligand on the Ir(III) complexes. By employing a hole-blocking layer between the emissive layer and the cathode of the PLEDs (*i.e.* enhancing the recombination efficiency for the injected holes and electrons), external quantum efficiencies of 6.9% for **RPP**, 11% for **GPP**, and 6.6% for **BPP** were achieved.[217]

Efficient blue electrophosphorescence was obtained from Ir(III) *bis*-[(4,6-difluorophenyl)pyridinato-*N*,*C*$^{2'}$]picolinate (Irpic) that was attached to the carbazole-based polymer poly-(9-dodecyl-3-vinylcarbazole) as host (Scheme 25).[219] The molar masses of the copolymers containing Irpic pendants (**CP*n***) could be varied from 18\,000 to 33\,700 g mol^{-1} by utilizing FRP. The molar content of the Irpic-containing monomer units was varied between 0.8 to 10.6% (**CP1**: 0.8%, **CP2**: 2.9%, **CP3**: 5.3%, **CP4**: 10.6%). Phase segregation in the **CP*n*** copolymers was significantly suppressed and the photoluminescence spectra of the carbazole-based polymer hosts overlapped with the absorption band of the Irpic guest. Furthermore the triplet energy level of the polymer host (-2.6 eV) was higher than that of the Irpic (-3.1 eV) ensuring efficient energy transfer and resulted in highly efficient blue phosphorescence. The device of the **VPP** copolymer (Scheme 25) showed an external quantum efficiency of 4.4%.[220]

In general, the efficiency of an emitting device with a single emitting layer depends on the balance of holes and electrons. Doping with oxadiazoles, as electron transporter (ET) molecules, and triphenylamines, working as hole transporters (HT), had beneficial effects on the performance of solution-processed PLED devices.[221] Incorporation of both HT and ET functionalities into copolymers featured a significant advantage over the ET-doping strategy preventing possible phase separation and crystallization of small molecular ET.

The synthesis of copolymers containing acrylic and styrenic oxadiazoles (ET), triphenylamines (HT) and functionalized β-diketone monomers by nitroxide-mediated radical polymerization (NMP) was described by Fréchet *et al.*[222,223] Utilization of a second-generation nitroxide initiator allowed the polymerization into homo-polymers as well as random and block co- and terpolymers with predictable molar masses and relatively low PDI values (Scheme 26, **Ir-IV**).[222] The polymers bearing HT and ET moieties were either directly used, as a matrix, for doping with luminescent molecules or were coordinated with phosphorescent Ir(III) complexes. The terpolymer **Ir-IVc** displayed the highest external quantum efficiency in a PLED device so far ($\sim$10%). Moreover, the group of Fréchet designed two heteroleptic Ir(III) complexes bearing a pendant styrene substituent, which enabled a radical polymerization (Scheme 26, **Ir-V**).[223]

The polymerizable ancillary ligands, *p*-tolylpyrazole styrene and *p*-tolylpyridine styrene, were chosen for their high triplet
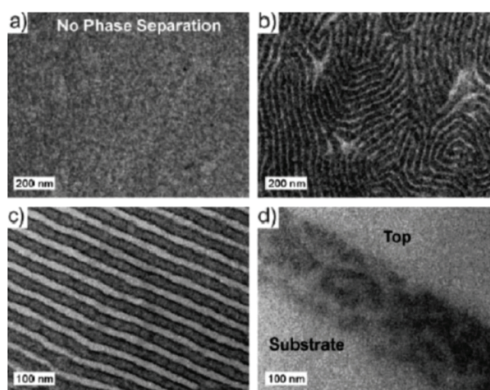
Fig. 19 TEM images of **Ir-V** polymers having different molar masses: (a) $M_n = 30\,000$ g mol^{-1}, $n/m = 10/0.5$, (b) $M_n = 100\,000$ g mol^{-1}, $n/m = 10/1$, (c) $M_n = 150\,000$ g mol^{-1}, $n/m = 10/2$, (d) cross-sectional view of polymer **Ir-V** with $M_n = 150\,000$ g mol^{-1} in thin film (reproduced from ref. 223 with permission by Wiley-VCH).

energies and, thus, the phosphorescent emission color was determined by the cyclometalating ligands. As a result, the phosphorescent emission color was located in the green/blue and orange/red region of the visible spectrum, respectively. The target block copolymers **Ir-V** could be varied within a range of 30\,000 to 150\,000 g mol^{-1}, but the lengths of the two blocks were kept equal in order to study the morphology at different sizes. Diblock copolymers were obtained by NMP by preparing the first and the second block *via* a random copolymerization, consecutively. The film morphology of three white-emitting **Ir-V** copolymers was explored by transmission electron microscopy (TEM) (Fig. 19). Fig. 19a indicated a homogeneous film and no phase separation of the polymer with $M_n = 30\,000$ g mol^{-1}. In contrast, the higher molar mass polymers (Fig. 19b and c) showed clear nanometre-sized features (lamellar morphology), which explained the suppressed energy transfer in these materials.[223]

Conclusions

In this review a summary of metal-containing polymers is provided focusing on the heavy d^6 transition metal ions Ru(II), Os(II), Re(I) as well as Ir(III), where the polymers mainly bear the metal subunit as a pendant group. Research on these polymers is mainly concentrated on photophysical, electrochemical and material processing issues. The key polymerization techniques for the polymer synthesis are free radical polymerization (uncontrolled manner), ring-opening metathesis polymerization (controlled manner) and reversible addition–fragmentation transfer radical polymerization (controlled manner) by incorporating the metal complexes into the polymeric backbone *via* copolymerization and grafting techniques, respectively. The first part was dedicated to fundamentals of photophysical and photochemical processes with the intent to widen the reader's comprehension.

The incorporated Ru(II) complexes exclusively contained 4-functionalized 2,2′-bipyridines possessing additional amide-,

methacrylate-, vinyl or hydroxyl-moieties, which allowed the preparation of macromolecules with Ru(II) complexes being attached to the polymer side chains. The hydroxy- and amide functionalized Ru(II) complexes were grafted onto polystyrene, whereas the amide functionalization was further exploited in ring-opening metathesis polymerization as well as a tool for Merrifield solid-phase peptide synthesis as a supplementary polymerization method. The ring-opening metathesis polymerization and the solid-phase peptide synthesis provided access to Ru(II)-containing polymers with control of the local array of added functional groups.

Osmium(II) complexes were introduced into the polymeric side chain to create redox active polymers which were capable of functioning, as a mediator, in biosensing applications (e.g. supporting electrooxidation of glucose). The Os(II) complexes enclosed 2,2'-bipyridine and bis(1H-imidazole) as chelating ligands and were grafted onto poly(4-vinylpyridine) and poly-(vinylimidazole), respectively. The resulting redox polymers were applied in biosensing applications, e.g. electrooxidation of glucose. Furthermore, a library of Os(II)-containing polymers based on poly(acrylate) was established in order to evolve the optimal conditions in electron transfer reactions with a selected enzyme.

Rhenium(I) complexes were installed, as pendant groups, in the polymer side chain as well as fixed in the polymer main chain. Grafting of the [Re(CO)₃bpy]⁺ entity to poly(4-vinyl-pyridine) and poly(styrene)–poly(4-vinylpyridine) block polymers led to macromolecules forming micellar aggregates in selective solvents. Furthermore, 2,2'-bipyridine as a part of the main chain of polyarylene ethynylenes and polyfluorenes, served as a coordinating element for [Re(CO)₃Cl]⁺ chromophores. The obtained Re(I)-containing macromolecules were applied, as emissive layers, in light-emitting devices leading to a performance enhancement.

Functionalized phenylpyridine and/or bipyridine-based bidentate ligands were used to coordinate Ir(III) ions. The corresponding neutral and cationic iridium(III) complexes, respectively, were covalently introduced, as pendant groups, on the polymeric side chain and were found to have beneficial processing features in thin film light-emitting devices. In particular, further incorporation of hole and electron transporter functionalities into the iridium copolymers showed a supplementary advantage compared to the doping strategy preventing possible phase separation and crystallization.

Notes and references

1 J.-M. Lehn, Angew. Chem., Int. Ed. Engl., 1988, 27, 89–112.
2 D. J. Cram, Angew. Chem., Int. Ed. Engl., 1988, 27, 1009–1020.
3 C. J. Pedersen, Angew. Chem., Int. Ed. Engl., 1988, 27, 1021–1027.
4 U. S. Schubert and C. Eschbaumer, Angew. Chem., Int. Ed., 2002, 41, 2893–2926.
5 H. Hofmeier and U. S. Schubert, Chem. Soc. Rev., 2004, 33, 373–399.
6 C. D. Eisenbach and U. S. Schubert, Macromolecules, 1993, 26, 7372–7374.
7 C. R. K. Glasson, L. F. Lindoy and G. V. Meehan, Coord. Chem. Rev., 2008, 252, 940–963.
8 A. Juris, V. Balzani, F. Barigelletti, S. Campagna, P. Belser and A. von Zelewsky, Coord. Chem. Rev., 1988, 84, 85–277.
9 K. Kalyanasundaram, Coord. Chem. Rev., 1982, 46, 159–244.
10 S. M. Baxter, W. E. Jones, E. Danielson, L. Worl, G. Strouse, J. Younathan and T. J. Meyer, Coord. Chem. Rev., 1991, 111, 47–71.
11 J. F. Rabek, Prog. Polym. Sci., 1988, 13, 83–188.
12 J. Sýkora and J. Šima, Coord. Chem. Rev., 1990, 107, 1–212.
13 S. M. Aly, C.-L. Ho, W.-Y. Wong, D. Fortin and P. D. Harvey, Macromolecules, 2009, 42, 6902–6916.
14 S. M. Aly, C.-L. Ho, D. Fortin, W.-Y. Wong, A. S. Abd-El-Aziz and P. D. Harvey, Chem.–Eur. J., 2008, 14, 8341–8352.
15 L. Prodi, F. Bolletta, M. Montalti and N. Zaccheroni, Coord. Chem. Rev., 2000, 205, 59–83.
16 A. Heller and B. Feldman, Chem. Rev., 2008, 108, 2482–2505.
17 A. P. Doherty, R. J. Forster, M. R. Smyth and J. G. Vos, Anal. Chim. Acta, 1991, 255, 45–52.
18 C. Qin, W.-Y. Wong and L. Wang, Macromolecules, 2010, 44, 483 489.
19 V. Marin, E. Holder, R. Hoogenboom and U. S. Schubert, Chem. Soc. Rev., 2007, 36, 618–635.
20 W. K. Chan, P. K. Ng, X. Gong and S. J. Hou, J. Mater. Chem., 1999, 9, 2103–2108.
21 B. O'Regan and M. Grätzel, Nature, 1991, 353, 737–740.
22 C. Ulbricht, B. Beyer, C. Friebe, A. Winter and U. S. Schubert, Adv. Mater., 2009, 21, 4418–4441.
23 W. K. Chan, C. S. Hui, K. Y. K. Man, K. W. Cheng, H. L. Wong, N. Zhu and A. B. Djurisic, Coord. Chem. Rev., 2005, 249, 1351–1359.
24 K. Kalyanasundaram and M. Grätzel, Coord. Chem. Rev., 1998, 177, 347–414.
25 W.-Y. Wong and C.-L. Ho, Acc. Chem. Res., 2010, 43, 1246–1256.
26 W.-Y. Wong, Macromol. Chem. Phys., 2008, 209, 14–24.
27 W.-Y. Wong, X.-Z. Wang, Z. He, A. B. Djurisic, C.-T. Yip, K.-Y. Cheung, H. Wang, C. S. K. Mak and W.-K. Chan, Nat. Mater., 2007, 6, 521–527.
28 W.-Y. Wong, X.-Z. Wang, Z. He, K.-K. Chan, A. B. Djurišić, K.-Y. Cheung, C.-T. Yip, A. M.-C. Ng, Y. Y. Xi, C. S. K. Mak and W.-K. Chan, J. Am. Chem. Soc., 2007, 129, 14372–14380.
29 Q. Wang, Z. He, A. Wild, H. Wu, Y. Cao, U. S. Schubert, C.-H. Chui and W.-Y. Wong, Chem.–Asian J., 2011, 6, 1766–1777.
30 W.-Y. Wong and P. D. Harvey, Macromol. Rapid Commun., 2010, 31, 671–713.
31 W.-Y. Wong, Dalton Trans., 2007, 4495–4510.
32 W.-Y. Wong and C.-L. Ho, Coord. Chem. Rev., 2006, 250, 2627–2690.
33 G.-J. Zhou and W.-Y. Wong, Chem. Soc. Rev., 2011, 40, 2541–2566.
34 G.-J. Zhou, W.-Y. Wong, Z. Lin and C. Ye, Angew. Chem., Int. Ed., 2006, 45, 6189–6193.
35 G. J. Zhou, W. Y. Wong, C. Ye and Z. Lin, Adv. Funct. Mater., 2007, 17, 963–975.
36 V. Balzani, G. Bergamini, S. Campagna and F. Puntoriero, Photochemistry and Photophysics of Coordination Compounds I, Springer-Verlag, Berlin, 2007, vol. 280, pp. 1–36.
37 S. Campagna, F. Puntoriero, F. Nastasi, G. Bergamini and V. Balzani, Photochemistry and Photophysics of Coordination Compounds I, Springer-Verlag, Berlin, 2007, vol. 280, pp. 117–214.
38 R. A. Kirgan, B. P. Sullivan and D. P. Rillema, Photochemistry and Photophysics of Coordination Compounds II, Springer-Verlag, Berlin, 2007, vol. 281, pp. 45–100.
39 V. Balzani, A. Juris, M. Venturi, S. Campagna and S. Serroni, Chem. Rev., 1996, 96, 759–833.
40 J. N. Demas, J. Chem. Educ., 1983, 60, 803–808.
41 X.-Y. Wang, A. Del Guerzo and R. H. Schmehl, J. Photochem. Photobiol., C, 2004, 5, 55–77.
42 P. J. Steel, Acc. Chem. Res., 2005, 38, 243–250.
43 U. S. Schubert, H. Hofmeier and G. R. Newkome, Modern Terpyridine Chemistry, Wiley-VCH, 2006.
44 R. C. Evans, P. Douglas and C. J. Winscom, Coord. Chem. Rev., 2006, 250, 2093–2126.
45 J.-M. Lehn, Supramolecular Chemistry, Concepts and Perspectives, Wiley-VCH, 1995.
46 G. R. Whittell, M. D. Hager, U. S. Schubert and I. Manners, Nat. Mater., 2011, 10, 176–188.
47 G. Zhou, Y. He, B. Yao, J. Dang, W.-Y. Wong, Z. Xie, X. Zhao and L. Wang, Chem.–Asian J., 2010, 5, 2405–2414.
48 K. Liu, C.-L. Ho, S. Aouba, Y.-Q. Zhao, Z.-H. Lu, S. Petrov, N. Coombs, P. Dube, H. E. Ruda, W.-Y. Wong and I. Manners, Angew. Chem., Int. Ed., 2008, 47, 1255–1259.

49 W.-Y. Wong, *J. Inorg. Organomet. Polym. Mater.*, 2005, **15**, 197–219.

50 W. K. Chan, *Coord. Chem. Rev.*, 2007, **251**, 2104–2118.

51 R. Shunmugam, G. J. Gabriel, K. A. Aamer and G. N. Tew, *Macromol. Rapid Commun.*, 2010, **31**, 784–793.

52 A. Wild, A. Winter, F. Schlütter and U. S. Schubert, *Chem. Soc. Rev.*, 2011, **40**, 1459–1511.

53 U. S. Schubert, A. Winter and G. R. Newkome, *Terpyridine-based Materials For Catalytic, Optoelectronic and Life Science Applications*, Wiley-VCH, Weinheim, 2011.

54 E. C. Constable, *Chem. Soc. Rev.*, 2007, **36**, 246–253.

55 I. Eryazici, C. N. Moorefield and G. R. Newkome, *Chem. Rev.*, 2008, **108**, 1834–1895.

56 E. A. Medlycott and G. S. Hanan, *Coord. Chem. Rev.*, 2006, **250**, 1763–1782.

57 P. R. Andres and U. S. Schubert, *Adv. Mater.*, 2004, **16**, 1043–1068.

58 G. R. Newkome, E. He and C. N. Moorefield, *Chem. Rev.*, 1999, **99**, 1689–1746.

59 U. S. Schubert, G. R. Newkome and I. Manners, *Metal-Containing and Metallosupramolecular Polymers and Materials*, ACS, Washington, DC, 2006.

60 D. Kumaresan, K. Shankar, S. Vaidya and R. H. Schmehl, *Photochemistry and Photophysics of Coordination Compounds II*, Springer-Verlag, Berlin, 2007, vol. 281, pp. 101–142.

61 L. Flamigni, A. Barbieri, C. Sabatini, B. Ventura and F. Barigelletti, *Photochemistry and Photophysics of Coordination Compounds II*, Springer-Verlag, Berlin, 2007, vol. 281, pp. 143–203.

62 A. I. Baba, J. R. Shaw, J. A. Simon, R. P. Thummel and R. H. Schmehl, *Coord. Chem. Rev.*, 1998, **171**, 43–59.

63 C. M. Flynn and J. N. Demas, *J. Am. Chem. Soc.*, 1974, **96**, 1959–1960.

64 J. N. Demas and B. A. DeGraff, *Anal. Chem.*, 1991, **63**, 829A–837A.

65 E. M. Kober, B. P. Sullivan, W. J. Dressick, J. V. Caspar and T. J. Meyer, *J. Am. Chem. Soc.*, 1980, **102**, 7383–7385.

66 A. J. Lees, *Chem. Rev.*, 1987, **87**, 711–743.

67 G. J. Kavarnos and N. J. Turro, *Chem. Rev.*, 1986, **86**, 401–449.

68 F. Scandola and V. Balzani, *J. Chem. Educ.*, 1983, **60**, 814–823.

69 J. Olmsted and T. J. Meyer, *J. Phys. Chem.*, 1987, **91**, 1649–1655.

70 I. V. Khudyakov, Y. A. Serebrennikov and N. J. Turro, *Chem. Rev.*, 1993, **93**, 537–570.

71 G. J. Kavarnos, *Top. Curr. Chem.*, 1990, **156**, 21–58.

72 J. N. Demas and G. A. Crosby, *J. Mol. Spectrosc.*, 1968, **26**, 72–77.

73 R. J. Watts, *Comments Inorg. Chem.*, 1991, **11**, 303–337.

74 N. Sutin, C. Creutz and E. Fujita, *Comments Inorg. Chem.*, 1997, **19**, 67–92.

75 T. J. Meyer, *Acc. Chem. Res.*, 1989, **22**, 163–170.

76 N. Sutin and C. Creutz, *Pure Appl. Chem.*, 1980, **52**, 2717–2738.

77 M. Kirch, J.-M. Lehn and J.-P. Sauvage, *Helv. Chim. Acta*, 1979, **62**, 1345–1384.

78 J. H. Alstrum-Acevedo, M. K. Brennaman and T. J. Meyer, *Inorg. Chem.*, 2005, **44**, 6802–6827.

79 T. Nishijima, T. Nagamura and T. Matsuo, *J. Polym. Sci., Part C: Polym. Lett.*, 1981, **19**, 65–73.

80 S. F. Chan, M. Chou, C. Creutz, T. Matsubara and N. Sutin, *J. Am. Chem. Soc.*, 1981, **103**, 369–379.

81 G. M. Brown, B. S. Brunschwig, C. Creutz, J. F. Endicott and N. Sutin, *J. Am. Chem. Soc.*, 1979, **101**, 1298–1300.

82 K. Okeyoshi and R. Yoshida, *Soft Matter*, 2009, **5**, 4118–4123.

83 P. M. Ennis, J. M. Kelly and C. M. Oconnell, *J. Chem. Soc., Dalton Trans.*, 1986, 2485–2491.

84 M. Suzuki, M. Kimura, K. Hanabusa and H. Shirai, *J. Chem. Soc., Faraday Trans.*, 1997, **93**, 4137–4143.

85 M. Kaneko, M. Ochiai, K. Kinosita and A. Yamada, *J. Polym. Sci., Part A: Polym. Chem.*, 1982, **20**, 1011–1019.

86 T. Abe and M. Kaneko, *Prog. Polym. Sci.*, 2003, **28**, 1441–1488.

87 M. Suzuki, S. Kobayashi, S. Uchida, M. Kimura, K. Hanabusa and H. Shirai, *Polymer*, 1998, **39**, 1539–1543.

88 M. Sykora, K. A. Maxwell, J. M. DeSimone and T. J. Meyer, *Proc. Natl. Acad. Sci. U. S. A.*, 2000, **97**, 7687–7691.

89 V. Balzani, A. Credi and M. Venturi, *ChemSusChem*, 2008, **1**, 26–58.

90 J. N. Younathan, S. F. McClanahan and T. J. Meyer, *Macromolecules*, 1989, **22**, 1048–1054.

91 G. F. Strouse, L. A. Worl, J. N. Younathan and T. J. Meyer, *J. Am. Chem. Soc.*, 1989, **111**, 9101–9102.

92 W. E. Jones, S. M. Baxter, G. F. Strouse and T. J. Meyer, *J. Am. Chem. Soc.*, 1993, **115**, 7363–7373.

93 L. A. Worl, W. E. Jones, G. F. Strouse, J. N. Younathan, E. Danielson, K. A. Maxwell, M. Sykora and T. J. Meyer, *Inorg. Chem.*, 1999, **38**, 2705–2708.

94 L. M. Dupray and T. J. Meyer, *Inorg. Chem.*, 1996, **35**, 6299–6307.

95 C. N. Fleming, L. M. Dupray, J. M. Papanikolas and T. J. Meyer, *J. Phys. Chem. A*, 2002, **106**, 2328–2334.

96 L. A. Worl, G. F. Strouse, J. N. Younathan, S. M. Baxter and T. J. Meyer, *J. Am. Chem. Soc.*, 1990, **112**, 7571–7578.

97 G. B. Shaw and J. M. Papanikolas, *J. Phys. Chem. B*, 2002, **106**, 6156–6162.

98 L. M. Dupray, M. Devenney, D. R. Striplin and T. J. Meyer, *J. Am. Chem. Soc.*, 1997, **119**, 10243–10244.

99 C. N. Fleming, M. K. Brennaman, J. M. Papanikolas and T. J. Meyer, *Dalton Trans.*, 2009, 3903–3910.

100 M. H. V. Huynh, D. M. Dattelbaum and T. J. Meyer, *Coord. Chem. Rev.*, 2005, **249**, 457–483.

101 R. M. Leasure, T. Kajita and T. J. Meyer, *Inorg. Chem.*, 1996, **35**, 5962–5963.

102 T. Kajita, R. M. Leasure, M. Devenney, D. Friesen and T. J. Meyer, *Inorg. Chem.*, 1998, **37**, 4782–4794.

103 C. N. Fleming, K. A. Maxwell, J. M. DeSimone, T. J. Meyer and J. M. Papanikolas, *J. Am. Chem. Soc.*, 2001, **123**, 10336–10347.

104 D. A. Friesen, T. Kajita, E. Danielson and T. J. Meyer, *Inorg. Chem.*, 1998, **37**, 2756–2762.

105 C. N. Fleming, P. Jang, T. J. Meyer and J. M. Papanikolas, *J. Phys. Chem. B*, 2004, **108**, 2205–2209.

106 S. L. Mecklenburg, B. M. Peek, J. R. Schoonover, D. G. McCafferty, C. G. Wall, B. W. Erickson and T. J. Meyer, *J. Am. Chem. Soc.*, 1993, **115**, 5479–5495.

107 D. G. McCafferty, B. M. Bishop, C. G. Wall, S. G. Hughes, S. L. Mecklenberg, T. J. Meyer and B. W. Erickson, *Tetrahedron*, 1995, **51**, 1093–1106.

108 C. A. Slate, D. R. Striplin, J. A. Moss, P. Y. Chen, B. W. Erickson and T. J. Meyer, *J. Am. Chem. Soc.*, 1998, **120**, 4885–4886.

109 D. R. Striplin, S. Y. Reece, D. G. McCafferty, C. G. Wall, D. A. Friesen, B. W. Erickson and T. J. Meyer, *J. Am. Chem. Soc.*, 2004, **126**, 5282–5291.

110 S. L. Gilat, A. Adronov and J. M. J. Fréchet, *Angew. Chem., Int. Ed.*, 1999, **38**, 1422–1427.

111 A. Adronov, S. L. Gilat, J. M. J. Frechet, K. Ohta, F. V. R. Neuwahl and G. R. Fleming, *J. Am. Chem. Soc.*, 2000, **122**, 1175–1185.

112 X. Schultze, J. Serin, A. Adronov and J. M. J. Fréchet, *Chem. Commun.*, 2001, 1160–1161.

113 J. Serin, X. Schultze, A. Adronov and J. M. J. Fréchet, *Macromolecules*, 2002, **35**, 5396–5404.

114 V. Marin, E. Holder and U. S. Schubert, *J. Polym. Sci., Part A: Polym. Chem.*, 2004, **42**, 374–385.

115 E. Holder, M. A. R. Meier, V. Marin and U. S. Schubert, *J. Polym. Sci., Part A: Polym. Chem.*, 2003, **41**, 3954–3964.

116 E. Tekin, E. Holder, V. Marin, B. J. de Gans and U. S. Schubert, *Macromol. Rapid Commun.*, 2005, **26**, 293–297.

117 T. Taniguchi, M. Kuroki and T. Miyashita, *Colloid Polym. Sci.*, 1996, **274**, 717–722.

118 K. B. Blodgett and I. Langmuir, *Phys. Rev.*, 1937, **51**, 964–982.

119 T. Taniguchi, Y. Fukasawa and T. Miyashita, *J. Phys. Chem. B*, 1999, **103**, 1920–1924.

120 M. K. Nazeeruddin, A. Kay, I. Rodicio, R. Humphry-Baker, E. Mueller, P. Liska, N. Vlachopoulos and M. Graetzel, *J. Am. Chem. Soc.*, 1993, **115**, 6382–6390.

121 G. Decher, *Science*, 1997, **277**, 1232–1237.

122 T. Fushimi, A. Oda, H. Ohkita and S. Ito, *J. Phys. Chem. B*, 2004, **108**, 18897–18902.

123 A. A. Farah, J. G. C. Veinot, M. Najman and W. J. Pietro, *J. Macromol. Sci., Pure Appl. Chem.*, 2000, **37**, 1507–1529.

124 A. A. Farah and W. J. Pietro, *Polym. Bull. (Berlin)*, 1999, **43**, 135–142.

125 E. K. Pefkianakis, N. P. Tzanetos and J. K. Kallitsis, *Chem. Mater.*, 2008, **20**, 6254–6262.

126 J. W. Oh, C. S. Choi, Y. Jung, C. Lee and N. Kim, *J. Mater. Chem.*, 2009, **19**, 5765–5771.

127 M. R. Buchmeiser, *Chem. Rev.*, 2000, **100**, 1565–1604.

128 R. Grubbs and W. Tumas, *Science*, 1989, **243**, 907–915.
129 R. Kröll, C. Eschbaumer, U. S. Schubert, M. R. Buchmeiser and K. Wurst, *Macromol. Chem. Phys.*, 2001, **202**, 645–653.
130 C. R. South, C. Burd and M. Weck, *Acc. Chem. Res.*, 2007, **40**, 63–74.
131 D. Smith, E. B. Pentzer and S. T. Nguyen, *Polym. Rev.*, 2007, **47**, 419–459.
132 M. Weck, *Polym. Int.*, 2007, **56**, 453–460.
133 B. Z. Chen and H. F. Sleiman, *Macromolecules*, 2004, **37**, 5866–5872.
134 K. L. Metera and H. Sleiman, *Macromolecules*, 2007, **40**, 3733–3738.
135 A. Rezvani, H. S. Bazzi, B. Chen, F. Rakotondradany and H. F. Sleiman, *Inorg. Chem.*, 2004, **43**, 5112–5119.
136 N. B. Sankaran, A. Z. Rys, R. Nassif, M. K. Nayak, K. Metera, B. Z. Chen, H. S. Bazzi and H. F. Sleiman, *Macromolecules*, 2010, **43**, 5530–5537.
137 M. Wilchek and E. A. Bayer, *Methods Enzymol.*, 1990, **184**, 5–13.
138 S.-J. Liu, Q. Zhao, B.-X. Mi and W. Huang, *Polyfluorenes*, Springer-Verlag, Berlin, 2008, vol. 212, pp. 125–144.
139 I. Manners, *Synthetic Metal-Containing Polymers*, Wiley-VCH, Weinheim, 2004.
140 G. R. Whittell and I. Manners, *Adv. Mater.*, 2007, **19**, 3439–3468.
141 Y. Liu, Y. Li and K. S. Schanze, *J. Photochem. Photobiol., C*, 2002, **3**, 1–23.
142 W.-Y. Wong, *Coord. Chem. Rev.*, 2005, **249**, 971–997.
143 M. V. Pishko, I. Katakis, S.-E. Lindquist, L. Ye, B. A. Gregg and A. Heller, *Angew. Chem., Int. Ed. Engl.*, 1990, **29**, 82–84.
144 Y. Degani and A. Heller, *J. Am. Chem. Soc.*, 1989, **111**, 2357–2358.
145 A. Heller, *J. Phys. Chem.*, 1992, **96**, 3579–3587.
146 S. M. Zakeeruddin, D. M. Fraser, M. K. Nazeeruddin and M. Grätzel, *J. Electroanal. Chem.*, 1992, **337**, 253–283.
147 A. Heller, *Acc. Chem. Res.*, 1990, **23**, 128–134.
148 T. J. Ohara, R. Rajagopalan and A. Heller, *Anal. Chem.*, 1993, **65**, 3512–3517.
149 F. Mao, N. Mano and A. Heller, *J. Am. Chem. Soc.*, 2003, **125**, 4951–4957.
150 T. J. Ohara, R. Rajagopalan and A. Heller, *Anal. Chem.*, 1994, **66**, 2451–2457.
151 S. Timur, Y. Yigzaw and L. Gorton, *Sens. Actuators, B*, 2006, **113**, 684–691.
152 K. Habermüller, A. Ramanavicius, V. Laurinavicius and W. Schuhmann, *Electroanalysis*, 2000, **12**, 1383–1389.
153 W. Schuhmann, C. Kranz, H. Wohlschläger and J. Strohmeier, *Biosens. Bioelectron.*, 1997, **12**, 1157–1167.
154 S. Reiter, K. Habermüller and W. Schuhmann, *Sens. Actuators, B*, 2001, **79**, 150–156.
155 A. Deronzier and J.-C. Moutet, *Coord. Chem. Rev.*, 1996, **147**, 339–371.
156 S. Warren, R. Doaga, T. McCormac and E. Dempsey, *Electrochim. Acta*, 2008, **53**, 4550–4556.
157 S. De Vito and C. R. Martin, *Chem. Mater.*, 1998, **10**, 1738–1741.
158 V. M. Cepak, J. C. Hulteen, G. Che, K. B. Jirage, B. B. Lakshmi, E. R. Fisher and C. R. Martin, *J. Mater. Res.*, 1998, **13**, 3070–3080.
159 A. Badura, D. Guschin, B. Esper, T. Kothe, S. Neugebauer, W. Schuhmann and M. Rogner, *Electroanalysis*, 2008, **20**, 1043–1047.
160 J. W. Gallaway and S. A. C. Barton, *J. Am. Chem. Soc.*, 2008, **130**, 8527–8536.
161 R. J. Forster and J. G. Vos, *Macromolecules*, 1990, **23**, 4372–4377.
162 V. Coman, T. Gustavsson, A. Finkelsteinas, C. von Wachenfeldt, C. Hagerhall and L. Gorton, *J. Am. Chem. Soc.*, 2009, **131**, 16171–16176.
163 A. Badura, B. Esper, K. Ataka, C. Grunwald, C. Wöll, J. Kuhlmann, J. Heberle and M. Rögner, *Photochem. Photobiol.*, 2006, **82**, 1385–1390.
164 J. Maly, J. Krejci, M. Ilie, L. Jakubka, J. Masojídek, R. Pilloton, K. Sameh, P. Steffan, Z. Stryhal and M. Sugiura, *Anal. Bioanal. Chem.*, 2005, **381**, 1558–1567.
165 D. A. Guschin, J. Castillo, N. Dimcheva and W. Schuhmann, *Anal. Bioanal. Chem.*, 2010, **398**, 1661–1673.
166 S. Calabrese Barton, J. Gallaway and P. Atanassov, *Chem. Rev.*, 2004, **104**, 4867–4886.
167 E. Wolcan and M. R. Feliz, *Photochem. Photobiol. Sci.*, 2003, **2**, 412–417.
168 E. Wolcan, J. L. Alessandrini and M. R. Féliz, *J. Phys. Chem. B*, 2005, **109**, 22890–22898.
169 M. R. Feliz and G. Ferraudi, *Inorg. Chem.*, 2004, **43**, 1551–1557.
170 E. Wolcan, *J. Phys. Chem. A*, 2000, **104**, 9281–9286.
171 S. Hou and W. K. Chan, *Macromol. Rapid Commun.*, 1999, **20**, 440–443.
172 C. A. Bignozzi, V. Ferri and M. Scoponi, *Macromol. Chem. Phys.*, 2003, **204**, 1851–1862.
173 W. R. Seitz and M. J. Sepaniak, *CRC Crit. Rev. Anal. Chem.*, 1988, **19**, 135–173.
174 C. A. Bignozzi, J. R. Schoonover and F. Scandola, *Prog. Inorg. Chem.*, 1997, **44**, 1–95.
175 C. W. Tse, L. S. M. Lam, K. Y. K. Man, W. T. Wong and W. K. Chan, *J. Polym. Sci., Part A: Polym. Chem.*, 2005, **43**, 1292–1308.
176 Q. Wang and L. P. Yu, *J. Am. Chem. Soc.*, 2000, **122**, 11806–11811.
177 T. A. Skotheim, R. L. Elsenbaumer and J. R. Reynolds, *Handbook of Conducting Polymers*, New York, 2nd edn, 1998.
178 J. R. Sheats and P. F. Barbara, *Acc. Chem. Res.*, 1999, **32**, 191–192.
179 J. R. Sheats, Y.-L. Chang, D. B. Roitman and A. Stocking, *Acc. Chem. Res.*, 1999, **32**, 193–200.
180 F. Garnier, *Acc. Chem. Res.*, 1999, **32**, 209–215.
181 T. Kugler, M. Lögdlund and W. R. Salaneck, *Acc. Chem. Res.*, 1999, **32**, 225–234.
182 P. F. Van Hutten, V. V. Krasnikov and G. Hadziioannou, *Acc. Chem. Res.*, 1999, **32**, 257–265.
183 S. H. Chan, L. S. M. Lam, C. W. Tse, K. Y. K. Man, W. T. Wong, A. B. Djurišić and W. K. Chan, *Macromolecules*, 2003, **36**, 5482–5490.
184 P. K. Ng, X. Gong, S. H. Chan, L. S. M. Lam and W. K. Chan, *Chem.–Eur. J.*, 2001, **7**, 4358–4367.
185 C. S. Hui, L. S. M. Lam, C. Yin, W. K. Chan and A. B. Djurišić, *J. Polym. Sci., Part A: Polym. Chem.*, 2003, **41**, 1708–1715.
186 K. D. Ley and K. S. Schanze, *Coord. Chem. Rev.*, 1998, **171**, 287–307.
187 K. D. Ley, Y. Li, J. V. Johnson, D. H. Powell and K. S. Schanze, *Chem. Commun.*, 1999, 1749–1750.
188 K. D. Ley, K. A. Walters and K. S. Schanze, *Synth. Met.*, 1999, **102**, 1585–1586.
189 K. A. Walters, K. D. Ley, C. S. P. Cavalaheiro, S. E. Miller, D. Gosztola, M. R. Wasielewski, A. P. Bussandri, H. van Willigen and K. S. Schanze, *J. Am. Chem. Soc.*, 2001, **123**, 8329–8342.
190 K. D. Ley, C. E. Whittle, M. D. Bartberger and K. S. Schanze, *J. Am. Chem. Soc.*, 1997, **119**, 3423–3424.
191 Y. Zhang, Z. Huang, W. Zeng and Y. Cao, *Polymer*, 2008, **49**, 1211–1219.
192 M. A. Baldo, D. F. O'Brien, Y. You, A. Shoustikov, S. Sibley, M. E. Thompson and S. R. Forrest, *Nature*, 1998, **395**, 151–154.
193 M. A. Baldo, M. E. Thompson and S. R. Forrest, *Nature*, 2000, **403**, 750–753.
194 Q. A. Zhao, S. J. Liu and W. Huang, *Macromol. Rapid Commun.*, 2010, **31**, 794–807.
195 E. Tekin, P. J. Smith and U. S. Schubert, *Soft Matter*, 2008, **4**, 703–713.
196 B. J. de Gans, P. C. Duineveld and U. S. Schubert, *Adv. Mater.*, 2004, **16**, 203–213.
197 J. X. Jiang, C. Y. Jiang, W. Yang, H. G. Zhen, F. Huang and Y. Cao, *Macromolecules*, 2005, **38**, 4072–4080.
198 X. W. Chen, J. L. Liao, Y. M. Liang, M. O. Ahmed, H. E. Tseng and S. A. Chen, *J. Am. Chem. Soc.*, 2003, **125**, 636–637.
199 C. Y. Mei, J. Q. Ding, B. Yao, Y. X. Cheng, Z. Y. Xie, Y. H. Geng and L. X. Wang, *J. Polym. Sci., Part A: Polym. Chem.*, 2007, **45**, 1746–1757.
200 N. R. Evans, L. S. Devi, C. S. K. Mak, S. E. Watkins, S. I. Pascu, A. Kohler, R. H. Friend, C. K. Williams and A. B. Holmes, *J. Am. Chem. Soc.*, 2006, **128**, 6647–6656.
201 W.-Y. Wong and C.-L. Ho, *Coord. Chem. Rev.*, 2009, **253**, 1709–1758.
202 C.-L. Ho and W.-Y. Wong, *Coord. Chem. Rev.*, 2011, **255**, 2469–2502.
203 S. J. Liu, W. J. Xu, T. C. Ma, Q. Zhao, Q. L. Fan, Q. D. Ling and W. Huang, *Macromol. Rapid Commun.*, 2010, **31**, 629–633.
204 S. J. Liu, Q. Zhao, R. F. Chen, Y. Deng, Q. L. Fan, F. Y. Li, L. H. Wang, C. H. Huang and W. Huang, *Chem.–Eur. J.*, 2006, **12**, 4351–4361.

- 129 -

205 T. Ito, S. Suzuki and J. Kido, *Polym. Adv. Technol.*, 2005, **16**, 480–483.

206 J. Langecker and M. Rehahn, *Macromol. Chem. Phys.*, 2008, **209**, 258–271.

207 G. L. Schulz, X. W. Chen, S. A. Chen and S. Holdcroft, *Macromolecules*, 2006, **39**, 9157–9165.

208 H. Y. Zhen, C. Y. Jiang, W. Yang, J. X. Jiang, F. Huang and Y. Cao, *Chem.–Eur. J.*, 2005, **11**, 5007–5016.

209 C. Ulbricht, C. R. Becer, A. Winter and U. S. Schubert, *Macromol. Rapid Commun.*, 2010, **31**, 827–833.

210 C. Ulbricht, C. R. Becer, A. Winter, D. Veldman and U. S. Schubert, *Macromol. Rapid Commun.*, 2008, **29**, 1919–1925.

211 E. Holder, V. Marin, D. Kozodaev, M. A. R. Meier, B. G. G. Lohmeijer and U. S. Schubert, *Macromol. Chem. Phys.*, 2005, **206**, 989–997.

212 W. Y. Lai, J. W. Levell, P. L. Burn, S. C. Lo and I. D. W. Samuel, *J. Mater. Chem.*, 2009, **19**, 4952–4959.

213 Y. Koga and K. Matsubara, *J. Polym. Sci., Part A: Polym. Chem.*, 2009, **47**, 4358–4365.

214 H. Kim, Y. Y. Lyu, K. Choi, R. Zentel, S. H. Lee and K. Char, *Macromol. Rapid Commun.*, 2009, **30**, 1232–1237.

215 X. Y. Wang, A. Kimyonok and M. Weck, *Chem. Commun.*, 2006, 3933–3935.

216 X. Y. Wang, R. N. Prabhu, R. H. Schmehl and M. Weck, *Macromolecules*, 2006, **39**, 3140–3146.

217 S. Tokito, M. Suzuki and F. Sato, *Thin Solid Films*, 2003, **445**, 353–357.

218 S. Tokito, M. Suzuki, F. Sato, M. Kamachi and K. Shirane, *Org. Electron.*, 2003, **4**, 105–111.

219 Y. You, S. H. Kim, H. K. Jung and S. Y. Park, *Macromolecules*, 2006, **39**, 349–356.

220 C. L. Lee, N. G. Kang, Y. S. Cho, J. S. Lee and J. J. Kim, *Opt. Mater. (Amsterdam)*, 2002, **21**, 119–123.

221 M. Suzuki, S. Tokito, F. Sato, T. Igarashi, K. Kondo, T. Koyama and T. Yamaguchi, *Appl. Phys. Lett.*, 2005, **86**, 103507.

222 L. Deng, P. T. Furuta, S. Garon, J. Li, D. Kavulak, M. E. Thompson and J. M. J. Fréchet, *Chem. Mater.*, 2006, **18**, 386–395.

223 D. A. Poulsen, B. J. Kim, B. Ma, C. S. Zonte and J. M. J. Fréchet, *Adv. Mater.*, 2010, **22**, 77–82.

- 130 -

Publication A4

SYNTHESIS AND RESONANCE ENERGY TRANSFER STUDY ON A RANDOM TERPOLYMER CONTAINING A 2-(PYRIDINE-2-YL)THIAZOLE DONOR-TYPE LIGAND AND A LUMINESCENT [RU(BPY)$_2$(2-(TRIAZOL-4-YL)PYRIDINE)]$^{2+}$ CHROMOPHORES

Bobby Happ, Johann Schäfer, Roberto Menzel, Martin D. Hager, Andreas Winter, Jürgen Popp, Rainer Beckert,* Benjamin Dietzek,* Ulrich S. Schubert*

Macromolecules

Synthesis and Resonance Energy Transfer Study on a Random Terpolymer Containing a 2-(Pyridine-2-yl)thiazole Donor-Type Ligand and a Luminescent [Ru(bpy)₂(2-(triazol-4-yl)pyridine)]²⁺ Chromophore

Bobby Happ,[†,‡,§] Johann Schäfer,[§,||] Roberto Menzel,[†,§] Martin D. Hager,[†,‡,§] Andreas Winter,[†,‡,§] Jürgen Popp,[§,||,⊥] Rainer Beckert,[*,†,§] Benjamin Dietzek,[*,§,||,⊥] and Ulrich S. Schubert[*,†,‡,§]

[†]Laboratory of Organic and Macromolecular Chemistry (IOMC), Friedrich-Schiller-University Jena, Humboldtstrasse 10, 07743 Jena, Germany

[‡]Dutch Polymer Institute (DPI), P.O. Box 902, 5600 AX Eindhoven, The Netherlands

[§]Jena Center for Soft Matter (JCSM), Friedrich-Schiller-Universität Jena, Humboldtstrasse 10, 07743 Jena, Germany

[||]Institute for Photonic Technology Jena (IPhT), Albert-Einstein-Strasse 9, 07745 Jena, Germany

[⊥]Institute for Physical Chemistry, Friedrich-Schiller-University Jena, Helmholtzweg 4, 07743 Jena, Germany

S *Supporting Information*

ABSTRACT: A statistical terpolymer, containing a 2-(pyridine-2-yl)-1,3-thiazole donor-type system and an acceptor-type [Ru(bpy)₂-(2-(triazol-4-yl)pyridine)]²⁺ chromophore as well as methyl methacrylate as comonomer, was synthesized using the controlled reversible addition—fragmentation chain transfer polymerization (RAFT) approach. Additionally, the appropriate donor- and acceptor-type copolymers were synthesized, whereas only a maximum content of 5 mol % of the ruthenium(II) chromophore could be incorporated into the macromolecules caused by its nitro-functionalization. The resulting terpolymer exhibited a direct Förster resonance energy transfer from the thiazole to the ruthenium(II) subunit as indicated by emission spectroscopy of the Ru(II) phosphorescence as well as lifetime measurements and quantum yield determinations of the thiazole fluorescence. The efficiency of the energy transfer was found to be higher than 70%.
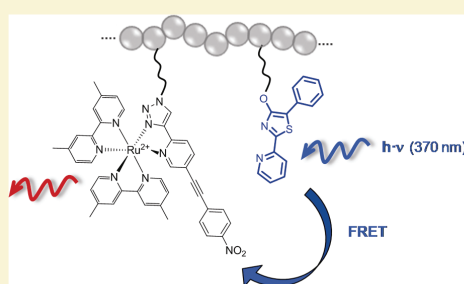
■ INTRODUCTION

Relating to artificial photosynthetic systems which are capable to harvest and exploit photons enabled by solar energy, ruthenium(II) complexes coordinated by *N*-heterocycles, such as 2,2′-bipyridines (bpy) and 2,2′:6′,2″-terpyridines (tpy), have been widely studied due to their predictable coordination behavior as well as their interesting photophysical and electrochemical properties.[1−19] Ruthenium—polypyridine complexes have particularly drawn significant interest, since they are able to catalyze reduction and oxidation processes under visible light irradiation enclosing a broad range of substrates. These privileges could be utilized for applications including, e.g., the photocatalytic decomposition of water and the implementation in photovoltaic devices.[20−26] The light sensitizing feature of ruthenium coordination compounds has been further used as luminescent chemosensors as well as for the production of singlet molecular oxygen.[27−31]

Thus, considerable effort in the synthesis of metal-containing polymers has been accomplished for combining the beneficial properties of a metal ion complex, which provides the optoelectronic capacity, and a polymer backbone enhancing the processability

of the materials. Applications in the field of supramolecular chemistry, conducting and photoresponsive materials, and catalysis were established.[5,7,32−37] In particular, the work of Fréchet and Meyer is noteworthy regarding the synthesis of linear macromolecules containing bipyridine-functionalized ruthenium(II) complexes. Fréchet et al. synthesized polymers containing coumarin and Ru(dmbpy)₃²⁺ (dmbpy = 4,4′-dimethyl-2,2′-bipyridine) chromophores using a grafting as well as a copolymerization approach utilizing free radical polymerization procedures. The resulting bichromophoric macromolecules exhibited enhanced absorption and luminescence properties compared to the single Ru(II) complexes due to an efficient (>95%) energy transfer between the coumarin donor dyes and the ruthenium subunit.[38,39] Meyer et al. established a molecular assembly that combined both the light-harvesting and electron transfer properties of a natural photosynthetic system within a single macromolecule.[33] The

Scheme 1. Schematic Representation of the Various Synthesized Polymer Systems
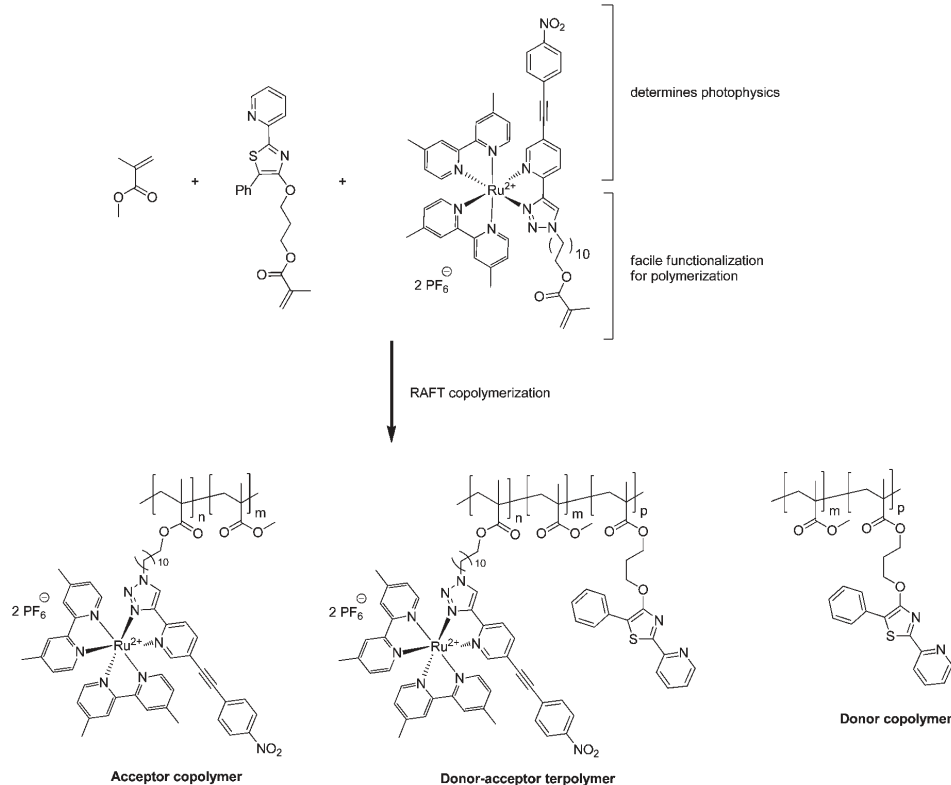
support material in these studies was a mixed styrene-based copolymer, which was prepared by free radical random copolymerization of styrene with p-(chloromethyl)styrene. This copolymer pictured a versatile precursor for the addition of a variety of functional groups by nucleophilic substitution of chloride from the pendant chloromethyl groups.[40]

However, the functionalization of polypyridine-based chelators with polymerizable groups can be synthetically troublesome and, therefore, requires new approaches in the preparation of analogous bidentate chelating ligands that also possess well-defined coordination properties and can be prepared as well as modified with high effectiveness.[41] In this respect the Cu^I-catalyzed 1,3-cycloaddition of organic azides with terminal alkynes (the CuAAC reaction) has a great potential due to its mild reaction conditions and wide range of usable substrates.[42,43] The development of the CuAAC reaction resulted in an increased interest toward the coordination chemistry of 1,4-functionalized $1H$-[1,2,3]triazoles due to their potential as N-donor ligands.[44−49]

In this contribution, the synthesis of a light-harvesting terpolymer by controlled reversible addition−fragmentation chain transfer (RAFT) radical polymerization is reported, comprising a luminescent ruthenium(II) complex coordinated by a 2-($1H$-[1,2,3]triazol-4-yl)pyridine system (trzpy) and a

2-(pyridine-2-yl)thiazole donor-type system (Scheme 1). This terpolymer is designed in order to mimic natural strategies for light harvesting and—potentially—to be incorporated in supramolecular systems for conversion of energy from sunlight into chemical energy.[12,50−52] The thiazole dye absorbs light and transfers a fraction of the excitation energy to a ruthenium(II) complex, where a metal-to-ligand charge-transfer (MLCT) state is directly excited for charge separation. Hence, the transition metal complex can act as a primary electron donor when, in perspective, combined with an electron acceptor, e.g., a semiconductor nanoparticle.[50,53] Thus, the photoinduced molecular processes resemble those in natural light harvesting, where the capability of the special pair to harvest sunlight is increased by dressing it with extended antenna structures.[54−56] For the system under investigation the main focus is on the energy transfer taking place in the random donor—acceptor terpolymer. The donor and acceptor units are designed for efficient Förster resonance energy transfer (FRET) as reported by Schäfer et al.[57] The successful incorporation of the donor and acceptor has been confirmed by size exclusion chromatography (SEC) coupled with a photodiode array detector. The trzpy ligand coordinated to the ruthenium(II) ion included two features at the same time: (i) affording the polymerizable group and (ii) an electron-withdrawing moiety on the pyridine, which is responsible for the

Scheme 2. Schematic Representation of the Synthesis of the Acceptor-Type Ruthenium(II) Complex

I) Synthesis of the ligand scaffold

II) Functionalization with a polymerizable group

III) Synthesis of the Ru(II)-complex
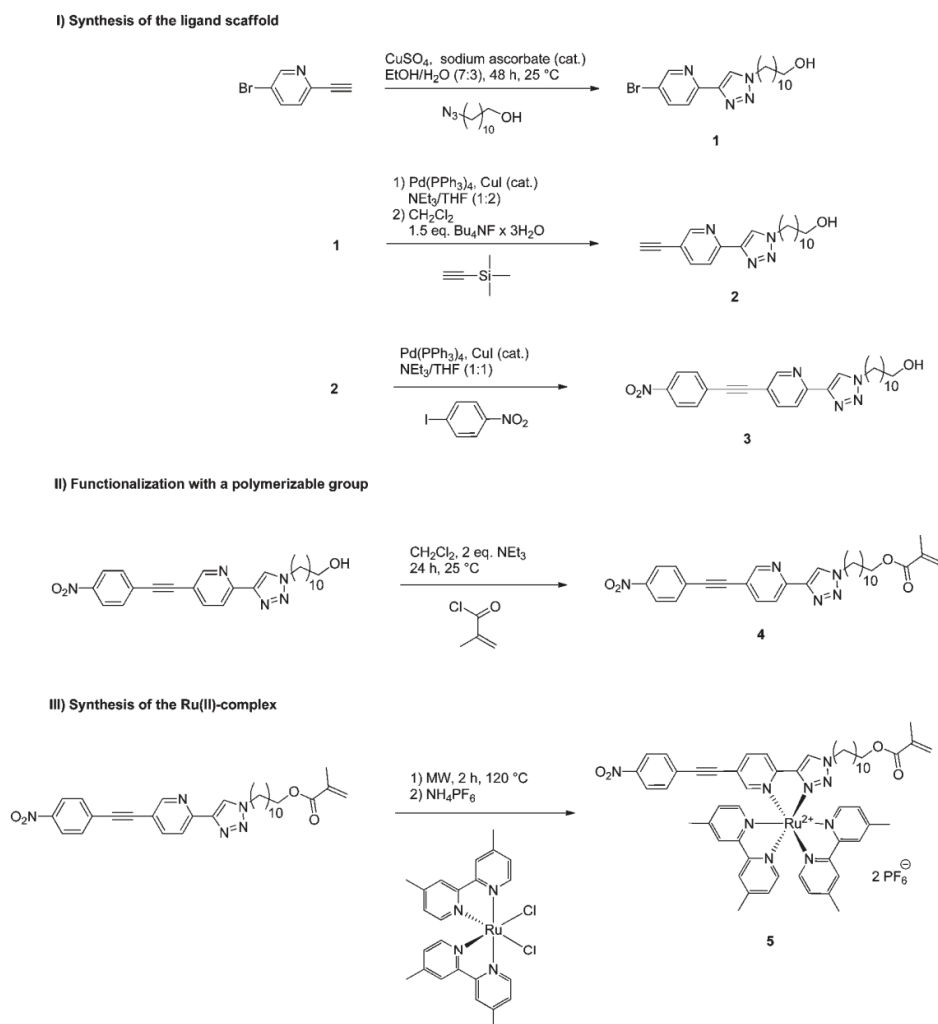
ruthenium complex luminescence. The latter consideration facilitated the energy transfer studies with respect to emission spectroscopy of the acceptor-type ruthenium subunit. The blue-fluorescent thiazole was characterized by a good stability toward the radical polymerization conditions as well as a considerable high luminescence quantum yield.[58]

■ RESULTS AND DISCUSSION

Synthesis of the Monomers. The general synthesis route of the acceptor-type ruthenium(II) complex **5** is depicted in Scheme 2. In the first three steps, copper(I)-catalyzed azide—alkyne coupling (CuAAC) and Pd(0)-catalyzed Sonogashira coupling were used to set up the trzpy scaffold bearing an electron-withdrawing 4-nitrophenylacetylene moiety on the

5-position of the pyridine ring. The copper(I)-catalyzed 1,3-dipolar cycloaddition of 2-ethynyl-5-bromopyridine and 11-azidoundecan-1-ol yielded **1** under typical CuAAC reaction conditions, whereas 10 mol % of $CuSO_4$ and 0.5 equiv of sodium ascorbate served as Cu(I) source.[43] Consecutive Sonogashira cross-coupling with trimethylsilylacetylene and $Pd^0(PPh_3)_4$, as catalytic active palladium(0) source, as well as subsequent deprotection of the trimethylsilyl-group by potassium fluoride afforded **2** in moderate yield (47%). The following Sonogashira coupling with 4-nitro-1-iodobenzene provided component **3**. The purity of the compounds has been proven by NMR spectroscopy, mass spectrometry, and elemental analysis. The hydroxyl moiety was changed to methyl methacrylate in order to introduce a polymerizable group. The straightforward esterification of **3** with methacryloyl chloride gave **4** in good yield (89%).

Scheme 3. Schematic Representation of the Synthesis of a Polymerizable Donor-Type Thiazole Ligand
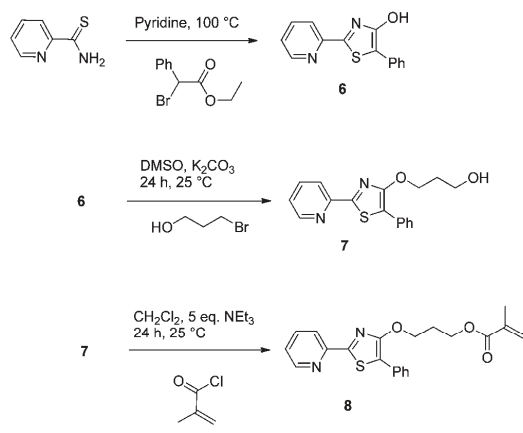
The heteroleptic ruthenium(II) complex **5** was synthesized by heating *cis*-dichlorobis(4,4′-dimethyl-2,2′-bipyridine)ruthenium(II) Ru(dmbpy)$_2$Cl$_2$[45] and ligand **4** under microwave irradiation (120 °C). The methacryl moiety was found to be stable under these conditions as confirmed by preliminary experiments. After the reaction was completed, a 10-fold excess of NH$_4$PF$_6$ was added to precipitate the ruthenium(II) complex. Precipitation occurred usually within 30 min, and the complex was finally purified by recrystallization from ethanol and subsequent washing with cold ethanol (yield >90%). The verification of the structure was carried out by ^{1}H and ^{13}C NMR spectroscopy as well as by high-resolution mass spectrometry (HR-ESI MS).

The 4-hydroxythiazole **6** was prepared by a cyclization process of pyridine-2-carbothioamide with ethyl 2-bromophenylacetate.[59] Williamson-type etherification of **6** with 3-bromopropan-1-ol as electrophile yielded **7** in good yield (68%) under mild conditions. Subsequently, the hydroxyl group was reacted with methacryloyl chloride under basic conditions to yield the polymerizable ester **8** (Scheme 3). All compounds had to be purified by column chromatography to ensure a proper reagent grade for the following radical polymerization reactions. The confirmation of the structures was performed by NMR spectroscopy, mass spectrometry, and elemental analysis.

Synthesis of the Polymers. Two copolymers and one terpolymer were synthesized based on a poly(methyl methacrylate) (PMMA) backbone, where **8** served as the donor and **5** as the acceptor unit, respectively (Scheme 4). In general, statistical RAFT copolymerizations were performed in concentrated solutions (~2 M solution of the monomer) to allow the polymerizations to proceed in a controlled manner.[60] 2-Cyanobutan-2-yl benzodithioate (CBBD) was used as RAFT agent, since it is known to provide a narrow molar mass distribution, in particular for PMMA, as it has been described in the literature.[61,62] The conversion of the reactions was driven to roughly 80% using a standard reaction time of 16 h. Because of the insolubility of **5** in commonly utilized solvents for radical polymerization (i.e., toluene, ethanol), the RAFT polymerizations were performed in *N,N*-dimethylacetamide (DMA), as described elsewhere.[63] After the reaction, **9b** was precipitated into cold diethyl ether

yielding the desired donor-type copolymer. The polymers **9a,c** were further purified by preparative SEC due to remaining monomer **5** (see SEC graphs in the Supporting Information). Selected characterization data of the final products are summarized in Table 1.

A noteworthy synthesis issue appeared concerning the copolymerization of the heteroleptic ruthenium(II) complex **5** and MMA. It was found after optimization of the reaction conditions (Table 2) that initiation of the polymerization only occurred if the molar content of **5** did not exceed 5 mol %. This fact was attributed to the retardation nature of the NO$_2$ group.[64] Consequently, the ruthenium(II) content of the terpolymer **9c** was kept below 5 mol % to ensure an efficient initiation of the reaction.

Energy Transfer Studies. When considering the emission and absorption spectra of the donor—acceptor pair **5** and **8** (Figure 1), it is apparent that the requirements for FRET are met, which were a significant emission quantum yield of the donor and a spectral overlap of the donor emission and the acceptor absorption band. The overlap between the donor (**8**) emission and the acceptor (**5**) extinction (hatched region in Figure 1) resulted in an overlap integral value of $J = 4.6$ M^{-1} cm^{-1} nm^4 (compare Table 3). The Förster radius, which corresponds to the distance between donor and acceptor at which the efficiency of FRET drops to 50%, was calculated to $R_0 = 4$ nm. The average distance between the donor and the acceptor units had to be smaller than R_0 in order to obtain efficient FRET, which was achieved by copolymerizing **5** and **8** in a polymer backbone delivering **9c**. In the terpolymer the thiazoles were randomly distributed in the vicinity of the Ru(II) complexes. Because of the fact that the geometrical constraints discussed above were met, FRET from the thiazole to the MLCT band of **5** (centered at 450 nm) was expected to occur in the polymer.

In order to verify the appearance of FRET in the donor—acceptor polymer **9c**, excitation spectra were recorded of the donor-type polymer **9b**, the acceptor-type polymer **9a**, and the donor—acceptor polymer **9c** (see Figure 2). For recording the luminescence excitation spectra of the Ru(II) subunit the emission was monitored at 620 nm, where no donor fluorescence from subunit **8** appeared. Therefore, a difference in the luminescence excitation spectra of **9a** and **9c** indicated contributions from thiazole excitation to the luminescence of the ruthenium-(II) unit as seen in the additional excitation band at 380 nm in **9c** (see Figure 2). This excitation band is spectrally centered, where the thiazole emission is excited in the donor-type polymer **9b** as indicated by the dashed line in Figure 2. These findings point toward FRET; i.e., excitation of the donor led to amplified luminescence of the acceptor.

The additional excitation band in the luminescence of the Ru(II) subunit is accompanied by a reduction of the donor-based quantum yield in the donor—acceptor polymer **9c** compared to that of **9b** (Table 3). While measuring the donor-based quantum yield in donor-type polymer **9b** was straightforward, the quantum yield measurement in the donor—acceptor polymer **9c** required adequate care: because of overlapping donor and acceptor absorptions (see Figures 1 and 2), it was not possible to exclusively excite donor molecules in the donor—acceptor polymer in order to directly measure the donor-based emission quantum yields. Taking into account these overlapping absorptions, the molar extinction coefficients of donor and acceptor at the excitation wavelength had to be considered as well as the ratio of donors and acceptors within the polymer chain. Considering these properties, the quantum yield measurement in the

Scheme 4. Schematic Representation of the Synthesis of the Statistical Copolymers 9a—c
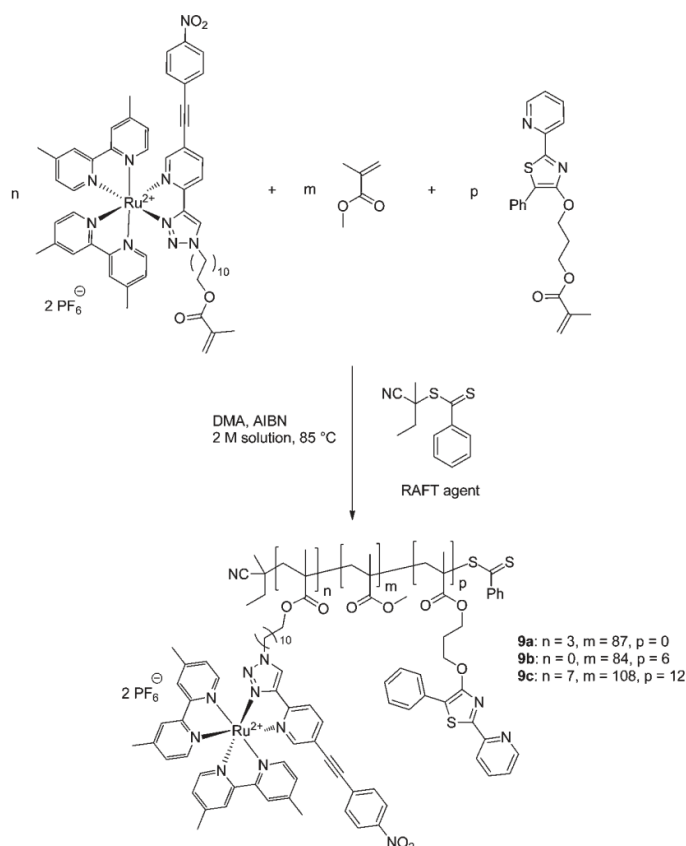
Table 1. Selected Characterization Data for the Polymers 9a—c

polymer	Ru(II) content [mol %][a]	dye content [mol %][a]	$M_{n,theo}$	$M_{n,NMR}$ [g mol^{-1}][a]	DP[a,b]	$M_{n,SEC}$ [g mol^{-1}][c]	PDI[d]
9a	3		8 500	9 000	90	5 000	1.32
9b		7	11 700	12 000	90	15 100	1.13
9c	6	10	11 200	12 800	127	8 000	1.32

[a] Determined by ^{1}H NMR spectroscopy. [b] Degree of polymerization. [c] Determined by SEC using PMMA calibration. [d] Polydispersity index determined by SEC.

donor—acceptor polymer **9c** followed the same procedure as the emission quantum yield measurements of **8** and **9b**.

In the work presented here the donor-type polymer **9b**, lacking acceptor molecules, was synthesized as reference system for **9c**. It is expected that the fluorescence quantum yield and the lifetime of the reference polymer are practical for calculating the transfer efficiency for energy transfer in the donor—acceptor polymer **9c**. The importance of using such a reference system instead of the monomeric unit **8** is obvious from Table 3. Upon integration into the polymer, the fluorescence quantum yield of the thiazole increased compared to the monomeric fluorophore. Such behavior is in agreement with the measured fluorescence

lifetimes, whereas the emission spectrum of **9b** was similar to that of **8** (see Figure 3). The reason for the increased lifetime was attributed to random coiling of the polymer in solution changing sufficiently the environment of individual dyes.[65] Nevertheless, choosing **9b** as reference was a critical step for the analysis of the excitation energy transfer in the donor—acceptor polymer **9c**: the lengths of **9b** and **9c** are not identical, and additionally, the reference polymer could exhibit a different coiling compared to the donor—acceptor polymer. Nonetheless, energy transfer efficiencies were calculated as described in the Experimental Section using the quantum yields and lifetime measurements from the reference system **9b** and the donor—acceptor polymer **9c**.

Table 2. Optimization of the Reaction Conditions of the Copolymerization of 5 and MMA

M/I ratio[a]	Ru(II) content [mol %]	t_R [h]	AIBN [mol %]	conv [%]
100	10	18	0.25	0
200	10	18	0.25	0
50	10	18	0.25	0
100	10	18	0.5	0
100	10	18	1	0
100	6	18	0.25	0
100	4	18	0.25	85

[a] Monomer/initiator ratio (MMA/CBBD).
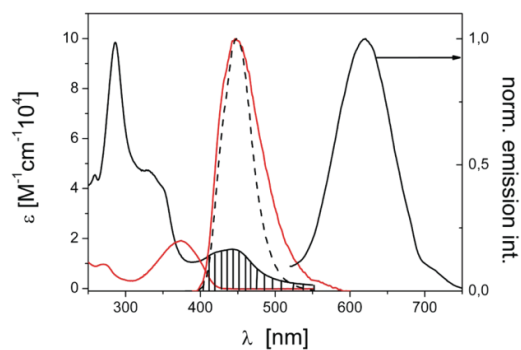
Figure 1. Extinction and emission spectra of **8** (red) and **5** (black) at room temperature measured in dichloromethane (excitation at 370 and 462 nm, respectively). The hatched region indicates the donor–acceptor spectral overlap, and the dashed line displays the integrand of the overlap integral.

Table 3. Representation of the Photophysical Properties from 8–9c

compd	$\lambda_{abs,max}$ (nm) [log ε]	$\lambda_{em,max}$ (nm) [excitation]	Φ^a	τ (ns)[b]	J (M^{-1} cm^{-1} nm^4)
8	375 [5.14]	447 [370]	0.40	1.8	
9a	286 [5.47]	620 [460]			
	330 [5.17]				
	443 [4.68]				
9b	375 [5.14]	447 [370]	0.58	2.7	0.064[c]
9c	285	449 [370]	0.06	$-e$	4.6[d]
	350				
	442				

[a] Emission quantum yield measured in dichloromethane at room temperature. [b] Lifetime measured in dichloromethane at room temperature. [c] Overlap integral considering homotransfer for **9b**. [d] Overlap integral of emission from **8** with absorption of **9a**. [e] No single-exponential decay was observed.

Time-resolved measurements of the donor lifetime in **9b** and **9c** (see Figure 4) revealed that the donor emission decayed more rapidly in the presence of an acceptor as the interaction between the donor and the acceptor quenched the donor emission. On the basis of the temporal emission profiles of the donor in **9b** and **9c**, the FRET efficiency E was calculated to be 70% (see
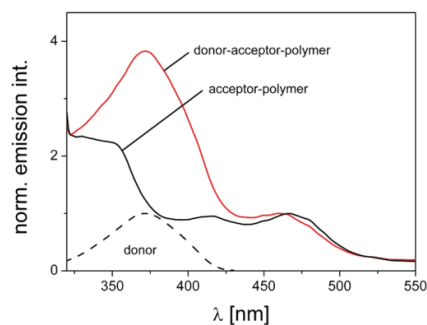
Figure 2. Excitation spectra of the donor–acceptor polymer **9c** (red) and the acceptor polymer **9a** (black) recorded by monitoring the luminescence of **5** at 620 nm (solid), normalized to maximal intensity in the MLCT excitation band at 460 nm. The donor polymer fluorescence excitation spectrum from **9b** recorded at 450 nm (dashed) was normalized to the maximal emission intensity. The spectra were taken in dichloromethane at room temperature.
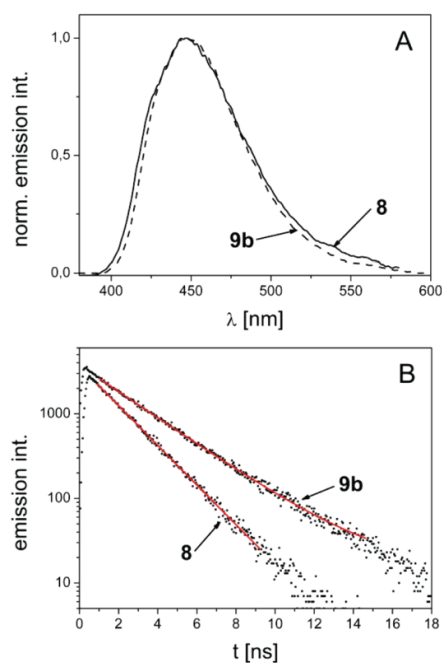
Figure 3. In panel A, the dashed line denotes the emission spectra of the reference polymer **9b** and the solid line the emission of the monomer **8** in dichloromethane, excited at 375 nm. In panel B, the red line fits the monoexponential decay of the measured data (dotted).

Experimental Section for details). Although there are many possibilities for excitation quenching in polymers—such as energy migration, exciton–exciton annihilation,[66–68] and excimer formation[69]—it was assumed that this shortening of the donor decay time in the donor–acceptor polymer is dominated by FRET. Because of the overlap between donor emission and
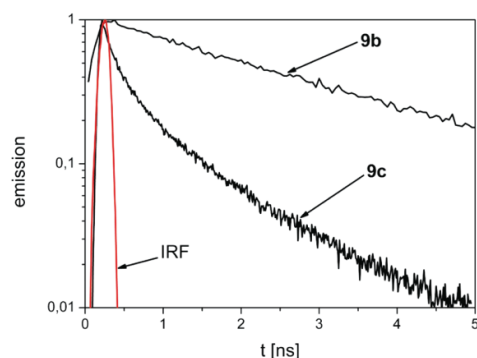
Figure 4. Donor decay profile of the reference polymer **9b** and the donor–acceptor polymer **9c** in dichloromethane at room temperature, excited at 290 nm. The instrument response function (IRF) was measured by scattered light.

Figure 5. Donor fluorescence curves of compound **9b** (donor alone polymer) and of **9c** (donor–acceptor polymer) in different solvents: acetonitrile (red squares), dichloromethane (blue circles), chloroform (black triangles). The longer living fluorescence (single-exponential decay) stems from the donor alone polymer and the shortened fluorescence (non-exponential decay) from the donor–acceptor polymer. Excitation wavelength: 290 nm.

donor absorption (see Figure 1) homoenergy transfer, i.e., FRET between dyes of the same type, is not excluded, but the calculated overlap integral for such energy transfer, and consequently the resulting transfer rate, was 2 orders of magnitude smaller than FRET between donor and acceptor molecules of the type **8** and **5** (see Table 3). Thus, in polymer **9c** no considerable homoenergy transfer will occur, even if there is a higher number of donor than acceptor molecules. Along the same lines contributions from back-energy transfer, i.e., FRET from the acceptor to the donor subunit, were excluded. Excimer formation was excluded as well because it typically causes an additional emission band beyond the red end of the fluorescence, which was not observed for **9c**.[70] Comparing the FRET results presented here to analogous work on other polymers and dendrimers,[65,71,72] it can be stated that in **9** effects, such as energy migration, excimer formation, or local concentration quenching, were avoided.[73] These effects cause a reduction of the emission quantum yield and a nonexponential emission decay. Neither of these effects were observed in the reference polymer **9b**. Probably this is caused by the low concentration of donor units in the polymer backbone compared to dendritic systems.[65]

Additionally, Figure 4 shows a nonexponential donor emission in the presence of acceptor units in the terpolymer. This is due to the fact that no fixed donor–acceptor distances existed within the polymer. This situation resulted in different FRET rates for individual donor–acceptor pairs and, therefore, different decay rates for individual photoexcited donors.

Moreover, preliminary solvent-dependent donor lifetime measurements were carried out and are depicted in Figure 5. The measured donor lifetimes in presence of the ruthenium(II) acceptor were shortened (non-single-exponential decay) compared to the donor alone lifetimes (single-exponential decay) due to the resonance energy transfer. The shape of the decay curves of the polymers themselves in different solvents are very similar, and thus, no significant change in the conformation of the polymers can be concluded. A comparison of the transfer efficiencies in the different solvents was not possible because the avalanche photodiode detects scattered photons from the excitation pulse as well. This may result in incorrect calculated transfer efficiencies.

Of course, any description of donor quenching in donor–acceptor polymers is incomplete using Förster's theory only; for

example, Dexter type energy transfer can also occur at donor–acceptor distances smaller than 10 Å, when donor emission and acceptor absorption spectrally overlap.[70] Furthermore, translational diffusion can cause an enhancement of the FRET efficiency compared to systems with a static distance distribution of donor and acceptor as reported by Lakowicz et al.[74] and Thomas et al.[75] Regardless of a possibly incomplete description of the excitation energy transfer only by FRET, the donor–acceptor polymers designed for efficient FRET allow enhanced light harvesting in a Ru(II) complex, whereupon energy is focused into the ^{1}MLCT band. By considering the charge separating character of the MLCT states, this process increased the accessibility of Ru(II) complexes as primary electron donors in photocatalytic systems.

■ CONCLUSIONS

Polymers containing a 1,3-thiazole dye (energy donor) and a ruthenium(II) chromophore (energy acceptor) were synthesized using a controlled RAFT polymerization procedure. The terpolymer was able to relay the absorbed energy by energy transfer from the thiazole donor to the ruthenium(II) acceptor. The ruthenium(II) content in the macromolecules was limited to 5 mol % at most, since for higher metal content the polymerization could not be initiated. The donor–acceptor functionalized terpolymer displayed a reasonable energy transfer efficiency of over 70%. Those polymeric systems will be practical, e.g., in terms of the synthesis of artificial photosynthetic systems, in which they can act as light-harvesting antennas.

■ EXPERIMENTAL SECTION

Materials and Instrumentation. All reagents were acquired from commercial sources and used without further purification. Solvents were dried and distilled according to standard procedures and stored under nitrogen. All reactions were performed in air-dried flasks under a nitrogen atmosphere, unless stated otherwise. For the Pd^0-catalyzed cross-coupling and the RAFT polymerization procedures, the solvents were degassed by bubbling with nitrogen 0.5 h before use. Purification of the reaction products was carried out by column chromatography using

40−63 μm silica gel. Analytical thin layer chromatography (TLC) was performed on aluminum sheets precoated with silica gel 60 F254, and visualization was accomplished with UV light (254 nm). Preparative size exclusion chromatography (SEC) was carried out on Bio-Rad S-X1 beads (size exclusion 600−14 000 g/mol), swollen in dichloromethane. The conversion of the copolymerization reactions was determined by ^{1}H NMR spectroscopy. The heteroleptic ruthenium(II) complexes were synthesized by microwave-assisted reactions using a Biotage Initiator ExpEU (maximum power: 400 W; working frequency: 2450 MHz) with closed reaction vials. During the experiments the temperature and the pressure profiles were detected. 1D (^{1}H and ^{13}C) and 2D ([1]H−^{1}H COSY) nuclear magnetic resonance spectra were recorded on a Bruker AC 300 (300 MHz) at 298 K. Chemical shifts are reported in parts per million (ppm, δ scale) relative to the signal of the applied solvent.

5-Bromo-2-ethynylpyridine,[45] 2-cyanobutan-2-yl benzodithioate,[61] dichloro(cycloocta-1,5-diene)ruthenium(II),[45] *cis*-dichlorobis(4,4′-dimethyl-2,2′-bipyridine)ruthenium(II),[45] and 5-phenyl-2-(pyridin-2-yl)-1,3-thiazol-4-ol[59] were synthesized according to literature reports.

Photophysical Measurements and Calculations. Measurements of the fluorescence intensity were carried out on a Perkin-Elmer lambda16 UV/vis spectrometer in the perpendicular excitation−emission geometry, while the absorbance at the excitation wavelength was <0.05. The calculation of fluorescence quantum yields was done according to following equation[76]

$$\Phi = \Phi_r \frac{I}{I_r} \frac{A_r}{A} \frac{n^2}{n_r^2} \tag{1}$$

where Φ is the quantum yield, I is the corrected integrated emission intensity, A is the absorbance at the excitation wavelength, and n is the refractive index of the solvent, i.e., in this study dichloromethane of spectroscopic grade from Sigma-Aldrich. The subscript "r" refers to a reference fluorophore of known quantum yield, whereas quinine sulfate ($\Phi = 0.55$) was used in our investigations.[76]

The fluorescence decay curves were obtained by a Hamamatsu streak scope C4334 in time-correlated single photon counting (TCSPC) modus. Triggering was carried out by the Hamamatsu trigger unit C4792-01. After excitation with a frequency-tripled Ti-sapphire laser (Tsunami, Newport Spectra-Physics GmbH), i.e., $\lambda_{ex} = 290$ nm, in perpendicular direction the fluorescence emission wavelength were separated by a Chromex 250IS imaging spectrograph. The repetition rate of the laser was adjusted to 0.8 MHz by a pulse selector (model 3980, Newport Spectra-Physics GmbH). All measurements were carried out at concentrations below 10^{-6} M. Solvent-dependent donor lifetime measurements were performed with a time-correlated single-photon counting module from Becker & Hickl using an avalanche photodiode as detector. The solvents were acetonitrile, dichloromethane, and chloroform.

In order to quantify the efficiency of FRET the time-dependent intensity decay curve of the donor-alone polymer **9b** was measured and compared to the respective intensity decay of **8** incorporated into the donor−acceptor polymer **9c** using eq 2, which can be derived from ref 77. Here, τ_D and τ_{DA} refer to the donor lifetime in the donor-alone polymer **9b** and to the donor lifetime in the donor−acceptor polymer **9c**, respectively. I_{DA} is the time-dependent intensity of the donor fluorescence in presence of an acceptor, which is normalized to the amplitude I_{DA}^0. The resultant efficiency E is 0.7.

$$E = 1 - \frac{\tau_{DA}}{\tau_D} = 1 - \frac{1}{\tau_D} \int \frac{I_{DA}(t)\,dt}{I_{DA}^0} \tag{2}$$

In analogy to the determination of the transfer efficiency based on time-resolved measurements, the emission quantum yield of the donor was measured in **9b** (donor-only polymer) and in the donor−acceptor polymer **9c** in order to calculate the transfer efficiency from eq 3, where Φ_{DA} and Φ_D refer to the donor emission quantum yield of **8** in **9c** and

9b, respectively (see Table 3).

$$E = 1 - \frac{\Phi_{DA}}{\Phi_D} \tag{3}$$

The obtained value of 90% for the transfer efficiency E is only an estimate because of the uncertainty for the measured quantum yields. But the significant reduction of the donor fluorescence quantum yield upon incorporation into the donor−acceptor polymer from $\Phi = 0.58$ (**9b**) to 0.06 (**9c**) proved FRET to take place. A more accurate value for E is achieved from the time-resolved measurements. Consequently, the value $E = 0.7$ in this article was discussed and assumed.

Synthesis of 11-(4-(5-Bromopyridin-2-yl)-1H-1,2,3-triazol-1-yl)undecan-1-ol (1). Sodium azide (590 mg, 9 mmol) was dissolved in dimethyl sulfoxide (20 mL), and 11-bromo-1-undecanol (1.5 g, 6 mmol) was added subsequently. After stirring 24 h at room temperature, water (30 mL) was added to quench the reaction, and the suspension was extracted three times with diethyl ether. The organic phases were combined, washed with brine, and dried over Na_2SO_4. The solution was subsequently concentrated *in vacuo* to yield 11-azido-1-undecanol as slight yellow oil (1.25 g, 98%).

To a solution of the organic azide, 2-ethynyl-5-bromopyridine (1.07 g, 5.9 mmol) and $CuSO_4$ (88 mg, 0.59 mmol, dissolved in 1 mL water) in an EtOH/water mixture (7:3 ratio, 50 mL) was added sodium ascorbate (570 mg, 2.9 mmol, dissolved in 2 mL of water), and the reaction was stirred for 72 h at room temperature. The yellow precipitate was filtered and recrystallized from ethanol, yielding the pure product as white solid (1.55 g, 68%). ^{1}H NMR (CDCl$_3$, 300 MHz): δ = 8.63 (s, 1H), 8.12−8.08 (m, 2H), 7.91 (dd, J = 8.5 Hz, J = 2.1 Hz, 1H), 4.42 (t, J = 7.2 Hz, 2H, N−CH$_2$), 3.67−3.61 (m, 2H, O−CH$_2$), 1.98−1.93 (m, 2H), 1.59−1.54 (m, 2H), 1.39−1.27 (m, 14H). ^{13}C NMR (CDCl$_3$, 75 MHz): δ = 150.4, 148.9, 147.4, 139.4, 121.9, 121.3, 119.3, 62.8, 50.5, 32.7, 30.0, 29.4, 29.3, 29.2, 28.8, 26.3, 25.7. ESI-TOF MS: m/z = 418.33 (15%, [M + Na]$^+$), 394.14 (100%, [M]$^+$). Anal. Calcd for $C_{18}H_{27}BrN_4O$: C, 54.69%; H, 6.88%; N, 14.17%. Found: C, 54.76%; H, 7.08%; N, 14.02%.

Synthesis of 11-(4-(5-Ethynylpyridin-2-yl)-1H-1,2,3-triazol-1-yl)undecan-1-ol (2). To a solution of 11-(4-(5-bromopyridin-2-yl)-1H-1,2,3-triazol-1-yl)undecan-1-ol (**1**, 1.5 g, 3.79 mmol), CuI (34 mg, 0.18 mmol), and tetrakis(triphenylphosphine)palladium(0) (220 mg, 0.18 mmol) in NEt$_3$/THF (1:1 ratio, 50 mL) was added trimethylsilylacetylene (280 mg, 2.8 mmol), and the mixture was stirred 48 h at 40 °C. After removal of the solvent under reduced pressure, the residue was purified by gel filtration on silica (CHCl$_3$/EtOAc 2:1 ratio).

For the deprotection, the product was dissolved in dichloromethane (30 mL) and treated with tetrabutylammonium fluoride trihydrate (1.8 g, 1.5 equiv). After 4 h, the solvent was removed and the crude product was finally purified by column chromatography on silica (EtOAc) yielding the product as off-white powder (580 mg, 45%). ^{1}H NMR (CDCl$_3$, 300 MHz): δ = 8.66 (s, 1H), 8.16−8.14 (m, 2H), 7.85 (dd, J = 8.2 Hz, J = 2.0 Hz, 1H), 4.41 (t, J = 7.1 Hz, 2H, N−CH$_2$), 3.64−3.59 (m, 2H, O−CH$_2$), 3.25 (s, 1H, C≡C−H), 1.95−1.92 (m, 2H), 1.56−1.51 (m, 2H), 1.33−1.25 (m, 14H). ^{13}C NMR (CDCl$_3$, 75 MHz): δ = 152.4, 149.7, 147.7, 139.9, 122.3, 119.3, 118.0, 80.8, 80.5, 62.9, 50.5, 32.7, 30.1, 29.4, 29.3, 29.2, 28.8, 26.3, 25.6. ESI-TOF MS: m/z = 340.24 (100%, [M]$^+$). Anal. Calcd for $C_{20}H_{28}N_4O$: C, 70.56%; H, 8.29%; N, 16.46%. Found: C, 70.22%; H, 7.98%; N, 16.41%.

Synthesis of 11-(4-(5-((4-Nitrophenyl)ethynyl)pyridine-2-yl)-1H-1,2,3-triazol-1-yl)undecan-1-ol (3). 11-(4-(5-Ethynylpyridin-2-yl)-1H-1,2,3-triazol-1-yl)undecan-1-ol (**2**, 450 mg, 1.32 mmol), 4-nitro-1-iodobenzene (336 mg, 1.35 mmol), tetrakis(triphenylphosphine)-palladium(0) (30 mg, 0.026 mmol), and CuI (5 mg, 0.026 mmol) were dissolved in a NEt$_3$/THF mixture (3:7, 30 mL), and the solution was stirred for 72 h at room temperature. The solution was evaporated under reduced pressure, and the pure product was isolated by column chromatography over silica (CHCl$_3$/EtOAc 8:1 ratio) as a slight yellow

Macromolecules

ARTICLE
ARTICLE

powder (560 mg, 92%). ^{1}H NMR (CDCl$_3$, 300 MHz): δ = 8.74 (s, 1H), 8.26−8.22 (m, 2H), 8.19−8.17 (m, 2H), 7.92 (dd, J = 8.2 Hz, J = 2.1 Hz, 1H), 7.71−7.68 (m, 2H), 4.42 (t, J = 7.1 Hz, 2H, N−CH$_2$), 3.63 (t, J = 6.6 Hz, 2H, O−CH$_2$), 1.99−1.93 (m, 2H), 1.58−1.53 (m, 2H), 1.34−1.27 (m, 14H). ^{13}C NMR (CDCl$_3$, 75 MHz): δ = 152.0, 149.9, 147.5, 147.3, 139.6, 132.3, 129.4, 123.7, 122.4, 119.5, 118.0, 91.2, 90.8, 62.9, 50.5, 32.7, 30.1, 29.4, 29.3, 29.2, 28.8, 26.3, 25.6. ESI-HRMS calcd for C$_{26}$H$_{32}$N$_5$O$_3$ [M + H]$^-$: 462.2500. Found: 462.2486.

Synthesis of 11-(4-(5-((4-Nitrophenyl)ethynyl)pyridine-2-yl)-1H-1,2,3-triazol-1-yl)undecyl Methacrylate (4). 11-(4-(5-((4-Nitrophenyl)ethynyl)pyridin-2-yl)-1H-1,2,3-triazol-1-yl)undecan-1-ol (3, 400 mg, 0.88 mmol) and triethylamine (240 μL, 1.76 mmol) were dissolved in dry dichloromethane (10 mL). The solution was cooled to 0 °C, methacryloyl chloride (200 μL, 2 mmol) was added, and subsequently the solution was stirred for 2 h at 0 °C and further 24 h at room temperature. The reaction mixture was washed with saturated NaHCO$_3$ solution, and after drying of the organic layer over MgSO$_4$, the solvent was removed in vacuo. The crude product was purified by column chromatography on silica (EtOAc/CHCl$_3$ 3:1) providing the pure product as slight yellow solid (410 mg, 88%). ^{1}H NMR (CDCl$_3$, 300 MHz): δ = 8.75 (s, 1H), 8.27−8.24 (m, 2H), 8.21−8.17 (m, 2H), 7.94 (dd, J = 8.2 Hz, J = 2.1 Hz, 1H), 7.72−7.69 (m, 2H), 6.09 (s, 1H, C = CH$_2$), 5.54 (s, 1H, C = CH$_2$), 4.42 (t, J = 7.1 Hz, 2H, N−CH$_2$), 4.13 (t, J = 6.7 Hz, 2H, O−CH$_2$), 2.01−1.97 (m, 2H), 1.93 (s, 3H, CH$_3$), 1.70−1.64 (m, 2H), 1.35−1.26 (m, 14H). ^{13}C NMR (CDCl$_3$, 75 MHz): δ = 167.5, 151.7, 149.8, 147.3, 139.8, 136.5, 132.4, 129.3, 125.1, 123.7, 122.6, 119.7, 118.1, 91.0, 64.8, 50.6, 30.2, 29.41, 29.38, 29.31, 29.1, 28.9, 28.5, 26.4, 25.9, 18.3. ESI-HRMS calcd for C$_{30}$H$_{35}$N$_5$NaO$_4$ [M + Na]$^+$: 552.2587. Found: 552.2580.

Synthesis of Bis(4,4′-dimethyl-2,2′-bipyridine)-[11-(4-(5-((4-nitrophenyl)ethynyl)pyridin-2-yl)-1H-1,2,3-triazol-1-yl)-undecyl methacrylate]ruthenium(II) Hexafluorophosphate (5). cis-Dichlorobis(4,4′-dimethyl-2,2′-bipyridine)ruthenium(II) (87 mg, 0.16 mmol) and 11-(4-(5-((4-nitrophenyl)ethynyl)pyridin-2-yl)-1H-1,2,3-triazol-1-yl)undecyl methacrylate (4, 85 mg, 0.16 mmol) were suspended in ethanol (10 mL). After heating under microwave irradiation at 125 °C for 2 h, the red solution was filtered and treated with a 10-fold excess of NH$_4$PF$_6$. Subsequently, precipitation occurred within 30 min, and the red precipitate was filtered off after 1 day. The precipitate was washed twice with cold ethanol, and recrystallization from ethanol yielded the pure product as red powder (184 mg, 89%). ^{1}H NMR (CD$_2$Cl$_2$, 300 MHz): δ = 8.75 (s, 1H), 8.29−8.07 (m, 8H), 7.73−7.46 (m, 7H), 7.31−7.26 (m, 3H), 7.16 (d, J = 5.9 Hz, 1H), 6.07 (s, 1H, C=C−H), 5.56 (m, 1H, C=C−H), 4.39 (t, J = 7.4 Hz, 2H, N−CH$_2$), 4.12 (t, J = 6.7 Hz, 2H, C(O)O−CH$_2$), 2.61−2.56 (m, 12H, CH$_3$), 1.92−1.87 (m, 2H), 1.67−1.59 (m, 6H), 1.34−1.24 (m, 14H). ^{13}C NMR (CD$_2$Cl$_2$, 75 MHz): δ = 156.9, 156.7, 156.3, 152.8, 151.0, 150.8, 150.7, 150.6, 150.5, 147.9, 147.0, 140.4, 132.7, 128.8, 128.7, 128.6, 128.0, 127.7, 126.0, 124.9, 124.85, 124.6, 124.5, 124.2, 124.1, 123.7, 122.4, 121.5, 93.5, 87.9, 64.7, 29.5, 29.4, 29.38, 29.34, 29.2, 28.8, 28.6, 26.2, 26.0, 21.1, 21.06, 21.02, 18.0. ESI-TOF MS: m/z = 1144.33 (5%, [M−PF$_6$]$^+$), 499.69 (100%, [M−2PF$_6$]$^{2+}$). ESI-HRMS calcd for C$_{54}$H$_{59}$N$_9$O$_4$Ru [M−2PF$_6$]$^{2+}$: 499.6861. Found: 499.6881.

Synthesis of 3-((5-Phenyl-2-(pyridine-2-yl)thiazol-4-yl)oxy)-propan-1-ol (7). To a solution of 5-phenyl-2-(pyridine-2-yl)thiazol-4-ol (6, 4.0 g, 15.8 mmol) and 3-bromopropan-1-ol (2.60 g, 18.9 mmol) in dimethyl sulfoxide (100 mL) was added fine ground K$_2$CO$_3$ (2.60 g, 18.9 mmol). The purple mixture was stirred for 24 h at room temperature followed by addition of 200 mL of H$_2$O. The solution was extracted with CHCl$_3$ (3 × 100 mL). The combined organic phases were washed with H$_2$O (3 × 100 mL) to remove the dimethyl sulfoxide, dried over MgSO$_4$, and concentrated in vacuo. The brown oil was purified using gel filtration (silica, CHCl$_3$) to yield the pure ether as a yellow oil (3.35 g, 68%). ^{1}H NMR (CDCl$_3$, 250 MHz): δ = 8.59 (d, J = 4.8 Hz, 1H), 8.05 (d, J = 8.0 Hz, 1H), 7.82−7.71 (m, 3H), 7.44−7.34

(m, 2H), 7.33−7.24 (m, 2H), 4.69 (t, J = 5.9 Hz, 2H, O−CH$_2$), 3.87 (t, J = 5.9 Hz, 2H, CH$_2$−OH), 2.90 (s, 1H, OH), 2.10 (p, J = 5.9 Hz, 2H, CH$_2$). ^{13}C NMR (CDCl$_3$, 63 MHz): δ = 160.9, 159.2, 150.9, 149.5, 137.0, 131.5, 128.7, 126.97, 126.96, 124.3, 118.9, 115.0, 67.7, 59.2, 32.8. EI MS: m/z = 312.09 (100%, [M]$^+$), 254.05 (75%, [M−C$_3$H$_6$O]$^+$). Anal. Calcd for C$_{17}$H$_{16}$N$_2$O$_2$S: C, 65.36%; H, 5.16%; N, 8.97%; S, 10.26%. Found: C, 65.38%; H, 5.18%; N, 9.10%; S, 9.92%.

Synthesis of 3-((5-Phenyl-2-(pyridin-2-yl)thiazol-4-yl)oxy)-propyl Methacrylate (8). To a solution of 3-((5-phenyl-2-(pyridin-2-yl)thiazol-4-yl)oxy)propan-1-ol (7, 1.40 g, 4.48 mmol) and triethylamine (2.24 g, 22.4 mmol) in dry CH$_2$Cl$_2$ (30 mL) was added methacryloyl chloride (0.94 g, 8.96 mmol). The reaction was stirred for 24 h at ambient temperature, and subsequently, the organic phase was thoroughly washed with water (3 × 20 mL) and saturated NaHCO$_3$ solution to hydrolyze the excess acid chloride. After drying of the organic phase over MgSO$_4$ and evaporation of the solvent (T < 40 °C), the crude product was purified using column chromatography on silica (CHCl$_3$) yielding the pure product as yellow oil (1.5 g, 88%). ^{1}H NMR (CDCl$_3$, 250 MHz): δ = 8.60 (d, J = 4.70 Hz, 1H), 8.09 (d, J = 7.9 Hz, 1H), 7.83−7.67 (m, 3H), 7.45−7.32 (m, 2H), 7.32−7.19 (m, 2H), 6.13 (s, 1H, C=C−H), 5.55 (s, 1H, C=C−H), 4.64 (t, J = 6.3 Hz, 2H, O−CH$_2$), 4.40 (t, J = 6.3 Hz, 2H, C(O)O−CH$_2$), 2.26 (p, J = 6.3 Hz, 2H, CH$_2$), 1.95 (s, 3H, CH$_3$). ^{13}C NMR (63 MHz, CDCl$_3$): δ = 167.4, 160.5, 158.9, 151.2, 149.4, 136.9, 136.3, 131.6, 128.8, 126.94, 126.85, 125.5, 124.2, 118.9, 114.8, 67.1, 61.7, 29.0, 18.3. EI MS: m/z = 380.12 (30%, [M]$^+$), 254.05 (10%, [M−C$_7$H$_{11}$O$_2$]$^+$). Anal. Calcd for C$_{21}$H$_{20}$N$_2$O$_3$: C, 66.29%; H, 5.30%; N, 7.36%; S, 8.43%. Found: C, 66.41%; H, 5.32%; N, 7.22%; S, 7.98%.

General RAFT Copolymerization Procedure. The respective methacrylate-functionalized monomer, methyl methacrylate (125 μL, 1.163 mmol), 2-cyanobutan-2-yl benzodithioate (2.7 mg, 1.6 μmol, 1 mol %), and 2,2′-azobis(2-methylpropionitrile) (0.5 mg, 0.4 μmol, 0.25 mol %) were dissolved in N,N-dimethylacetamide (600 μL) in a 2 mL microwave vial. The vial was sealed, and the solution was degassed for 0.5 h under nitrogen. Subsequently, the reaction mixture was stirred at 85 °C (oil bath temperature) for 16 h. The crude product was precipitated in cold diethyl ether and purified by preparative size exclusion chromatography (BioBeads S-X1, CH$_2$Cl$_2$ as eluent) yielding the pure desired copolymer.

Synthesis of Polymer 9a. According to the general procedure, bis(4,4′-dimethyl-2,2′-bipyridine)-[11-(4-(5-((4-nitrophenyl)ethynyl)-pyridin-2-yl)-1H-1,2,3-triazol-1-yl)undecyl methacrylate]ruthenium-(II) hexafluorophosphate (5, 60 mg, 0.047 mmol) was reacted to yield the product as red solid (106 mg, 45%). ^{1}H NMR (CDCl$_3$, 300 MHz): δ = 8.80 (br), 8.35−8.10 (br), 7.70−7.50 (br), 7.45−7.25 (br), 7.15−7.08 (br), 4.40 (br), 3.95 (br), 3.58 (s), 2.60−2.45 (br), 2.05−1.65 (br), 1.45−1.15 (br), 1.0 (s), 0.8 (s). ^{13}C NMR (CDCl$_3$, 75 MHz): δ = 178.1, 177.8, 176.9, 157.0, 156.6, 156.3, 152.9, 150.9, 150.8, 147.8, 147.1, 140.4, 132.7, 128.8, 128.7, 128.0, 127.7, 126.0, 124.9, 124.6, 124.2, 124.1, 123.7, 122.4, 121.5, 93.7, 87.7, 54.4−51.8, 44.9, 44.5, 29.4, 21.5, 21.2, 18.7, 16.5.

Synthesis of Polymer 9b. According to the general procedure, 3-((5-phenyl-2-(pyridin-2-yl)thiazol-4-yl)oxy)propyl methacrylate (8, 35 mg, 0.093 mmol) was reacted to yield the product as orange solid (81 mg, 51%). ^{1}H NMR (CDCl$_3$, 300 MHz): δ = 8.59 (br), 8.15−8.0 (br), 7.8−7.70 (br), 7.40−7.30 (br), 4.60 (br), 4.20 (br), 3.70−3.45 (br), 2.2−1.70 (br), 1.48−1.30 (br), 1.0 (br), 0.83 (br). ^{13}C NMR (CDCl$_3$, 75 MHz): δ = 178.1, 177.8, 176.9, 160.4, 158.7, 151.1, 149.3, 148.3, 137.1, 131.5, 128.9, 128.7, 126.9, 124.2, 123.1, 119.0, 114.7, 66.9, 65.8, 54.3−51.7, 44.8, 44.5, 18.7, 16.4, 15.2.

Synthesis of Polymer 9c. According to the general procedure, bis(4,4′-dimethyl-2,2′-bipyridine)-[11-(4-(5-((4-nitrophenyl)ethynyl)-pyridin-2-yl)-1H-1,2,3-triazol-1-yl)undecyl methacrylate]ruthenium-(II) hexafluorophosphate (5, 60 mg, 0.047 mmol) and 3-((5-phenyl-2-(pyridin-2-yl)thiazol-4-yl)oxy)propyl methacrylate (8, 35 mg, 0.093 mmol) were reacted to yield the product as red solid (42 mg, 36%). ^{1}H NMR

6285   dx.doi.org/10.1021/ma201193e |Macromolecules 2011, 44, 6277−6287

- 141 -

(CDCl$_3$, 300 MHz): δ = 8.58 (br), 8.30−7.90 (br), 7.85−7.30 (br), 7.20−7.0 (br), 4.51 (br), 4.15 (br), 3.55 (s), 2.50 (br), 1.92−1.70 (br), 1.34−1.24 (br), 1.0 (br), 0.83 (br). ^{13}C NMR (CDCl$_3$, 75 MHz): δ = 178.1, 177.8, 177.0, 151.1−150.0, 149.5, 137.0, 136.70, 136.24, 132.9, 131.6, 128.8−126.9, 124.3, 123.6, 118.9, 67.0, 54.4, 51.8, 44.9, 44.5, 29.7−28.5, 26.3, 26.0, 21.2, 18.7, 16.5.

■ ASSOCIATED CONTENT

ⓢ **Supporting Information.** SEC traces of all polymers as well as UV/vis absorption and emission spectra. This material is available free of charge via the Internet at http://pubs.acs.org.

■ AUTHOR INFORMATION

Corresponding Author
*Fax +49 (0)3641 948212, e-mail c6bera@uni-jena.de (R.B.); Fax +49 (0)3641 206399, e-mail benjamin.dietzek@uni-jena. de (B.D.); Fax +49 (0)3641 948202, e-mail ulrich.schubert@ uni-jena.de (U.S.S.).

■ ACKNOWLEDGMENT

■ REFERENCES

(1) Juris, A.; Balzani, V.; Barigelletti, F.; Campagna, S.; Belser, P.; von Zelewsky, A. *Coord. Chem. Rev.* **1988**, *84*, 85–277.

(2) Lehn, J.-M. *Angew. Chem., Int. Ed.* **1988**, *27*, 89–112.

(3) Balzani, V.; Juris, A.; Venturi, M.; Campagna, S.; Serroni, S. *Chem. Rev.* **1996**, *96*, 759–833.

(4) Baba, A. I.; Shaw, J. R.; Simon, J. A.; Thummel, R. P.; Schmehl, R. H. *Coord. Chem. Rev.* **1998**, *171*, 43–59.

(5) Newkome, G. R.; He, E.; Moorefield, C. N. *Chem. Rev.* **1999**, *99*, 1689–1746.

(6) Schubert, U. S.; Eschbaumer, C. *Angew. Chem., Int. Ed.* **2002**, *41*, 2893–2926.

(7) Hofmeier, H.; Schubert, U. S. *Chem. Soc. Rev.* **2004**, *33*, 373–399.

(8) Siebert, R.; Winter, A.; Dietzek, B.; Schubert, U. S.; Popp, J. *Macromol. Rapid Commun.* **2010**, *31*, 883–888.

(9) Siebert, R.; Winter, A.; Schubert, U. S.; Dietzek, B.; Popp, J. *J. Phys. Chem. C* **2010**, *114*, 6841–6848.

(10) Siebert, R.; Winter, A.; Schubert, U. S.; Dietzek, B.; Popp, J. *Phys. Chem. Chem. Phys.* **2011**, *13*, 1606–17.

(11) Siebert, R.; Akimov, D.; Schmitt, M.; Winter, A.; Schubert, U. S.; Dietzek, B.; Popp, J. *ChemPhysChem* **2009**, *10*, 910–919.

(12) Tschierlei, S.; Presselt, M.; Kuhnt, C.; Yartsev, A.; Pascher, T.; Sundström, V.; Karnahl, M.; Schwalbe, M.; Schäfer, B.; Rau, S.; Schmitt, M.; Dietzek, B.; Popp, J. *Chem.—Eur. J.* **2009**, *15*, 7678–7688.

(13) Tschierlei, S.; Dietzek, B.; Karnahl, M.; Rau, S.; MacDonnell, F. M.; Schmitt, M.; Popp, J. *J. Raman Spectrosc.* **2008**, *39*, 557–559.

(14) Heller, M.; Schubert, U. S. *J. Org. Chem.* **2002**, *67*, 8269–8272.

(15) Heller, M.; Schubert, U. S. *Macromol. Rapid Commun.* **2001**, *22*, 1358–1363.

(16) Schubert, U. S.; Eschbaumer, C.; Hochwimmer, G. *Synthesis* **1999**, 779–782.

(17) Hochwimmer, G.; Nuyken, O.; Schubert, U. S. *Macromol. Rapid Commun.* **1998**, *19*, 309–313.

(18) Eisenbach, C. D.; Schubert, U. S. *Macromolecules* **1993**, *26*, 7372–7374.

(19) Schubert, U. S.; Eschbaumer, C.; Andres, P.; Hofmeier, H.; Weidl, C. H.; Herdtweck, E.; Dulkeith, E.; Morteani, A.; Hecker, N. E.; Feldmann, J. *Synth. Met.* **2001**, *121*, 1249–1252.

(20) Kalyanasundaram, K.; Grätzel, M. *Coord. Chem. Rev.* **1998**, *177*, 347–414.

(21) Rabek, J. F. *Prog. Polym. Sci.* **1988**, *13*, 83–188.

(22) Meyer, T. J. *Acc. Chem. Res.* **1989**, *22*, 163–170.

(23) Alstrum Acevedo, J. H.; Brennaman, M. K.; Meyer, T. J. *Inorg. Chem.* **2005**, *44*, 6802–6827.

(24) Kiwi, J.; Gratzel, M. *Nature* **1979**, *281*, 657–658.

(25) O'Regan, B.; Gratzel, M. *Nature* **1991**, *353*, 737–740.

(26) Balzani, V.; Credi, A.; Venturi, M. *ChemSusChem* **2008**, *1*, 26–58.

(27) Szaciłowski, K.; Macyk, W.; Drzewiecka-Matuszek, A.; Brindell, M.; Stochel, G. *Chem. Rev.* **2005**, *105*, 2647–2694.

(28) Prodi, L.; Bolletta, F.; Montalti, M.; Zaccheroni, N. *Coord. Chem. Rev.* **2000**, *205*, 59–83.

(29) DeRosa, M. C.; Crutchley, R. J. *Coord. Chem. Rev.* **2002**, *233*, 351–371.

(30) Rogers, C. W.; Wolf, M. O. *Coord. Chem. Rev.* **2002**, *233*, 341–350.

(31) Kuhnt, C.; Karnahl, M.; Tschierlei, S.; Griebenow, K.; Schmitt, M.; Schäfer, B.; Krieck, S.; Görls, H.; Rau, S.; Dietzek, B.; Popp, J. *Phys. Chem. Chem. Phys.* **2010**, *12*, 1357–1368.

(32) Manners, I. *Synthetic Metal-Containing Polymers*; Wiley-VCH: Weinheim, 2004.

(33) Sykora, M.; Maxwell, K. A.; DeSimone, J. M.; Meyer, T. J. *Proc. Natl. Acad. Sci. U. S. A.* **2000**, *97*, 7687–7691.

(34) Schubert, U. S.; Winter, A.; Newkome, G. R. *Terpyridine-Based Materials*; Wiley-VCH: Weinheim, 2011.

(35) Whittell, G. R.; Manners, I. *Adv. Mater.* **2007**, *19*, 3439–3468.

(36) Suzuki, M.; Kobayashi, S.; Kimura, M.; Hanabusa, K.; Shirai, H. *Chem. Commun.* **1997**, 227–228.

(37) Whittell, G. R.; Hager, M. D.; Schubert, U. S.; Manners, I. *Nature Mater.* **2011**, *10*, 176–188.

(38) Schultze, X.; Serin, J.; Adronov, A.; Frechet, J. M. J. *Chem. Commun.* **2001**, 1160–1161.

(39) Serin, J.; Schultze, X.; Adronov, A.; Frechet, J. M. J. *Macromolecules* **2002**, *35*, 5396–5404.

(40) Huynh, M. H. V.; Dattelbaum, D. M.; Meyer, T. J. *Coord. Chem. Rev.* **2005**, *249*, 457–483.

(41) Newkome, G. R.; Patri, A. K.; Holder, E.; Schubert, U. S. *Eur. J. Org. Chem.* **2004**, 235–254.

(42) Kolb, H. C.; Finn, M. G.; Sharpless, K. B. *Angew. Chem., Int. Ed.* **2001**, *40*, 2004–2021.

(43) Rostovtsev, V. V.; Green, L. G.; Fokin, V. V.; Sharpless, K. B. *Angew. Chem., Int. Ed.* **2002**, *41*, 2596–2599.

(44) Happ, B.; Friebe, C.; Winter, A.; Hager, M. D.; Hoogenboom, R.; Schubert, U. S. *Chem.—Asian J.* **2009**, *4*, 154–163.

(45) Happ, B.; Escudero, D.; Hager, M. D.; Friebe, C.; Winter, A.; Görls, H.; Altuntas, E.; Gonzalez, L.; Schubert, U. S. *J. Org. Chem.* **2010**, *75*, 4025–4038.

(46) Schulze, B.; Friebe, C.; Hager, M. D.; Winter, A.; Hoogenboom, R.; Görls, H.; Schubert, U. S. *Dalton Trans.* **2009**, 787–794.

(47) Brombosz, S. M.; Appleton, A. L.; Zappas, A. J.; Bunz, U. H. F. *Chem. Commun.* **2010**, *46*, 1419–1421.

(48) Beyer, B.; Ulbricht, C.; Escudero, D.; Friebe, C.; Winter, A.; Gonzalez, L.; Schubert, U. S. *Organometallics* **2009**, *28*, 5478–5488.

(49) Meudtner, R. M.; Ostermeier, M.; Goddard, R.; Limberg, C.; Hecht, S. *Chem.—Eur. J.* **2007**, *13*, 9834–9840.

(50) Rau, S.; Schäfer, B.; Gleich, D.; Anders, E.; Rudolph, M.; Friedrich, M.; Görls, H.; Henry, W.; Vos, J. G. *Angew. Chem., Int. Ed.* **2006**, *45*, 6215–6218.

(51) Tschierlei, S.; Karnahl, M.; Presselt, M.; Dietzek, B.; Guthmuller, J.; González, L.; Schmitt, M.; Rau, S.; Popp, J. *Angew. Chem., Int. Ed.* **2010**, *49*, 3981–4.

(52) Dietzek, B.; Kiefer, W.; Blumhoff, J.; Böttcher, L.; Rau, S.; Walther, D.; Uhlemann, U.; Schmitt, M.; Popp, J. *Chem.—Eur. J.* **2006**, *12*, 5105–5115.

(53) Bard, A. J.; Fox, M. A. *Acc. Chem. Res.* **1995**, *28*, 141–145.

(54) Terazono, Y.; Kodis, G.; Liddell, P. a.; Garg, V.; Moore, T. a.; Moore, A. L.; Gust, D. *J. Phys. Chem. B* **2009**, *113*, 7147–55.

(55) Kodis, G.; Liddell, P.; de la Garza, L.; Clausen, P. C.; Lindsey, J. S.; Moore, A. L.; Moore, T.; Gust, D. *J. Phys. Chem. A* **2002**, *106*, 2036–2048.

(56) Johnson, J. M.; Chen, R.; Chen, X.; Moskun, A. C.; Zhang, X.; Hogen-Esch, T. E.; Bradforth, S. E. *J. Phys. Chem. B* **2008**, *112*, 16367–16381.

(57) Schäfer, J.; Menzel, R.; Weiss, D.; Dietzek, B.; Beckert, R.; Popp, J. *J. Lumin.* **2011**, *131*, 1149–1153.

(58) Menzel, R.; Breul, A.; Pietsch, C.; Schäfer, J.; Friebe, C.; Täuscher, E.; Weiss, D.; Dietzek, B.; Popp, J.; Beckert, R.; Schubert, U. S. *Macromol. Chem. Phys.* **2011**10.1002/macp.201000752.

(59) Menzel, R.; Täuscher, E.; Weiss, D.; Beckert, R.; Görls, H. *Z. Anorg. Allg. Chem.* **2010**, *636*, 1380–1385.

(60) Chiefari, J.; Chong, Y. K.; Ercole, F.; Krstina, J.; Jeffery, J.; Le, T. P. T.; Mayadunne, R. T. A.; Meijs, G. F.; Moad, C. L.; Moad, G.; Rizzardo, E.; Thang, S. H. *Macromolecules* **1998**, *31*, 5559–5562.

(61) Benaglia, M.; Rizzardo, E.; Alberti, A.; Guerra, M. *Macromolecules* **2005**, *38*, 3129–3140.

(62) Rizzardo, E.; Chen, M.; Chong, B.; Moad, G.; Skidmore, M.; Thang, S. H. *Macromol. Symp.* **2007**, *248*, 104–116.

(63) Happ, B.; Friebe, C.; Winter, A.; Hager, M. D.; Schubert, U. S. *Eur. Polym. J.* **2009**, *45*, 3433–3441.

(64) Odian, G. In *Principles of Polymerization*, 4th ed.; Wiley-VCH: New York, 2004; pp 255—263.

(65) Adronov, A.; Gilat, S. L.; Frechet, J. M. J.; Ohta, K.; Neuwahl, F. V. R.; Fleming, G. R. *J. Am. Chem. Soc.* **2000**, *122*, 1175–1185.

(66) Ozcelik, S. *J. Phys. Chem. B* **1997**, *5647*, 3021–3024.

(67) Gulbinas, V.; Mineviciūte, I.; Hertel, D.; Wellander, R.; Yartsev, a.; Sundström, V. *J. Chem. Phys.* **2007**, *127*, 144907.

(68) Kuhnt, C.; Karnahl, M.; Schmitt, M.; Rau, S.; Dietzek, B.; Popp, J. *Chem. Commun.* **2011**, 3820–3821.

(69) Ghiggino, K. P.; Smith, T. A. *Prog. React. Kinet.* **1993**, *18*, 375–436.

(70) Turro, N. J.; Ramamurthy, V.; Scaiano, J. C. *Principles of Molecular Photochemistry*; University Science Books: Sausalito, CA, 2009.

(71) Ghiggino, K. P.; Smith, T. a.; Haines, D. J.; Wilson, G. J. *Can. J. Chem.* **1995**, *73*, 2015–2020.

(72) Adronov, A.; Robello, D. R.; Fréchet, J. M. J. *J. Polym. Sci., Part A: Polym. Chem.* **2001**, *39*, 1366–1373.

(73) Bojarski, P. *Chem. Phys. Lett.* **1997**, *278*, 225–232.

(74) Lakowicz, J. R.; Szmacinski, H.; Gryczynski, I.; Wiczk, W.; Johnson, M. L. *J. Phys. Chem.* **1990**, *94*, 8413–8416.

(75) Thomas, D. D.; Carlsen, W. F.; Stryer, L. *Proc. Natl. Acad. Sci. U. S. A.* **1978**, *75*, 5746–5750.

(76) Montalti, M.; Credi, A.; Prodi, L.; Gandolfi, M. T. *Handbook of Photochemistry*; Taylor & Francis Group: Boca Raton, FL, 2006.

(77) Lakowicz, J. R. *Principles of Fluorescence Spectroscopy*, 3rd ed.; Springer: Baltimore, MD, 2006.

Publication A5

CLICK CHEMISTRY MEETS POLYMERIZATION: CONTROLLED INCORPORATION OF AN EASILY ACCESSIBLE RUTHENIUM(II) COMPLEX INTO A PMMA BACKBONE VIA RAFT COPOLYMERIZATION

Bobby Happ, Christian Friebe, Andreas Winter, Martin D. Hager, Ulrich S. Schubert*

Click chemistry meets polymerization: Controlled incorporation of an easily accessible ruthenium(II) complex into a PMMA backbone *via* RAFT copolymerization

Bobby Happ [a,b], Christian Friebe [a,b], Andreas Winter [b,c], Martin D. Hager [a,b], Ulrich S. Schubert [a,b,c,*]

[a] Laboratory of Organic and Macromolecular Chemistry, Friedrich-Schiller-University Jena, Humboldtstrasse 10, 07743 Jena, Germany
[b] Dutch Polymer Institute (DPI), P.O. Box 902, 5600 AX Eindhoven, The Netherlands
[c] Laboratory of Macromolecular Chemistry and Nanoscience, Eindhoven University of Technology, P.O. Box 513, 5600 MB Eindhoven, The Netherlands

ARTICLE INFO

ABSTRACT

The copper(I)-catalyzed azide-alkyne cycloaddition provided an easy and efficient access to a functionalized heteroleptic ruthenium(II) complex monomer. A grafted copolymer with the heteroleptic ruthenium(II) complex and methyl methacrylate (MMA) as comonomer was synthesized by reversible addition fragmentation chain transfer (RAFT) polymerization. The product was characterized by means of ^{1}H NMR spectroscopy, UV/vis spectroscopy and size exclusion chromatography coupled with a photodiode array detector. The RAFT process itself led to a grafted copolymer with a low polydispersity index.

© 2009 Published by Elsevier Ltd.

1. Introduction

The processing of well-known (co)polymers functionalized with light-interacting systems represents an interesting topic due to their remarkable photophysical and electrochemical properties [1–4]. Hence, a general target of current research is to develop new synthetic approaches allowing the facile and straightforward covalent linkage of functionalized ligands or transition metal complexes to polymers. Such covalent linkages are the basis for potential functional materials, which are able to avoid aggregation of incorporated metal complexes while maintaining the photophysical properties of the appropriate complex at

the same time. The prevention of aggregation can yield advanced materials processable by spin-coating [6] and ink-jet-printing [7], respectively.

The construction of metal-containing macromolecules contains mainly two variable components: The ligand(s) of the metal complex and the polymer backbone. The thermodynamic and kinetic stability as well as the photophysical properties of the metal complex are mainly determined by the nature of the used ligands. In addition, copolymerization represents a fashionable route to incorporate ligands and their metal complexes, respectively, whereupon the metal complex itself maintains the optical properties in the polymer [8–10].

In general, metal-containing polymers can be generated either by allowing to react a reactive heteroleptic metal complex (*i.e.* having a reactive ligand side-chain) with another monomer leading to the respective polymer (copolymers) or the polymer backbone bears the ligand units as side-chains, which then can be coordinated to metal-ions

later [4a,4b,8]. The basic prerequisite for all strategies is in general the good synthetic accessibility of the ligands and metal complexes which are connected to the monomer.

One of the most interesting ligands for the complexation of transition metal-ions is 2,2′-bipyridine (see *e.g.* Schubert et. al. Ref. [11a]). However, by contrast the use of functionalized 4-(pyridin-2-yl)-1*H*-1,2,3-triazole ligands for the complexation of ruthenium(II) overcomes the troublesome synthesis of *mono*-functionalized bipyridines [4d,11b] (Scheme 1) and provides a fast access to a functionalized ruthenium(II) complex. Such *mono*-functionalized 4-(pyridin-2-yl)-1*H*-1,2,3-triazole ligands were synthesized in good yields and in a one-step procedure using the copper(I)-catalyzed azide-alkyne cycloaddition ("click" chemistry) [12]. This is in contrast to the well-established 2,2′-bipyridines, for which at least two synthesis steps are necessary containing the synthesis of the 4,4′-substituted 2,2′-bipyridine itself [4b] usually utilizing the hazardous Stille-coupling followed by the *mono*-functionalization of the 4,4′-substituted 2,2′-bipyridine, which normally is not simple to purify and ends up in relatively low yields [4d].

Almost all monomers, which contain one carbon–carbon double bond, will undergo radical polymerization. By contrast, ionic polymerizations are highly selective due to the very strict requirements for stabilization concerning the anionic or the cationic propagating species [13,14]. Furthermore, the reactivity of the monomer significantly

changes with the electronic nature of its substituents [13]. The controlled introduction of thiocarbonylthio-compounds in the field of radical polymerization reactions, which serve as reversible addition fragmentation chain transfer (RAFT) agents and ensure good control of the process, was first reported in 1998 [15].

Since that time it has been established that RAFT polymerization represents an extremely versatile process [15–17] and the main advantages are that it can be applied to prepare polymers or copolymers with narrow polydispersity indices starting from a large variety of monomers, which are able to undergo radical polymerization. Furthermore, it is possible to drive the RAFT polymerization to high conversions to obtain relatively high polymerization rates and a wide range of functionalities in the monomers, even metal complexes, are tolerated. Star-shaped, block, hyper-branched structures as well as supramolecular assemblies and other complex architectures are accessible *via* this technique. Thus, this controlled process overcomes most drawbacks of a conventional free-radical polymerization [5,15,16].

In the present study we describe the facile and straightforward synthesis of a *mono*-functionalized ruthenium complex and its controlled radical RAFT copolymerization with methyl methacrylate yielding a well-defined grafted copolymer. The resulting copolymer was characterized in detail by ^{1}H NMR spectroscopy, UV/vis spectroscopy and size exclusion chromatography (SEC) with

Synthesis of mono-functionalized 2,2'-bipyridines

One-step synthesis of mono-functionalized 4-(pyridin-2-yl)-1*H*-1,2,3-triazoles
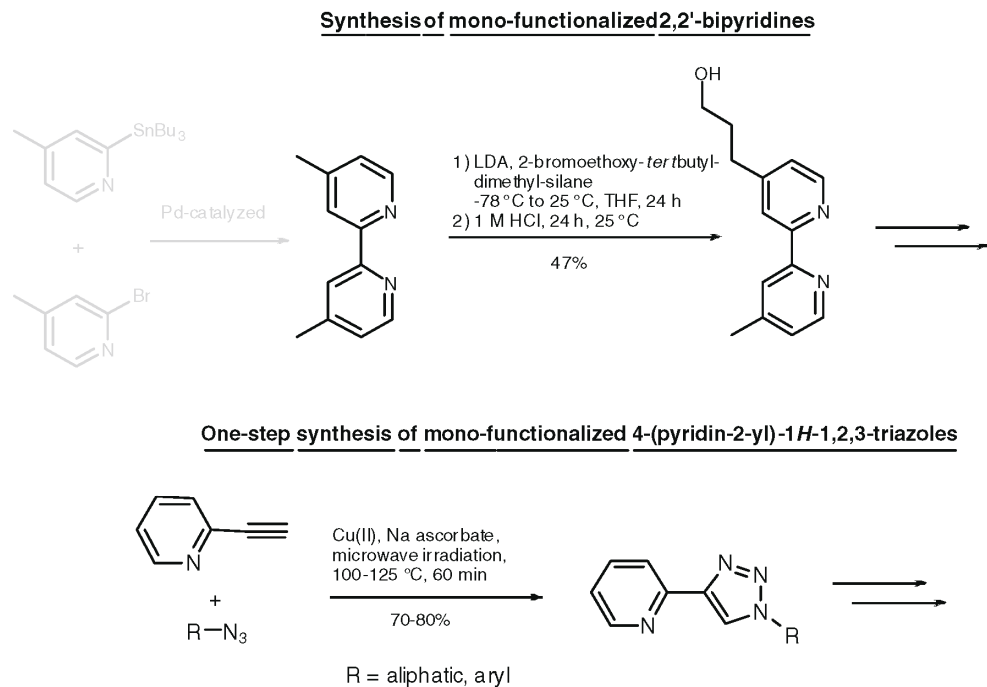
Scheme 1. Schematic representation of the synthesis of *mono*-functionalized 4-(pyridin-2-yl)-1*H*-1,2,3-triazoles [12] and 4-substituted 2,2′-bipyridines [4d] for further reactions.

a refractive-index as well as a photodiode array detector. The obtained copolymer was spin-coated on a glass substrate and characterized by means of UV/vis- and emission spectroscopy.

2. Experimental section

2.1. Materials and instrumentation

Unless stated otherwise, all reagents and solvents were purchased from commercial sources and used without further purification. For the synthesis of the transition metal complexes, the solvents were previously degassed under reflux, applying a vigorous argon flow for at least 1 h. The progress of the reactions was controlled either by GC–MS (Shimadzu QP5050 and electron ionization (EI) as ion source) or by thin-layer chromatography using aluminum sheets pre-coated with silica gel 60 F_{254} or neutral aluminum oxide 60 F_{254} (Merck). Standardized aluminum oxide 90 and silica gel purchased from Merck were used for preparative column chromatography. Preparative size exclusion chromatography (SEC) was carried out on Bio-Rad S-X1 beads (size exclusion 600–14,000 g/mol), swollen in dichloromethane. Microwave-assisted reactions were carried out in a Biotage Initiator ExpEU (maximum power: 400 W, working frequency: 2450 MHz) using closed reaction vials. During the experiments the temperature and the pressure profiles were detected. 1D-(^{1}H and ^{13}C) and 2D-(^{1}H–1H gCOSY) nuclear magnetic resonance (NMR) spectra were recorded on a Varian Mercury 400 MHz instrument at 298 K in deuterated solvents (Cambridge Isotope Laboratories Inc.). Chemical shifts are reported in parts per million (ppm, δ scale) relative to the signal of the applied solvent. Coupling constants are given in Hertz. MALDI-TOF mass spectra were measured on a Voyager-DE PRO biospectrometry workstation (Applied Biosystems) time-of-flight mass spectrometer with dithranol as matrix. Elemental analysis was carried out on an EuroVector EuroEA3000 elemental analyzer for CHNS-O. UV/vis spectra were recorded on a Perkin Elmer Lambda 45 (1 cm cuvettes) using velocities of 480 nm/min. Size exclusion chromatograms (SEC) for non-metal-containing polymers were recorded with a Shimadzu system equipped with a SCL-A10 system controller, a LC-10AD pump, a RID-10A refractive-index detector, a SPD-10A UV-detector at 254 nm and a PLgel 5 mm Mixed-D column at 50 °C utilizing a chloroform/triethylamine/2-propanol (94:4:2 ratio) mixture as eluent at a flow rate of 1 mL/min. The molar masses were calculated against linear poly(methyl methacrylate) standards. For the metal-containing polymers SEC was carried out on a Waters SEC system consisting of a 717 Plus autosampler, an isocratic pump, a solvent degasser, a column oven and a Styragel HT 4 GPC column with a precolumn equipped either with a 2414 refractive-index (RI) or a 2996 photodiode array (PDA) detector. DMF (containing 5 mM NH$_4$PF$_6$) was used as eluent at a column temperature of 50 °C and a flow rate of 0.5 mL/min. For both systems, poly(methyl methacrylate) standards have been applied to determine the molar masses.

Films were prepared *via* spin-coating from an acetonitrile solution containing 5 mg mL^{-1} of the copolymer onto quartz glass substrates. UV/vis spectroscopy of the received films were measured with a Perkin Elmer Lambda 19 (absorption) and a Hitachi F-4500 (emission).

2.2. Synthesis of 11-(4-(pyridin-2-yl)-1H-1,2,3-triazole-1-yl)-undecan-1-ol

To a suspension of sodium azide (195 mg, 3.0 mmol), 1-bromoundecan-11-ol (703 mg, 2.8 mmol) and 2-ethynylpyridine (290 mg, 2.8 mmol) in a EtOH/water mixture (7:3 ratio, 8 mL) filled in a 20 mL microwave vial were added CuSO$_4$ × 5 H$_2$O (23 mg, 5 mol%) and subsequently sodium ascorbate (90 mg, 25 mol%). This mixture has been irradiated in the microwave at 125 °C for 20 min. After this time additional CuSO$_4$ × 5 H$_2$O (23 mg, 5 mol%) was added into the reaction mixture and the brown solution was irradiated for another 25 min. Subsequently, a large excess of water was added to the suspension. The off-white precipitate was filtered to yield 11-(4-(pyridin-2-yl)-1H-1,2,3-triazole-1-yl)undecan-1-ol as white powder after gel filtration on silica (ethyl acetate) and precipitation from CH$_2$Cl$_2$/n-pentane (644 mg, 72%).

^{1}H NMR (CDCl$_3$, 400 MHz): δ = 1.28–1.36 (m, 14H, CH$_2$), 1.55 (m, 2H, HO—CH$_2$—CH$_2$), 1.69 (s, 1H, OH), 1.95 (m, 2H, N—CH$_2$—CH$_2$), 3.63 (m, 2H, HO—CH$_2$—CH$_2$), 4.41 (t, ^3J = 7.1 Hz, 2H, N—CH$_2$—CH$_2$), 7.22 (ddd, $^3J_{5,4}$ = 7.5 Hz, $^3J_{5,6}$ = 5.1 Hz, $^4J_{5,3}$ = 1.0 Hz, 1H, H^5), 7.78 (dt, $^3J_{4,3}$ = 7.9 Hz, ^4J = 1.8 Hz, 1H, H^4), 8.13 (s, 1H, H$^{5'}$), 8.18 (d, $^3J_{3,4}$ = 8 Hz, 1H, H^3), 8.57 (m, 1H, H^6).

^{13}C NMR (CDCl$_3$, 100.63 MHz): δ = 25.7, 26.3, 28.8, 29.1, 29.2, 29.2, 29.3, 30.1, 32.7, 50.4 (N—CH$_2$), 62.6 (HO—CH$_2$), 120.2 (C^3), 121.8 (C$^{5'}$), 122.7 (C^5), 136.9 (C^4), 148.1 (C$^{4'}$), 149.2 (C^6), 150.2 (C^2).

IR-ATR (cm^{-1}): 751, 785, 997, 1054, 1259, 1417, 1465, 1600, 2849, 2922, 3130, 3420.

MALDI-TOF MS (dithranol): m/z = 317.23 (100%) [M+H]$^+$.

UV/vis (CH$_2$Cl$_2$) (ε in M^{-1} cm^{-1}): λ_{max}/nm = 280 (8900), 246 (13,000).

Emission (CH$_2$Cl$_2$): λ_{max}/nm = 324.

Anal. calcd. for C$_{18}$H$_{28}$N$_4$O: C 68.32, H 8.92, N 17.71; found: C 68.06, H 9.12, N 17.46.

2.3. Synthesis of bis(4,4'-dimethyl-2,2'-bipyridine)-{11-(4-(pyridin-2-yl)-1H-1,2,3-triazole-1-yl)undecan-1-ol} ruthenium(II) hexafluorophosphate

Cis-dichloro-*bis*(4,4'-dimethyl-2,2'-bipyridine) ruthenium(II) (43 mg, 0.08 mmol) and 11-(4-(pyridin-2-yl)-1H-1,2,3-triazole-1-yl)undecan-1-ol (26, mg, 0.08 mmol) were suspended in degassed ethanol (8 mL). After an irradiation time of 2 h at 125 °C in the microwave, the red solution was treated with a 10-fold excess of NH$_4$PF$_6$ and was subsequently stirred for approximately 2 h until precipitation occurred. The orange precipitate was purified by washing twice with water, ethanol and diethyl ether providing the pure product (72 mg, 90%).

^{1}H NMR (CD$_2$Cl$_2$, 400 MHz): δ = 1.18–1.3 (m, 12H), 1.52 (m, 4H), 1.86 (m, 2H, N—CH$_2$—CH$_2$), 2.56 (s, 3H, CH$_3$), 2.58 and 2.59 (s, 9H, CH$_3$), 3.59 (t, ^3J = 6.6 Hz, 2H, HO—CH$_2$), 4.38

B. Happ et al./European Polymer Journal 45 (2009) 3433–3441

(t, ^3J = 7.4 Hz, 2H, N—CH$_2$—CH$_2$), 7.15 (dd, $^3J_{5,6}$ = 5.8 Hz, $^4J_{5,3}$ = 0.8 Hz, 1H, H^5-Mepy), 7.23–7.31 (m, 4H, H^5-py, 3 × H^5-Mepy), 7.52 (d, $^3J_{6,5}$ = 5.8 Hz, 1H, H^6-Mepy), 7.56–7.62 (m, 4H, H^6-py, 3 × H^6-Mepy), 7.94 (dt, $^3J_{4,3}$ = 7.8 Hz, ^4J = 1.4 Hz 1H, H^4-py), 8.13 (d, $^3J_{3,4}$ = 7.8 Hz, 1H, H^3-py), 8.16 (s, 1H, H^3-Mepy), 8.20 (s, 1H, H^3-Mepy), 8.24 (s, 1H, H^3-Mepy), 8.26 (s, 1H, H^3-Mepy), 8.67 (s, 1H, H^5').

^{13}C NMR (CD$_2$Cl$_2$, 100.63 MHz): δ = 18.2, 21.0, 21.0, 21.0, 25.7, 26.1, 28.7, 29.3, 29.3, 29.3, 29.5, 29.4, 32.7, 52.5, 62.6, 122.7, 124.0, 124.3, 124.6, 124.8, 125.1, 125.9, 127.6, 128.4, 128.5, 128.6, 137.9, 149.8, 150.3, 150.4, 150.5, 150.8, 150.9, 150.9, 151.1, 156.3, 156.7, 156.8, 156.9, 157.1.

MALDI-TOF MS (dithranol): m/z = 470.04 (48%) [M−2PF$_6$−pytrz+H]$^+$, 602.17 (23%) [M−2PF$_6$−dmbpy+H]$^+$, 695.04 (25%) [M−2PF$_6$−pytrz+matrix]$^+$, 786.18 (35%) [M−2PF$_6$]$^+$, 931.12 (100%) [M−PF$_6$]$^+$.

UV/vis (CH$_2$Cl$_2$) (ε in M^{-1} cm^{-1}): λ_{max}/nm = 451 (12,500), 418 (10,200), 380sh (7500), 286 (70,600), 261sh (32,400), 249 (28,720).

Anal. calcd. for C$_{42}$H$_{52}$F$_{12}$N$_8$OP$_2$Ru: C 46.89, H 4.87, N 10.41; found: C 47.09, H 5.17, N 10.06.

2.4. Synthesis of bis(4,4'-dimethyl-2,2'-bipyridine) {11-(4-(pyridin-2-yl)-1H-1,2,3-triazol-1-yl)undecyl methacrylate} ruthenium(II) hexafluorophosphate (2)

Bis(4,4'-dimethyl-2,2'-bipyridine)-{11-(4-(pyridin-2-yl)-1H-1,2,3-triazol-1-yl)undecan-1-ol} ruthenium(II) hexafluorophosphate[15] (1, 150 mg, 0.14 mmol) and triethylamine (60 μL, 0.44 mmol) were dissolved in dry dichloromethane (10 mL). The solution was cooled to 0 °C under an argon flow. Then methacryloyl chloride (50 μL, 0.5 mmol) was added and the red solution was stirred for 2 h at 0 °C and further 24 h at room temperature. Subsequently, the reaction mixture was washed with saturated NaHCO$_3$ solution and twice with water. After drying over MgSO$_4$, the solvent was removed *in vacuo*. The crude product was purified by column chromatography on aluminum oxide (acetonitrile/toluene 5:1) providing the pure product as red oil (122 mg, 76%).

^{1}H NMR (CD$_2$Cl$_2$, 400 MHz): δ = 1.15–1.40 (m, 14H, alkyl-*H*), 1.67 (m$_c$, 2H, alkyl-*H*), 1.87 (m$_c$, 2H, alkyl-*H*), 1.93 (s, 3H, methacrylate-C*H*$_3$), 2.56 (s, 3H, dmbpy-C*H*$_3$), 2.6 (s, 9H, dmpby-C*H*$_3$), 4.12 (t, ^3J = 6.7 Hz, 2H, alkyl-*H*), 4.38 (t, ^3J = 7.4 Hz, 2H, alkyl-*H*), 5.55 (m$_c$, 1H, methacrylate-*H*), 6.07 (m$_c$, 1H, methacrylate-*H*), 7.15 (m$_c$, 1H, dmbpy-*H*^{5}), 7.23–7.31 (m, 4H, pyr-*H*^{5}, dmbpy-*H*^{5}), 7.52 (d, ^3J = 5.8 Hz, 1H, dmbpy-*H*^{6}), 7.56–7.62 (m, 4H, pyr-*H*^{6}, dmbpy-H^6-Mepy), 7.95 (m, 1H, pyr-*H*^{4}), 8.12 (d, ^3J = 7.8 Hz, 1H, pyr-*H*^{3}), 8.14 (s, 1H, dmbpy-*H*^{3}), 8.17 (s, 1H, dmbpy-*H*^{3}), 8.22 (s, 1H, dmbpy-*H*^{3}), 8.23 (s, 1H, dmbpy-*H*^{3}), 8.65 (s, 1H, triazole-*H*) ppm.

^{13}C NMR (CD$_2$Cl$_2$, 100.63 MHz): δ = 18.3, 21.2, 21.1, 25.9, 26.2, 28.6, 28.7, 29.2, 29.3, 29.4, 29.5, 52.5, 64.6, 122.8, 124.0, 124.3, 124.6, 124.7, 125.1, 125.9, 127.6, 128.5, 128.6, 128.7, 137.9, 147.4, 149.7, 150.3, 150.4, 150.6, 150.8, 150.9, 151.1, 156.3, 156.7, 156.7, 156.9 ppm.

MALDI-TOF MS (dithranol): m/z = 695.12 (43%, [M−2PF$_6$−pyridyl-triazole+matrix]$^+$), 854.27 (32%, [M−2PF$_6$+H]$^+$), 999.24 (100%, [M−PF$_6$]$^+$).

UV/vis (CH$_2$Cl$_2$,): $\lambda_{max}(\varepsilon)$ = 451 (12,500), 418 (10,200), 380sh (7500), 286 (70,600), 261sh (32,400), 249 (28,700 M^{-1} cm^{-1}) nm.

Anal. calcd. for C$_{46}$H$_{56}$F$_{12}$N$_8$O$_2$P$_2$Ru: C 48.30, H 4.93, N 9.80; found: C 47.92, H 5.23, N 9.63.

2.5. RAFT copolymerization

Bis(4,4'-dimethyl-2,2'-bipyridine)-{11-(4-(pyridin-2-yl)-1H-1,2,3-triazol-1-yl)undecyl methacrylate} ruthenium(II) hexafluorophosphate (2, 200 mg, 0.117 mmol), methyl methacrylate (154 mg, 1.54 mmol), (4-cyanopentanoic acid)-4-dithiobenzoate (RAFT-agent, 4.6 mg, 0.017 mmol, 1 mol%) and AIBN (0.7 mg, 4.26 μmol, 0.25 mol%) were dissolved in *N,N*-dimethyl acetamide (DMA, 0.85 mL) in a 2 mL microwave vial. The red solution was degassed for 1 h under argon. Subsequently, the reaction mixture was stirred at 80 °C for 9 h. The crude product was precipitated in cold *n*-hexane and purified by preparative size exclusion chromatography (BioBeads S-X1, CH$_2$Cl$_2$ as eluent) yielding the desired copolymer **3** as a red powder (271 mg, yield: 40% with respect to MMA).

^{1}H NMR (CD$_2$Cl$_2$, 400 MHz): δ = 0.82 (br, PMMA backbone), 1.00 (br, PMMA backbone), 1.24 (br, PMMA backbone and alkyl-*H*), 1.80 (br, PMMA backbone and alkyl-*H*), 2.58 (br, dmbpy-C*H*$_3$), 3.59 (br, PMMA backbone), 3.93 (br, 2H, alkyl-*H*), 4.39 (br, 2H, alkyl-*H*), 7.15 (m$_c$, Ru-complex), 7.25–7.40 (br, Ru-complex and RAFT-agent), 7.52 (m$_c$, Ru-complex), 7.56–7.61 (m$_c$, Ru-complex and RAFT-agent), 7.93 (br, Ru-complex and RAFT-agent), 8.18–8.26 (br, Ru-complex), 8.7 (br, 1H, triazole-*H*) ppm.

UV/vis (CH$_2$Cl$_2$): $\lambda_{max}(\varepsilon)$ = 450 (12,000), 418 (10,000), 381 (7100), 286 (71,000), 260 (31,500 M^{-1} cm^{-1}) nm.

GPC (5 mM NH$_4$PF$_6$ in DMF, PMMA calibration): M_n = 4000 g/mol, M_w = 4500 g/mol, PDI = 1.13.

3. Results and discussion

The synthesis of the N^1-alcohol-substituted ligand **1** has been performed under microwave-assisted click conditions, starting from 2-ethynylpyridine and the corresponding aliphatic azide compounds, which utilize copper(II) sulfate in the presence of sodium ascorbate as the catalytic system (Scheme 2) [12]. The azide compound has been prepared from the respective alkyl bromide in a microwave-assisted nucleophilic substitution reaction by using an excess of NaN$_3$. The organic azide has been used without any purification or isolation. The final product was isolated in good yield (72%). Subsequently, the bidentate 1H-1,2,3-triazole ligand **1** was coordinated to the ruthenium(II) precursor [Ru(dmbpy)$_2$]Cl$_2$ by using microwave-assisted reaction conditions yielding the heteroleptic complex **2** in very good yields (90%) (Scheme 2) [12]. The purity of **1** and **2** has been confirmed by NMR spectroscopy, mass spectrometry, and elemental analysis.

A controlled RAFT radical polymerization was performed in order to covalently incorporate the heteroleptic ruthenium(II) complex **2** into a (PMMA) polymer backbone in form of a grafted copolymer avoiding phase separation phenomenon of the materials. In order to synthesize a suit-
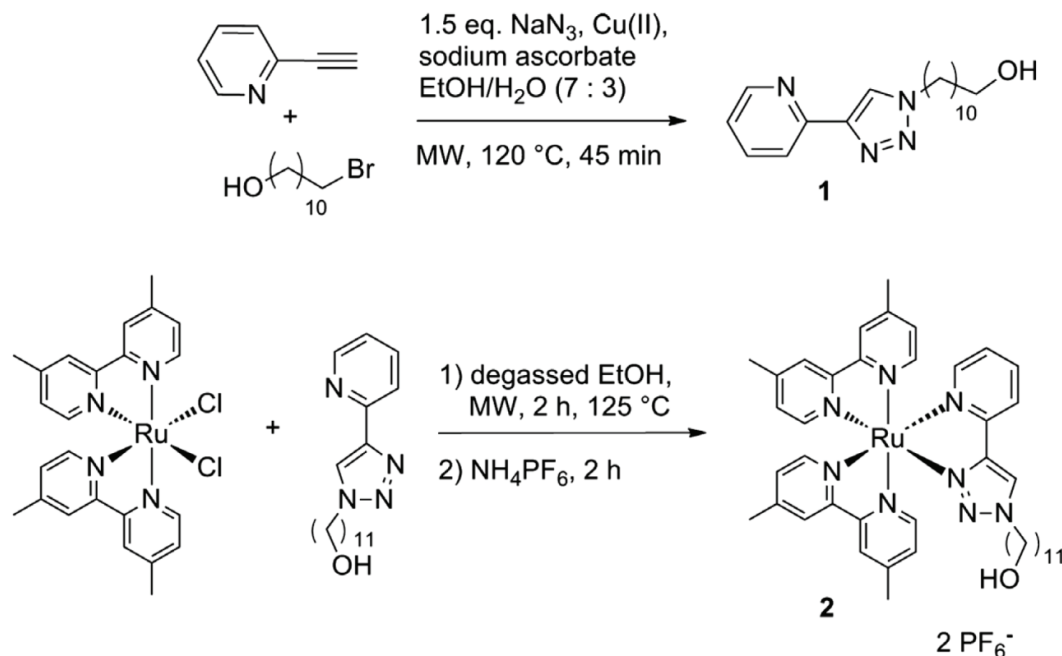
Scheme 2. Schematic representation of the monomer synthesis.

able monomer for the copolymerization with methyl methacrylate (MMA) the OH-functionalized complex **2** was reacted with an excess of methacryloyl chloride in anhydrous dichloromethane in the presence of triethylamine as base (Scheme 3) [11b]. The methacrylate-modified ruthenium(II) complex **3** was isolated in good yield (76%) after purification by washing the reaction mixture with a saturated potassium hydrogen carbonate solution and subsequent column chromatography on aluminum oxide (acetonitrile/toluene 5:1). The purity of the monomer complex **3** was confirmed by ^{1}H NMR spectroscopy (Fig. 4), UV/vis absorption spectroscopy, MALDI-TOF mass spectrometry as well as elemental analysis.

As expected, the ruthenium(II) complex **3** revealed nearly the same UV/vis absorption behavior as complex **2** (Fig. 1). Previously, we examined the optical properties of ruthenium(II) complexes by UV/vis absorption spectroscopy with respect to the number of (1,2,3-1H-triazol-5-yl)-pyridine (pytrz) ligands in the complex on the one hand and the influence of various aromatic and aliphatic substituents on the triazole unit on the other hand. Here, a strong dependence of the number of these pytrz-ligands on the MLCT absorption band could be observed. Increasing the number of the latter the MLCT band of the ruthenium(II) complex shifts to higher energy. This observation was confirmed by cyclic voltammetry, which revealed an increasing HOMO–LUMO energy band gap
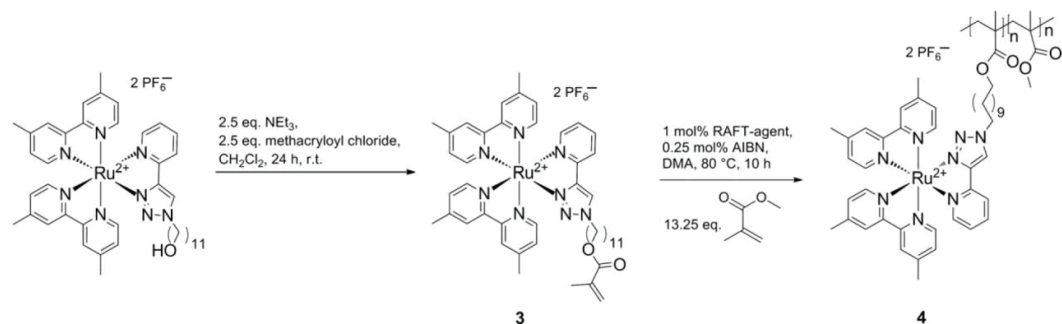
Scheme 3. Schematic representation of the synthesis of the Ru(II) complex containing monomer **3** and the grafted copolymer **4** via RAFT polymerization.
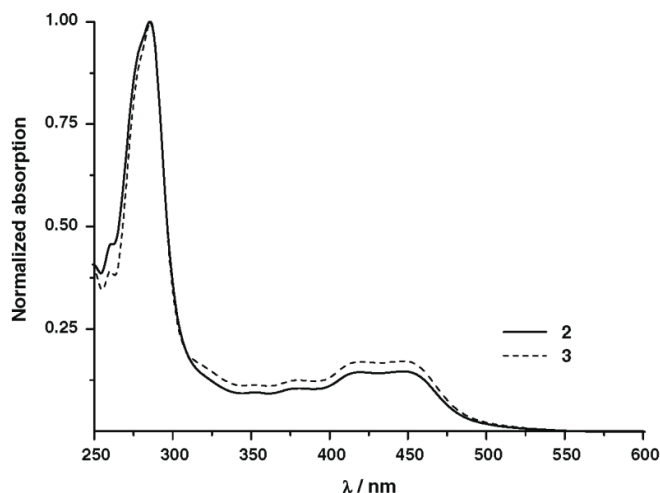
Fig. 1. UV/vis absorption spectra of the ruthenium(II) complexes **2** and **3**; for both spectra: $\sim 10^{-6}$ M in CH_2Cl_2. The MLCT absorption band shows its maximum at 430 nm.

with increasing number of pytrz-ligands, since the metal-based $d\pi$ HOMO is stabilized and the ligand-based π^* LUMO is destabilized by the triazole-containing ligand. Above all, the energy of the metal to ligand charge transfer absorption band in complexes of the general type $[Ru(dmbpy)_2(\{1,2,3-1H\text{-}triazol-5-yl\}pyridine)](PF_6)_2$, where dmbpy represents 4,4′-dimethyl-2,2′-bipyridine, was found to be independent from the nature of lateral substituents (*i.e.* aromatic and aliphatic groups) on the triazole-moiety, which reveals the dominant role of the dmbpy ligands with respect to the optical properties of the complexes [12].

In general, the RAFT polymerizations were performed in concentrated solutions (*i.e.* ~ 2 M solution of the monomer) to allow the polymerization to proceed in a controlled manner. 4-Cyanopentanoic acid-4-dithiobenzoate was used as RAFT agent, since it is known to provide a narrow molar mass distribution, in particular for PMMA as described in literature [5b]. A relatively short reaction time (10 h) was chosen in order to prevent undesired recombination of the polymer radicals [5]. Since **3** was found to be insoluble in organic solvents commonly used for RAFT polymerizations (*i.e.* toluene or ethanol), a test homo-polymerization was carried out using MMA as monomer and
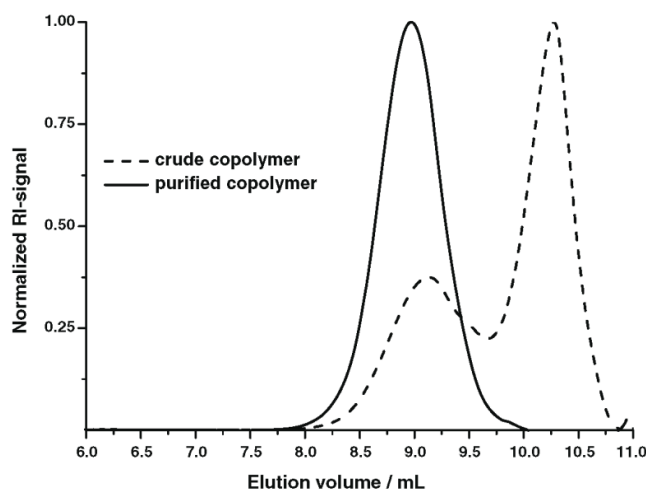
Fig. 2. Left: SEC traces of the crude and purified copolymer **4**; for both chromatograms: 5 mM NH_4PF_6 in DMF as eluent.

N,*N*-dimethyl-acetamide (DMA) as solvent following a literature procedure (MMA/RAFT agent ratio of 100:1) [5]. The obtained poly(methyl methacrylate) was purified by two times precipitation into cold methanol ($-20\,°C$) and characterized by SEC (CHCl$_3$/NEt$_3$/*iso*-PrOH 94:4:2 as eluent) showing a *mono*-modal distribution with a
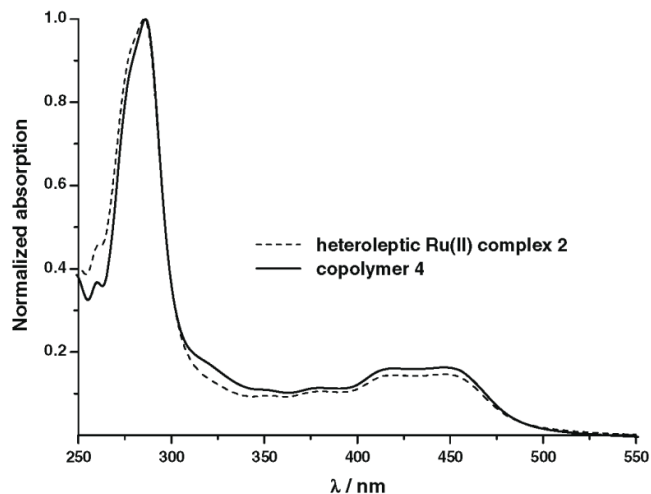
Fig. 3. UV/vis absorption spectra of **2** and **4**; for both spectra: $\sim 10^{-6}$ M in CH$_2$Cl$_2$.
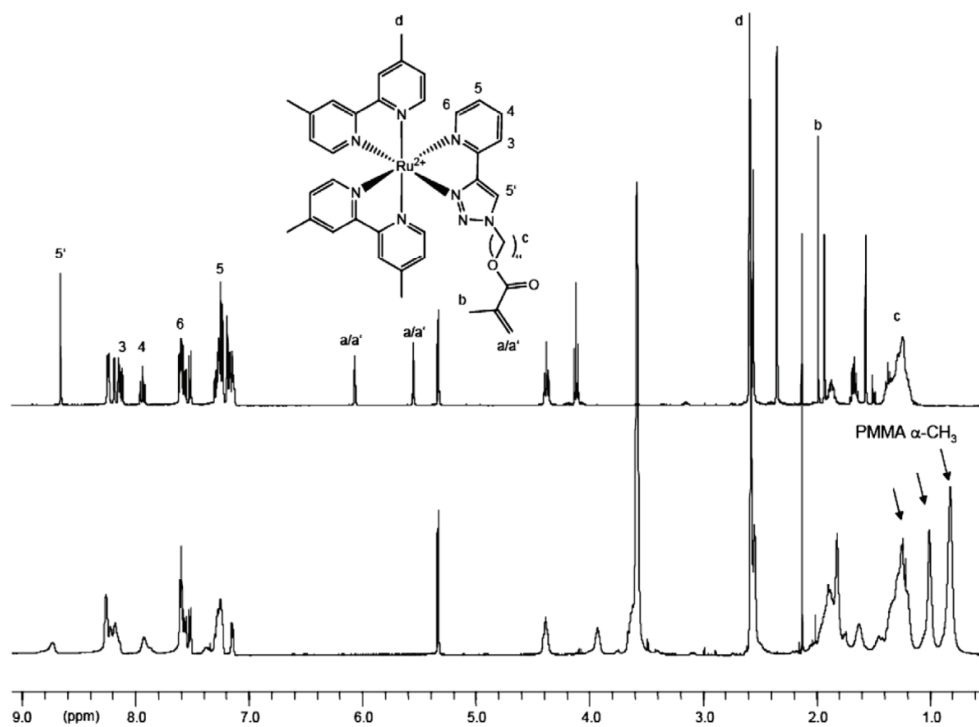
Fig. 4. ^{1}H NMR spectra of the monomer **3** (top) and the grafted copolymer **4** (bottom), for both spectra: 400 MHz, CD$_2$Cl$_2$, 298 K.

retention time of 8.2 min. The molar masses were estimated using a linear PMMA calibration (M_n = 7100 g/mol, M_w = 8400 g/mol) and were slightly lower than the value calculated from the ^{1}H NMR spectrum by comparing the integrals of the aromatic signals corresponding to the RAFT agent to those of the polymer backbone (M_n = 9500 g/mol).

The copolymer 4 was then synthesized employing the same conditions as for the RAFT test-polymerization (MMA: 3 ratio of 13.25:1; ~2 M solution of monomers). After a reaction time of 10 h, the reaction mixture was precipitated into cold methanol (−20 °C) and the crude reddish polymer was purified by preparative size exclusion chromatography (Fig. 2). The characterization by SEC (for the characterization of metal-containing polymers by SEC, see e.g. Ref. [18]) revealed a mono-modal distribution for the finally obtained copolymer 4 (M_n = 4000 g/mol, PDI = 1.13). A ruthenium(II) complex content of 9.8% was estimated from the ^{1}H NMR spectrum corresponding to ten ruthenium(II) complex units per polymer chain, which is consistent with the used monomer ratio (1:13, complex:MMA). As expected, 4 reveals the same photophysical absorption behavior as the small-molecule counterpart 2 (Fig. 3).

The purity of the copolymer 4 was additionally confirmed by ^{1}H NMR spectroscopy (Fig. 4). The disappearance of the H^a- and $H^{a'}$-proton signals of the methacrylate group lead to the conclusion that monomer 3 was incorporated into the copolymer and that no unpolymerized monomer was left.

Moreover, the obtained copolymer 4 was investigated using SEC coupled with a photodiode array detector (PDA) in order to further confirm the incorporation of the ruthenium(II) complex 3 into the polymer backbone (Fig. 5). Fig. 5 shows the 3D-plot of the copolymer 4, which reveals the characteristic metal to ligand charge transfer (MLCT) transition at 430 nm. This correlates exactly with the UV/vis absorption behavior of the ruthenium(II) model complex. Therefore, the successful incorporation of the ruthenium(II) complex 3 into the polymer structure can be concluded.

Furthermore, we investigated the optical properties of thin films and compared the results with the solution measurements. As a result, nearly the same absorption behavior was observed in both cases (Fig. 6). The MLCT at 435 nm of the ruthenium(II) system in solution was observed in the film absorption at 435 nm as well. In addition, neither the film nor the solution of the copolymer exhibited any observable luminescence. Therefore, the further existence of intact, metal complexes in the film can be concluded.
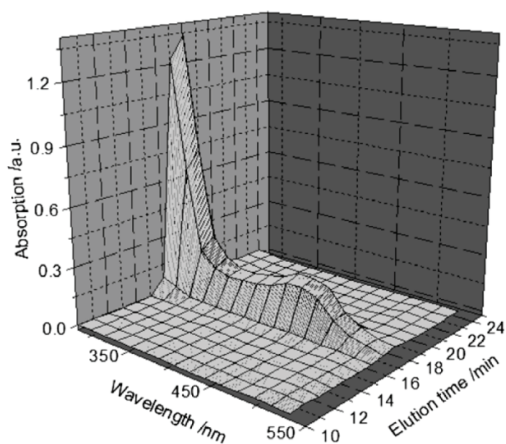
Fig. 5. SEC coupled with a photodiode array detector (DMF containing 5 mM NH$_4$PF$_6$ as eluent) of the copolymer 4 (elution time = 17.6 min).
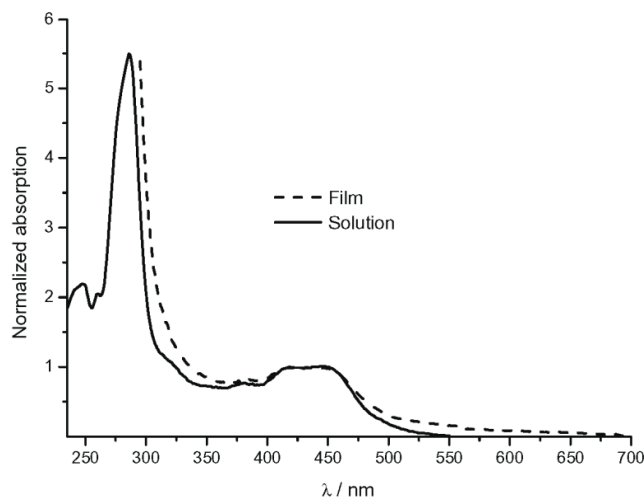
Fig. 6. Comparison of the film and solution UV/vis absorption behavior of the copolymer 4.

3441

4. Conclusion

A hydroxy-functionalized 2-(1*H*-1,2,3-triazole)pyridine ligand was synthesized in a one-pot procedure by using the copper(I)-catalyzed alkyne-azide cycloaddition overcoming the troublesome synthesis of *mono*-functionalized 4,4′-bipyridines at the same time. A ruthenium(II) complex containing 4,4′-dimethyl-2,2′-bipyridine and a hydroxy-functionalized 2-(1*H*-1,2,3-triazole)pyridine system was synthesized in high yield (90%) and converted to the corresponding methacrylate derivative. The latter was successfully incorporated into a PMMA backbone by performing a controlled radical copolymerization (RAFT) [5] with MMA. The obtained grafted copolymer was identified by ^{1}H NMR spectroscopy and size exclusion chromatography (SEC). A ruthenium(II) complex content of 10% was estimated from the ^{1}H NMR spectrum corresponding to an average of ten ruthenium(II) complex units per polymer chain. This is consistent with the used monomer ratio of 1:13 (complex:MMA). As expected, the grafted copolymer reveals the same photophysical absorption behavior as the small-molecule counterpart. Moreover, the successful incorporation of the ruthenium(II) complex into the polymer backbone was further proven by using SEC coupled with a photodiode array detector (PDA).

With this copolymer in hand we were able to spin-coat the copolymer on a glass substrate obtaining a thin film, which revealed the same optical properties as in solution.

Acknowledgement

References

[1] Balzani V, Juris A, Venturi M, Campagna S, Serroni S. Luminescent and redox-active polynuclear transition metal complexes. Chem Rev 1996;96:759–833.

[2] Holder E, Langeveld BMW, Schubert US. New trends in the use of transition metal-ligand complexes for applications in electroluminescent devices. Adv Mater 2005;17:1109–21.

[3] Yang SY, Rubner MF. Micropatterning of polymer thin films with pH-sensitive and cross-linkable hydrogen-bonded polyelectrolyte multilayers. J Am Chem Soc 2002;124:2100–1.

[4] (a) Marin V, Holder E, Hoogenboom R, Schubert US. Functional ruthenium(II)- and iridium(III)-containing polymers for potential electro-optical applications. Chem Soc Rev 2007;36:618–35;
(b) Newkome GR, Patri AK, Holder E, Schubert US. Synthesis of 2,2-bipyridines: versatile building blocks for sexy architectures and functional nanomaterials. Eur J Org Chem 2004:235–54;
(c) Holder E, Marin V, Alexeev A, Schubert US. Greenish-yellow-, yellow-, and orange-light-emitting iridium(III) polypyridyl complexes with poly(ε-caprolactone)-bipyridine macroligands. J Polym Sci A Polym Chem 2005;43:2765–76;
(d) Marin V, Holder E, Schubert US. Polymeric ruthenium bipyridine complexes: new potential materials for polymer solar cells. J Polym Sci A Polym Chem 2004;42:374–85.

[5] (a) Benaglia M, Rizzardo E, Alberti A, Guerra M. Searching for more effective agents and conditions for the RAFT polymerization of MMA: influence of dithioester substituents, solvent and temperature. Macromolecules 2005;38:3129–40;

(b) Rizzardo E, Chen M, Chong B, Moad G, Skidmore M, Thang SH. RAFT polymerization: adding to the picture. Macromol Symp 2007;248:104–16.

[6] Rudmann H, Shimada S, Rubner MF. Solid-state light-emitting devices based on the tris-chelated ruthenium(II) complex, 4. High-efficiency light-emitting devices based on derivatives of the tris(2,2′-bipyridyl) ruthenium(II) complex. J Am Chem Soc 2002;124:4918–21.

[7] (a) Tekin E, Holder E, Marin V, Gans BJ, Schubert US. Ink-jet printing of luminescent ruthenium- and iridium-containing polymers for applications in light-emitting devices. Macromol Rapid Commun 2005;26:293–7;
(b) Marin V, Holder E, Hoogenboom R, Tekin E, Schubert US. Light-emitting iridium(III) and ruthenium(II) polypyridyl complexes containing quadruple hydrogen-bonding moieties. J Chem Soc Dalton Trans 2006:1636–44;
(c) de Gans BJ, Duineveld PC, Schubert US. Inkjet printing of polymers: state of the art and future developments. Adv Mater 2004;16:203–13.

[8] (a) Schubert US, Eschbaumer C. Macromolecules containing bipyridine and terpyridine metal complexes: towards metallosupramolecular polymers. Angew Chem Int Ed 2002;41:2892–926;
(b) Hofmeier H, Schubert US. Recent developments in the supramolecular chemistry of terpyridine–metal complexes. Chem Soc Rev 2004;33:373–99;
(c) Younathan JN, McClanahan SF, Meyer TJ. Synthesis and characterization of soluble polymers containing electron- and energy-transfer reagents. Macromolecules 1989;22:1048–54;
(d) Jones W, Baxter SM, Strouse GF, Meyer TJ. Mimicking the antenna-electron transfer properties of photosynthesis. J Am Chem Soc 1993;115:7363–73.

[9] (a) Chen M, Ghiggino KP, Thang SH, Wilson GJ. Star-shaped light-harvesting polymers incorporating an energy cascade. Angew Chem Int Ed 2005;44:4368–72;
(b) Fustin CA, Guillet P, Schubert US, Gohy JF. Metallo-supramolecular block copolymers. Adv Mater 2007;19:1665–73;
(c) Meier MAR, Wouters D, Ott C, Guillet P, Fustin CA, Gohy JF, Schubert US. Supramolecular ABA triblock copolymers via a polycondensation approach: synthesis, characterization, and micelle formation. Macromolecules 2006;39:1569–76;
(d) Hofmeier H, Schmatloch S, Wouters D, Schubert US. Linear terpyridine–ruthenium(II) poly(ethylene glycol) coordination polymers. Macromol Chem Phys 2003;204:2197–203.

[10] Friesen DA, Kajita T, Danielson E, Meyer TJ. Preparation and photophysical properties of amide-linked, polypyridylruthenium-derivatized polystyrene. Inorg Chem 1998;37:2756–62.

[11] (a) Eisenbach CD, Schubert US. Synthesis and chain extension of bipyridine-terminated polyethers with copper(I) ions. Macromolecules 1993;26:7372–4;
(b) Holder E, Meier MAR, Marin V, Schubert US. New soluble functional polymers by free-radical copolymerization of methacrylates and bipyridine ruthenium complexes. J Polym Sci A Polym Chem 2003;41:3954–64.

[12] Happ B, Friebe C, Winter A, Hager MD, Hoogenboom R, Schubert US. Synthesis of functionalized bipyridine analogs by click-chemistry: tuning the optical properties of ruthenium(II) complexes. Chem Asian J 2009;4:154–63.

[13] Matyjaszewski K. Macromolecular engineering by controlled/living ionic and radical polymerizations. Macromol Symp 2001;174:51–67.

[14] Chiefari J, Chong YK, Ercole F, Krstina J, Jeffery J, Le TPT, et al. Living free-radical polymerization by reversible addition–fragmentation chain transfer: the RAFT process. Macromolecules 1998;31:5559–62.

[15] Moad G, Rizzardo E, Thang SH. Living radical polymerization by the raft process. Aust J Chem 2005;58:379–410.

[16] Moad G, Rizzardo E, Thang SH. Living radical polymerization by the RAFT process: a first update. Aust J Chem 2006;59:669–92.

[17] (a) Hoogenboom R, Schubert US, Camp WV, Du Prez FE. RAFT polymerization of 1-ethoxyethyl acrylate: a novel route toward near-monodisperse poly(acrylic acid) and derived block copolymer structures. Macromolecules 2005;38:7653–9;
(b) Fijten MWM, Paulus RM, Schubert US. Systematic parallel investigation of RAFT polymerizations for eight different (meth)acrylates: a basis for the designed synthesis of block and random copolymers. J Polym Sci A Polym Chem 2005;43: 3831–9.

[18] Meier MAR, Lohmeijer BGG, Schubert US. Characterization of defined metal-containing supramolecular block copolymers. Macromol Rapid Commun 2003;24:852–7.

Publication A6

SELF-ASSEMBLY OF 3,6-BIS(4-TRIAZOLYL)PYRIDAZINE LIGANDS WITH COPPER(I) AND SILVER(I) IONS: TIME-DEPENDANT 2D-NOESY AND ULTRACENTRIFUGE MEASUREMENTS

Bobby Happ, Georges M. Pavlov, Esra Altuntas, Christian Friebe, Martin D. Hager, Andreas Winter, Helmar Görls, Wolfgang Günther, Ulrich S. Schubert*

Self-Assembly of 3,6-Bis(4-triazolyl)pyridazine Ligands with Copper(I) and Silver(I) Ions: Time-Dependant 2D-NOESY and Ultracentrifuge Measurements

Bobby Happ,[a] Georges M. Pavlov,[a] Esra Altuntas,[a] Christian Friebe,[a] Martin D. Hager,[a] Andreas Winter,[a] Helmar Görls,[b] Wolfgang Günther,[a] and Ulrich S. Schubert*[a]

Abstract: Two 3,6-bis(R-1H-1,2,3-triazol-4-yl)pyridazines (R=mesityl, monodisperse $(CH_2-CH_2O)_{12}CH_3$) were synthesized by the copper(I)-catalyzed azide–alkyne cycloaddition and self-assembled with tetrakis(acetonitrile)copper(I) hexafluorophosphate and silver(I) hexafluoroantimonate in dichloromethane. The obtained copper(I) complexes were characterized in detail by time-dependent 1D [^{1}H, ^{13}C] and 2D [^{1}H-NOESY] NMR spectroscopy, elemental analysis, high-resolution ESI-TOF mass spectrometry, and analytical ultracentrifugation. The latter characterization methods, as well as the comparison to analog 3,6-di(2-pyridyl)pyridazine (dppn) systems and their corresponding copper(I) and silver(I) complexes indicated that the

Keywords: analytical ultracentrifugation · heterocycles · NMR spectroscopy · self-assembly · supramolecular chemistry

herein described 3,6-bis(1H-1,2,3-triazol-4-yl)pyridazine ligands form [2×2] supramolecular grids. However, in the case of the 3,6-bis(1-mesityl-1H-1,2,3-triazol-4-yl)pyridazine ligand, the resultant red-colored copper(I) complex turned out to be metastable in an acetone solution. This behavior in solution was studied by NMR spectroscopy, and it led to the conclusion that the copper(I) complex transforms irreversibly into at least one different metal complex species.

Introduction

A renewed interest in pyridazine chemistry has arisen, due to the wide range of interesting features, in particular, being useful for polynuclear coordination assemblies with structures including grids,[1–4] metallocryptand cages,[5] and helices.[6] In this respect, 3,6-di(2-pyridyl)pyridazine (dppn) and its derivatives are a well-known and well-studied class of compounds.[7] The nitrogen atoms present manifold coordination sites and their attachment to a variety of metal centers including Cu^I and Ag^I ions triggered investigations of the resulting photophysical, magnetic, and electrochemical properties.[8] The sterical hindrance of substituents on the pyridazine ring can force the adjacent aromatic rings to rotate away from the pyridazine ring plane and, consequently, ruling the overall coordination environment.[9] However, synthesis-wise there are limitations for the dppn systems, as they can only be synthesized indirectly by an inverse electron-demand Diels–Alder reaction between 1,2,4,5-tetrazines and acetylenes, whereby the 1,2,4,5-tetrazine acts as the electron-deficient diene (Scheme 1).[10]

Over the years, several groups have shown that the 1H-1,2,3-triazole ring has the potential to replace pyridine as a nitrogen-donor ligand for transition-metal ion complexation.[11] As a consequence, our interest was to synthesize dppn-analogous structures by replacing the pyridine rings with 1,2,3-triazole rings, whilst maintaining the ditopic building block. The direct synthesis of the 3,6-bis(1H-1,2,3-triazol-4-yl)pyridazine system (dtpn) was accomplished by starting with the ethynylation of 3,6-dibromopyridazine followed by the copper(I)-catalyzed azide–alkyne cycloaddition

[a] B. Happ, Dr. G. M. Pavlov, E. Altuntas, C. Friebe, Dr. M. D. Hager, Dr. A. Winter, Dr. W. Günther, Prof. Dr. U. S. Schubert
Laboratory of Organic and Macromolecular Chemistry (IOMC)
Friedrich-Schiller-University Jena
Humboldtstr. 10, 07743 Jena (Germany)
Fax: (+49)3641-9482-02
E-mail: ulrich.schubert@uni-jena.de

[b] Dr. H. Görls
Laboratory of Inorganic and Analytical Chemistry
Friedrich-Schiller-University Jena
Lessingstraße 8, 07743 Jena (Germany)

Supporting information for this article is available on the WWW under http://dx.doi.org/10.1002/asia.201000737.

FULL PAPERS
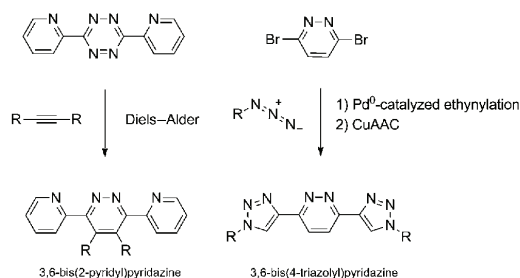
Scheme 1. Schematic representation of the structural analogy and the general synthesis of 2-pyridyl and 4-triazolyl pyridazines, respectively.

(CuAAC; Scheme 1). By utilizing the CuAAC as the final step, the moiety at position one of the triazole ring could be controlled. In this present study, the synthesis and characterization of dtpn systems bearing an aromatic or a polymeric moiety are described. These organic ligands have the capability to complex transition-metal ions, such as copper(I) and silver(I) (Scheme 2). In order to verify the metal complex, geometry spectroscopic tools such as 1D and 2D NMR
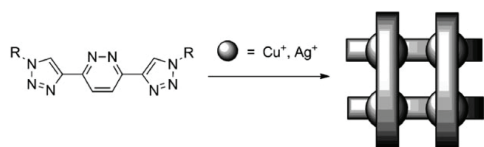
Scheme 2. Schematic representation of the self-assembly of 3,6-bis(1H-1,2,3-triazol-4-yl)pyridazines using copper(I) and silver(I) ions.

Abstract in German: Die Kupfer(I)-katalysierte Azid–Alkin Cycloaddition ermöglichte die Synthese der organischen Liganden 3,6-Bis(R-1H-1,2,3-triazol-4-yl)pyridazin (R = Mesityl, monodisperses methoxy-PEG12), die als Strukturanaloga zu 3,6-Bis(2-pyridyl)pyridazinen gesehen werden können. Diese ditopen Liganden wurden mit Tetrakis(acetonitril)-kupfer(I)hexafluorophosphat und Silber(I)hexafluoroantimonat in Dichlormethan umgesetzt. Der erhaltene Kupfer(I)-Komplex wurde mittels zeitabhängiger ¹H NMR Spektroskopie, Elementaranalyse, hochauflösender Massenspektrometrie sowie analytischer Ultrazentrifugation detailliert charakterisiert. Auf Grund der Ergebnisse letzterer Methoden, sowie des Vergleichs zu literaturbekannten 3,6-Bis(2-pyridyl)pyridazin Systemen kann angenommen werden, dass diese Liganden ebenfalls [2×2]-Metallgitter bilden. Weiterhin konnte mittels ¹H NMR Spektroskopie nachgewiesen werden, dass es sich im Falle des Kupfer(I)-Komplexes des Liganden 3,6-Bis(1-mesityl-1H-1,2,3-triazol-4-yl)pyridazin in Aceton um ein metastabiles System handelt, welches sich in Lösung irreversibel in mindestens eine weitere Spezies umwandelt.

spectroscopy, elemental analysis, high-resolution ESI-TOF mass spectrometry as well as analytical ultracentrifugation have been used.

Results and Discussion

Synthesis and Characterization

Substituted 3,6-Bis(4-triazolyl)pyridazines: The synthesis of the N-heterocyclic ligands 2 and 4 is outlined in Scheme 3. The palladium(0)-catalyzed Sonogashira cross-coupling of 3,6-dibromopyridazine, which was synthesized according to the literature procedure using maleic hydrazide,[12] and the subsequent deprotection of the trimethylsilyl-group (TMS) with potassium fluoride provided the desired intermediate 1 in moderate yield. The following CuAAC reaction of 1 with mesitylazide, utilizing copper(II) sulphate and sodium ascorbate as a copper(I) source, yielded the desired product 2 in a one-pot reaction.[13] However, cleavage of the TMS-group of intermediate 3 was inefficient due to the instability of compound 1 under ambient conditions. Consequently, the dtpn system 4 was synthesized by in situ deprotection of the TMS-groups of 3 and subsequent CuAAC reaction with the monodisperse methoxy poly(ethylene oxide) azide to yield the final product 4 bearing an oligomeric moiety. It is noteworthy that, during the CuAAC reactions, a considerable amount of the copper(I) ions was complexed by the dtpn ligands formed, and thus the reaction with ethylenediaminetetraacetic acid (EDTA) represented a crucial step of purification.

The final products were purified by column chromatography and, in the case of 4, by preparative size-exclusion chromatography (BioBeads SX-3) had to be applied additionally to remove the remaining impurities. The purity of the compounds was confirmed by elemental analysis, high-resolution mass spectrometry (HR-ESI MS) as well as ¹H and ¹³C NMR spectroscopy. Single crystals suitable for X-ray crystallographic analysis were obtained for ligand 2 by slow evaporation of chloroform from a chloroform/methanol solution. The ORTEP plot of the molecular structure and the packing diagram of the unit cell are shown in Figure 1. The two molecules exhibit relatively high torsion angles between the mesityl and the triazole ring of 60.0° and 65.7°, respectively. Hydrogen bonds between the nitrogen atoms of the pyridazine ring and the hydrogen atoms of the opposed pyridazine ring as well as the hydrogen bonds of the opposed triazole rings imply that two molecules of 2 interact at the same time. In the packing diagram, a π–π interaction of the mesityl units can be observed.

Complexation Investigations of 3,6-Bis(4-triazolyl)pyridazines with Copper(I) and Silver(I)

The ligands 2 and 4 were investigated with respect to their capability for supramolecular entropy-driven self-assembly into grid-like structures using copper(I) and silver(I) ions (Scheme 1). The ditopic ligand 2 was chosen as a model
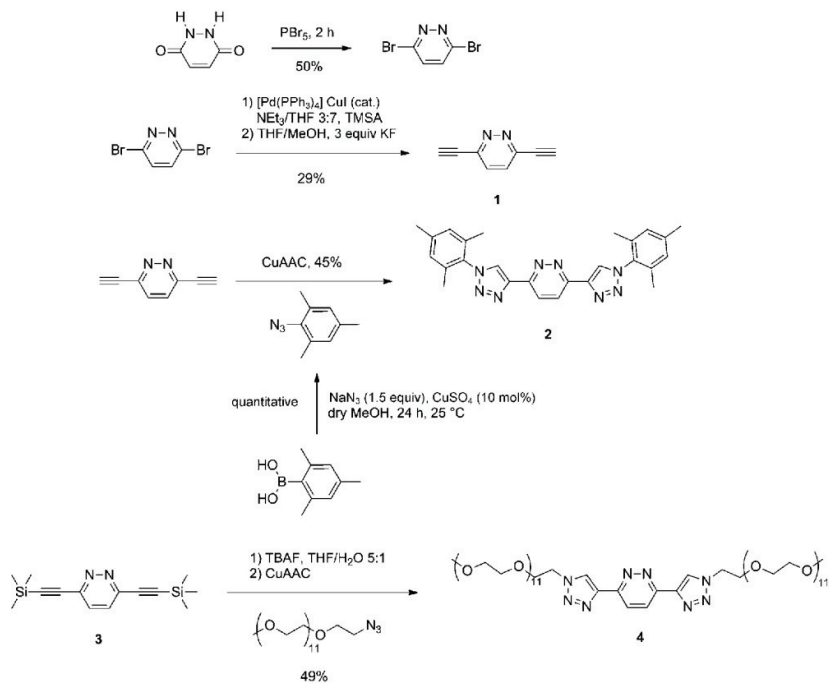
Scheme 3. Schematic representation of the synthesis of 3,6-bis(4-triazolyl)pyridazine ligands **2** and **4**.

Figure 1. Top: ORTEP plot (50% probability level) of **2**. Bottom: Space-fill packing diagram of **2** illustrating the π–π interaction of the mesityl moieties. Hydrogen atoms are omitted for clarity.

system in order to gain knowledge of the coordination behavior. The self-assembly experiment with copper(I) ions was performed by adding a solution of **2** (1 equiv) in dichloromethane to a solution of tetrakis(acetonitrile)cop-

5, M = Cu, X = PF_6
6, M = Ag, X = SbF_6

Scheme 4. Schematic representation of the synthesis of the metal complexes.

per(I) hexafluorophosphate. An instantaneous formation of the copper grid **5** was observed as a red precipitate (Scheme 4). The silver(I) complex **6** was prepared in a similar way, whereby ligand **2** (1 equiv) in dichloromethane was added to a solution of silver(I) hexafluoroantimonate (1 equiv) in dichloromethane. After 1 hour of stirring, the resulting product was obtained by precipitation with diethyl ether as a white solid. Compound **5** was only soluble in warm acetone and methanol, whereas the silver(I) species **6**

FULL PAPERS

was soluble in dichloromethane. Previously reported analogous [2×2]-grids of copper(I) and silver(I) showed similar solubility behavior.[8b,14] ^{1}H NMR spectroscopy revealed three aromatic signals for the obtained grids **5** and **6** (Scheme 4). This expresses the high symmetry of the complexes and, consequently, indicates the formation of defined grid-like architectures rather than polymeric species. In particular, the proton signals of the pyridazine ring and the triazole ring of **5** were significantly shifted downfield upon complexation compared to the free ligand (Figure 2), which confirmed the successful complexation.
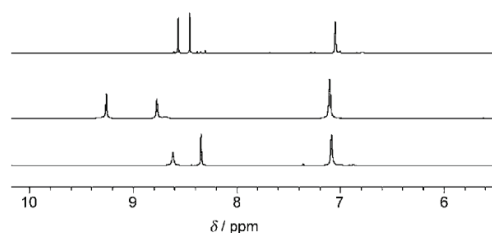
Figure 2. ^{1}H NMR spectra of ligand **2** (top, [D6]acetone), the corresponding copper(I) complex **5** (middle, [D6]acetone), and silver(I) complex **6** (bottom, [D6]acetone).

UV/vis spectra in methanol were recorded for **5** and are depicted in Figure 3. The appearance of the absorption maximum at 380 nm upon complexation with copper(I) ions in
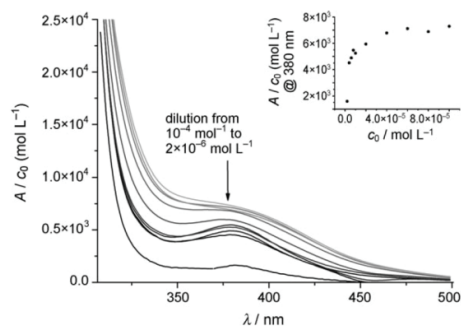
Figure 3. UV/vis absorption spectra of **5** in methanol at different concentrations.

contrast to the free ligand was observed. This fact has also been described in the literature for the formation of analogous copper(I) grids.[1a,7a] Diluting the UV/vis solution by two orders of magnitude, resulted in a successive decrease in the molar extinction coefficient at 380 nm (see inset Figure 3). This was attributed to the metastable nature of **5**,

which was investigated in more detail. In the case of silver(I) complex **6**, a similar absorption behavior to that of **2** was observed (spectrum not shown).

Furthermore, the copper(I) complex **7** of ligand **4** was prepared by adding a solution of **4** (1 equiv) in dichloromethane to a solution of [Cu(CH$_3$CN)$_4$]PF$_6$ (Scheme 5). The
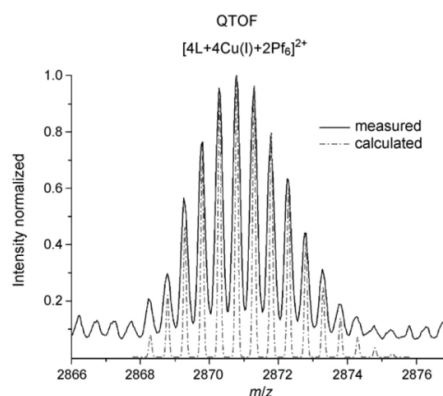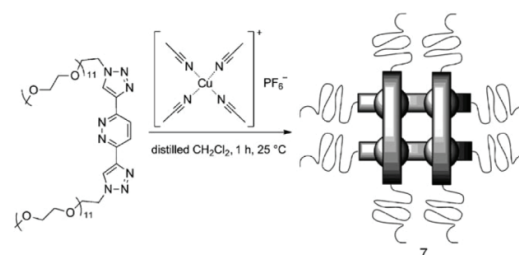
Scheme 5. Top: Schematic representation of the synthesis of a [2×2] copper(I) grid-like structure bearing eight polymer side chains. Bottom: ESI-Q-TOF-MS spectrum of **7** superimposed with the calculated spectrum indicating the existence of [2×2] grid-like species.

pure, oily product was obtained after purification by using preparative size-exclusion chromatography. The ESI-Q-TOF-MS spectrum of **7** revealed the existence of the complete [2×2] copper(I) grids as shown in Scheme 5. Peaks corresponding to fragments with four copper centers such as [Cu$_4$L$_4$X$_2$]$^{2+}$ and [Cu$_4$L$_4$X]$^{3+}$ (X=PF$_6^-$) were observed. The isotopic pattern is accurately consistent with the simulated one. HR-ESI MS of **7** further confirmed the stoichiometry of the fragments. Moreover, in contrast to **5**, the long-term durability of the absorption maximum of 376 nm as well as the aromatic ^{1}H NMR signals demonstrate the structural stability of **7**.

In the case of **5** and **6**, the ESI-Q-TOF-MS spectra did not reveal signals of the entire grid. Only fragments corresponding to the successive loss of one bar of the [2×2]-grid structure were observed, namely, [Cu$_2$L$_3$X]$^+$ (X=PF$_6^-$) and

$[Ag^2L_3X]^+$ ($X = SbF_6^-$) as well as $[Cu_2L_2X]^+$ ($X = PF_6^-$), and $[Ag^2L_2X]^+$ ($X = SbF_6^-$), respectively.

Sedimentation Velocity Experiments

In order to retrieve further confirmation for the integrity of the supramolecular structure of the metal complexes **5** and **6**, analytical ultracentrifugation experiments were carried out in solution.[2c] Figure 4 represents the comparison of dif-
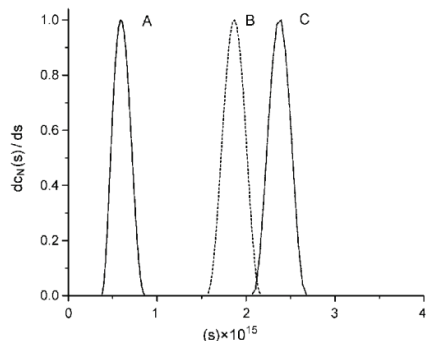
Figure 4. Normalized differential distributions dc(s)/ds of sedimentation coefficients obtained with a regularization procedure and a confidence level of 0.90 for the initial ligand **2** (A), copper(I) complex **5** (B), and silver(I) complex **6** (C).

ferential distribution of the initial ligand **2** and the supramolecular systems versus the intrinsic sedimentation coefficient ($(s) \equiv s_0\eta_0/(1-\upsilon\rho_0)$). Sedimentation velocity experiments of **5** and **6** in acetone clearly showed single species in solution (Figure 4) and illustrate that the assembly of the initial ligands with metal ions occurred. The distributions were normalized on the values of the maximal peak ordinates. By estimation, the obtained values were close to the theoretical ones of the $[2 \times 2]$ Cu^I and $[2 \times 2]$ Ag^I grid-like structure.

Detailed Characterizations of the Copper(I) Complexes

NMR Spectroscopic Investigations of Copper(I) Complex 5: In order to gain more insight into its behavior in solution, copper(I) complex **5** was characterized further by time-dependant 1D (^1H) and 2D (^1H-NOESY) NMR spectroscopy. The ^1H-NOESY spectrum of **5** in deuterated acetone, which was recorded after one day of standing in the NMR glass tube, is depicted in Figure 5. A correlation between the pyrimidine ring proton C and the triazole ring proton B indicates the successful complexation with copper(I) ions. A second correlation arises between proton B and the broad signal next to it at 8.72 ppm. The latter correlation suggests the presence of at least one more copper(I) complex species.

Figure 6 displays seven ^1H NMR spectra of **5**, which have been recorded within a time frame of two and a half weeks.
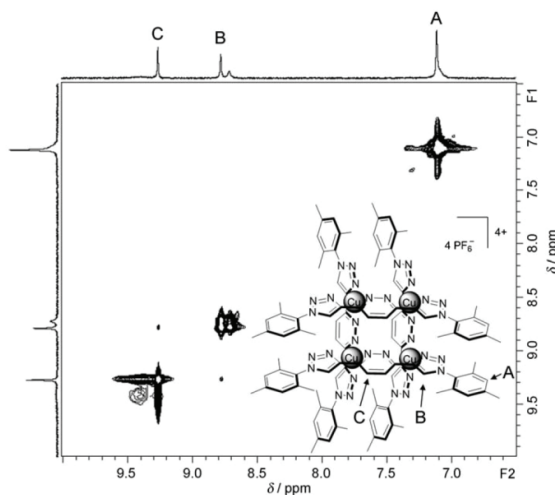
Figure 5. ^1H-NOESY spectrum (400 MHz, 25°C, [D$_6$]acetone) of copper(I) complex **5** after one day.
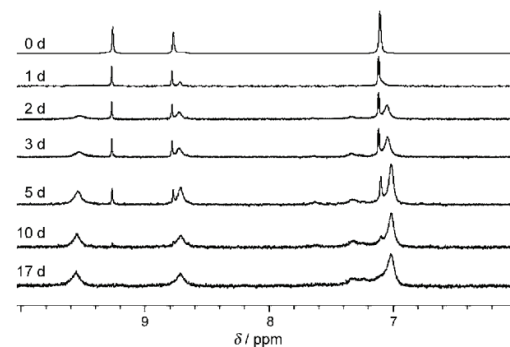
Figure 6. ^1H NMR spectra (250 MHz, [D$_6$]acetone) of copper(I) complex **5** followed over time.

After 17 days, the three primary signals had completely vanished and three broadened signals were mainly present. The ^1H NMR spectrum did not transform anymore at this stage. This leads to the conclusion that the initial red material is only metastable in acetone solution. The new species is assumed to be a symmetrical copper(I) complex, as the symmetry in the ^1H NMR spectrum is similar to the former spectrum, and the NMR solution is still orange colored after 17 days.

Conclusions

The successful synthesis of 3,6-bis(1H-1,2,3-triazol-4-yl)pyridazine systems was described using the palladium(0)-catalyzed Sonogashira coupling as well as the copper(I)-cata-

FULL PAPERS

lyzed azide–alkyne coupling reaction. These ligands were characterized in detail by 1D (^{1}H, ^{13}C) and 2D (^{1}H–^{1}H COSY, NOESY) NMR spectroscopy, elemental analysis, HR-ESI-MS, and an X-ray crystal structure was obtained for 3,6-bis(1-mesityl-1H-1,2,3-triazol-4-yl)pyridazine (**2**). The ditopic N-heterocyclic ligands were investigated with respect to their complexation capability of singly charged d^{10} metal ions (copper and silver). In this context, ^{1}H NMR spectroscopy and ESI-Q-TOF-MS of copper complex **7** indicated the existence of a stable [2×2] grid-like structure. The copper complex **5** turned out to be metastable in solution as confirmed by time-dependant 1D (^{1}H) and 2D (^{1}H-NOESY) NMR spectroscopy experiments. The latter experiments suggested the presence of at least one more copper(I) complex species.

Experimental Section

General Methods

Unless noted otherwise, all reagents were acquired from commercial sources and used without further purification. Solvents were dried and distilled according to standard procedures and stored under argon. Tetrakis(acetonitrile)copper(I) hexafluorophosphate, silver(I) hexafluoroantimonate, and mesitylboronic acid were purchased from Aldrich. Monodisperse methoxy poly(ethylene glycol) azide, containing 12 repeating units (m-dPEG$_{12}$-N$_3$) was obtained from Celares (Berlin, Germany). 3,6-Dibromopyridazine was synthesized according to a literature procedure.[7] Purification of the reaction products was carried out by column chromatography using 40–63 μm silica gel. Preparative size-exclusion chromatography (SEC) was carried out on Bio-Rad S-X3 beads (size exclusion 2000 g mol^{-1}), swollen in dichloromethane. Analytical thin-layer chromatography (TLC) was performed on silica sheets precoated with silica gel 60 F254 and visualization was accomplished with UV light (254 nm).

Instrumentation

The 1D (^{1}H and ^{13}C) and 2D NMR (^{1}H–^{1}H COSY, NOESY) experiments were recorded in deuterated solvents at 25°C on a Bruker DRX 400 or AC 250 instrument. ESI-Q-TOF-MS measurements were performed with a microTOF (Bruker Daltonics) mass spectrometer equipped with an automatic syringe pump, which is supplied from KD Scientific for sample injection. The mass spectrometer was operating in the positive-ion mode. The standard electrospray ion (ESI) source was used to generate the ions. The ESI-Q-TOF-MS instrument was calibrated in the m/z range 50–3000 by using an internal calibration standard (Tunemix solution), which was supplied from Agilent. Data were processed with Bruker Data Analysis software version 4.0. HRMS calculations have been made by using this software. Elemental analysis was carried out on a CHN-932 Automat Leco instrument. UV/vis absorption spectra were recorded on a Perkin–Elmer Lambda 45 UV/vis spectrophotometer using methanol (spectroscopy grade) in 1 cm cuvettes at 25°C. Electrochemical measurements were performed on a Metrohm Autolab PGSTAT30 potentiostat with a standard three-electrode configuration using a graphite disk working electrode, a platinum-rod auxiliary electrode, and an Ag/AgCl reference electrode; scan rates from 100 to 500 m·Vs^{-1} were applied. The experiments were carried out in degassed acetonitrile (spectroscopy grade) containing *tetra-n*-butylammonium hexafluorophosphate salt (0.1 m; dried previously by heating at 100°C and stored under vacuum). At the end of each measurement, ferrocene was added as an internal standard.

Sedimentation Velocity Instrument

Analytical ultracentrifugation was performed on a ProteomeLabTM XLI (Beckman Coulter) at a rotor speed of 40000 rpm. Double sector cells with 12 mm optical path length using interference and absorbance optics

(400 nm) were used. Scans were measured overnight in intervals of 2 to 5 min. Sedimentation coefficients (s), and frictional ratios (f/f$_{sph}$) were obtained with Sedfit.[15] Thereby, f is the translational friction coefficient of the macromolecules and f$_{sph}$ is the translational friction coefficient of a sphere with the same molar mass.[16] Velocity sedimentation of supramolecular structures was studied in acetone and deuterated acetone containing NH$_4$PF$_6$ (0.8 mol %). The initial pyridazine ligands were studied in dimethylformamide (DMF) and deuterated DMF without salt. The concentrations of the solutions of the supramolecular structures were 1.0–1.5 mg mL^{-1}. The use of deuterated and nondeuterated solvents was necessary to estimate the value of the partial specific volume (υ) of the dissolved molecules from the following relation: $\upsilon = (s_2\eta_2 - s_1\eta_1)/(s_2\eta_2\rho_1 - s_1\eta_1\rho_2)$, where η_1, η_2 are the viscosity and ρ_1, ρ_2 are density of deuterated and nondeuterated solvents, correspondingly. The molar masses may be estimated from the modified Svedberg relationship ($M_{fs} = 9 \cdot \pi \cdot 2^{1/2} N_A \cdot ((s)(f/f_{sph})_0)^{3/2} \cdot \upsilon^{1/2})$.[17]

Crystal Structure Determination

The intensity data for the compounds were collected on a Nonius KappaCCD diffractometer using graphite-monochromated Mo$_{K\alpha}$ radiation. Data were corrected for Lorentz and polarization effects but not for absorption effects.[18,19] The structure was solved by direct methods (SHELXS)[20] and refined by full-matrix least squares techniques against Fo^2 (SHELXL-97).[20] All hydrogen atoms were included at calculated positions with fixed thermal parameters. All non-hydrogen atoms were refined anisotropically.[20] XP (SIEMENS Analytical X-ray Instruments, Inc.) was used for structure representations.

3,6-Bis(ethynyl)pyridazine (1): 3,6-Bis(trimethylsilyl)ethynyl)pyridazine (1.92 g, 7.06 mmol) was dissolved in degassed tetrahydrofuran (THF)/MeOH (1:1, 30 mL) and potassium fluoride (1.2 g, 3 equiv) was added to the stirred solution. After 24 h the suspension was filtered and purified by column chromatography on silica gel (chloroform/ethyl acetate 2:1), thus providing the product as an off-white solid (269 mg, 29 %). The pure product decomposes under ambient conditions. ^{1}H NMR (250 MHz, CDCl$_3$, 25°C): $\delta = 7.57$ (s, 2H), 3.52 ppm (s, 2H). ^{13}C NMR (75 MHz, CDCl$_3$, 25°C): $\delta = 145.4$, 129.1, 83.6, 79.7 ppm. Elemental analysis: calcd (%) for C$_8$H$_4$N$_2$: C 74.99, H 3.15, N 21.86; found: C 74.64, H 3.19, N 21.67.

3,6-Bis(1-mesityl-1H-1,2,3-triazol-4-yl)pyridazine (2): Sodium azide (238 mg, 3.66 mmol) and anhydrous CuSO$_4$ (39 mg, 0.24 mmol) were dissolved in absolute methanol (25 mL) successively. Mesitylboronic acid (400 mg, 2.44 mmol) was added to the brown solution and the reaction mixture was stirred for 24 h at room temperature. The conversion was controlled by TLC on silica gel (chloroform). Sodium ascorbate (241 mg, 1.22 mmol, in 3 mL of water), 3,6-bis(ethynyl)pyridazine (125 mg, 0.98 mmol), and water (5 mL) were added. The reaction was stirred for 48 h at 50°C. After that, an excess of water (30 mL, containing an appropriate amount of EDTA) was added to the reaction mixture and the precipitate was filtered off. The filtrate was cautiously extracted with CHCl$_3$ and the organic extract was combined with the precipitate. The CHCl$_3$ solution was dried over NaSO$_4$, filtered, and the solvent was evaporated. Column chromatography on silica (CH$_2$Cl$_2$/ethyl acetate 3:1) and subsequent recrystallization from ethanol provided the pure product as a white powder (200 mg, 45 %). Slow evaporation from a CHCl$_3$/MeOH mixture provided crystals of the product suitable for crystallographic analysis. ^{1}H NMR (250 MHz, CDCl$_3$, 25°C): $\delta = 8.56$ (s, 2H), 8.45 (s, 2H), 7.04 (s, 4H), 2.38 (s, 6H), 2.05 ppm (s, 12H). ^{13}C NMR (75 MHz, CDCl$_3$, 25°C): $\delta = 152.6$, 145.1, 140.4, 134.9, 133.2, 129.2, 124.6, 124.2, 21.1, 17.4 ppm. Elemental analysis: calcd (%) for C$_{26}$H$_{26}$N$_8$: C 69.31, H 5.82, N 24.87; found: C 69.04, H 5.89, N 24.67.

Crystal data for 2: C$_{26}$H$_{26}$N$_8$, M = 450.55 g mol^{-1}, colorless prism, size 0.06×0.06×0.05 mm^3, orthorhombic, space group Pna2$_1$, $a = 37.4888(9)$, $b = 11.1633(3)$, $c = 11.4326(3)$ Å, $V = 4784.5(2)$ Å^3, $T = -140$°C, $Z = 8$, $\rho_{calcd.} = 1.251$ gcm^{-3}, μ (Mo$_{K\alpha}$) = 0.79 cm^{-1}, F(000) = 1904, 23206 reflections in h(−48/33), k(−13/14), l(−14/13), measured in the range $2.55° \leq \Theta \leq 27.51°$, completeness Θmax = 97.7 %, 5643 independent reflections, $R_{int} = 0.0369$, 5172 reflections with F$_o$ > 4σ(F$_o$), 625 parameters, 1 restraints, R$^1_{obs}$ = 0.0477, wR$^2_{obs}$ = 0.1146, R$^1_{all}$ = 0.0543, wR$^2_{all}$ = 0.1191, GOOF =

1.091, Flack-parameter 0(10), largest difference peak and hole: 0.220/ -0.229 e Å^{-3}.

3,6-Bis(trimethylsilyl)ethynyl)pyridazine (3): Trimethylsilylacetylene (2.85 mL, 20.2 mmol) was added through a syringe to a degassed solution of 3,6-dibromopyridazine (2 g, 8.4 mmol), CuI (32 mg, 0.17 mmol), and Pd(PPh$_3$)$_4$ (200 mg, 0.17 mmol) in THF/NEt$_3$ (7:3, 60 mL), and the solution was stirred for 24 h at 25 °C. The salts formed were filtered off, and the filtrate was evaporated under reduced pressure. The residue was purified by column chromatography on silica gel (chloroform as an eluent), providing the product as an off-white powder (1.92 g, 84%). ^{1}H NMR (250 MHz, CDCl$_3$, 25 °C): $\delta = 7.49$ (s, 2H, CH), 0.29 ppm (s, 18H, CH$_3$). ^{13}C NMR (75 MHz, CDCl$_3$, 25 °C): $\delta = 145.5$, 128.9, 102.3, 100.4, -0.5 ppm. Elemental analysis: calcd (%) for C$_{14}$H$_{20}$N$_2$Si$_2$: C 61.71, H 7.40, N 10.28; found: C 61.59, H 7.66, N 10.07.

3,6-Bis(1-(2,5,8,11,14,17,20,23,26,29,32,35-dodecaoxaheptatriacontan-37-yl)-1H-1,2,3-triazol-4-yl)pyridazine (4): 3,6-Bis(trimethylsilyl)ethynyl)pyridazine (50 mg, 0.2 mmol) was dissolved in a deaerated THF/water mixture (5:1, 15 mL) and treated with a 3-fold excess of tris[(1-benzyl-1H-1,2,3-triazol-4-yl)methyl]amine (TBTA; 200 mg, 0.6 mmol) under an argon atmosphere. After 30 min the m-dPEG$_{12}$ azide (250 mg, 0.43 mmol), CuSO$_4$ (70 mg, 0.43 mmol), and sodium ascorbate (90 mg, 0.45 mmol, in 1 mL of water) was added and the suspension was stirred for 72 h at 25 °C under an argon atomsphere. The solvent was evaporated under vacuum and the residue was extracted by using chloroform/water (containing an appropriate amount of EDTA). The organic phase was dried over NaSO$_4$, filtered, and the solvent was evaporated. Column chromatography on silica acetone/methanol (1:1) and subsequent preparative size-exclusion chromatography (BioBeads SX-3, CH$_2$Cl$_2$) provided the pure product as a brown oil (129 mg, 49%). ^{1}H NMR (250 MHz, CD$_2$Cl$_2$, 25 °C): $\delta = 8.56$ (s, 2H), 8.38 (s, 2H), 4.68 (t, ^3J(H,H) = 5.0 Hz, 4H), 3.98 (t, ^3J(H,H) = 5.0 Hz, 4H), 3.61–3.55 (m, 88H), 3.35 ppm (s, 6H, CH$_3$). ^{13}C NMR (75 MHz, CDCl$_3$, 25 °C): $\delta = 71.8$, 70.4, 69.2, 58.5 ppm (aromatic carbon signals are too low in intensity). MS (ESI): m/z (%): 1299.74 (100) [M+H]$^+$, 1321.72 (60) [M+Na]$^+$. HRMS (ESI) calcd for C$_{58}$H$_{107}$N$_8$O$_{24}$ [M+H]$^+$: 1299.7393; found: 1299.7345.

Copper(I) complex of 3,6-bis(1-mesityl-1H-1,2,3-triazol-4-yl)pyridazine (5): 3,6-Bis(1-mesityl-1H-1,2,3-triazol-4-yl)pyridazine (25 mg, 0.055 mmol) in CH$_2$Cl$_2$ (2 mL) was added dropwise to a solution of tetrakis(acetonitrile)copper(I) hexafluorophosphate (21 mg, 0.055 mmol) in CH$_2$Cl$_2$ (2 mL). The immediate red precipitate formed was filtered off after 30 min and washed twice with CH$_2$Cl$_2$, yielding the pure product as a red powder (35 mg, 98%). ^{1}H NMR (250 MHz, [D$_6$]acetone, 25 °C): $\delta = $ 9.26 (s, 8H, H-pyridazine), 8.77 (s, 8H, H-triazol), 7.10 (s, 16H, H-mesityl), 2.35 (s, 24H, CH$_3$), 1.92 ppm (s, 48H, CH$_3$). ^{13}C NMR (75 MHz, [D$_6$]acetone, 25 °C): $\delta = 151.5$, 143.2, 142.3, 135.3, 133.1, 130.3, 130.1, 129.8, 21.1, 17.3 ppm. MS (ESI): m/z (%): 963.38 (70) [2L+Cu]$^+$, 1623.51 (10) [3L+2Cu+PF$_6$]$^+$. Elemental analysis: calcd (%) for C$_{104}$H$_{104}$Cu$_4$F$_{24}$N$_{32}$P$_4$: C 47.38, H 3.98, N 17.00; found: C 47.69, H 3.91, N 17.32.

Silver(I) complex of 3,6-bis(1-mesityl-1H-1,2,3-triazol-4-yl)pyridazine (6): 3,6-Bis(1-mesityl-1H-1,2,3-triazol-4-yl)pyridazine (25 mg, 0.055 mmol) in CH$_2$Cl$_2$ (2 mL) was added dropwise to a solution of silver(I) hexafluoroantimonate (19 mg, 0.055 mmol) in CH$_2$Cl$_2$ (2 mL), and the solution was stirred for 1 h at room temperature. After the addition of diethyl ether (10 mL), the white precipitate was filtered off. The pure product was obtained after recrystallization from dichloromethane/diethyl ether (1:1) as a white powder (32 mg, 73%). ^{1}H NMR (250 MHz, CD$_2$Cl$_2$, 25 °C): $\delta = $ 8.61 (s, 8H, H-pyridazine), 8.34 (s, 8H, H-triazole), 7.08 (s, 16H, H-mesityl), 2.40 (s, 24H, CH$_3$), 1.97 ppm (s, 48H, CH$_3$). ^{13}C NMR (75 MHz, [D$_6$]acetone, 25 °C): $\delta = 150.2$, 142.5, 141.7, 134.7, 132.0, 129.4, 127.7, 127.2, 20.9, 16.9 ppm. MS (ESI): m/z (%):557.13 (100) [2L+2Ag]$^{2+}$, 1005.34 (40) [2L+Ag]$^+$, 1349.13 (5) [2L+2Ag+SbF$_6$]$^+$, 1799.40 (4) [3L+2Ag+SbF$_6$]$^+$. HRMS (ESI) calcd for C$_{78}$H$_{78}$Ag$_2$N$_{24}$SbF$_6$ [M−L−2Ag−3SbF$_6$]$^+$: 1799.3880; found: 1799.3703. Elemental analysis: calcd (%) for C$_{104}$H$_{104}$Ag$_4$F$_{24}$N$_{32}$Sb$_4$: C 39.32, H 3.30, N 14.11; found: C 39.29, H 3.31, N 14.01.

Copper(I) complex of 3,6-bis(1-(2,5,8,11,14,17,20,23,26,29,32,35-dodecaoxaheptatriacontan-37-yl)-1H-1,2,3-triazol-4-yl)pyridazine (7): 3,6-Bis(1-

(2,5,8,11,14,17,20,23,26,29,32,35-dodecaoxaheptatriacontan-37-yl)-1H-1,2,3-triazol-4-yl)pyridazine (69 mg, 0.053 mmol) in CH$_2$Cl$_2$ (2 mL) was added dropwise to a solution of tetrakis(acetonitrile)copper(I) hexafluorophosphate (19 mg, 0.053 mmol) in CH$_2$Cl$_2$ (2 mL) and the solution was stirred for 1 h at room temperature. After the addition of diethyl ether (10 mL), the brown suspension was allowed to stand in the fridge overnight. The diethyl ether was decanted and the pure product was obtained after subsequent preparative size-exclusion chromatography (BioBeads SX-3, CH$_2$Cl$_2$) as a brown oil (58 mg, 73%). ^{1}H NMR (250 MHz, CD$_2$Cl$_2$, 25 °C): $\delta = 8.79$ (s, 8H, H-pyridazine), 8.38 (s, 8H, H-triazol), 4.66 (br, 16H, CH$_2$), 4.01–3.35 (br, 392H, CH$_2$ and CH$_3$) ppm. ^{13}C NMR (75 MHz, CD$_2$Cl$_2$, 25 °C): $\delta = 71.6$, 70.3, 69.0, 58.5 ppm. (aromatic carbon signals are too low in intensity). MS (ESI): m/z (%): 1321.71 (100) [L+Na]$^+$, 1865.83 (10) [4L+4Cu+PF$_6$]$^{3+}$, 2870.25 (10) [4L+4Cu+2PF$_6$]$^{2+}$. HRMS (ESI) calcd for C$_{232}$H$_{424}$N$_{32}$O$_{96}$Cu$_4$PF$_6$ [M−3PF$_6$]$^{3+}$: 1865.5384; found: 1865.5397. HRMS (ESI) calcd for C$_{232}$H$_{424}$N$_{32}$O$_{96}$Cu$_4$P$_2$F$_{12}$ [M−2PF$_6$]$^{2+}$: 2870.7900; found: 2870.7826.

CCDC 787347 (2) contains the supplementary crystallographic data for this paper. These data can be obtained free of charge from The Cambridge Crystallographic Data Centre via www.ccdc.cam.ac.uk/data_request/cif

[1] a) R. Hoogenboom, G. Kickelbick, U. S. Schubert, *Eur. J. Org. Chem.* **2003**, 4887–4896; b) W. Kaim, *Coord. Chem. Rev.* **2002**, *230*, 127–139; c) L. K. Thompson, *Coord. Chem. Rev.* **2002**, *233–234*, 193–206.

[2] a) M. Schmittel, V. Kalsani, D. Fenskeb, A. Wiegrefea, *Chem. Commun.* **2004**, 490–491; b) M. Schmittel, V. Kalsani, J. W. Bats, *Inorg. Chem.* **2005**, *44*, 4115–4117; c) M. Schmittel, V. Kalsani, R. S. K. Kishore, H. Colfen, J. W. Bats, *J. Am. Chem. Soc.* **2005**, *127*, 11544–11545.

[3] S. De, K. Mahata, M. Schmittel, *Chem. Soc. Rev.* **2010**, *39*, 1555–1575.

[4] M. Ruben, J.-M. Lehn, G. Vaughan, *Chem. Commun.* **2003**, 1338–1339.

[5] V. J. Catalano, M. A. Malwitz, S. J. Horner, J. Vasquez, *Inorg. Chem.* **2003**, *42*, 2141–2148.

[6] L. Carlucci, G. Ciani, D. M. Proserpio, A. Sironi, *Inorg. Chem.* **1998**, *37*, 5941–5943.

[7] a) Z. Xu, L. K. Thompson in *Comprehensive Coordination Chemistry II, Vol. 1* (Eds.: J. A. McCleverty, T. J. Meyer), Elsevier, Oxford, **2004**, pp. 63–95; b) P. N. W. Baxter in *Comprehensive Supramolecular Chemistry, Vol. 9* (Eds.: J. L. Atwood, J. E. D. Davies, D. D. Macnicol, F. Vögtle), Pergamon, Oxford, **1996**, pp. 165–211; c) F. Thébault, A. J. Blake, C. Wilson, N. R. Champness, M. Schröder, *New J. Chem.* **2006**, *30*, 1498–1508; d) E. C. Constable, C. E. Housecroft, M. Neuburger, S. Reymann, S. Schaffner, *Eur. J. Org. Chem.* **2008**, 1597–1607.

[8] a) M.-T. Youinou, N. Rahmouni, J. Fischer, J. A. Osborn, *Angew. Chem.* **1992**, *104*, 771–773; *Angew. Chem. Int. Ed. Engl.* **1992**, *31*, 733–735; b) B. L. Schottel, H. T. Chifotides, M. Shatruk, A. Chouai, L. M. Perez, J. Basca, K. R. Dunbar, *J. Am. Chem. Soc.* **2006**, *128*, 5895–5912; c) N.-D. Sung, K.-S. Yun, T.-Y. Kim, K.-Y. Choi, M. Suh, J.-G. Kim, I.-H. Suh, J. Chin, *Inorg. Chem. Commun.* **2001**, *4*, 377–380; d) N. Tsukada, T. Sato, H. Mori, S. Sugawara, C. Kabuto, S. Miyano, Y. Inoue, *J. Organomet. Chem.* **2001**, *627*, 121–126.

[9] E. C. Constable, C. E. Housecroft, M. Neuburger, S. Reymann, S. Schaffner, *Chem. Commun.* **2004**, 1056–1057.

FULL PAPERS

[10] a) W. A. Butte, F. H. Case, *J. Org. Chem.* **1961**, *26*, 4690–4692; b) J. Sauer in *Comprehensive Heterocyclic Chemistry II, Vol. 6*, Pergamon, London, **1996**, pp. 901–965.

[11] a) D. Schweinfurth, K. I. Hardcastle, U. H. F. Bunz, *Chem. Commun.* **2008**, 2203–2205; b) Y. Li, J. C. Huffman, A. H. Flood, *Chem. Commun.* **2007**, 2692–2694; c) R. M. Meudtner, M. Ostermeier, R. Goddard, C. Limberg, S. Hecht, *Chem. Eur. J.* **2007**, *13*, 9834–9840; d) B. Schulze, C. Friebe, M. D. Hager, A. Winter, R. Hoogenboom, H. Goerls, U. S. Schubert, *Dalton Trans.* **2009**, 787–794; e) B. Happ, C. Friebe, A. Winter, M. D. Hager, R. Hoogenboom, U. S. Schubert, *Chem. Asian J.* **2009**, *4*, 154–163; f) B. Beyer, C. Ulbricht, D. Escudero, C. Friebe, A. Winter, L. Gonzalez, U. S. Schubert, *Organometallics* **2009**, *28*, 5478–5488.

[12] Y. S. Park, D. Kim, H. Lee, B. Moon, *Org. Lett.* **2006**, *8*, 4699–4702.

[13] B. Happ, D. Escudero, M. D. Hager, C. Friebe, A. Winter, H. Goerls, E. Altuntas, L. Gonzalez, U. S. Schubert, *J. Org. Chem.* **2010**, *75*, 4025–4038.

[14] B. R. Manzano, F. A. Jalon, I. M. Ortiz, M. L. Soriano, F. G. de La Torre, J. Elguero, M. A. Maestro, K. Mereiter, T. D. W. Claridge, *Inorg. Chem.* **2008**, *47*, 413–428.

[15] P. Schuck, *Biophys. J.* **2000**, *78*, 1606–1619.

[16] C. Tanford, in *Physical Chemistry of Macromolecules*, Wiley, New York, London, **1961**.

[17] G. M. Pavlov, D. Amoros, C. Ott, I. I. Zaitseva, J. G. de La Torre, U. S. Schubert, *Macromolecules* **2009**, *42*, 7447–7455.

[18] COLLECT, Data Collection Software; B. V. Nonius, Netherlands, **1998**.

[19] Z. Otwinowski, W. Minor in *Methods in Enzymology, Macromolecular Crystallography Part A, Vol. 276* (Eds.: C. W. Carter, R. M. Sweet), Academic Press, **1997**, pp. 307–326.

[20] G. M. Sheldrick, *Acta Crystallogr. Sect. A* **2008**, *64*, 112–122.

- 166 -

Publication A7

INDUCED CHARGE EFFECT BY CO^II-COMPLEXATION ON THE CONFORMATION OF A COPOLYMER CONTAINING A BIDENTATE 2-(1,2,3-TRIAZOL-4-YL)PYRIDINE CHELATING UNIT

Bobby Happ, Georges M. Pavlov, Igor Perevyazko, Martin D. Hager, Andreas Winter, Ulrich S. Schubert*

Full Paper

Induced Charge Effect by Co(II) Complexation on the Conformation of a Copolymer Containing a Bidentate 2-(1,2,3-Triazol-4-yl)pyridine Chelating Unit

Bobby Happ, Georges M. Pavlov, Igor Perevyazko, Martin D. Hager, Andreas Winter, Ulrich S. Schubert*

Poly(alkyl methacrylate) copolymers embedding bidentate trzpy chelating units as comonomer in the side chains are synthesized utilizing the controlled radical RAFT polymerization process. The free trzpy units are complexed by iron(II) and cobalt(II) ions, which results in characteristic UV-Vis absorption bands and an increase of solution viscosity. The intramolecular complexation with Co(II) ions is studied by different analytical ultracentrifugation experiments. Following the addition of a small amount of Co(II) ions, a significant decrease of the intrinsic sedimentation coefficient is observed that can be explained by the elongation of the individual polymer coils due to the electrostatic repulsion of the coordinated Co(II) ions.
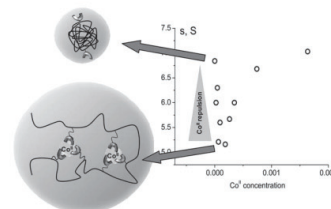
1. Introduction

An interesting approach in today's polymer chemistry is the conjunction of covalent linked polymer species with noncovalent interactions to establish new polymeric systems. For this purpose, supramolecular polymers containing reversible metal–ligand interactions have been widely studied.[1–6] In particular, copolymers containing supramolecular entities as well as crosslinking units have become appealing systems in material science during the past years due to their feasibility to assemble advanced materials with reversible and addressable properties, respectively, such as switchable adhesives and self-healing materials.[7–10] Important representative architectures, which have emerged are among others: linear polymers,[11] block copolymer,[12] star-like systems,[13–15] and micelles.[16–18]

Crosslinked supramolecular polymers based on 2,2′-bipyridine (bpy) were first reported in the 1990s by Lewis and Miller[19] and Chujo et al.[20,21] exhibiting thermal reversibility and membrane utilization. Chujo et al. obtained intermolecular crosslinked metal complexes between 2,2′-bipyridine-branched polyoxazolines and Fe(II) and Co(II) ions, which revealed a thermally reversible behavior. A series of biocompatible, star-shaped polylactides (PLA) and polyesters (PE) as well as various copolymer analogs with either labile Fe(II) or luminescent *tris*-(2,2′-bipyridine)ruthenium(II) cores has been

B. Happ, Dr. G. M. Pavlov, I. Perevyazko, Dr. M. D. Hager, Dr. A. Winter, Prof. Dr. U. S. Schubert
Laboratory of Organic and Macromolecular Chemistry (IOMC), Friedrich-Schiller-University Jena,
Humboldtstr. 10, 07743 Jena, Germany
E-mail: ulrich.schubert@uni-jena.de
B. Happ, Dr. G. M. Pavlov, I. Perevyazko, Dr. M. D. Hager, Dr. A. Winter, Prof. Dr. U. S. Schubert
Jena Center for Soft Matter (JCSM),
Humboldtstr. 10, 07743 Jena, Germany
B. Happ, Dr. M. D. Hager, Dr. A. Winter, Prof. Dr. U. S. Schubert
Dutch Polymer Institute (DPI), P. O. Box 902, 5600 AX Eindhoven, the Netherlands
Dr. G. M. Pavlov
Institute of Macromolecular Compounds,
RAS, Bolshoy pr. 31, St. Petersburg, 199004 Russia

1339

described by Fraser and co-workers.[13,14] These polymers were assembled by a convergent approach that enclosed the attachment of bpy ligands to PLA- and PE-containing arms and subsequent coordination of the macroligands to Fe(II) or Ru(II) ions.

In the recent years, the development of the copper(I)-catalyzed azide–alkyne cycloaddition[22,23] (CuAAC) reaction resulted in an increased interest toward the coordination chemistry of 1,4-functionalized 1H-[1,2,3]triazoles due to their potential as N-donor ligands. In particular, the coordination chemistry of bi- and tridentate ligand systems with common d^6, d^8, and d^{10} metal ions, such as Ru(II), Ir(III), Pd(II), Re(I), Cu(I), and Ag(I), has been investigated and, thus, a large variety of novel metal chelators emerged, while the synthetic effort was reduced at the same time.[24–29] However, there are only a few examples in literature that deal with the incorporation of the latter chelates into polymeric structures.

Consequently, this contribution focuses on the complexation and decomplexation behavior of 2-(1H-1,2,3-triazol-4-yl)pyridine-containing copolymers by Fe(II) and Co(II) ions. The copolymers were synthesized using the controlled reversible addition–fragmentation transfer (RAFT) polymerization technique. Subsequently, the macromolecules were treated with Fe(II) and Co(II) salts and the coordination performance was studied by means of UV-Vis spectroscopy and titration experiments. Viscosity measurements and detailed analytical ultracentrifugation experiments were executed to study the intra- and intermolecular complexation behavior of Co(II) ions in solution. A strong competitive ligand was used to examine the reversibility of the metal complexation in low concentrated solutions by means of UV-Vis spectroscopy.

2. Experimental Section

2.1. General Methods and Materials

All chemicals were purchased from Fluka, Aldrich, Acros Organics as well as Alfa Aesar and were used without further purification unless otherwise specified. The solvents were dried and distilled according to standard procedures. Preparative size-exclusion chromatography (SEC) was performed on BioRad S-X1 (size exclusion limit: 16 000 g mol^{-1}) with dichloromethane as eluent. 11-[4-(Pyridin-2-yl)-1H-1,2,3-triazol-1-yl]undecan-1-ol was synthesized according to a literature procedure.[30] Methyl methacrylate (MMA) and butyl methacrylate (BMA) were treated with an inhibitor remover before usage in order to remove the stabilizer.

The reversibility studies on the copolymers, that is, complexation and decomplexation investigations employing Fe(II) and Co(II) ions, were carried out in a cuvette using 2.5 mL of a 7.6×10^{-5} M dichloromethane solution of the polymer. Decomplexation was accomplished by using a methanolic trisodium N-(2-hydroxyethyl)ethylenediamine triacetate (HEEDTA-Na$_3$) solution.

2.2. Instrumentation

1D (^{1}H, ^{13}C) and 2D NMR spectra were recorded on a Bruker AC 300 instrument (300 MHz) at 298 K. Chemical shifts are reported in parts per million (δ scale) relative to the residual signal of the deuterated solvent. Coupling constants are given in Hz. UV-Vis absorption spectra were recorded on an Analytik Jena SPECORD 250 spectrometer at 298 K relative to a blank of the pure solvent (1 cm path length of the quartz cuvette).

Sedimentation velocity experiments were performed using a Beckman XLI analytical ultracentrifuge (ProteomeLab XLI Protein Characterization System) at a rotor speed of 40 000 rpm and at 20 °C, using interference optics and Al double-sector cells of an optical path of 12 mm. The samples dissolved in acetone were studied in the concentration range of high dilution.

The continuous particle size distribution $c(s)$ of Sedfit[31,32] was used for sedimentation velocity data analysis, where s is the velocity sedimentation coefficient. The Tikhonov-Philips 2nd derivative regularization method was used with a confidence level of 0.7–0.9 (corresponding F-ratio). As a result, the continuous sedimentation coefficient distribution and the weight-average frictional ratio (f/f_{sph}) of all species were obtained for studied solutions.

Viscosity measurements were conducted using an AMVn viscometer (Anton Paar, Graz, Austria) with the capillary/ball combination of the measuring system. The respective times of the fall of the steel ball in a viscous medium of the solvent and polymer solutions, τ_0 and t, were measured at 20 °C, the relative viscosities $\eta_r = t/\tau_0$ being in the range 1.15 to 1.8. The extrapolation to zero concentration was made by using both the Huggins and the Kraemer equations, and the average values were considered as the value of the intrinsic viscosity (Figure S8, Supporting Information).

Density measurements were carried out using a DMA 02 density meter (Anton Paar, Graz, Austria) according to the procedure of Kratky et al. (Figure 4S, Supporting Information).[33] Acetone (HPLC-grade, ≥99.9%; Chromasolv) was obtained from Sigma–Aldrich. It has the following characteristics (at 20 °C): dynamic viscosity $\eta_0 = 0.339 \times 10^{-2}$ mPa s; density $\rho_0 = 0.791$ g cm^{-3}. Deuterated acetone was obtained from Euriso-Top with the following characteristics (at 20 °C): dynamic viscosity $\eta_0 = 0.374 \times 10^{-2}$ mPa s; density $\rho_0 = 0.874$ g cm^{-3}.

Electron spay ionization quadrupole time-of-flight mass spectrometry (ESI-Q-TOF-MS) measurements were performed in the positive ion mode with a microTOF (Bruker Daltonics) mass spectrometer equipped with an automatic syringe pump, which was supplied from KD Scientific for sample injection. The standard electrospray ion (ESI) source was used to generate the ions. The concentration of the samples was 10 μg mL^{-1} and all samples were injected using a constant flow rate (180 μL h^{-1}) of sample solution. The ESI-Q-TOF-MS instrument was calibrated in the m/z range of 50 to 3000 using an internal calibration standard (Tunemix solution, Agilent). Data were processed via Bruker Data Analysis software version 4.0. HR-MS calculations have been made by using this software. Elemental analysis was carried out on a CHN-932 Automat Leco instrument. Size-exclusion chromatograms were recorded on a Waters SEC system equipped with a DG-980-50 degasser, HPLC 1515 pump, Column Heater 1500 oven, photo diode array (PDA) detector 2996, RI

detector 2414, and Waters pre/Phenomenex Phenogel 10^3 Å/10^5 Å column using dimethylacetamide (DMA) with 0.08 mol% NH_4PF_6 as solvent with a flow rate of 1 mL min^{-1} at 50 °C.

2.3. ^{1}H NMR Titration of the trzpy Ligand with Fe(II)

A stock solution of ligand **2** (18.19 mg in 1 mL of CDCl$_3$) was prepared, whereby 0.5 mL of the solution was transferred into the NMR tube. FeCl$_2$ · 4H$_2$O (31.34 mg in 1 mL of CD$_3$OD) was used as standard solution ($c = 0.158$ M) SnCl$_2$ · 4H$_2$O as stabilizer. The deuterated methanolic FeCl$_2$ · 4H$_2$O solution was added to the analyte solution in the NMR tube in steps of 20 µL. After every addition, a ^{1}H NMR spectrum was recorded after a reaction time of 5 min.

2.4. UV Titrations for Determination of the trzpy Ligand Content in the Polymers

A stock solution of polymer **3** (4 mg) and polymer **4** (5.92 mg), respectively, was prepared in a volumetric flask (50 mL) with dichloromethane as solvent, whereby 2.5 mL of the solution was used for the measurement in the quartz cuvette (1 cm path length). FeCl$_2$ × 4H$_2$O was used as standard solution ($c = 5.754 \times 10^{-4}$ M in MeOH), whereby SnCl$_2$ · 4H$_2$O ($I = 0.1$ M) served as oxidation inhibitor for the Fe(II) ions and maintained a constant ionic strength during the titration experiments. The methanolic FeCl$_2$ · 4H$_2$O solution was directly added to the analyte solution in the UV cuvette in steps of 10 µL. After every addition, a UV-Vis spectrum was recorded after 10 min. The absorption value of the maximum of the metal-to-ligand charge-transfer band (MLCT) at 433 nm was used to obtain the titration curve.

2.5. Complexation and Decomplexation Studies of Polymer 2 with HEEDTA by Absorption Spectroscopy

The reversibility investigations employing Fe(II) and Co(II) ions were carried out in a cuvette using 2.5 mL of the dichloromethane stock solution of polymer **3** ($c = 8.0 \times 10^{-5}$ M). After that, 100 µL of the respective methanolic metal salt solution (FeCl$_2$ · 4H$_2$O and CoBF$_4$ · 6H$_2$O, both: 5.8×10^{-4} M) was added to establish the corresponding *tris*-complex, which was confirmed by the appearance of the MLCT band at 433 and 320 nm, respectively. Decomplexation was observed by appending a fivefold excess of a methanolic HEEDTA solution. The disappearance of the MLCT band verified the decomplexation.

2.6. 11-[4-(Pyridin-2-yl)-1*H*-1,2,3-triazol-1-yl]undecyl Methacrylate (2)

11-[4-(Pyridin-2-yl)-1*H*-1,2,3-triazol-1-yl]undecan-1-ol (700 mg, 2.2 mmol) and triethylamine (0.55 mL, 4 mmol) were dissolved in dry dichloromethane (10 mL). The solution was cooled to 0 °C, methacryloyl chloride (350 µL, 3.5 mmol) was added and, subsequently, the solution was stirred for 2 h at 0 °C and further 24 h at room temperature. The reaction mixture was washed with saturated NaHCO$_3$ solution and, after drying of the organic layer over MgSO$_4$, the solvent was removed in vacuo. The crude product

was purified by recrystallization from ethanol providing the pure product as white solid (740 mg, 87%).

^{1}H NMR (300 MHz,CHCl$_3$-d_6, δ): 8.52 (d, $J = 4.8$ Hz, 1H), 8.12 (d, $J = 8$ Hz, 1H), 8.06 (s, 1H), 7.71 (m, 1H), 7.16 (m, 1H), 6.06 (s, 1H, C=CH$_2$), 5.47 (m, 1H, C=CH$_2$), 4.35 (t, $J = 7.2$ Hz, 2H), 4.04 (m, 2H), 1.98 (s, 3H, CH$_3$), 1.87 (m, 2H), 1.62–1.55 (m, 2H), 1.27–1.17 (m, 14H); ^{13}C NMR (75 MHz, CDCl$_3$, δ): 167.5, 150.2, 149.2, 148.1, 136.9, 136.5, 125.2, 122.7, 121.8, 120.2, 64.8, 50.4, 32.7, 30.1, 29.3, 29.28, 29.23, 29.1, 28.8, 26.3, 25.7, 18.3; UV-Vis (CH$_2$Cl$_2$): λ_{max} (ε) = 282 (8100), 244 nm (13500); ESIMS m/z (%): 385.26 (100) [M$^+$ + H]; C$_{22}$H$_{32}$N$_4$O$_2$: Calcd. C 68.72, H 8.39, N 14.57; found: C 69.02, H 8.46, N 14.30.

2.7. General Procedure for RAFT Polymerization

MMA (0.69 mL, 6.5 mmol) and BMA (1.03 mL, 6.5 mmol), respectively, ligand **1** (250 mg, 0.65 mmol), 2-cyanobutan-2-yl benzodithioate (RAFT agent, 10 mg, 0.043 mmol) and 2,2′-azobis(2-methylpropionitrile) (AIBN) (1.8 mg, 0.01 mmol) were charged in the reaction vial (5 mL microwave vial) and dissolved in *N,N*-dimethylacetamide (3 mL). The vial was sealed and the reaction solution was purged with a flow of nitrogen for 30 min. Subsequently, the reaction was performed in an oil bath at 80 °C for 16 h. The crude polymers were incorporated into chloroform and washed three times with brine. The organic phase was dried over Na$_2$SO$_4$. After evaporation of the solvent, the pure polymers were obtained after preparative SEC (Bio-Rad SX-1 beads and CH$_2$Cl$_2$ as eluent).

2.8. Polymer (2-*stat*-MMA) (3)

^{1}H NMR (300 MHz,CHCl$_3$-d_6, δ): 8.57, 8.17, 7.78, 7.23, 4.42, 3.91, 3.58 (b, OCH$_3$^{MMA}), 1.95–1.80, 1.42–1.24, 1.0 (b, CH$_3$^{backbone}), 0.83 (b, CH$_3$^{backbone}); ^{13}C NMR (75 MHz, CDCl$_3$, δ): 178.1, 177.8, 150.3, 149.3, 148.2, 136.9, 128.0, 127.96, 127.93, 127.8, 127.6, 122.8, 121.87, 121.85, 120.2, 54.4, 51.7, 50.5, 44.8, 44.5, 31.9, 30.2, 29.68, 29.64, 29.45, 29.43, 29.3, 28.9, 26.4, 22.6, 18.7, 16.5, 16.4, 14.1; Conversion (^{1}H NMR): 74%; SEC (DMA, PMMA calibration): $\overline{M}_n = 14\ 100$ g mol^{-1}, $\overline{M}_w = 17\ 480$ g mol^{-1}, PDI = 1.24, degree of polymerization (DP) = 112.

2.9. Polymer (2-*stat*-BMA) (4)

^{1}H NMR (300 MHz,CHCl$_3$-d_6, δ): 8.57, 8.17, 7.78, 7.23, 4.42, 3.93 (b), 3.74, 3.39, 1.97–1.75, 1.60 (b), 1.42–1.26, 1.06–0.86; ^{13}C NMR (75 MHz, CDCl$_3$, δ): 177.8, 177.5, 176.7, 149.3, 136.9, 122.8, 121.8, 120.2, 120.01, 64.6, 54.5, 54.1, 50.5, 45.0, 44.7, 30.1, 29.4, 26.4, 25.9, 19.2, 18.5, 18.3, 16.4, 13.6; Conversion (^{1}H NMR): 75%; SEC (DMA, PMMA calibration): $\overline{M}_n = 23\ 500$ g mol^{-1}, $\overline{M}_w = 27\ 700$ g mol^{-1}, PDI = 1.18, DP = 135.

3. Results and Discussion

3.1. Synthesis and Characterization of the Copolymers

The copper(I)-catalyzed azide–alkyne cycloaddition of 2-ethynylpyridine and 11-azidoundecan-1-ol provided
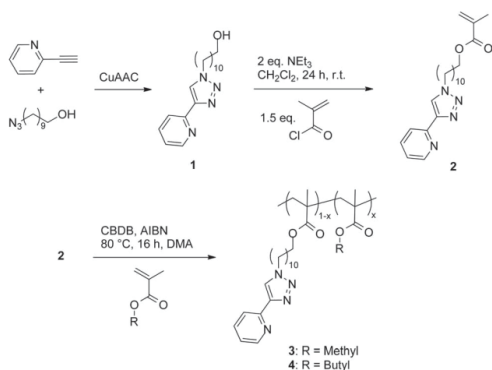
Scheme 1. Schematic representation of the synthesis of the methacrylate-functionalized 2-(1,2,3-triazol-4-yl)pyridine monomer **2** and the corresponding copolymerization.

the alcohol-functionalized trzpy ligand **1** described by our group earlier.[34] Compound **1** was esterified in good yield (87%) with methacryloyl chloride to yield monomer **2** (Scheme 1). A controlled RAFT radical copolymerization was performed to covalently incorporate the bidentate ligand **2** into two different polymer backbones, whereby MMA and BMA were used as comonomers. This polymerization technique was used due to its tolerance to a great number of functional groups. The RAFT polymerizations were performed in concentrated solutions (i.e., ≈2 M solution of the monomer in DMA) to allow the polymerization to proceed in a controlled manner. 2-Cyanobutan-2-yl benzodithioate was utilized as RAFT agent, since it is known to provide a narrow molar mass distribution.[35] AIBN has been used as initiator. A reaction time of 16 h was chosen to drive the conversion of the reaction to approximately 80%. The obtained copolymers **3** and **4** were purified by preparative SEC and characterized by ^{1}H NMR spectroscopy, UV-Vis titration experiments as well as SEC (see Figure S1–S6, Supporting Information). The SEC coupled with a photodiode array detector revealed a typical UV-Vis absorption spectrum of the *N*-heterocyclic trzpy ligand (λ_{max} = 286 nm), which confirmed the incorporation into the backbone of

copolymers **3** and **4** (see Figure S3–S4, Supporting Information). The molar masses were estimated by SEC using a linear PMMA calibration and the molar fraction (*x*) of trzpy-ligands was determined by both ^{1}H NMR spectroscopy and UV-Vis titration experiments (Table 1, for UV-Vis titration experiments see Figure S5 and S6, Supporting Information). The molar fraction did not significantly deviate from the theoretical values and both characterization techniques revealed comparable results (Table 1).

A typical ^{1}H NMR spectrum of the PMMA copolymer **4** is shown in Figure 1. The spectrum shows the characteristic aromatic signals of the trzpy ligand from δ = 7.2 to 8.6 as well as the polymeric backbone proton signals below δ = 2.0. The disappearance of the vinylic protons at δ = 5.9 and 6.3 of the monomers indicated the formation of a copolymer. Integration of the appropriate aromatic proton signals provided the molar fraction of the trzpy ligand, which are specified in Table 1 (compare x values with Scheme 1) for both copolymers.

The molar fraction of the trzpy was further determined by UV-Vis titration experiments with Fe(II) ions (for details see Experimental Section). A linear increase of the MLCT band at 433 nm (formation of the *tris*-complex: $[Fe(trzpy)_3]^{2+}$) was observed up to a ligand-to-Fe(II) stoichiometry of 3:1. This point of equivalence was used to calculate the molar fraction, whereby an underestimation was ascertained in comparison to the ^{1}H NMR calculation. The underestimation can be attributed to uncompleted complexation of the iron metal ions caused by the bulkiness of the polymer coils. After the point of equivalence, the MLCT absorption principally stayed constant. This indicated a high stability of the formed polymeric network in contrast to the Fe(II) UV-Vis titration experiments with the trzpy ligand itself (see Figure S5 and S6, Supporting Information). In the latter case, the absorption of the MLCT band decreases after reaching the point of equivalence.

In order to verify the formation of the $[Fe(trzpy)_3]^{2+}$ species, a ^{1}H NMR titration experiment of ligand **2** with Fe(II) ions was carried out (Figure 2). The spectrum at the top was recorded at a ligand-to-Fe(II) stoichiometry of 3:1. All typical ligand signals in the aromatic region vanished and, thus, the formation of the *tris*-complex can be concluded.

Table 1. Experimental details and characterization data of the copolymers **3** and **4**.

	Ligand/MMA (calc.)	MMA/CBDB/AIBN	Conv.[a] [%]	$\overline{M}_n$[b] (g mol^{-1})	PDI[c]	x[a]	x[d]	DP[e]
3	10/90	150/1/0.25	74	14 100[b]	1.24	0.89	0.90	112
4	10/90	150/1/0.25	75	23 500[b]	1.18	0.91	0.92	135

[a]Determined by ^{1}H NMR spectroscopy; [b]Determined by SEC (PMMA calibration); [c]Polydispersity index; [d]Determined by UV-Vis titration using Fe(II) ions; [e]Degree of polymerization.

- 172 -
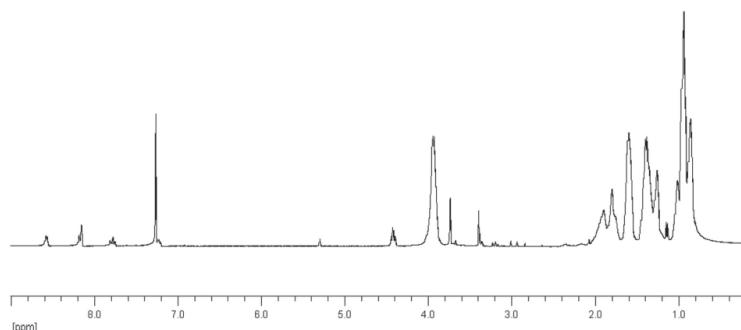
■ *Figure 1.* ^{1}H NMR spectrum of copolymer **4** (300 MHz, CDCl$_3$).

Additionally, a UV-Vis absorption spectrum of the NMR solution was recorded and showed a similar absorption behavior compared to the UV-Vis titration experiments (MLCT absorption maximum at 433 nm).

Moreover, copolymer **4** was characterized by the methods of macromolecular hydrodynamics application, which has been described by Schubert et al. in literature.[36–38] From the analysis of the sedimentation velocity, the following experimental values were obtained: velocity sedimentation coefficient extrapolated to the condition of infinite dilution of polymer solution $s_0 = (6.90 \pm 0.04) \times 10^{-13}$ s; concentration Gralen coefficient $k_s = (20 \pm 1)$ cm^3 g^{-1}; frictional ratio $(f/f_{sph})_0 = 1.43 \pm 0.01$, intrinsic viscosity

value $[\eta] = (8.5 \pm 0.2)$ cm^3 g^{-1} (see Figure S8 to S11, respectively, Supporting Information). Copolymer **4** (dissolved in acetone) was also characterized by the value of the partial specific volume $\upsilon = (0.88 \pm 0.01)$ cm^3 g^{-1} and the increment of the refraction index $\Delta n/\Delta c = (0.139 \pm 0.002)$ cm^3 g^{-1}. The molar mass of **4** was estimated from the modified Svedberg relationship: $M_{sD} = (RT/(1 - \upsilon\rho_0)(s_0/D_0) = 9\pi\ 2^{1/2}N_A([s](f/f_{sph})_0)^{3/2}\upsilon^{1/2}$, where R is the gas constant, T is the temperature in K, N_A is Avogadro's constant and $[s] \equiv s_0\eta_0/(1 - \upsilon\rho_0)$ is the intrinsic sedimentation coefficient. The obtained value of $\overline{M}_{Sd} = 27\ 600$ g mol^{-1} was in good agreement with the estimation obtained by SEC analysis ($\overline{M}_n = 23\ 500$ g mol^{-1}).
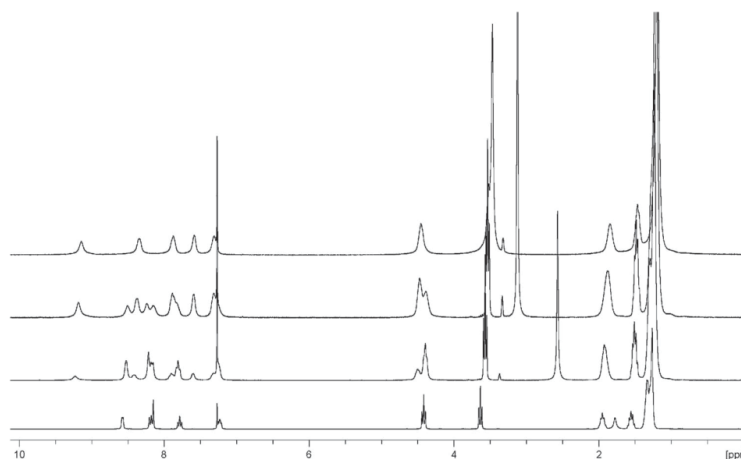
Figure 2. ^{1}H NMR (300 MHz) titration spectra of **2** (0.047 M in CDCl$_3$) by increasing Fe(II) ion content (from bottom to the top: pure ligand, ligand/Fe(II) = 9:1, ligand/Fe(II) = 6:1, ligand/Fe(II) = 3:1).

B. Happ et al.

conc. CH$_2$Cl$_2$ solution of polymer 3

Co^{II}(BF$_4$)$_2$ Fe^{II}Cl$_2$
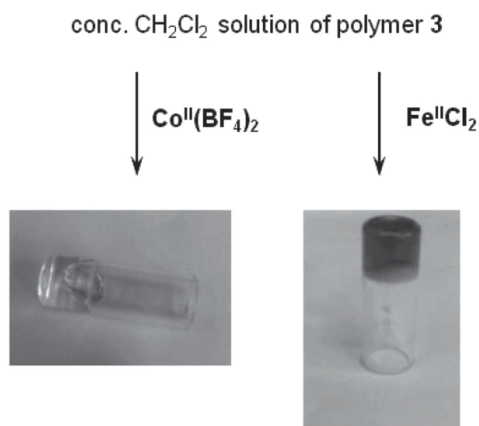
Figure 3. Gelation upon metal coordination of a concentrated solution of copolymer **3** in CH$_2$Cl$_2$.

3.2. Complexation and Decomplexation Studies

In a preliminary experiment, a concentrated dichloromethane solution of copolymers **3** or **4** ($c > 10$ mg mL^{-1}) was prepared and subjected to gelation via metal coordination using a methanolic Fe(II) or Co(II) solution (Figure 3). In the case of Fe(II), a red solid was obtained upon crosslinking each with three trzpy units. The crosslinking procedure with Co(II) ions led to a highly viscous solution, which was fluid yet. The reversibility of the crosslinking was examined by UV-Vis spectroscopy experiments utilizing a strong competitive chelating agent (Scheme 2). HEEDTA metal complexes are known to have high complex formation constants (see also Supporting Information for metal complex formation constants of [M(trzpy)$_3$]$^{2+}$ species).[39] At first, a UV-Vis absorption spectrum of a dichloromethane solution of copolymer **3** was measured as a blank (Figure 4 and Figure 5). The absorption spectrum exhibited a maximum

at 286 nm, which can be assigned to electronic transitions of the trzpy moiety of the copolymer. After that, the appropriate amount of metal salt, as methanolic Fe(II) or Co(II) solution, was added to obtain a ligand–metal stoichiometry of 3:1. The UV-Vis spectrum was remeasured and the appearance of the MLCT bands at 433 (Fe(II) *tris*-complex) and 320 nm [Co(II) *tris*-complex], respectively, verified the complexation of the bidentate ligands by the metal ions. For the meanwhile, there is no possibility to distinguish between intermolecular and intramolecular complexation as two possible complexation modes. By adding 10 equivalents of a methanolic HHEDTA solution, subsequently, the MLCT absorption bands vanished for both metals upon decomplexation (Figure 4 and Figure 5).

3.3. Supramolecular Crosslinking Studies

To gain detailed insights into the crosslinking process and the metal complexation, respectively, viscosity titration experiments at different concentrations of copolymer **4** and Co(II) ions were performed in acetone. Fe(II) ions could not be investigated by this method, since the acetone solution of iron(II) salts was not stable yielding an off-white precipitate after a few minutes. The Co(BF$_4$)$_2 \cdot$ 6H$_2$O salt was dissolved in acetone and added in stepwise portions to a solution of the polymer with known concentration ($c_{\text{poly}}^{\text{init}}$). The dynamic viscosity (η) was measured after each step utilizing an AMVn viscosimeter. After the addition of the metal salt, the final solutions were shaken for a sufficient time to enable homogenization. The polymer concentration was kept constant by the addition of the corresponding amount of the polymer solution with the concentration $c = 2c_{\text{poly}}^{\text{init}}$. The results of this rheological study are presented in Figure 6. The dynamic viscosity of the solutions containing the Co(II) salts strongly depended on the initial polymer concentration. For the concentrated solutions, where the degree of dilution (product of intrinsic viscosity of the polymer and its concentration in the solution ([η]c) was higher than
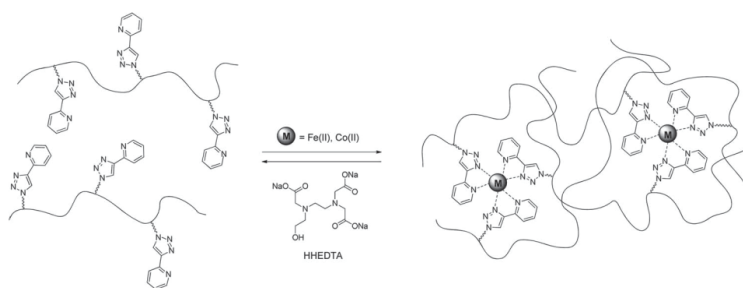
■ *Scheme 2.* Complexation of polymer **3** and decomplexation with HHEDTA.

- 174 -
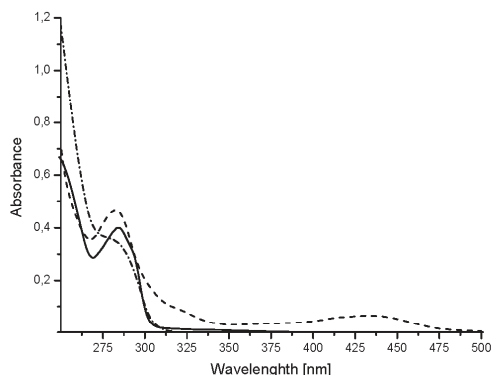
Figure 4. UV-Vis spectra (in CH$_2$Cl$_2$) of the blank copolymer 3 (solid), complexation with Fe(II) metal ions (dash) and decomplexation with methanolic HHEDTA solution (dash-dot).

Figure 6. Dynamic viscosity of the acetone solutions of 4 in dependence on the weight concentration (wt%) of Co(BF$_4$)$_2$ · 6H$_2$O. The dotted line 4 corresponds to the polymer solutions without the cobalt(II) salt.

0.5 (50% of the volume is occupied by macromolecules), an exponential increase of the dynamic viscosity value was observed with increasing Co(II) concentration. For $[\eta]c \approx 0.8$, the dynamic viscosity value increased approximately 20-fold compared with the initial one at a molar cobalt(II) concentration of $c(Co) = 3.66 \times 10^{-3}$ M (Figure 6, line 1). When the degree of dilution was low ($[\eta]c \leq 0.25$), the dynamic viscosity value increased only about 3 times and after further addition of Co(II) ions a declining tendency of the η value was observed.

The remarkable large increase of the dynamic viscosity in a concentrated copolymer solution with increasing Co(II) concentration was attributed to the formation of
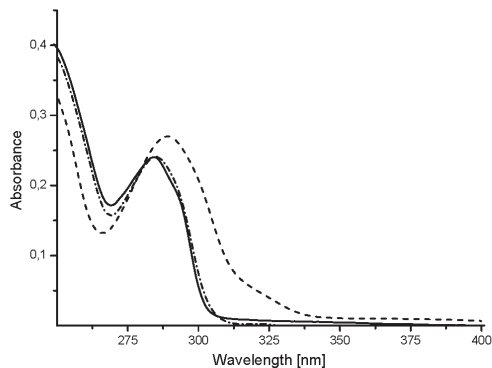
Figure 5. UV-Vis spectra (in CH$_2$Cl$_2$) of the blank copolymer 3 (solid), complexation with Co(II) ions (dash) and decomplexation with methanolic HHEDTA solution (dash-dot).

crosslinked structures (intermolecular complexation) in which Co(II) ions are linked to several different copolymer chains. The average molar mass of a crosslinked macromolecule can be estimated from the dynamic viscosity value. It is known that the dynamic viscosity of various polymer–solvent systems at high concentrations above some critical molar mass (M_{cr}) is related to the molar mass by the equation $\eta = K_h\,M^{3.4}$,[40] Below M_{cr}, the value of the dynamic viscosity is directly proportional to the molar mass. Considering the latter two extremes, the following estimation was obtained for the solute with $c_{poly} = 0.096$ g cm^{-3} and $c(Co^{II}) = 3.66 \times 10^{-3}$ M: $70 < M \times 10^{-3}$ g mol$^{-1} < 500$. A more precise estimation can be obtained by comparing the values of the dynamic viscosity of the solution of known molar masses of different PMMA samples in acetone with the η value of the copolymer solution in presence of the cobalt salt (Figure 7), whereby PMMA was considered as a modeling system for the copolymer 4 as a first approximation. This comparison yielded the value of $\overline{M}_n = 150\,000$ g mol^{-1}. This means that on average five initial copolymer macromolecules form the crosslinked unit. Along the intermolecular crosslinking also intramolecular complexation occurred at a higher degree of dilution (Figure 6, line 3).

The stability of the network observed at high concentrated copolymer solution with Co(II) ions was further studied. For this purpose, the comparison of the velocity sedimentation of two solutions was accomplished. One solution was obtained by diluting a highly concentrated solution ($c = 9.05 \times 10^{-2}$ g cm^{-3}, degree of dilution is $c[\eta] = 0.77$), where a strong increase of the dynamic viscosity in the presence of Co(II) ions was observed, and a second solution by diluting a less concentrated solution
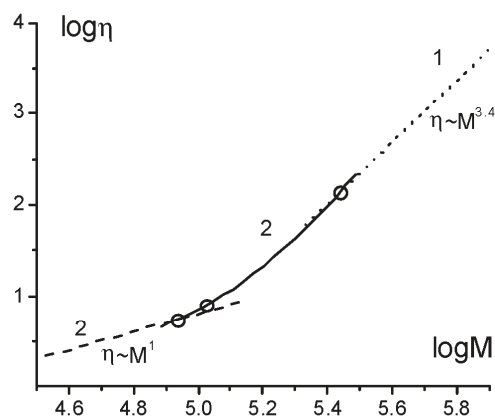
Figure 7. Double logarithmic plot of the dynamic viscosity (η) of PMMA samples in acetone (c_{poly} = 0.096 g cm^{-3}) versus molar mass. Dashed line 1 corresponds to the law $\eta = K_h\,M^{3.4}$ and line 2 corresponds to $\eta = K_1\,M^{1.0}$. Line 3 is related to the following data obtained for solutions of PMMA samples: $\overline{M}_w$ = 86 000 g mol^{-1}, η = 5.15 cP; $\overline{M}_w$ = 106 000 g mol^{-1}, η = 7.915 cP and $\overline{M}_w$ = 274 000 g mol^{-1}, η = 136 cP.

(c = 0.71 × 10^{-2} g cm^{-3}, degree of dilution is $c[\eta]$ = 0.06). Figure 8 shows the comparisons of the distributions of the velocity sedimentation coefficients obtained for two Co(II) concentrations by least-squares boundary modeling.[31,32] The distributions in both cases are practically the same, which indicates that the network is not stable and destroyed during the dilution caused by Brownian thermal movements of the molecules.

3.4. Induced Charge Effect on the Macromolecule Conformation During the Copolymer Complexation

The intramolecular complexation of such kind of copolymers with multi-valence ions may be observed and studied in the regime of very dilute solutions (Figure 6, line 3). The velocity sedimentation of the solutions with the polymer concentration c = (0.070 ± 0.005) × 10^{-2} g cm^{-3} was studied as function of the concentration of the Co(BF$_4$)$_2$ · 6H$_2$O salt. This polymer concentration corresponds to a very high degree of dilution $c[\eta]$ = 0.006. Such degree of dilution means that only 0.6% of solution volume is occupied by the macromolecules. Hence, the macromolecules are separated by the distance larger than their hydrodynamic size and the information obtained at this condition concern virtually the properties of individual macromolecules. Figure 8 represents the dependence of the intrinsic velocity sedimentation coefficient [s] on the molar salt concentration in the semilogarithmic scale. The intrinsic velocity sedimentation coefficient [s] is a value, which depends only on the macromolecular characteristics, such as the molar mass M and the mean square of the end-to-end distance of the linear chain ($<h^2>$): $[s] \equiv s_0\eta_0/(1 - v\rho_0) = M/N_A P <h^2>^{1/2}$, where N_A is Avogadro's constant and P is the dimensionless Flory hydrodynamic parameter.

When the solution of Co(BF$_4$)$_2$ · 6H$_2$O salt is added into a diluted polymer solution first a significant decrease of the velocity sedimentation coefficient was observed (Figure 9a, region 1). This experimental fact can be explained by an increase of the proportion of Co(II) ions bound to ligands of the polymeric chain. This leads to an increase of the number of electrical charges on individual macromolecules and, consequently, allows the raise of the translational friction coefficient due to the additional friction losses resulting from the electrostatic expansion of

Figure 8. The distribution of the velocity sedimentation coefficient g*(s) obtained by least-squares boundary modeling (ls-g*(s)) for copolymer **4** (c_{poly} = 7 × 10^{-4} g cm^{-3} in acetone) using different weight concentration of the Co(II) salt. a) 0.008, b) 0.315 wt%. 1) Velocity sedimentation distribution for the solutions obtained by the dilution of the high concentrated solution (c_{poly} = 9.05 × 10^{-2} g cm^{-3}) and 2) obtained by the dilution of the moderately concentrated solution (c_{poly} = 0.71 × 10^{-2} g cm^{-3}).
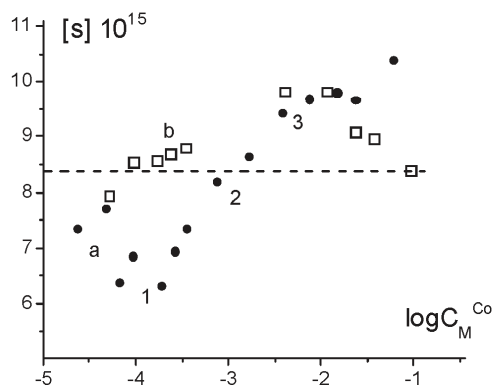
Figure 9. Dependence of the intrinsic velocity sedimentation coefficient measured for the copolymer **4** ($c_{poly} = 7 \times 10^{-4}$ g cm^{-3} in acetone) on different molar concentrations of cobalt salt without (●) and with 0.05 M NH$_4$PF$_6$ (□) using a semilogarithmic scale.

Figure 10. Sedimentation coefficient distribution g∗(s) obtained by least-squares boundary modeling (ls-g∗(s)) for copolymer **4** ($c_{poly} = 7 \times 10^{-4}$ g cm^{-3} in acetone) with different concentrations of cobalt salt: 1) 0, 2) 0.008, 3) 0.32, 4) 6.3, and 5) 0.004 wt% + 0.05 M NH$_4$PF$_6$.

the chains and from the electrostatic interactions between distant macromolecules. The increase in the translational friction coefficient f results in a decrease in the velocity sedimentation coefficient, as $s \approx Mf^{-1}$. In the range of the Co(II) salt concentration $c(Co) \approx 0.2 \times 10^{-3}$ M, the minimum of the velocity sedimentation coefficient was observed. As a result, the average number of Co(II) ions connected with one macromolecule may be estimated. The ratio of the polymer molar concentration to the cobalt salt molar concentration gives the number of the repeating units of the copolymer (molar masses of comonomers averaged), which corresponds to one cobalt ion. The number was calculated to be 23. Since the average degree of polymerization is 135, six Co(II) ions are approximately connected with one macromolecule. The argument to prove that the decrease of the velocity sedimentation coefficient is related with the charge effect of the coordinated Co(II) ions was supported by the addition of a one-to-one ion salt NH$_4$PF$_6$ (0.05 M) to the cobalt-containing solution. The velocity sedimentation coefficients take values close to that obtained for pure acetone without Co(II) salt (Figure Figure 9b and Figure 10). After reaching a minimum, the value of the velocity sedimentation coefficient begins to increase as function of the concentration of cobalt salt. Presumably, in this case, the main effect is the screening of charges on the polymer chains by additional charges appearing in solution and a large part of the new added ions are not bound by the polymer chains anymore. The changes of the hydrodynamic and conformational characteristics of the macromolecules (Figure 9a, region 2) are supposedly related with the increasing of the ionic strength of the solution, which may be reached
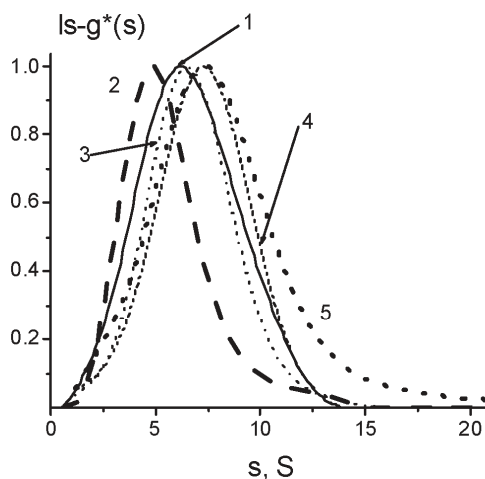
by the addition of any other soluble one-to-one ion salt (Figure 9, region 3).

4. Conclusion

A bidentate 2-(1*H*-1,2,3-triazol-4-yl)pyridine chelating unit was copolymerized with two different methacrylate-based comonomers (MMA and BMA). The RAFT polymerization technique led to well-defined copolymers as confirmed by ^{1}H NMR spectroscopy, SEC coupled with a photodiode array detector, and UV-Vis titration experiments. The copolymers were investigated toward their gelation properties against Fe(II) and Co(II) ions. Both metal salts showed a crosslinking ability in concentrated solution ($c > 10$ mg mL^{-1}), whereby in the case of cobalt a highly viscous fluid was observed. The reversibility of the crosslinking was demonstrated by UV-Vis spectroscopy experiments utilizing the strong competitive chelate HHEDTA. Moreover, the differentiation between intermolecular and intramolecular complexation, respectively, was achieved by viscosity titration experiments at different concentrations of the copolymer in acetone using Co(II) ions. In concentrated solutions, that is, with a degree of dilution higher than 0.5 of the polymer, intermolecular complexation of the Co(II) ion with different macromolecule chains was deduced from the latter experiments. The complexes were destroyed during the dilution

of the solutions. The intramolecular complexation with Co(II) ions was studied in highly diluted acetone solution of the trzpy-containing copolymer by means of different analytical ultracentrifuge experiments. By the addition of a small amount of Co(II) ions, a significant decrease of the intrinsic sedimentation coefficient was observed, which could be explained by the elongation of the individual polymer coils upon the electrostatic repulsion of the coordinated Co(II) ions.

Supporting Information

[1] J.-M. Lehn, *Supramolecular Chemistry, Concepts and Perspectives*, Wiley-VCH, Weinheim **1995**.
[2] U. S. Schubert, C. Eschbaumer, *Angew. Chem. Int. Ed.* **2002**, *41*, 2893.
[3] M. Weck, *Polym. Int.* **2007**, *56*, 453.
[4] G. R. Whittell, I. Manners, *Adv. Mater.* **2007**, *19*, 3439.
[5] U. S. Schubert, A. Winter, G. R. Newkome, Terpyridine-based *Materials: For Catalytic, Optoelectronic and Life Science Applications*, Wiley-VCH, Weinheim **2011**.
[6] H. Hofmeier, U. S. Schubert, *Chem. Soc. Rev.* **2004**, *33*, 373.
[7] A. W. Bosman, R. Vestberg, A. Heumann, J. M. J. Fréchet, C. J. Hawker, *J. Am. Chem. Soc.* **2002**, *125*, 715.
[8] M. D. Hager, P. Greil, C. Leyens, S. van der Zwaag, U. S. Schubert, *Adv. Mater.* **2010**, *22*, 5424.
[9] G. R. Whittell, M. D. Hager, U. S. Schubert, I. Manners, *Nat. Mater.* **2011**, *10*, 176.
[10] I. Luzinov, S. Minko, V. V. Tsukruk, *Prog. Polym. Sci.* **2004**, *29*, 635.
[11] C. D. Eisenbach, U. S. Schubert, *Macromolecules* **1993**, *26*, 7372.
[12] J.-F. Gohy, *Coord. Chem. Rev.* **2009**, *253*, 2214.
[13] C. L. Fraser, A. P. Smith, X. Wu, *J. Am. Chem. Soc.* **2000**, *122*, 9026.
[14] P. S. Corbin, M. P. Webb, J. E. McAlvin, C. L. Fraser, *Biomacromolecules* **2001**, *2*, 223.
[15] G. Hochwimmer, O. Nuyken, U. S. Schubert, *Macromol. Rapid Commun.* **1998**, *19*, 309.
[16] J. F. Gohy, B. G. G. Lohmeijer, S. K. Varshney, B. Décamps, E. Leroy, S. Boileau, U. S. Schubert, *Macromolecules* **2002**, *35*, 9748.
[17] Y. Yan, J. Huang, *Coord. Chem. Rev.* **2010**, *254*, 1072.
[18] P. Guillet, C. Mugemana, F. J. Stadler, U. S. Schubert, C.-A. Fustin, C. Bailly, J.-F. Gohy, *Soft Matter* **2009**, *5*, 3409.
[19] A. L. Lewis, J. D. Miller, *J. Mater. Chem.* **1993**, *3*, 897.
[20] Y. Chujo, K. Sada, T. Saegusa, *Macromolecules* **1993**, *26*, 6315.
[21] Y. Chujo, K. Sada, T. Saegusa, *Macromolecules* **1993**, *26*, 6320.
[22] H. C. Kolb, M. G. Finn, K. B. Sharpless, *Angew. Chem. Int. Ed.* **2001**, *40*, 2004.
[23] V. V. Rostovtsev, L. G. Green, V. V. Fokin, K. B. Sharpless, *Angew. Chem. Int. Ed.* **2002**, *41*, 2596.
[24] H. Struthers, T. L. Mindt, R. Schibli, *Dalton Trans.* **2010**, *39*, 675.
[25] B. Schulze, D. Escudero, C. Friebe, R. Siebert, H. Gorls, U. Kohn, E. Altuntas, A. Baumgaertel, M. D. Hager, A. Winter, B. Dietzek, J. Popp, L. Gonzalez, U. S. Schubert, *Chem. Eur. J.* **2011**, *17*, 5494.
[26] I. Stengel, A. Mishra, N. Pootrakulchote, S.-J. Moon, S. M. Zakeeruddin, M. Gratzel, P. Bauerle, *J. Mater. Chem.* **2011**, *21*, 3726.
[27] B. Happ, G. M. Pavlov, E. Altuntas, C. Friebe, M. D. Hager, A. Winter, H. Görls, W. Günther, U. S. Schubert, *Chem. Asian J.* **2011**, *6*, 873.
[28] M. Obata, A. Kitamura, A. Mori, C. Kameyama, J. A. Czaplewska, R. Tanaka, I. Kinoshita, T. Kusumoto, H. Hashimoto, M. Harada, Y. Mikata, T. Funabiki, S. Yano, *Dalton Trans.* **2008**, 3292.
[29] B. Beyer, C. Ulbricht, D. Escudero, C. Friebe, A. Winter, L. González, U. S. Schubert, *Organometallics* **2009**, *28*, 5478.
[30] B. Happ, C. Friebe, A. Winter, M. D. Hager, U. S. Schubert, *Eur. Polym. J.* **2009**, *45*, 3433.
[31] P. Schuck, *Biophys. J.* **2000**, *78*, 1606.
[32] http://www.analyticalultracentrifugation.com/sedphat/sedphat.htm.
[33] O. Kratky, H. Leopold, H. Stabinger, *Methods Enzymol.* **1973**, *27*, 98.
[34] B. Happ, C. Friebe, A. Winter, M. D. Hager, R. Hoogenboom, U. S. Schubert, *Chem. Asian J.* **2009**, *4*, 154.
[35] E. Rizzardo, M. Chen, B. Chong, G. Moad, M. Skidmore, S. H. Thang, *Macromol. Symp.* **2007**, *248*, 104.
[36] G. M. Pavlov, D. Amorós, C. Ott, I. I. Zaitseva, J. Garcia de la Torre, U. S. Schubert, *Macromolecules* **2009**, *42*, 7447.
[37] G. M. Pavlov, I. Perevyazko, U. S. Schubert, *Macromol. Chem. Phys.* **2010**, *211*, 1298.
[38] G. M. Pavlov, I. Y. Perevyazko, O. V. Okatova, U. S. Schubert, *Methods* **2011**, *54*, 124.
[39] S. Chaberek, A. E. Martell, *J. Am. Chem. Soc.* **1955**, *77*, 1477.
[40] R. H. Colby, L. J. Fetters, W. W. Graessley, *Macromolecules* **1987**, *20*, 2226.